Characterization, Optimization and Design of

The Sorbent System for a Continuous Direct Air Capture System

Gijs Mulder

TU Delft

Characterization, Optimization and Design of the Sorbent System for a Continuous Direct Air Capture System.

by

Gijs Mulder

to obtain the degree of Master of Science
at the Delft University of Technology,
to be defended publicly on May 20, 2021 at 13:00.

”Life is like riding a bicycle. To keep your balance, you must keep moving.”

Albert Einstein

Student number:	4174925	
Project duration:	June 1, 2020 – May 20, 2021	
Thesis committee:	Prof. dr. ir. E. Goetheer,	TU Delft, supervisor
	Prof. dr. ir. W. De Jong,	TU Delft
	Prof. dr. ir. B. J. Boersma,	TU Delft
	Ir. M. Sinha,	Zero Emission Fuels

This thesis is confidential and cannot be made public until May 20, 2023

Abstract

With the influx of the industrial revolution of the past centuries, the global energy demand has grown proportional to the global economical growth. Consequently, an enormous rise in greenhouse gas emissions has been observed, where the major contribution to global warming comes from the rising concentration of CO_2. Therefore, the concept of capturing CO_2 directly from the air (DAC) has gained world wide attention as it can reduce the carbon footprint of men kind.

Zero Emission Fuels (ZEF), an inspiring start-up based in Delft, aims to develop a micro plant that utilizes the DAC concept to produce methanol as a fuel, using only the sun as its energy source. CO_2 and H_2O is captured directly from the atmosphere by the DAC unit which operates continuously with the help of an amine sorbent that flows through an absorption and stripping column. Previous research shows pure tetraethylenepentamine (TEPA) having great potential as a CO_2 capturing sorbent. However, it has some limitations regarding slow absorption and desorption kinetics due to a high sorbent viscosity, that prevent ZEF from reaching their goal of capturing 825 grams of CO_2 per DAC unit in eight hours of operation.

The focus of this research is on the sorbent selection process of ZEF's DAC system. Research has shown that adding a diluent to TEPA could potentially improve the performance of the ZEF DAC unit. Therefore, a total of nine diluents, *DEG, PEG-200, PEG-400, PEG-600, selexol-250, selexol-500, glycerol, 1,4-butanediol, sulfolane*, mixed in different ratio's with TEPA, have been put to the test through the developed framework of sorbent selection.

In the framework of sorbent selection all the sorbents are tested through four different experiments, keeping efficiency and costs in consideration. The Airfarm experiments are used to evaluate absorption capacity and viscosity of the sorbent at specific ambient conditions. The Vapor-Liquid-Equilibrium (VLE) experiments are utilized to evaluate the desorption characteristics of the sorbent from where the regeneration energy demand can be calculated with the help of a mathematical model. The re-pumping experiments are used to evaluate the absorption kinetics of the sorbent and lastly, the degradation experiments are used to evaluate the sorbent life time performance. After the experimental procedure the sorbents can be judged on the key performance indicators regarding the ZEF DAC unit operated in a specific climate.

It was concluded through the literature research and proved by an extensive experimental research that *selexol, glycerol and sulfolane* did not improve the characteristics of the sorbent. However, adding *DEG, PEG or 1,4-butanediol* to TEPA did have a profound positive effect on the overall performance of the DAC unit. Since the diluents reduce the sorbent viscosity, and therefore, increase the absorption and desorption kinetics.

Based on the experimental results and the design specifications set by ZEF, *PEG-200* proved the most promising out of all diluents in the mixing ratio *TEPA:PEG-200 2:5*. This sorbent has been tested for two different climates; the dry Sahara climate and the more humid Mediterranean climate to see how the sorbent would have to be changed for different climates. It was concluded, for a more humid climate, it requires less diluent for the sorbent to stay within the 2 $Pa \cdot s$ viscosity limit.

The experimental results were included in a full DAC model to design the DAC unit utilizing the optimized sorbent for the two different climates considering the design specifications set by ZEF. Following a sensitivity analysis an optimized conceptual DAC design was obtained for both climates. Where it was concluded that the optimized sorbent resulted in reduction in energy requirement for regeneration of the sorbent, where 1554 kWh/ton_{CO_2} is needed for the Sahara climate and 1636 kWh/ton_{CO_2} for the Mediterranean climate. Finally, a cost analysis has been performed regarding the operational and capital costs of the newly designed conceptual DAC units for both climates.

Acknowledgements

Through the journey I have made over the past 12 months at ZEF I have matured a lot. It has made me stronger as a person, as it has boosted the confidence in myself and provided me with a strong sense of purpose for the goals I want to achieve in life. Although this was not all to my own doing. Throughout the journey of this research project I was blessed and lucky to have received a great deal of support and assistance.

First and foremost I would like to thank my parents, **Luc & Nelleke Mulder**, for always supporting me throughout my entire life. Believing in me, inspiring me and showering me with love and support. Without you, I would have never be able to build this solid foundation for my future.

I would like to express my gratitude and appreciation for my twin brother, **Bart Mulder**. As we rocked our studies here in Delft together, always helping, pushing and learning together along the way, making your guidance, support and encouragement invaluable throughout my entire life.

Furthermore, I would like to thank my rock in the sea, **Rachelle Moll**, for always supporting me and pushing me beyond my own limits to achieve the absolute maximum, I love you.

I would like to thank Zero Emission Fuels, for providing the opportunity to indulge myself in this highly inspiring environment and do both my internship and thesis project with them. Within ZEF, they guided me throughout this journey.

Therefore, I would like to thank my supervisor at ZEF, **Mrigank Sinha**, whose expertise was invaluable in formulating the research questions and methodology. Your insightful feedback, perseverance and dedication pushed me to sharpen my thinking and brought my work to a higher level.

Furthermore, I would like to thank **Ulrich Starke** and **Jan van Kranendonk**. I have learned a lot under their guidance. They guided me from day one and through my entire journey with patience, perseverance and above all great enthusiasm which made working at ZEF not only very educational but also a lot of fun. Naturally not all things that had to be done were always fun to do, but from this valuable lessons were learned since it represents real life challenges. The organizational skills of Ulrich were very helpful from the first day at ZEF, from getting to know the ZEF way, to arranging everything around this thesis project at ZEF. Furthermore the ability of Jan to keep track with everyone's work and how he guides the entire company in the right direction is an admirable quality. I have learned a lot from Jan's analytical way of thinking.

Lastly from ZEF, I would like to recognize the invaluable effect **Hessel Jongebreur** has on the the whole team of ZEF. His uplifting spirit and ability to see possibilities in nearly every situation helped a lot.

I would like to pay my special regards to the way the ZEF team dealt with the situation when the Covid-19 virus hit the Netherlands. The company kept their work flow going with everyone working from home and through online meetings on Skype the project was continued.

I would also like to thank Professor **Earl Goetheer** for being my thesis supervisor and motivating me in many ways throughout my thesis. Thank you for the early morning meetings and your enthusiasm regarding the DAC concept during this thesis project.

I would like to acknowledge my fellow students at ZEF for their wonderful collaboration. **Rahul Pougat, Ved Dubhashi, Andrea De Matteis, Nelson van de Poll, Samir den Haan, Tom Kleist and Bart Boons.**

Furthermore, I want to thank my brother and sister, **Stijn & Besty Mulder**, for always helping me wherever they could and just for being awesome. You guys rock!

Finally, I could not have completed this dissertation without the support of my friends, **Jelmer Hollanders, Aron van Stijn, Boss Priester, Brandon & Kevin ten Hoeve, Jimi & Mick Burgwal, Thijmen Tijhuis, Patrick Schilperoort, Wessel Willemsen, Karim Yafrah and Nick rutten**, who provided stimulating discussions as well as happy distractions to rest my mind outside of my research.

Contents

List of Figures

List of Tables

Nomenclature

Table 1: List of molecules mentioned in this research project including their description.

Molecular structure	Description
$(C_2H_5N)_n$	Polyethylenimine
$C_{2n}H_{4n+2}O_{n+1}$	Polyethylene glycol
$C_{2n+2}H_{4n+6}O_{n+1}$	Selexol
$C_3H_8O_3$	Glycerol
$C_4H_{10}O_2$	1,4-Butanediol
$CaCO_3$	Calcium Carbonate
CaO	Calcium Oxide
$Ca(OH)_2$	Calcium Hydroxide
CH_3	Methyl group
CH_3OH	Methanol
CH_4	Methane
$(CH_2)_4SO_2$	Sulfolane
CO_2	Carbon Dioxide
H_2	Hydrogen
H_2O	Water
HCl	Hydrochloric acid
K_2CO_3	Potassium Carbonate
NaOH	Sodium Hydroxide
Na_2CO_3	Sodium Carbonate
N_2O	Nitrous Oxide
O_2	Oxygen
OH	Hydroxyl group

Table 2: List of abbreviations used in this research project including their description part 1.

Abbreviation	Description
3D	Three Dimensional
AEC	Alkaline Electrolysis Cell
CAD	Computer Aided Design
CCS	Carbon Capture and Sequestration
CCU	Carbon Capture and Utilization
CDRA	Carbon Dioxide Removal Assembly
DAC	Direct Air Capture
DEA	Diethanolamine
DEG	Diethylene Glycol
DEPG	Dimethyl Ethers of Polyethylene Glycol
DETA	Diethylenetriamine
DS	Distillation column
EDA	Ethylenediamine
EOR	Enhanced Oil Recovery
et al.	et alia, meaning and others
FM	Fluid Machinery
FTIR	Fourier Transform Infrared Spectroscopy
HEX	Heat exchanger

Table 3: List of abbreviations used in this research project including their description part 2.

ID	Identification Document or tag
IPCC	Intergovernmental Panel on Climate Change
i.e.	id est, meaning that is
KPI	Key Performance Indicator
kWh	kiloWatt-hours
LD_{50}	Amount of material to cause 50% of tested animals to be killed
LNG	Liquid Natural Gas
MDEA	Methyldiethanolamine
MEA	Monoethanolamine
MOF	Metal Organic Frameworks
MS	Methanol Synthesis reactor
MSA	Moisture Swing Absorption
N/A	Not applicable
NTC	Negative Temperature Coefficient
PCB	Printed Circuit Board
PEG	Polyethylene glycol
PEI	Polyethylenimine
PFA	Perfluoroalkoxy
pH	Power of Hydrogen, scale for acidity or basicity
PLA	Polyactic Acid
ppm	Parts Per Million
PV	Photo-Voltaic
PSA	Pressure Swing Adsorption
PZ	Piperazine
rpm	revolutions per minute
SOL	Solar panel
STP	Standard Temperature and Pressure
STY	Space-Time-Yield
TEPA	Tetraethylenepentamine
[TEPA]Ac	Tetraethylenepentamine acetic acid
TETA	Triethylenetetramine
TSA	Temperature Swing Adsorption
TU	Technical University
TVS	Temperature-Vacuum-Swing cycling
TWh	TeraWatt-hours
USA	United States of America
VLE	Vapor Liquid Equilibrium
ZEF	Zero Emission Fuels

Table 4: List of symbols used in this research project including their description and unit part 1.

Symbol	Description	Unit
A	Area	$[m^2]$
A_i	Additional mass flow into stripper stage i	$[mol/s]$
β	Thermal expansion coefficient	$[K^{-1}]$
B	Bottom product mass flow	kg/s
CC	Cyclic capacity	$[mol_{CO_2}/kg_{TEPA\ or\ sorbent}]$
C_p	Specific heat	$[kJ/kg \cdot K]$
$C_{p,liq}$	Specific heat of liquid	$[kJ/kg \cdot K]$
$C_{p,vap}$	Specific heat of vapor	$[kJ/kg \cdot K]$
c_{gas}	Solubility of gas	$[mol/L]$
c_{Ai}	concentration of A at position i	$[wt\%]$
$\bar{c}_A$	average bulk concentration of A	$[wt\%]$
D	Diffusion coefficient or diffusivity	$[m^2/s]$
$D_{A,L}$	Diffusion coefficient of species A in liquid L	$[m^2/s]$
$D_{top,product}$	Top product mass flow	$[kg/s]$
$\frac{dc_A}{dz}$	Molar concentration gradient	$[mol/m^3m]$
E	Energy demand of stripper for CO_2	$[kJ/mol_{CO_2}]$
$E_{3:1}$	Energy demand of stripper when 3:1 product stream is satisfied	$[kJ/mol_{CO_2}]$
$E_{absorption}$	Energy of absorption	$[W]$
$E_{regeneration}$	Regeneration energy demand	$[W]$
$E_{sensible}$	Sensible heat	$[W]$
$E_{vaporization}$	Energy for vaporization	$[W]$
ϕ_i	Fugacity coefficient	[-]
F_{rich}	Molar flow of the feed of the stripper column	$[mol/s]$
γ_i	Activity coefficient	[-]
γ_{feed}	Loading of the feed of the stripper column	$[mol_{CO_2}/kg_{TEPA}]$
$\gamma_{sorbent}$	Loading into the sorbent	$[mol_{CO_2}/kg_{sorbent}]$
γ_{TEPA}	Loading into the sorbent	$[mol_{CO_2}/kg_{TEPA}]$
H_{abs}	Heat of absorption	$[kJ/mol]$
H_{gas}	Henry's constant	$[L \cdot bar/mol]$
H_{vap}	Heat of vaporization	$[kJ/kg]$
J	Diffusion flux	$[mol/m^2s]$
k_B	Boltzmann Constant	$[m^2kg/s^2]$
k_{CO_2}	Space-Time-Yield or mass transfer coefficient	$[mol/m^2s]$
Λ	Wilson parameter	[-]
L	Length	$[m]$
L_{cond}	Condensed vapor mass flow	$[kg/s]$
L_i	Liquid mass flow entering stage i	$[mol/s]$
μ	dynamic viscosity of fluid	$[Pa \cdot s]$
M_L	Molecular weight of L	$[g/mol]$
$\dot{m}$	Mass flow	$[kg/s]$
$m_{sorbent}$	Mass of sorbent	$[g]$
N	Number of stages in stripper column	$[-]$
$\dot{n}_A$	Rate of absorption	$[mol/s]$
n_{CO_2,H_2O}	Total amount absorbed in VLE test vessel	$[mol]$
$n_{CO_2,abs}$	Amount of CO_2 absorbed by the sorbent	$[mol]$
$n_{CO_2,g}$	Amount of CO_2 in the gas phase	$[mol]$
n_{puff}	Number of puffs in the VLE test setup	$[Puffs]$
O_L	association factor of absorbent	[-]
P_{abs}	Absolute pressure	$[bar]$
P_{STP}	Standard pressure	$[Pa]$
P_i^{sat}	Saturation vapor pressure	$[Pa]$
p_{gas}	Partial pressure of gas	$[bar]$
Q_i	Heat flow into stage i	$[W]$
Q_{reb}	Heat duty of the reboiler	$[W]$

Table 5: List of symbols used in this research project including their description and unit part 2.

Symbol	Description	Unit
R	Universal gas constant	$[J/(K \cdot mol)]$
R_{rich,H_2O}	Water ratio in rich sorbent stream	$[kg_{H_2O}/kg_{TEPA}]$
R_{top}	Product vapor ratio of stripper column	[−](H_2O:CO_2
RH	Relative Humidity	[%]
RR	Reflux Ratio	[−]
RR_{min}	Minimum reflux ratio	[−]
r	Radius of spherical particle	[m]
STY	Space-Time-Yield	$[mol/m^2 s]$
T	Temperature	$[K$ or $^\circ C]$
δT	Temperature step change	$[^\circ C]$
T_{des}	Desorption temperature	$[K$ or $^\circ C]$
T_{feed}	Feed temperature	$[K$ or $^\circ C]$
T_{reb}	Reboiler temperature	$[^\circ C]$
T_{STP}	Standard temperature	$[K]$
t	Time	$[s]$
V	Liquid mass flow back to column	kg/s
ΔV	Difference in volume due to temperature change	$[m^3]$
V_0	liquid volume of original sample	$[m^3]$
V_A	Molecular volume of A	$[m^2/mol]$
V_{i+1}	Vapor flow entering stage i	$[mol/s]$
V_{puff}	Volume of one puff in VLE test setup	$[l]$
W	Width	$[m]$
χ	Mass fraction	$[wt\%]$
x_i	liquid phase mole fraction	[-]
y_i	Vapor mole fraction	[-]
$z_{i,j}$	Composition of additional mass flow into stage i	[-]

1

Introduction

In this inaugural chapter, one of the major global problems on Earth is concisely discussed as well as its cause and effects. Thereafter, a number of solutions are elaborated along with the motivation for this thesis. Subsequently, the scope and research objectives of this thesis are established and the chapter ends with the thesis approach and the outline of this report.

1.1. A Problem of Global Scale

The human evolution essentially started 4.1 billion years ago when life originated on planet Earth [125]. The Homo sapiens have walked this planet for more than 300.000 years. However, arguably the biggest steps in the evolution of science have only been made in the last few centuries. This jump in scientific development has benefited the average life quality of the human race greatly, but on the other hand, has profound negative effects on the natural equilibrium of life which has directed this planet ever since life originated on it.

1.1.1. Global Energy Demand

With the influx of the industrial revolution of the past centuries, the global energy demand has grown proportional to the global economical growth. Figure 1.1 shows the enormous increase in global primary energy consumption of the past two centuries.

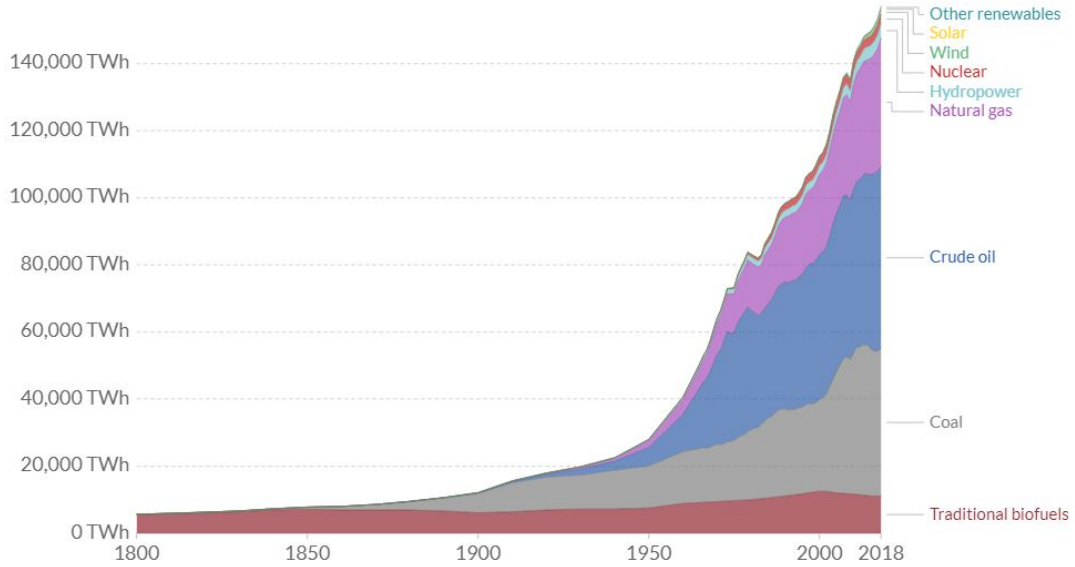

Figure 1.1: Global primary energy consumption, measured in terawatt-hours (TWh) per year.[113]

1.1.2. Primarily Fossil Based

The resources for this increasing energy demand are primarily fossil based, such as coal, natural gas and crude oil as can be seen in figure 1.1. Figure 1.2 shows the increase in energy consumption per source. A close inspection points out that even nowadays, the depletion of these fossil based resources is increasing at a steady pace. Meanwhile, compared to the growth of the fossil based resources, the growth of renewable energy sources is very slim.

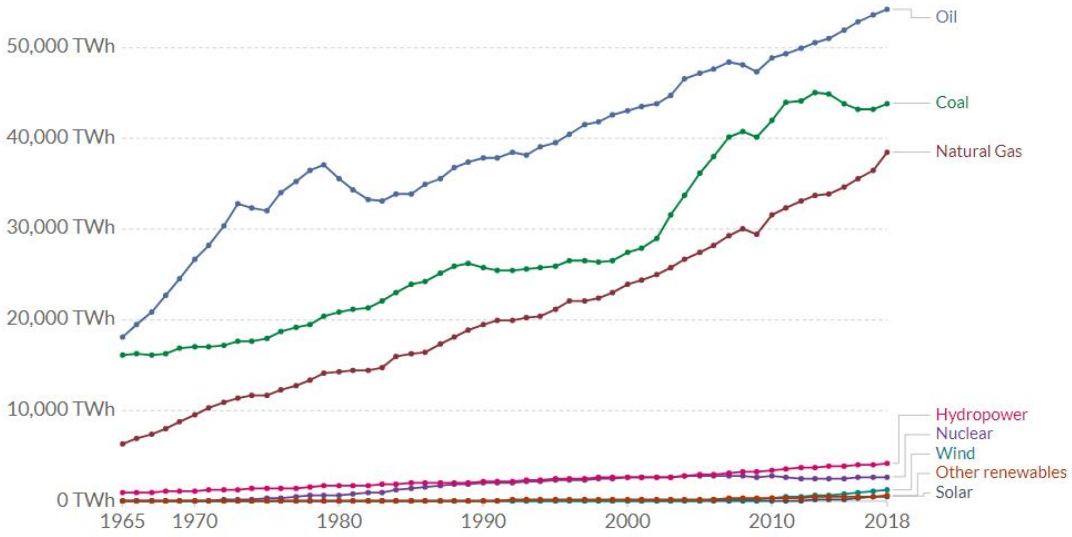

Figure 1.2: Global primary energy consumption by source, measured in terawatt-hours (TWh) per year.[113]

When these fossil resources are burned to produce energy they emit harmful gasses into the atmosphere, increasing the greenhouse gas emissions. Furthermore, since these resources are obtained from Earth, their availability on Earth is limited. So, not only are we polluting the air surrounding our planet, we are also depleting our planet from its fossil resources.

1.1.3. CO_2 Emissions

One of the end products of the combustion of fossil fuels is carbon-dioxide (CO_2), which account for the majority of greenhouse gas emissions. Ever since the industrial revolution the concentration of CO_2 in the atmosphere has increased exponentially as can be seen in figure 1.3. Resulting in a CO_2 concentration in the atmosphere of 417ppm [28] in the year of 2020, which is an increase of 25% over the last 70 years. That value is higher than it has been at any point for at least the past 800,000 years [77].

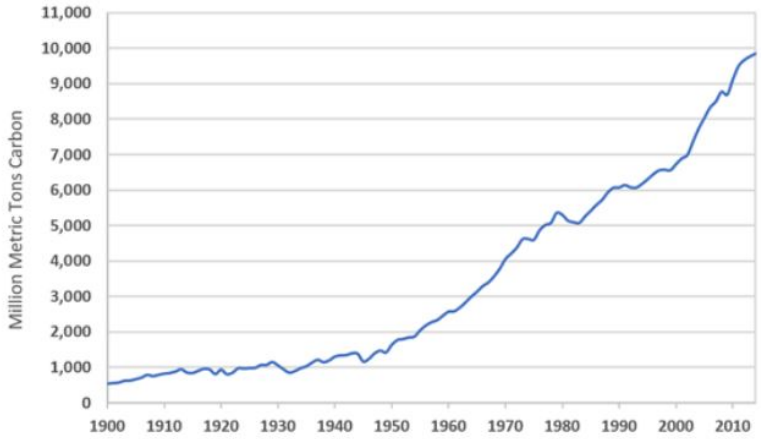

Figure 1.3: Global carbon emissions from fossil fuels, 1900-2014 [14]

1.1.4. Consequences

The ever growing amount of CO_2 trap heat inside the atmosphere. This heat would have otherwise radiated into space and as a consequence heats up the earth, which changes the global climate for the worse. Since the pre-industrial era (1880-1900) the average surface temperature of the Earth has increased by two degrees [43]. This might seem small, but considering the tremendous heat capacity of the global oceans, this two degree increase equals a massive amount of extra heat being captured within the atmosphere. That extra heat is ramping up regional and seasonal temperatures, resulting in more severe weather conditions, higher sea levels due to the reduction in snow cover and sea ice, air pollution, acidic oceans and shrinking wildlife numbers around the world. Furthermore, with the exponential growth of the world's population, the global energy demand will only increase in the coming decades, resulting in an increase in consumption of fossil fuels, even higher CO_2 emissions, and therefore accelerated global warming. Not to mention the inevitable scenario where the world's fossil resources are totally depleted and the world as we now know would seize to exist.

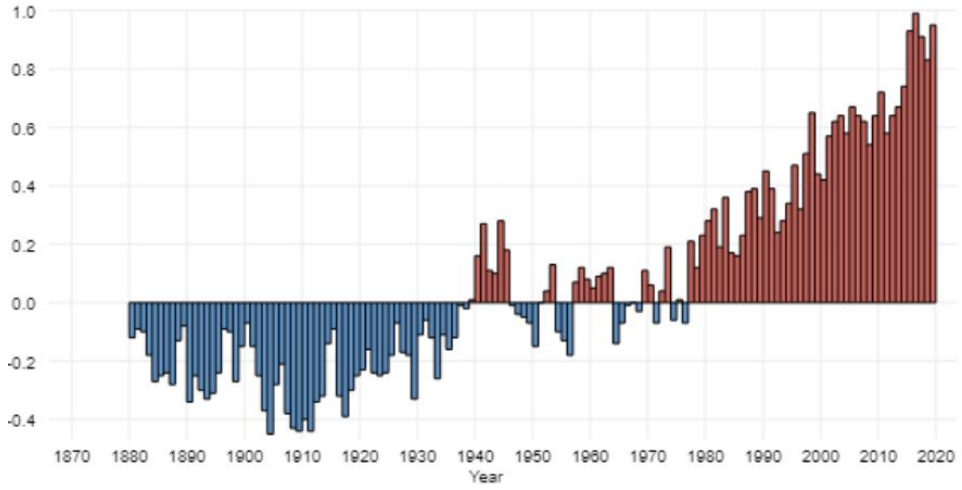

Figure 1.4: Global average surface temperature anomaly compared tot 1901-2000 in °C [43]

Fortunately, global awareness is increasing and the willingness to make a change increases with it. This is brought to light by events like the Paris Agreement of 2015, which is signed by 189 countries worldwide. The Paris Agreement aims to restrict the temperature increase of the earth to 1.5°C by reducing the emission of greenhouse gasses. For mankind to reach this goal it is now high time to work on mitigation techniques and implement them on a large scale. Techniques that will stagnate or reduce the CO_2 concentration in the atmosphere.

1.2. Mitigation

This section briefly discusses the mitigation techniques which are already implemented and used to reduce CO_2 emissions, whereafter the concept of Direct Air Capture is introduced, the chosen technique for this thesis.

1.2.1. Present Mitigation Techniques

Nowadays, there are a lot of mitigation techniques which are already implemented and used throughout the world. First of which, is the world wide consensus on being as energy efficient as possible. This is done through energy efficiency measures and increased electrification. Yet more importantly, this is achieved by consuming less. As now-a-days almost every product money can buy is processed and therefore, requires a certain amount of energy to produce. By just consuming less as a person would already make a very big difference in global emissions. Another mitigation technique which is already implemented is large scale carbon capture from point sources. According to a particular process where CO_2 capture can be implemented, there are three main approaches; pre-combustion capture, capture during combustion or post-combustion capture [39]. After the CO_2 is captured there are two options; first of which is Carbon Capture and Sequestration or CCS. This technique aims at the

large scale capturing of CO_2 from point sources, followed by concentration, pressurization and storage in a (semi)permanent state, which is generally in geological formations, such as empty oilfields[127]. The second option is Carbon Capture and Utilization or CCU, where the CO_2 captured from large point sources is utilized for the production of higher value products, such as concrete, plastics or bio fuel. These point sources are largely coal-fired power plants, which account for roughly one-third of the total global CO_2 emissions. Unfortunately, CCS and CCU can only slow down the rate of increase of CO_2 concentration in the atmosphere, as it only utilizes the CO_2 coming from large, stationary point sources. Where approximately half of the total annual global CO_2 emissions come from distributed sources, such as the transportation sector, this sector is therefore still polluting the atmosphere. Consequently, only capturing CO_2 from large point sources is not sufficient if we want to reach the goals set by the Paris agreement. As a matter of fact, the latest report from the Intergovernmental Panel on Climate Change (IPCC) from Working Group III even indicates that modern day society has reached a point where only mitigating the current CO_2 emissions is not sufficient, but negative CO_2 emissions are needed to stabilize the atmosphere at twice the preindustrial level as can be seen in figure 1.5. Consequently, more carbon capture techniques will have to be developed and implemented, which leads us to the main subject of this thesis; Direct Air Capture.

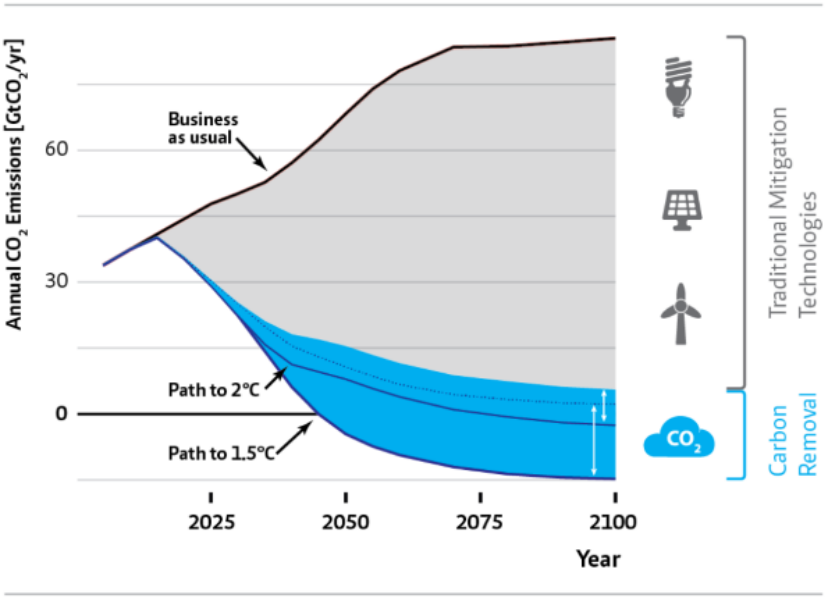

Figure 1.5: Annual CO_2 emission prediction in order to stay within 2°C of global temperature rise. [124]

1.2.2. Introduction to Direct Air Capture

Direct Air Capture (DAC) is a method which aims at capturing CO_2 directly from ambient air, rather than conventional CO_2 capture technologies which capture CO_2 from large point sources. Which is its biggest advantage, since a system utilizing the DAC method can be implemented anywhere in the world and is not restricted to these large point sources such as power plants. Accordingly, the DAC method can compensate for mobile CO_2 emissions as well, which account for between one-third and on-half of society's total CO_2 emissions[67]. The emissions from the transport sector can therefore be addressed using the DAC method, while maintaining the transportation infrastructure of the modern society. However, there has to be a purpose for the captured CO_2 for DAC to become profitable. For instance, the use of CO_2 to synthesize carbon-based fuels. The use of carbon-based fuels can be made to be sustainable, if these carbon-based fuels are to be synthesized from air-captured CO_2, closing the carbon cycle as can be seen in figure 1.6. Another big advantage of this method is that it can be used to actually reduce the concentration of CO_2 in the atmosphere rather than just slowing down the increase in CO_2 concentration. With the increasing amount of CO_2 used as a feed stock for higher value products, the ability of the DAC method to provide this CO_2 anywhere on the planet is in that regard highly advantageous. The DAC method can even compensate for the CO_2 leakage

from geologic storage sites. The concept was first introduced for climate change mitigation by Lackner in 1999 [39], and is since then becoming a rapidly growing environmental technology. An extensive description of the DAC concept along with its working principles is provided in section 2.2. Although there are plenty of advantages which favor the DAC concept, there are still many uncertainties and unknowns that require further research, that is where Zero Emission Fuels comes into play.

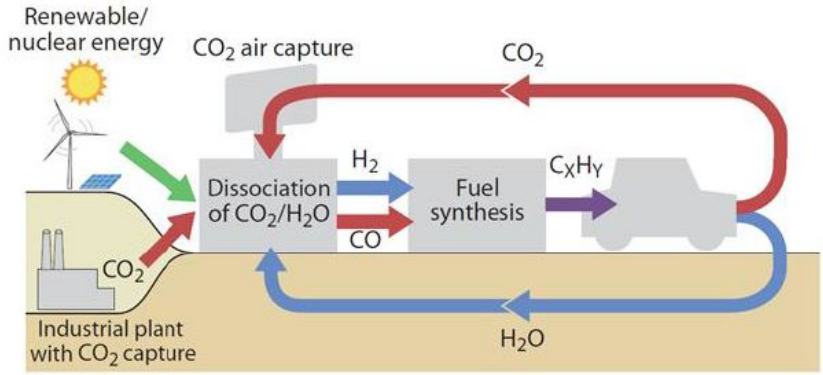

Figure 1.6: Schematic interpretation of the closed carbon cycle.[49]

1.3. Zero Emission Fuels

Zero Emission Fuels B.V. or ZEF aims to develop a plant that produces a fuel with zero emissions. To achieve this goal a fully automated, modular, air to methanol micro-plant, which will be connected directly to a solar panel, is developed. [70] ZEF is a small start-up company, founded by Jan van Kranendonk, Ulrich Starke and Hessel Jongebreur, is located in Delft and is in direct contact with the Technical University of Delft to be on the forefront of technological advancement. The system is highly dynamic since it is relying on the energy of the sun for the production of methanol. Considering this dynamic nature of the system, it is favourable for the system to have a fast start-up procedure, so fast heating and cooling has to be possible. Consequently the choice was made to keep the scale of the plant on the level of a household fridge. This small scale makes fast development possible, since the cost of prototyping is relatively low. Furthermore, after the initial development phase the risks associated with scaling up will be low. Scaling up in numbers means that the plant has to be mass manufactured, which in turn results in lower capital costs. The methanol can be produced with CO_2 as a feedstock. This CO_2 has to be obtained utilizing the DAC concept since the application of the system is therefore not limited to the use on an existing plant, but can be applicable on existing PV (photo-voltaic) fields everywhere in the world. The ZEF concept will aim to mitigate the rising CO_2 concentrations, and use the already emitted CO_2 to produce a fuel which can be used in countless of ways. In order for this project to succeed the methanol has to be produced for a price competing with the ordinary way of producing methanol from natural gas. This presents one of many challenges ZEF is facing, but ZEF would not be ZEF if they were not up for a challenge.

1.3.1. The ZEF Concept

The ZEF concept basically corresponds to a micro plant, which is divided in different subsystems, all of which have their own function and are worked on separately by different student teams. These subsystems are:

- **The Direct Air Capture (DAC) unit**, which captures a mixture of CO_2 and H_2O directly from the atmosphere and separates this mixture into a stream of CO_2 and a stream of water (H_2O).
- **The Alkaline Electrolysis Cell (AEC)**, where the flow of H_2O is separated into hydrogen (H_2) and oxygen (O_2).
- **Fluid Machinery (FM)**, which compresses the CO_2 and H_2 to an operating pressure of 50 bar at which the methanol synthesis reactor operates.

- **The Methanol Synthesis reactor (MS)**, to which the purified CO_2 and H_2 are fed, and where they are converted to a mixture of methanol (CH_3OH) and water (H_2O).
- **The Distillation (DS) column**, where the methanol and water are separated resulting in the end product; pure methanol.
- **The Solar panel (SOL)**, which provides the power to drive the entire micro plant.

The energy needed for operation is provided by just three PV solar panels, of 300 Watts each. Figure 1.7 below shows a schematic flowchart of the ZEF system. Since this thesis concerns the DAC subsystem, the general specifications of the DAC system are now briefly presented whereafter the scope and research objectives of this project are discussed.

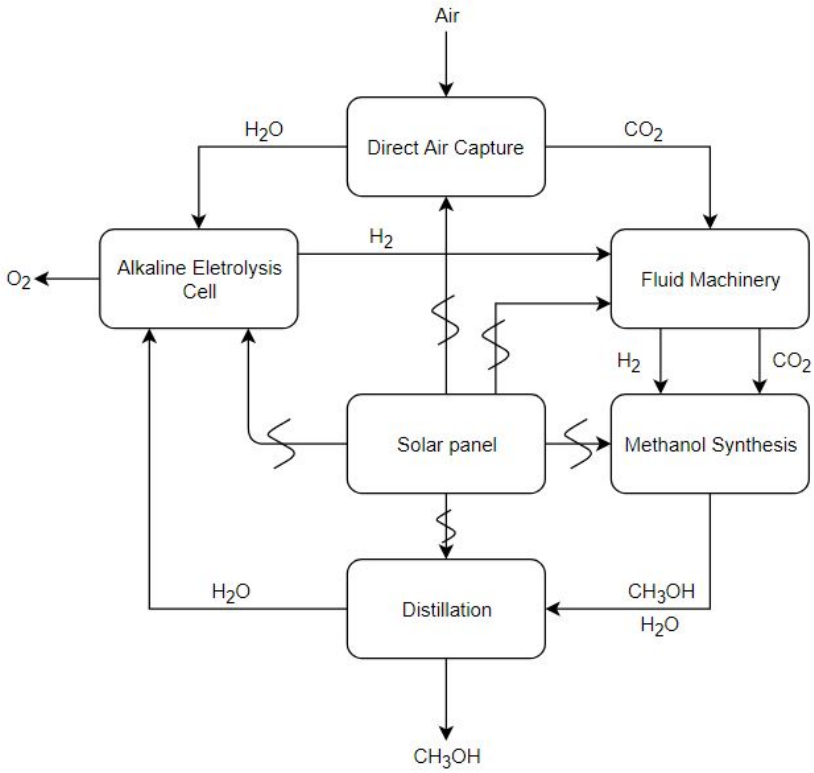

Figure 1.7: A schematic overview of the ZEF system [70]

1.3.2. The ZEF DAC System

For the ZEF system to be commercially attractive the goal is set to produce 600 grams of methanol per day for each micro plant. Considering the plant is powered by the sun, the system can operate for only eight hours per day, assuming the energy of the sun will only be strong enough to power the plant for eight hours per day. Within those eight hours, the DAC system has to capture enough CO_2 and H_2O for the plant to produce the 600 grams of methanol. It can be seen from the equilibrium reaction 1.1 for methanol production from CO_2 that one mole of CO_2 reacts with three moles of H_2 to form one mole of CH_3OH. Therefore, 825 grams of CO_2 has to react in the MS reactor to produce the target of 600 grams of CH_3OH. Hence, the capture target for the DAC system is 825 grams of CO_2 per eight hours.

$$CO_2 + 3H_2 \Leftrightarrow CH_3OH + H_2O \tag{1.1}$$

Although most DAC systems which are already used around the world use a batch process, the ZEF DAC system opts for a continuous process, since it is potentially a lot more energy efficient and mechanically simpler. An extensive overview of the history of the DAC system within ZEF is presented in section 2.4. The CO_2 and H_2O are absorbed from an airflow into a sorbent, which is flowing down a surface in the absorption column. The enriched sorbent flows into the desorption section, where the

sorbent is stripped from the CO_2 and H_2O, whereafter the lean sorbent flows back to the absorption column to be used again. The sorbent which is currently used is an ethyleneamine called Tetraethylene-pentamine (TEPA), although TEPA holds great potential as a carbon capturing sorbent compared to other amines, it does have a few drawbacks that prevent the DAC system from reaching the goal of 825 grams of CO_2 in eight hours. The kinetics of the CO_2 absorption, which can be described as the 'speed' of absorption, are too slow due to a number of reasons. The main reason for this is TEPA becoming really viscous when it absorbs CO_2, resulting in limited CO_2 absorption [112]. Preliminary research has indicated that adding a diluent to the sorbent can potentially improve the kinetics of the sorbent. Furthermore, previous research at ZEF indicates the thermal instability of TEPA [48]. When TEPA is heated for a longer duration of time, it degrades and therefore, looses part of its capability to absorb CO_2 from the atmosphere. These are the main problems concerning the current sorbent at ZEF. That is where the significance of this thesis comes to light.

1.4. Aim of this Thesis

The aim of this thesis is to develop a sorbent selection method and find an optimized sorbent which will help the DAC unit of ZEF reach the goals set by ZEF. The sorbent is the actual mixture of substances that absorbs the CO_2 and H_2O from the atmosphere. This sorbent will differ for every location on earth where a different location on earth will have different ambient conditions in terms of temperature and relative humidity. The 'perfect' sorbent for ZEF has to reach the CO_2 and H_2O capture targets, has to be fluid enough for pumping, has to be able to perform for more than a year, has to be within a specific cost limit, can not harm the environment and all the while has to be operated as energy efficient as possible.

The DAC goals set by ZEF are:

- Produce 825 grams of CO_2 per day.
- Work with a sorbent with a viscosity less than 2 $Pa \cdot s$.
- Produce CO_2 and H_2O at a pressure ratio of 1:3, which is optimal for the methanol synthesis reactor, where 1 mole of CO_2 reacts with 3 moles of H_2.
- The absolute pressure of the product has to be approximately 1 bar in order to be as efficient as possible.
- Keep size of the DAC system sensible, such that the microplant is of realistic size.

In order to achieve this a chronological method for sorbent selection will be developed and tested for ease of sorbent testing in the future of ZEF. Since there is not enough time during this thesis to test all the possible candidates thoroughly, this will provide a clear path for future students in order to find the optimal sorbent for ZEF.

1.5. Research Objectives & Questions

The research objectives of this thesis project can be divided in the following two parts:

Select a sorbent-diluent cocktail based on the key performance indicators to optimize ZEF's DAC process. This objective can be achieved by answering the following research questions:

1. What are the KPI's that influence the direct air capture process at ZEF?
2. How are these KPI's influenced by adding a diluent to the polyamine?
3. What is the effect of climate change on the characteristics of the optimized sorbent?

Design a sorbent system/process taking into account the optimum KPI's

1.6. Thesis Scope

Literature shows that TEPA holds great potential for the ZEF DAC appliance, but improvements can possibly be made be adding a diluent. Therefore, TEPA will remain the absorbing amine. There are a great amount of possible diluents in the world of chemicals. However, due to the time constraints of this thesis project a total of **nine diluents** will be tested according to the developed sorbent selection method and graded on the key performance indicators in phase one of testing, as can be seen in the thesis outline in figure 1.8. These diluents will be carefully selected from literature. Furthermore, since this thesis has to be finished within nine months, the ambient testing conditions for phase one will be limited to the average **conditions of the Sahara desert**, at 30°C and 25% relative humidity. The Sahara conditions where chosen because that is a place on Earth where the ZEF micro-plant could well be stationed due to the intense sun. Furthermore, this location poses a big challenge regarding the viscosity due to its extremely dry conditions as will later become apparent in this thesis. At the end of phase one the optimal sorbent will be selected, tested and optimized in phase two, where it will be tested at **different ambient conditions**. In order to make proven statements on which sorbent would work at other specific locations on Earth. In phase three, the optimized sorbent will be tested on it lifetime performance. After the test phase of this thesis, a full DAC model will be made with the goal to provide quantitative statements of the ZEF DAC unit utilizing the optimized sorbent.

The general outline of this thesis is presented on the next page in figure 1.8.

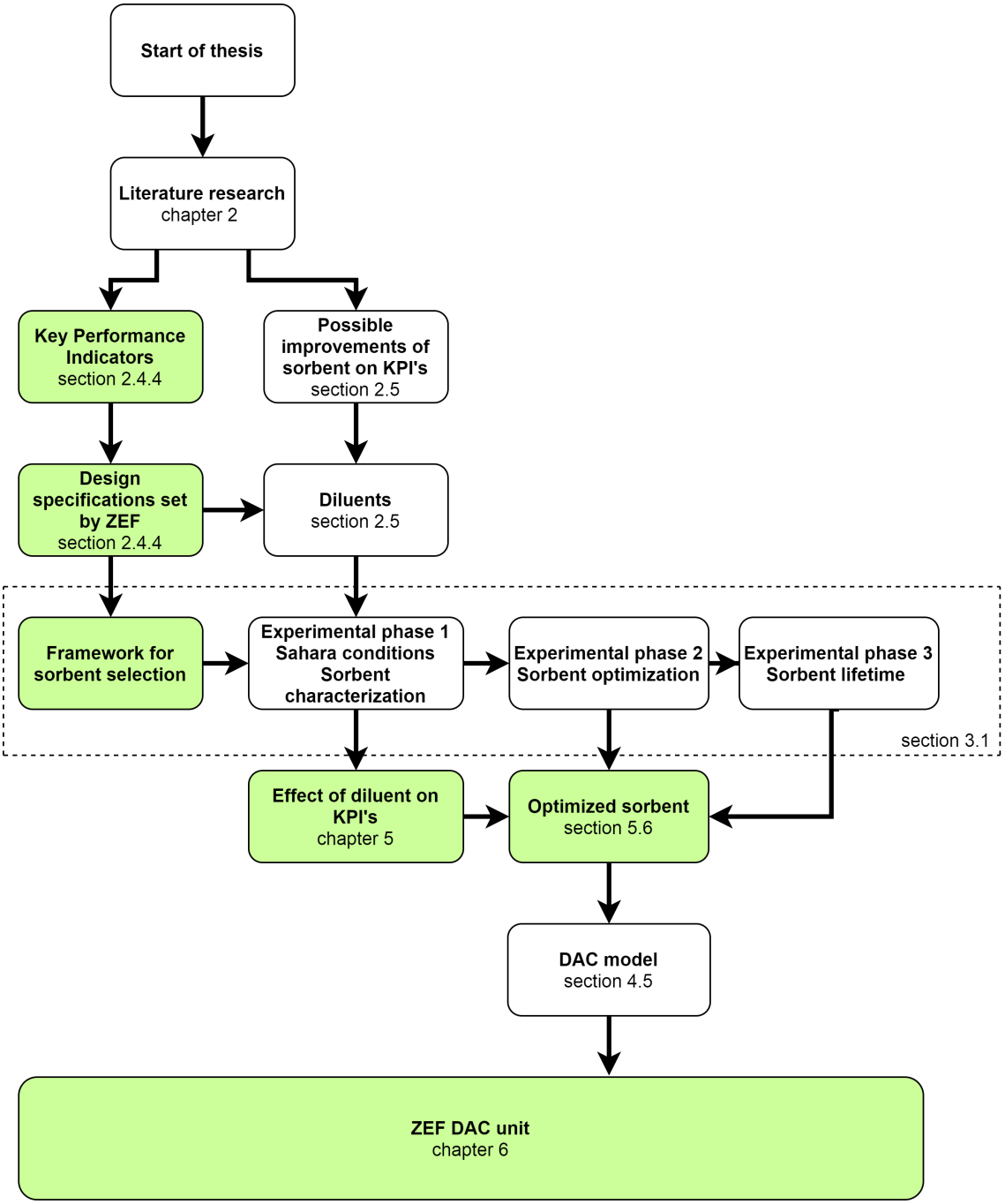

Figure 1.8: The general outline of this thesis

2

Background

In this chapter all the background information which is relevant for this thesis is provided. First a brief overview of CO_2 capture processes along with the relevant CO_2 separation technologies, which are used or developed nowadays around the world, ending with a focus on Direct Air Capture. Secondly, the DAC concept is thoroughly discussed along with an overview of different sorbents which are used in the industry. Thirdly, an elaborate explanation of amine-based carbon capture techniques is set out. Thereafter, the full history of sorbents within the ZEF DAC environment is discussed, from where the new heading of the sorbent selection will be drawn at the end of this chapter.

2.1. Carbon Capture

Ever since the world has reached a world wide consensus on the negative environmental effects of CO_2 emissions from fossil fuel combustion, the concept of carbon capture and storage has drawn extensive attention by researchers around the world. Resulting in numerous processes for capturing CO_2, each of which utilize different technologies. This section provides an overview of the current carbon capture processes and technologies which are already implemented around the world along with its history.

2.1.1. History

Technologies for capturing CO_2 were first put to use as early as the 1920s for separating CO_2 from natural gas for methane gas production [55]. Their aim was not to reduce the carbon emissions but to convert natural gas to methane, since there was a market for methane. The idea of capturing CO_2 and storing it, and therefore preventing it from entering the atmosphere originates back to 1977, although captured CO_2 was already being used since the early 1970s in Texas (USA) for Enhanced Oil Recovery (EOR) by injecting it into an oil field. EOR meant that there was a use for captured CO_2 and would therefore give CO_2 a value in monetary terms. As time progressed the severity of the green house gas effect became more apparent and with that the amount of research in carbon capture grew from which new technologies came to light.

2.1.2. CO_2 Capture Processes

Since CO_2 is not only emitted from large point sources but also from smaller sources which are spread out all over the world, like the transportation sector, CO_2 can and has to be captured in different processes. Therefore, a brief overview of the most prominent current CO_2 capture processes is provided in the sector.

Pre-Combustion

Capturing CO_2 at combustion processes before combustion of a fossil fuel is called pre-combustion carbon capture. This process usually involves a reaction between the carbon rich fuel and oxygen or air which is called partial oxidation like equation 2.1, or a reaction between the carbon rich fuel and steam which is called steam reforming like equation 2.2. Both these reactions produce a gas mixture called 'synthesis gas or syngas', which is mainly composed of carbon monoxide and hydrogen [31]. Whereafter CO_2 and more hydrogen are produced from a reaction between the carbon monoxide and

steam in a catalytic reactor called a water-gas shift converter as in equation 2.3. Lastly the CO_2 is separated from the hydrogen, resulting in a hydrogen-rich fuel which can be utilised in numerous applications, such as fuel cells, gas turbines and engines. This separation is usually done by a pressure swing absorption method or a cryogenic distillation method at low temperatures [110]. However, separation at high temperatures is preferable from an energy consumption and cost associated point of view since the reaction temperature of reaction 2.3 is around 200-400°C, thus using a membrane separation method would be the best option. These three methods will be explained briefly in section 2.1.3.

$$\text{Partial oxidation: } C_xH_y + \frac{x}{2}O_2 \Leftrightarrow xCO + \frac{y}{2}H_2 \quad \Delta H_{CH_4} = -36\ kJ/mol \tag{2.1}$$

$$\text{Steam reforming: } C_xH_y + xH_2O \Leftrightarrow xCO + (x + \frac{y}{2})H_2 \quad \Delta H_{CH_4} = 206\ kJ/mol \tag{2.2}$$

$$\text{Water-gas shift: } CO + H_2O \Leftrightarrow CO_2 + H_2 \quad \Delta H = -41\ kJ/mol \tag{2.3}$$

Post-Combustion
Post-combustion carbon capture technologies have become a world wide research topic, since power plants burning fossil fuels, especially coals, account for a very big part of the global CO_2 emissions. Currently, post-combustion CO_2 separation is mostly done via a scrubbing or a chemical absorption process. The flue gas emitted from a power station has a low concentration of CO_2 of around 4-14%, which means that a large volume of gas has to be processed making it rather energy intensive. Therefore, chemical absorption processes are likely to be replaced by membrane based separation processes, for they are less energy demanding. However membrane separation processes for CO_2 separation is still a relatively new technology so more research in that area is needed.

Oxy-fuel Combustion
Oxy-fuel combustion is a process where the fossil fuel is combusted with pure oxygen rather than with air, resulting in an increase of the CO_2 concentration in the flue gas up to 80%, which in turn makes it easier to separate the CO_2 from the flue gas. However, oxygen production from cryogenic air separation is very costly and energy intensive. New technology development for oxygen production could possible lower the energy and costs of this process in the future[50].

Biological Capture
Plants and organisms power their activities by converting solar energy into chemical energy via a photosynthesis process. This chemical energy is stored by carbohydrate molecules, like sugar which is synthesised from CO_2 and water. Microorganisms with carbon fixation rates even higher than those of terrestrial plants are microalgae and cyanobacteria (photosynthetic microorganism). Although this biological method holds great promise for not only CO_2 fixation but also for other organic and inorganic contaminants from contaminated air, this concept requires a huge surface of the planet in order to be effective at a large scale. Consequently, this concepts threatens biodiversity, water and food security, when implemented at a large scale. Hence this concept is not further investigated, since it is not within the scope of this thesis.

Direct Air Capture
The process of direct air capture of CO_2, which, as the name suggests, captures CO_2 directly from the air is the main subject of this thesis. This concept is listed here for completion of the list of current CO_2 processes but is extensively described in section 2.2.

2.1.3. CO_2 Separation Technologies
Current CO_2 capture processes make use of various technologies to separate the CO_2 from other substances. In this section a brief overview of the physicochemical technologies used for CO_2 is provided to get an overview of the state of art in CO_2 separation technologies.

Membrane-based Separation
A basic membrane based separation process for a post-combustion process is illustrated in figure 2.1. The flue gas is separated by a membrane, where part of the CO_2 permeate through the membrane to a stream with a higher CO_2 concentration, which is called the permeate stream. The stream leaving the membrane module with the lowered CO_2 concentration is called the retentate stream. In

post-combustion processes the flue gas is often cooled down in a wet scrubber before entering the membrane model to cool the flue gas down to the operational temperature of the membrane. A compressor before the membrane and vacuum pump after the membrane is used to increase the partial pressure difference of CO_2 across the membrane, which is essential as the partial pressure of CO_2 in the flue gas is very small. The compressor and the vacuum pump account for the majority of the energy consumption of this process. The material of the membrane plays a big role in separating the CO_2 from the flue gas. There are generally three types of membrane material: ceramic (inorganic), polymeric (organic) or a hybrid of these two, which utilizes the advantages of both materials. These materials each have their advantages at the two main properties for membrane materials: permeability and selectivity. The configuration of the membrane module plays another big role in separation performance. However, the selectivity of a membrane-based separation process is low, and therefore, only a small part of the CO_2 is captured. Additionally, for the same reason the purity of the captured CO_2 is low, so multistage separation is essential for capturing more CO_2 which in turn results in extra capital and operating costs.

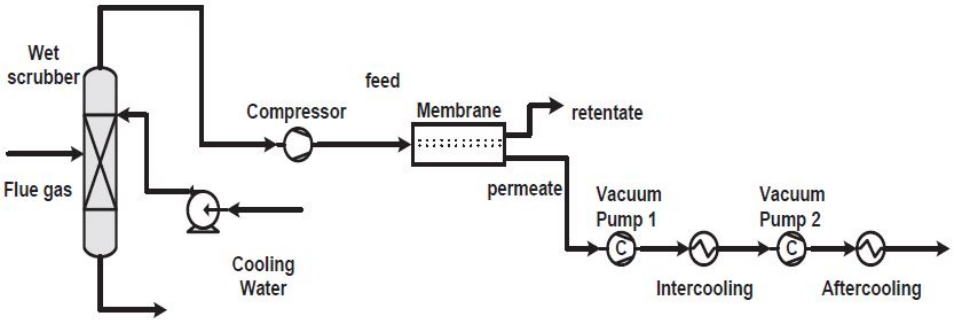

Figure 2.1: A schematic overview of a basic membrane based separation process for post-combustion CO_2 capture [128]

Cryogenic Separation

Cryogenic separation technology works by cooling down and/or pressurizing the feed gas until one of the substances in the feed gas condenses to a liquid, which makes it a lot easier to separate. CO_2 condenses at -56,6°C at atmospheric pressure [80]. This separation technique is typically used for CO_2 capture from an oxy-fuel combustion process, but cryogenic separation is often not considered as a realistic CO_2 capture technology for a post-combustion process as the expected cooling costs would be too high. Usually, the required cold duty for cryogenic CO_2 separation is obtained by integration with processes of LNG (liquid natural gas) regasification or/and cryogenic air separation, but significant energy savings can be made by integration with a cryogenic nitrogen removal process for natural gas cleaning [69]. No further research in this area is done since it is not within the scope of this thesis.

Adsorption

The physical process which involves the attachment of a gas or liquid to a solid surface is called adsorption. The CO_2 and the adsorbent are then separated by the reduction of pressure, called pressure swing adsorption (PSA) or by the application of heat, called temperature swing adsorption (TSA). Activated carbon, alumina, zeolites and metallic oxides are adsorbents which could be applied, but due to their low adsorption capacity, current adsorption systems are not seen as suitable for application in large-scale power plant flue gas treatment[80]. Furthermore, due to the generally low selectivity of most available adsorbents, the feed stream for separation via an adsorption process must have a high CO_2 concentration for the process to be effective. This makes it a less attractive process for direct air capture, since the concentration of CO_2 in air is only around 400 ppm.

Physical Absorption

The absorption process is based on Henry's law when the CO_2 is physically absorbed into a solvent. Henry's law states that the amount of dissolved gas in a liquid is proportional to its partial pressure above that liquid as is explained in section 2.3. The solvent and CO_2 can be separated by pressure reduction, heat application or both, whereafter the regenerated solvent can be recycled. Selexol (dimethyl

ethers of polyethylene glycol) and Rectisol (methanol) are typical solvents for a physical absorption process [80]. Physical absorption of CO_2 happens at high partial pressures of CO_2, and therefore, for this technology to work, the feed stream must be highly pressurized. Consequently, making the gas pressurization the main energy requirement. It is for this reason that physical absorption is not seen as an economically viable option for feed gas streams with CO_2 partial pressure lower than 15%, and as such, not an viable technology for direct air capture.

Membrane Absorption

With membrane absorption the membrane is used as a contacting device between the liquid solvent and the gas stream. As apposed to membrane-based separation, where selectivity is provided by the membrane itself, with membrane absorption the membrane itself does not necessarily have to provide additional selectivity. The membrane simply provides a large contact area between the solvent and the gas. Conventionally, packed beds are used as contacting devices in absorption processes, but they tend to be less compact and are susceptible to entrainment, channeling, foaming or flooding as opposed to membrane absorption modules. Just like a physical absorption process, the separation efficiency depends on the CO_2 partial pressure, thus membrane absorption processes are suitable for feed stream CO_2-concentrations above 20% [80], such as flue gas streams from oxy-fuel combustion processes.

Chemical Absorption

Chemical absorption of CO_2 into a sorbent is one of the leading techniques which is used throughout the world. The CO_2 is absorbed either into a liquid sorbent which is usually an amine, or a solid sorbent. The CO_2 chemically bonds with the sorbent in the absorber and is then separated in the stripper section, as the chemical bonds are released when energy in the form of heat is provided, producing the original solvent and a CO_2 stream. A schematic overview of a basic chemical absorption process is given in figure 2.2. The selectivity of this technique is high compared to the other separation techniques, and therefore, a relatively pure stream of CO_2 can be produced. This technique can be implemented for post-combustion carbon capture appliances, but also for direct air capture appliances. A more in dept explanation of this technique is provided in section 2.2

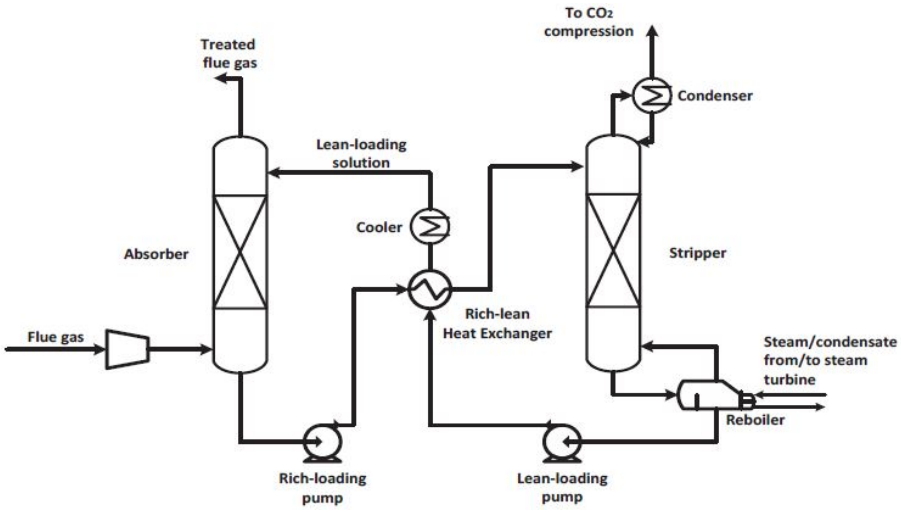

Figure 2.2: A schematic overview of a basic chemical absorption process for post-combustion CO_2 capture [128]

Hybrid Operation

Most modern CO_2 capture processes utilize not just one single separation technology but multiple at the same time. This is called hybrid technology, which aim is to exploit the advantages of more than one technology for a more economical, less energy demanding and therefore cleaner system. As is the case for the concept of direct air capture, which is reviewed accordingly in the next section.

2.2. Direct Air Capture

The ZEF micro-plant has to be able to operate anywhere on the planet and therefore, has to be able to capture CO_2 from the atmosphere anywhere on the planet. Hence direct air capture is the method utilized by ZEF to capture the required CO_2 for methanol production. Capturing CO_2 from ambient air was first used in cryogenic air separation plants in the 1930s and about 30 years later in life support systems of manned closed environments such as submarines and space stations [81]. The earlier life support systems date back to 1965 and where not able to regenerate the sorbent. Nowadays, all modern space shuttles are equipped with a Carbon Dioxide Removal Assembly (CDRA) which regenerates its sorbent. This system helps to maintain a habitable environment for the crew. In the 1960s, mobile nuclear power plants were considered for the production of hydrocarbon fuels from air captured CO_2 [33]. Direct air capture of CO_2 is increasingly discussed as a climate change mitigation option. Consequently, more and more research is done on this topic.

Most of the DAC systems used nowadays utilize either an adsorption or a chemical, a physical and/or a membrane absorption technology to separate the CO_2 from ambient air. A basic DAC model consists a contacting area, a sorbent and a regeneration stage as can be seen in figure 2.3. The contacting area facilitates the contact between the ambient air and the sorbent by inducing an airflow over the sorbent. Due to the very dilute concentration of CO_2 in the atmosphere, only 0.04%, chemical sorbents with strong binding qualities are mostly utilized in modern day systems. Furthermore, these sorbents are preferably of low cost while combining optimum uptake, kinetics, energetics, physical/chemical stability and have a high selectivity towards CO_2 compared to other present gasses in ambient air at atmospheric conditions. These chemical sorbents can either be liquid or solid, both requiring different systems to extract the CO_2 from ambient air which will be explained in the following sections.

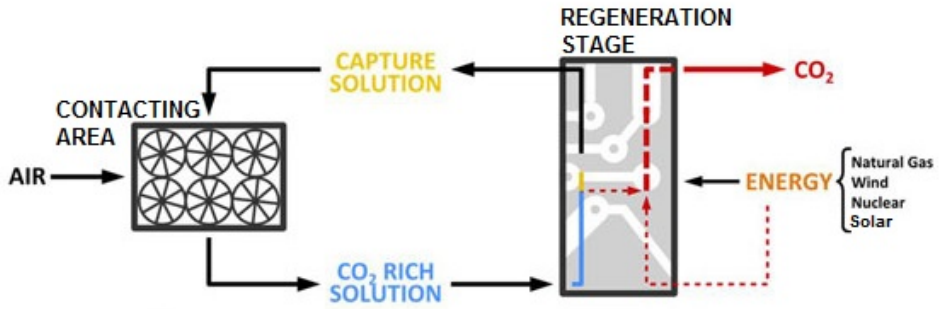

Figure 2.3: A schematic overview of a basic DAC system [40]

Solid Sorbent Systems

This technology usually requires a single unit containing the solid sorbent, where the CO_2 is captured via Temperature-Vacuum-Swing (TVS) cycling. The capturing of CO_2 via adsorption and regeneration of the sorbent via desorption happen consecutively. This process is schematically illustrated on the next page in figure 2.4, where in chronological order the following happens. The system is open and ambient air flows through the unit, either naturally or forced by a fan. The CO_2 chemically binds to the filter at ambient conditions and consequently, CO_2-poor air flows from filter until the sorbent is fully saturated with CO_2. At that point the unit is closed of from the surroundings and the remaining air is optionally removed via vacuuming or purging the system with steam. Hereafter, the system is heated to regenerate the sorbent, as the chemical bonds between the CO_2 and the sorbent are released when they are subjected to heat. The regeneration temperature is typically between 80°C and 150°C depending on the specific sorbent specifications. These regeneration temperatures are generally low compared to systems utilizing a liquid solvent. The CO_2 is released and exits through the product stream. For the system to start another cycle it has to be cooled back down to ambient conditions.

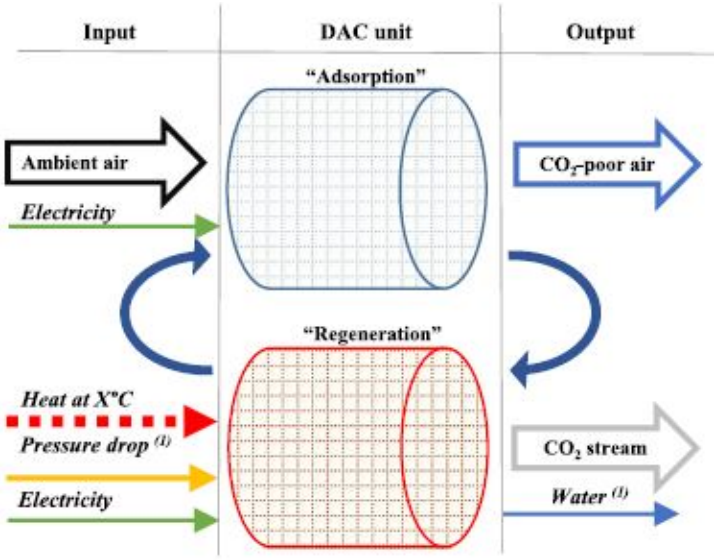

Figure 2.4: A schematic overview of a basic solid sorbent DAC system [81]

The systems conditions are sorbent specific and are listed in table 2.1. A solid organo-amine based chemisorbent, where the functional groups of the amine are either physically or chemically bonded to a membrane of cellulose, is typically employed by modern DAC systems [51]. **Climeworks** utilizes such an amine based filter supported on a special cellulose fiber, which not only capture CO_2 but also moisture, and therefore provides sufficient water for its own use [27]. A full cycle of this specific system takes around four to six hours.
The full cycle time can be a lot shorter as **Global Thermostat** has proven. By using an amino-polymer adsorbent, they have shortened the full cycle time to less than 30 minutes, with a regeneration time less than 100 seconds. They have achieved this by using saturated steam at sub-atmospheric pressure not only as a direct heat transferring fluid, but also as a sweeping gas [96].
A system using a silica sorbent (TRI-PE-MCM-41) was proposed by **Kulkarni and Sholl**, which utilizes a temperature swing system with steam at 110°C for the desorption of 88% CO_2 and 12% N_2 together with water as its products [71]. A similar system has been studied by **Sinha et al.**, where they analysed two different amino-modified Metal Organic Frameworks (MOF), namely: MIL-101(Cr)-PEI-800 and mmen-Mg_2 (dobpdc). Vacuuming the system before heating is necessary since the MOFs are likely to oxidate at high temperatures. The mmen-Mg_2 was concluded to be the best performer of these two MOFs, as it had the lower energy demand of the two.
A composite sorbent based on potassium carbonate (K_2CO_3) is utilised by the system of **Antecy**. A slightly lower regeneration temperature (80-100°C) compared to Climeworks is achieved by evacuating the air with water before regeneration. A system based on a K_2CO_3/Y_2O_3 sorbent was introduced by **Derevschikov et al.**, which utilizes wind energy as a clean power supply and regenerates at temperatures of 150-250°C. However, it is a very delicate system since the sorbent can be easily destroyed as it is sensitive to high temperatures.
The major technical specifications of the predominant solid sorbents found in literature are summarised in table 2.1. Where it can be seen that the amino-polymer used by Global Thermostat requires the least amount of energy per ton of CO_2 production.

Table 2.1: Solid sorbent DAC specifications

Sorbent	**CO_2 con.**	**adsorption**	**desorption**		**energy demand**			**cooling**		**CO_2 purity**	**reference**
	ppm	T [°C]	T[°C]	P [bar]	[kWhel/t]	[kWhth/t]	by	T [°C]	by	%	
amine-based	400	ambient	100	0.2	200-300	1500-2000	waste heat	15	air/water	99.9	[27]
amino-polymer	400	ambient	85-95	0.5-0.9	150-260	1170-1410	steam	ambient	water evaporation	>98.5	[96]
TRI-PE-MCM-41	400	ambient	110	1.4	218	1656	steam	-	-	88	[71]
MOF(Cr)	400	ambient	135-480	1	1420	-	HT steam	-	-	-	[111]
MOF(MG)	400	ambient	135-480	1	997	-	HT steam	-	-	-	
K_2CO_3/Y_2O_3	400	ambient	150-250	-	-	-	el. heater	-	-	-	[35]
K_2CO_3	-	ambient	80-100	-	694	2083	waste heat	ambient	airflow	-	[6]

Liquid Sorbent Systems

Liquid sorbent systems can be divided into two groups based on their sorbent: high temperature aqueous solution and low temperature amine adsorption. In contrary to solid sorbent systems, the systems utilizing a liquid sorbent can absorb and desorb simultaneously. A schematic overview of a system based on an aqueous solution of sodium hydroxide (NaOH) is presented in figure 2.5. The blue cycle represents the absorption cycle, where in the air contactor ambient air is brought into contact with sprayed NaOH, either by natural airflow or with fan power. The CO_2 reacts chemically at ambient conditions with NaOH to form a solution of sodium carbonate (Na_2CO_3) (Eq. 2.4). The beige cycle represents the regeneration cycle. In the causticicer solid calcium carbonate ($CaCO_3$) is formed from a reaction between Na_2CO_3 and calcium hydroxide ($Ca(OH)_2$) (Eq. 2.5). From the causticiser the NaOH is send back to the air contactor to conclude the absorption cycle and the formed $CaCO_3$ is transported to the calciner. This is where the $CaCO_3$ is heated up to 900°C in order to release the CO_2 (Eq 2.6). This step is the most energy intensive of this process with an overall heat demand of 1420-2250 kWh_{th} per ton of CO_2 according to literature. From there the calcium oxide (CaO) is mixed with water in the slaker to regenerate the $Ca(OH)_2$ (Eq 2.7).

$$\text{Contactor: } 2NaOH + CO_2 \Leftrightarrow Na_2CO_3 \tag{2.4}$$

$$\text{Causticiser: } Na_2CO_3 + Ca(OH)_2 \Leftrightarrow 2NaOH + CaCO_3 \tag{2.5}$$

$$\text{Calciner: } CaCO_3 + \textit{heat} \Leftrightarrow CaO + CO_2 \tag{2.6}$$

$$\text{Slaker: } CaO + H_2O \Leftrightarrow Ca(OH)_2 \tag{2.7}$$

The heat needed for regeneration for this system is mainly supplied by natural gas and is consequently, not a sustainable solution. Capturing one tonne of atmospheric CO_2 would release 0.44 tonnes of CO_2 from the burning of natural gas when 2000 kWh_{th} of heat would be delivered by oxy-fuel combustion of natural gas with an efficiency of 90%, without taking into account the life cycle emissions. Despite the fact that this released CO_2 can be captured again and utilized as feed stock for other purposes, it will eventually end up in the atmosphere after some cycles of utilization and as such, pollute the atmosphere as this process is still fossil fueled. Furthermore, besides heat, electrical power is also needed to drive the fans, to spray the aqueous solution and for transportation between units. According to literature, this electrical power is between 366-764 kWh_{el} per ton of CO_2 [81]. For this system to be sustainable the heating part should be fully electrified, which has been recently discussed in literature. Carbon Engineering released content on their website claiming a total energy demand of 1500 kWh_{el} per captured ton of CO_2 at 150 bar [40]. Due to the very high energy demand for regeneration of this type of sorbent more research has been done in the other group of liquid sorbent systems: aqueous amine adsorption. The chemical absorption of CO_2 in liquid amines for capturing CO_2 from post-combustion processes is already a very mature and promising technology, yet for the direct air capture of CO_2 from the atmosphere it still relatively new. This technology is thoroughly explained in section 2.3.

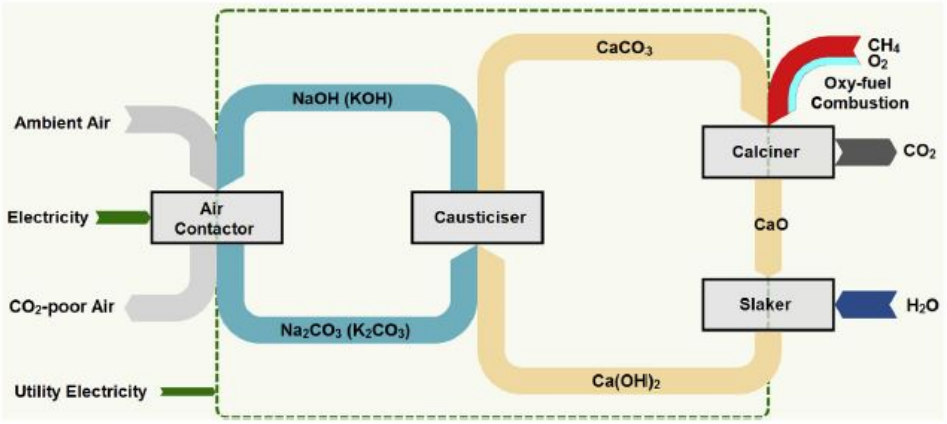

Figure 2.5: A schematic overview of a basic liquid sorbent DAC system based on an aqueous solution of sodium hydroxide (NaOH) [81]

Other Technologies

The three approaches for CO_2 capture described above are the dominant approaches for chemical absorption described in literature. CO_2 can also be captured through a physical absorption process, where the physical solvent can be stripped of the CO_2 by reducing the pressure without the application of heat. Physical absorption is the favoured approach when the partial pressure of CO_2 in the feed stream is high, as can be the case in flue gas streams [19]. Further research revealed more approaches, which are suggested in literature but are less mature. Electrochemical CO_2 capture at ambient temperature via a modified fuel cell was suggested by Eisaman et al. [38].

Lackner et al. [72] propose a system utilizing thin ion-exchanging resin sheets which can capture CO_2 at ambient conditions and can be regenerated using Moisture Swing Absorption (MSA). Lackner et al. claim an energy demand of only 326 kWh_{el}/ton_{CO2}, as the system utilizes the heat released from compression.

A complex DAC system has been proposed by Goldberg et al. [47], which cools down its captured CO_2 until it precipitates as dry ice and turns into a pressurized liquid after warming it back up. A mere 631 kWh_{el}/ton_{CO2} of wind energy is claimed to be needed for this system to operate.

A conceptual design of nanofactory based molecular filters which, when powered by solar energy, capture CO_2 from ambient air was proposed by Freitas et al. [62]. The system delivers pure CO_2 with an energy demand of only 333 kWh_{el}/ton_{CO2}. Resulting in an alleged production cost of only 14 €/ton_{CO2}. It can be a revolution for DAC technologies if this approach would make it to a commercial scale.

2.3. Amines

Amino alcohols have been industrially produced since the 1930s, but large-scale production really started after 1945, when the chlorohydrin route of production was replaced by a faster route; the alkoxylation with ethylene oxide and propylene oxide [78]. Amino alcohols are usually referred to as alkanolamines in industry, where ethanolamines and propanolamines are by far the most used compounds. An amine is essentially an organic compound or a functional group that contains a nitrogen atom alongside a lone pair of electrons. A lone pair of electrons is a pair of valence electrons that are not shared with another atom in a covalent bond. An organic compound is basically any chemical compound which contains carbon-hydrogen bonds. Typically, amines are derivatives of ammonia and can be classified into three subcategories based on the number of organic substitutes, such as an alkyl or aryl group, attached to the nitrogen atom as can be seen in figure 2.6, where R denotes an organic substituent and the dots denote the lone pair of electrons.

- Primary amines are connected to one organic substituent and two hydrogen atoms.
- Secondary amines are connected to two organic substitutes and one hydrogen atom.
- Tertiary amines are connected to three organic substitutes.

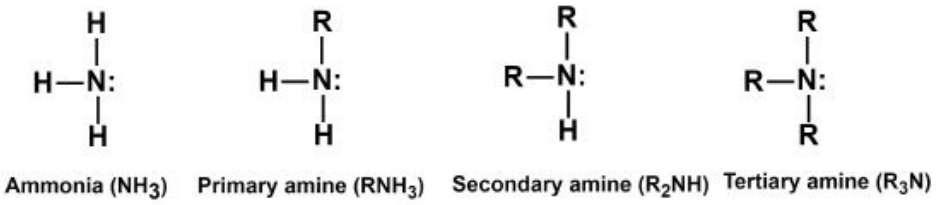

Figure 2.6: General structure of Ammonia, primary, secondary and tertiary amines [78]

Then there is a fourth subcategory which are sterically hindered amines. An amine is called sterically hindered when the adjacent group is blocking the way to the nitrogen atom and therefore, preventing reactions from occurring. This can happen when repulsive forces between overlapping electron clouds result in the *'blockage'* of the nitrogen atom, as is the case when primary amines are attached to a tertiary carbon atom and when secondary amines are attached to a secondary or tertiary carbon atom [116].

2.3.1. Amine Solvents for CO_2 Capture

The utilization of amines for CO_2 capture is getting more frequent these days. These amines can either be in a solid state bonded to a membrane or in a liquid state as a liquid sorbent. All ethanolamines absorb CO_2 and H_2O from air at ambient conditions, which is their main advantage for DAC appliances. In this section more insight in the physics and chemistry of absorption in amines is provided.

Physics of Absorption

How much of one material can be maximally dissolved in another material is called **solubility** [45]. When a material is dissolved in another material, it does not undergo any chemical change, only the environment around the dissolved material changes. Diffusion of one material in another is driven by the desire to move towards maximum disorder, thus towards the lowest entropy. The state of lowest entropy is reached when a soluble gas is distributed evenly between the gas and liquid phases to a point of equilibrium. Hence CO_2 will diffuse into the absorbent when the absorbent in which CO_2 is soluble comes into contact with CO_2 in the gas phase. The concentration gradient of CO_2 between the liquid and the gas phase is the **driving force** for the absorption of CO_2. The relationship between the partial pressure of a gas and the solubility of that gas into a solvent is constant at a fixed temperature. This constant is called the Henry constant.

Henry's law states (2.8) that the amount of gas that dissolves into a specific type and volume of liquid is directly proportional to the partial pressure of the gas in equilibrium with that liquid at a constant temperature [107]. Hence, according to Henry's law, the solubility of a gas in a liquid is directly proportional to the partial pressure of the gas above the liquid. The equation for Henry's law is the following.

$$H_{gas} = \frac{p_{gas}}{c_{gas}} \tag{2.8}$$

where

H_{gas} = Henry's constant [$L * bar/mol$]
p_{gas} = partial pressure of gas [bar]
c_{gas} = solubility of gas in a specific solvent at a fixed temperature [mol/L]

The **diffusion rate** at which the gas molecules diffuse through the gas and liquid phase determines the time to reach equilibrium. In the gas phase, molecules have more kinetic energy and are able to move with less resistance compared to the liquid phase, hence diffusion in the gas phase is generally faster than in the liquid phase and therefore, the time it takes to reach equilibrium generally depends on the diffusion rate inside the liquid [45]. The diffusion rate strongly depends on the molecular volume of the diffusing molecule and the viscosity of the liquid, as can be explained by the following laws for diffusion.

The diffusion rate can be calculated using **Fick's first law of diffusion** (2.9). In 1855, Adolf Flick, aged only 26 years old, reported this law governing the transport of mass through diffusive means [59]. Fick's first law provides a relation between the diffusion flux, which equals the diffusion rate per unit area, to the gradient in concentration. Fick's law is analogues to other physical relationships like Darcy's law (hydraulic flow), Ohm's law (charge transport) and Fourier's law (heat transport) which were discovered in that same era. The most common form of Fick's first law is stated below.

$$J = -D\frac{dc_A}{dz} \tag{2.9}$$

where

J = diffusion flux [$mol/m^2 s$]
D = diffusion coefficient or diffusivity [m^2/s]
$\frac{dc_A}{dz}$ = molar concentration gradient [$mol/m^3 m$]

Where the diffusion coefficient for a specific fluid can be calculated using the **Stokes-Einstein equation** (2.10). This equation gives a relation between the diffusion of spherical particles through a fluid and the viscosity of that fluid.

$$D = \frac{k_B T}{6\pi\mu r} \tag{2.10}$$

where

D = diffusion coefficient or diffusivity $[m^2/s]$
k_B = Boltzmann Constant $[m^2 kg/s^2]$
T = temperature of the fluid $[K]$
μ = dynamic viscosity of the fluid $[kg/ms = Pa \cdot s]$
r = radius of the spherical particle $[m]$

The most common correlation used in gas separation applications is the **Wilke and Chang** correlation (2.11)[126], which is an extension of the Stokes-Einstein equation. The Wilke-Chang correlation has been found empirically for higher concentrated solutions and is stated below.

$$D_{A,L} = 7.4 \times \frac{T \times 10^{-8} (O_L M_L)^{0.5}}{\mu_L V_A^{0.6}} \tag{2.11}$$

where

$D_{A,L}$ = diffusion coefficient or diffusivity of species A in liquid L $[m^2/s]$
T = temperature of the fluid $[K]$
O_L = association factor of absorbent
M_L = molecular weight of absorbent L $[g/mol]$
μ_L = viscosity of the absorbent $[mPa \cdot s]$
V_A = molecular volume of species A $[m^2/mol]$

Since CO_2 reacts chemically with the aqueous amine solution, the actual diffusion coefficient independent of these reactions is very hard to determine. **Cullinane and Rochelle** [30] and **Versteeg et al.** [120] have experimentally determined specific correlations for the diffusion coefficient of CO_2 ($D_{CO_2,amine}$) in aqueous amines. These correlations are based on the N_2O diffusion coefficient ($D_{N_2O,amine}$) in aqueous amines and the analogy that assumes the ratio $\frac{D_{CO_2,amine}}{D_{N_2O,amine}}$ to be constant and equivalent to that in water. This analogy was also used by Browling and Weiland to determine the Henry coefficient and to measure the CO_2 solubility in aqueous amine solutions [17], which were comparable with the results in water.

$$D_{N_2O,amine} = 5.533 \times 10^{-8} \frac{T}{\mu_{amine}^{0.545}} \tag{2.12}$$

$$D_{CO_2,amine} = D_{N_2O,amine} \times \frac{D_{CO_2,water}}{D_{N_2O,water}} \tag{2.13}$$

where

$D_{N_2O,amine}$ = diffusion coefficient or diffusivity of N_2O in aqueous amines $[m^2/s]$
$D_{CO_2,amine}$ = diffusion coefficient or diffusivity of CO_2 in aqueous amines $[m^2/s]$
$D_{CO_2,water}$ = diffusion coefficient or diffusivity of CO_2 in water $[m^2/s]$
$D_{N_2O,water}$ = diffusion coefficient or diffusivity of N_2O in water $[m^2/s]$
T = temperature of the fluid $[K]$
μ_{amine} = viscosity of the amine $[mPa \cdot s]$

So far, the solubility, driving force and diffusion rate have been explained, but when a gas is absorbed by a liquid the mass transfer across the gas-liquid interface also plays a big role in the kinetics of absorption. For a given moment in time the rate of absorption as a function of the mass transfer coefficient of CO_2, k_{CO_2} also referred to by **space-time-yield**, from the gas phase into a falling liquid film is given by equation 2.14. Sinha et al. [112] derived a general equation for the absorption rate of a gas into falling liquid film of height L and width W. With that general equation the analogy to heat transfer was made, together with the help of Newton's law of cooling he came up with equation 2.14 as stated on the next page.

$$\dot{n}_A = k_c A(c_{Ai} - \bar{c}_A) \tag{2.14}$$

where

$\dot{n}_A$ = rate of absorption [mol/s]
k_c = mass transfer coefficient or space-time-yield [$mol/m^2 s$]
A = mass transfer area (normal to the direction of mass transfer) [m^2]
c_{Ai} = concentration of gas A at position i [$wt\%$]
$\bar{c}_A$ = average bulk concentration of gas A in the liquid [$wt\%$]

Chemistry of Absorption

When CO_2 is absorbed by an aqueous amine it is not only physically absorbed by the amine but it also reacts chemically with it. In this section the chemical reactions which occur when CO_2 is absorbed in an aqueous amine are introduced, since it plays a big role in the kinetics of absorption.

Reactions

During the absorption of CO_2 there are a lot of reactions happening at once. These reactions occur instantaneous or take place over a measurable time. The reactions for primary/secondary amines differ from the reactions happening with tertiary amines.

Primary (RNH_2) **and Secondary Amines** (R_2NH)

Monoethanolamine (MEA), a primary amine, and diethanolamine (DEA), a secondary amine, are the most used primary and secondary alkanolamines in the industry. Aqueous MEA is seen as the benchmark solvent due to its low price and long-time use in the industry. Primary and secondary amines form stable carbamates when absorbing CO_2 and are therefore highly reactive. During the first reaction (2.15 and 2.18) a zwitterion, an ion with both a positive and negative charge, is formed. The zwitterion is then deprotonated to form a stable carbamate as can be seen in reactions 2.16 and 2.19 [88]. The formed carbamate can be hydrolysed at elevated pressure to form bicarbonates and a free amine (2.17 and 2.20). The latter will then react with CO_2 again. As can be observed in the reactions below, the maximum possible CO_2 loading is 0.5 mole of CO_2 per mole of amine as only one CO_2 molecule reacts with two amine molecules.

Primary amines:

$$CO_2 + RNH_2 \Leftrightarrow RNH_2^+COO^- \tag{2.15}$$
$$RNH_2 + RNH_2^+COO^- \Leftrightarrow RNH_2^+ + RNHCOO^- \tag{2.16}$$
$$RNHCOO^- + H_2O \Leftrightarrow RNH_2 + HCO_3^- \tag{2.17}$$

Secondary amines:

$$CO_2 + R_1R_2NH \Leftrightarrow R_1R_2NH^+COO^- \tag{2.18}$$
$$R_1R_2NH + R_1R_2NH^+COO^- \Leftrightarrow R_1R_2NH^+ + R_1R_2NCOO^- \tag{2.19}$$
$$R_1R_2NCOO^- + H_2O \Leftrightarrow R_1R_2NH + HCO_3^- \tag{2.20}$$

Tertiary Amines

Tertiary amines have a higher theoretical CO_2 loading than primary or secondary amines, as one mole of a tertiary amine can react with one mole of CO_2 to form a bicarbonate, as can be seen in equation 2.21. Furthermore, the regeneration energy demand for tertiary amines is lower compared to primary and secondary amines, since the heat of absorption of this reaction is lower. However, tertiary amines have low reactivity with CO_2 compared to primary or secondary amines [88]. Tertiary amines directly convert to bicarbonates as they don't have a proton as a migrating group. The most used tertiary amine is methyldiethanolamine (MDEA).

$$CO_2 + R_1R_2R_3 + H_2O \Leftrightarrow R_1R_2R_3NH^+ + HCO_3^- \tag{2.21}$$

Sterically Hindered Amines
Sterically hindered amine groups form carbamates, just like primary and secondary amines. However, they have a relatively lesser reactivity and lower heat of absorption, due to their instability.

Amine Performance Characteristics
Different solvents for DAC appliances are judged on performance on a number of characteristics. According to N. El Hadri and Zahra [88] the ideal solvent for CO_2 capture should score best on the following:

- High CO_2 absorption capacity at ambient temperature
- Low energy demand for regeneration
- Fast reaction kinetics

The energy demand for regeneration is the total heat required to desorb the CO_2 from a CO_2-amine-H_2O solution in the stripper column. It is contributed by three different energies as can be seen in equation 2.22.

$$E_{regeneration} = E_{sensible} + E_{vaporization} + E_{absorption} \tag{2.22}$$

The first term, E_{sensible}, is the **sensible heat** required to heat the CO_2 rich feed stream coming from the absorber to the desorption temperature, and can be calculated according to equation 2.23.

$$E_{sens} = \dot{m} \cdot C_p(T_{des} - T_{feed}) \tag{2.23}$$

where

$\dot{m}$	=	mass flow of sorbent $[kg/s]$
C_p	=	specific heat of sorbent $[kJ/kg \cdot K]$
T_{des}	=	desorption temperature $[K]$
T_{feed}	=	feed stream temperature $[K]$

The second term, $E_{vaporization}$, is the **heat of vaporization** required to bring the CO_2 and H_2O from the liquid phase into the gas phase. Sinha et al. estimated the heat of vaporization of H_2O in TEPA for different H_2O concentrations and found the value to be higher than the latent heat of H_2O. This implies that the heat of mixing, thus the formation and breaking of hydrogen bonds, adds up to the heat of vaporization of H_2O [112].

The third term, $E_{\text{absorption}}$, is the **heat of absorption**, which account for the heat required to reverse the reactions which occurred when the CO_2 was absorbed by the solvent, also the heat of physical dissolution of CO_2 into the solvent and the heat of non-ideal mixing as a result of new interaction inside the solvent. The absorption of CO_2 into an amine is exothermic, it releases energy. Therefore, for desorption, the reaction is endothermic i.e. it requires energy to break the chemical bonds. The heat of absorption accounts for 50-60 % of the total regeneration energy for MEA 30 $wt\%$ [88]. For primary and secondary amines this heat of absorption is usually high, resulting in a high regeneration energy demand for those amines. According to R. Wanderley et al. the heat of absorption of CO_2 for water lean sorbents can be assumed to be $\Delta H = 85\, kJ/mol_{CO_2}$ following the average of that obtained experimentally [100].

In order to quantify the three characteristics listed above the following properties are usually tested: nominal cyclic capacity, heat of reaction, reboiler duty, liquid film mass transfer coefficient, viscosity and thermal degradation. Since sorbent selection is the subject of this thesis an elaborate overview and explanation of all the important material properties is provided in section 2.4.4.

No sole primary, secondary or tertiary amine solvent scores high on all three requirements, where usually a high score on one requirement impedes the score on the other. Although, according to literature, amine blends of primary/secondary amines with tertiary amines improve the reactivity compared to the pure tertiary amine. Furthermore, they reduce the heat of absorption compared to pure

primary and secondary amines [88][105]. Thus, these amine blends utilize the advantages of both primary/secondary amines and tertiary amines. Since sterically hindered amines form carbamates of low stability, they too have a lower heat of absorption compared to pure primary, secondary or tertiary amines [15]. Consequently the direct route to bicarbonate is preferred over the carbamate route, since it results in a larger CO_2 capture capacity compared to unhindered primary/secondary amines.

2.3.2. Polyamines

Since the aforementioned amine blends offer favorable characteristics, the next step is to dive deeper into polyamines, as they could possibly offer the same or even better CO_2 capture characteristics. A polyamine is an organic compound that has more than two amino groups, which can be primary, secondary, tertiary or hindered amines. Accordingly, one polyamine molecule can react with more than two CO_2 molecules, and therefore, their CO_2 absorption capacity is likely to be higher compared to monoamines [66]. The specific molecular structure of the polyamine dictate its properties and potential for CO_2 capture appliances.

Relatively little research has been done on polyamines as CO_2 capturing solvents, with the exception for the diamine called: piperazine (PZ), which has been thoroughly studied by Rochelle's group [104]. Kim et al. tested the properties of three aqueous monoamines, six aqueous polyamines, four blends of polyamines with monoamines and compared them to each other. [66]. All six polyamines absorbed more CO_2 per mole of amine compared to the tested mono- or di-amines, but scored similar results on absorption capacity and cyclic capacity per kg of solvent. From their study they concluded that a blend of 2,6,10-Trimethyl-2,6,10-triazaundecane with Piperazine in the ratio of 2:1 and 70% H_2O had the fastest absorption rate, the best thermal stability and the lowest reboiler duty of all the amines tested. The effect of the number of amino groups on the absorption and desorption of CO_2 has been studied by Muchan et al., where they compared the behavior of ethylenediamine (EDA), diethylenetriamine (DETA), triethylenetetramine (TETA) and tetraethylenepentamine (TEPA) [94]. They concluded that having more amino groups in the polyamine resulted in a higher initial absorption rate and therefore, in a higher CO_2 loading per amine molecule and it also reduced the basicity. Furthermore, the energy demand for regeneration decreased with an increasing number of amino groups when they estimated the regeneration duty based on the absorption data. This was due to the weaker chemical bonds of secondary carbamates and bicarbamates compared to primary carbamates. Therefore, it costs less energy to break these bonds down. Their study concluded that TEPA holds the most promise as a CO_2 capturing sorbent. TEPA was also investigated by Aronu and al.. Their results showed fast reaction rates and a high absorption capacity of TEPA at low concentrations. Where TEPA was able to remove three times as much CO_2 per full absorption/desorption cycle as MEA at the same concentration, and therefore, concluded TEPA as a promising CO_2 capturing sorbent [7]. It is for these reasons TEPA was already the main focus of ZEF, the next step in the process is to investigate the evolution of sorbents at ZEF.

2.4. DAC at ZEF

Since this thesis covers the sorbent selection of the ZEF DAC team it is important to have an overview of all the research that has already been done at ZEF in the field of DAC sorbents. The evolution of the ZEF DAC unit with its sorbents is elaborated in this section whereafter the current test setups at ZEF are explained with their working principles including their latest findings and recommendations. Followed by a system overview of the ZEF DAC unit including the current sorbent challenges, and finally, the key performance indicators along with the sorbent background check are presented.

2.4.1. Sorbent Evolution

Since the birth of ZEF there there have been four complete prototypes build for the DAC application, which all utilized a different sorbent. **ZEF Team 1** started their DAC journey in February 2018 with their first prototype, which utilized a conventional batch process with a solid sorbent to subtract the CO_2 from ambient air via a temperature-vacuum swing operation [13]. A packed bed made out of **polyethylenimine** or **PEI** of higher molecular weight on a structure of silica could absorb CO_2 and H_2O from ambient air until it was saturated, whereafter the chamber was vacuumed to 0.1 bar and heated in order to release the absorbed CO_2 and H_2O. The system was then cooled to ambient temperature

and the absorption/desorption cycle started again. The isomeric assembly of the first prototype made by Azzalini et al. can be seen in figure 2.7. The whole unit had a large volume and the sorbent was relatively expensive compared to active carbon based sorbents. Therefore, they proposed a monolithic sorbent system for the next prototype.

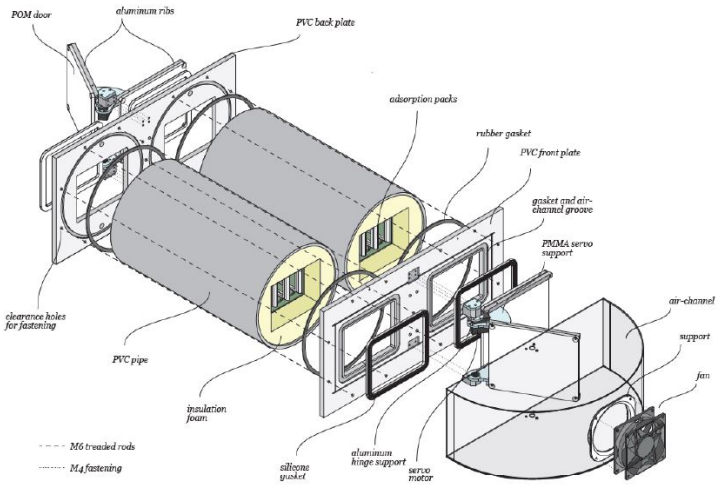

Figure 2.7: An isometric assembly of ZEF's DAC prototype 1 made by Azzalini et al.

The second prototype, as can be seen in figure 2.8, was build in July 2018 by **ZEF team 2** and also utilized a sorbent comprised of polyethylenimine, yet this time two different types of PEI where tested on an active carbon monolith. One type with a molecular weight of $1200\,g/mol$ and the other with a molecular weight of $10,000\,g/mol$. This prototype utilized the same working principle as the first prototype, where absorption/desorption would be realized via a temperature-vacuum swing process [13]. This prototype revealed a lot of major drawbacks, not only to this system but also to its sorbent. The active carbon proved to be very brittle which made it very difficult to impregnate it with PEI. Furthermore, it proved to be very hard to get a homogeneous distribution of PEI over the active carbon. And finally, getting the chamber to be leak tight was very difficult, hence this prototype was never fully functional and was therefore ultimately shelved [119].

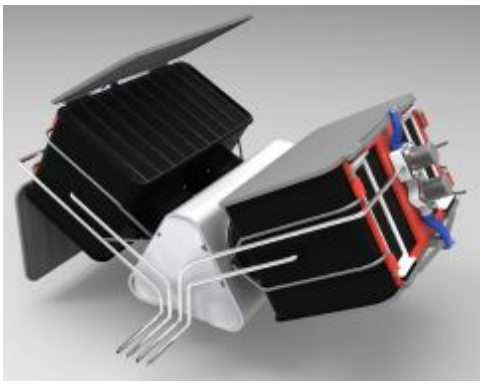

Figure 2.8: ZEF's DAC prototype 2 made by ZEF team 2 [118]

PEI

Polyethylenimine can either be a linear polymer of secondary amines with primary amines at the end or a branched polymer of primary, secondary and tertiary amines. The ratio of primary, secondary and tertiary amines depends on the molecular weight of the polymer, which varies with the number of repeating units. The repeating unit is an amino group with the chemical formula $(C_2H_5N)_n$ for its linear form as can be seen in figure 2.9a. It is important to note that the boiling temperature also scales with

the molecular weight, in other words, systems using amines with higher molar weights generally suffer less from evaporation losses.

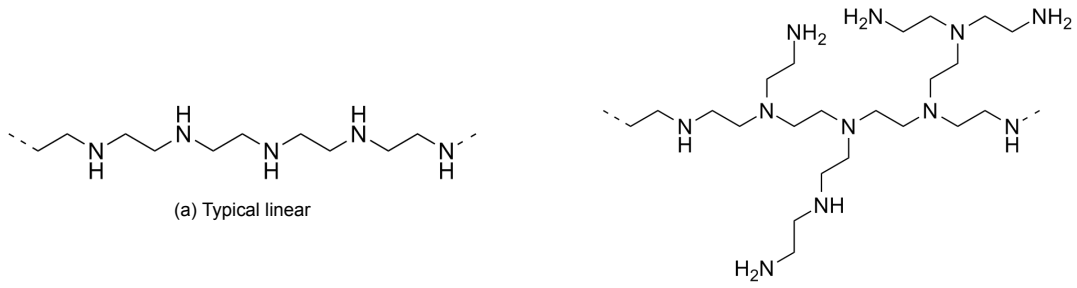

(a) Typical linear

(b) Typical branched

Figure 2.9: Typical structures of polyethylenimine

ZEF team 3 shifted their research from a batch process utilizing a solid sorbent to a continuous process utilizing a liquid sorbent. The third prototype consisted of a separate absorber and stripper, with a bulk amine as a sorbent, much like the chemical absorption technology for post-combustion CO_2 capture as reviewed in section 2.1.3. Compared to batch systems, a continuous systems would require less energy due to lesser valves and vacuum pumps. Team 3 concluded that PEI gets very viscous after it absorbs CO_2 to a point where it is too viscous to pump. Therefore, PEI with a molar of $600 g/mol$ was used as they learned that the viscosity remained lower on CO_2 absorption than that of PEI 1200 and PEI 10,000. With this discovery the challenge of finding the optimal sorbent for a continuous DAC system was born. Since it was found that a lighter molecule of PEI remained less viscous they proposed a different polyamine as a sorbent, namely **tetraethylenepentamine** or **TEPA**.

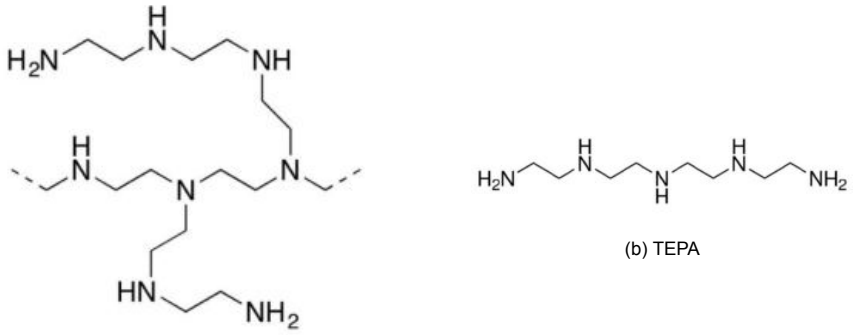

(a) PEI-600

(b) TEPA

Figure 2.10: Molecular structures of PEI-600 and TEPA

TEPA

Tetraethylenepentamine or TEPA is basically a linear iteration of PEI of lesser molecular weight, containing only 5 amino groups. Where PEI-600 is a branched polymer of primary, secondary and tertiary amines, TEPA only consists of primary and secondary amines as can be observed in figure 2.10. Therefor, TEPA binds with CO_2 via the carbamate route. The general properties of PEI-600 and TEPA are listed in table 2.2 for the sake of comparison.

Table 2.2: General properties of PEI-600 and TEPA

Sorbent	Molecular weight	Density at 20°C	Specific heat	Viscosity at 20°C	Heat of absorption*
Type	[g/mol]	[kg/m^3]	[kJ/kgK]	[mPa.s]	[kJ/mol$_{CO_2}$]
PEI-600	600 [79]	1029-1038 [79]	2.44 [20]	500-2500 [79]	-80 [123], -50 [2], -95 [20] (solid on silica)
TEPA	189.31 [91] [54]	993 [91], 991 [54]	2.554 [24]	23.4 [54], 80 [91]	-85 (liquid) [58], -50 (solid on silica) [58]

*Average value since heat of absorption varies with loading and temperature

ZEF team 4 divided their research into the absorption part and the desorption part. Barthe et al. focused on the absorption mechanisms of CO_2 into the sorbent, comparing TEPA and PEI. His main findings were [13]:

- The H_2O loading into the polyamine depends on the relative humidity of the ambient air.
- The CO_2 absorption process was identified to be diffusion limited.
- Pure TEPA has a higher absorption capacity of CO_2 than pure PEI.
- For TEPA, an increase in H_2O concentration improves the loading of CO_2. For PEI the opposite effect was observed.

Ovaa et al. focused his research on the desorption mechanisms, where his main work focused on the VLE setup. The VLE setup is used for testing at desorption conditions, thus at higher temperatures. VLE stands for vapor-liquid-equilibrium. This setup is used to calculate the amount of CO_2 and H_2O which is desorbed in the stripper and would prove to be one of the key features to this thesis and is further elaborated in section 3.3.

ZEF team 5 continued and expanded the research on the two amines, PEI-600 and TEPA, since a complete understanding of the continuous absorption and desorption characteristics was needed in order to decide which of the amines performed better for the ZEF DAC unit. As ZEF team 4 discovered that CO_2 absorption into the amine is diffusion limited and the diffusion coefficient scales inversely with viscosity, as can be derived from the Stokes-Einstein relation 2.10, the viscosity was a parameter of increasing importance for the ZEF DAC team. With that in mind Sinha et al. performed an elaborate viscosity test sequence, where the effect of CO_2 and H_2O concentration and the effect of temperature was mapped and modelled. He also mapped the effect of varying the H_2O concentration on the CO_2 capture rate and on the CO_2 loading capacity. In order to rank the amines on absorption performance he introduced a new parameter; the space time yield as can be seen in equation 2.14. Sinha et al. concluded that TEPA scored better based on the following absorption performance parameters:

- Higher space-time-yield of CO_2 absorbance
- Lower viscosity at varying temperatures, CO_2 and H_2O concentrations
- Higher CO_2 absorption capacity

Furthermore, TEPA is advantageous over PEI-600 looking at the chemical reactions. TEPA and PEI-600 are both made of primary and secondary amines. They differ in the fact that PEI-600 also contains tertiary amines. Tertiary amines react with CO_2 through the bicarbonate route as is stated in section 2.3.1. However, Sinha's experiments and literature both prove the absence of bicarbonates at lower CO_2 loading in the amine. Therefore, part of the PEI-600 does not contribute to the capture of CO_2. It is for these reasons Sinha et al. concluded that TEPA is the best option for the ZEF DAC unit.
Gowda et al. researched the degradation of the sorbent, comparing PEI-600 and TEPA on evaporation, CO_2 induced degradation and O_2 induced degradation. He found that both PEI-600 and TEPA do not experience evaporation losses at ambient conditions. However, in their pure form they both experience significant evaporation losses at 80, 100 and 120°C. On the other hand, a higher concentration of CO_2 and H_2O reduces the evaporation losses. Furthermore, incorporating a gas washer in the stripper column can prevent most of the evaporation losses of the sorbent in the stripper. Both TEPA and PEI-600 where susceptible to CO_2 induced degradation with the formation of urea after the muffle furnace experiments.

ZEF team 6 focused their research on TEPA as a sorbent. Dowling et al. researched and modelled the CO_2 absorption in aqueous solutions of 30, 70 and 80% TEPA [36]. She utilized a mechanically stirred and temperature controlled autoclave, varying to the temperature from 25 to 120°C and measured the CO_2 absorption until vapor-liquid equilibrium (VLE) was reached. This VLE setup is used for two types of experiments: vapor curve measurements and CO_2 loading measurements. Since an evolution of this setup is used for this research it is thoroughly elaborated in section 3.3. The heat of absorption of CO_2 into the TEPA was estimated to be between 75 and 80 kJ/mol_{CO_2} for 70 wt% TEPA using the Clausius Clapeyron equation. She also concluded that the sensible heat generally accounts for the biggest part of the regeneration energy demand, where the most energy efficient result she obtained for the regeneration energy was 533 kJ/mol_{CO_2} at $T_{ambient}$ of 20°C, $T_{stripper}$ of 130 °C and a cyclic capacity of 1.5 mol_{CO_2}/kg_{TEPA}. It must be stated that this result was obtained without a heat exchanger (HEX) between the rich and the lean stream, hence the use of a HEX was one of her recommendations. She also recommended to investigate the possibility to reduce the viscosity of TEPA by utilizing alternative sorbents or additives. ZEF team 6 eventually build a full DAC prototype as can be seen in figure 2.11, which utilized pure TEPA as a sorbent and was the first continuous absorption/desorption prototype at ZEF. One of the main bottlenecks resulting from tests on this prototype where the inability to precisely control the mass flow of the enriched sorbent to the distillation column, as the viscosity of the fluid influenced the speed of the pump. The other main conclusion was that the absorption column used was ineffective.

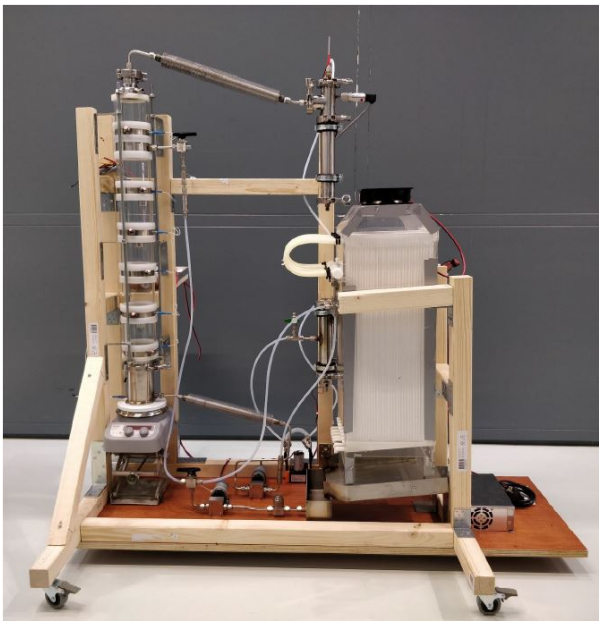

Figure 2.11: ZEF DAC prototype made by team 6 [121]

Matteis et al. focused his research on the absorption mechanism and how to improve the absorption process with TEPA as a sorbent [82]. His main findings where:

- The reactive absorption of CO_2 into TEPA can be explained by his ”Ice-Sheet” theory, which is thoroughly explained below.
- Actively mixing the sorbent in the absorption column proved more effective regarding the CO_2 capture rate compared to passive mixing.
- TEPA is far from the ideal sorbent due to the formation of the ”Ice-Sheet”, therefore, his main recommendation is to change the sorbent.

Matteis et al. developed a theory called: **the ”Ice-Sheet” theory**, which describes the absorption of CO_2 molecules into a polyamine sorbent on a molecular level [82]. The theory focuses only on diffusion in the liquid phase, where it is assumed that diffusion in the gas phase is instantaneously and that the

reaction time between the CO_2 molecules and the sorbent molecules is much shorter than the time it takes for the CO_2 molecules to diffuse into the sorbent.

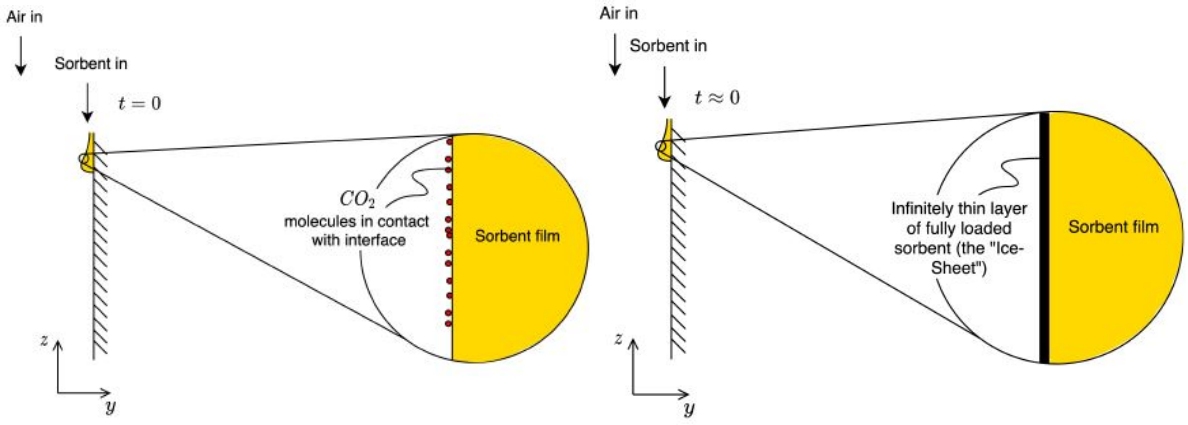

(a) step 1

(b) step 2

Figure 2.12: Absorption of CO_2 into a polyamine sorbent [82]

Figure 2.12a, at time t = 0, shows the yellow sorbent starting to flow down the absorption plate. CO_2 molecules come into contact with the gas-liquid interface via an airflow. At a time still very close to zero, the first CO_2 molecules will react with the sorbent, since it is assumed that the CO_2 molecules react extremely fast, up until the moment when saturation is reached in the sorbent close to the gas-liquid interface. An infinitely thin, fully loaded sorbent layer will be formed on the free surface of the sorbent which is graphically displayed as a black film in figure 2.12b. This layer is called the ”Ice-Sheet”.

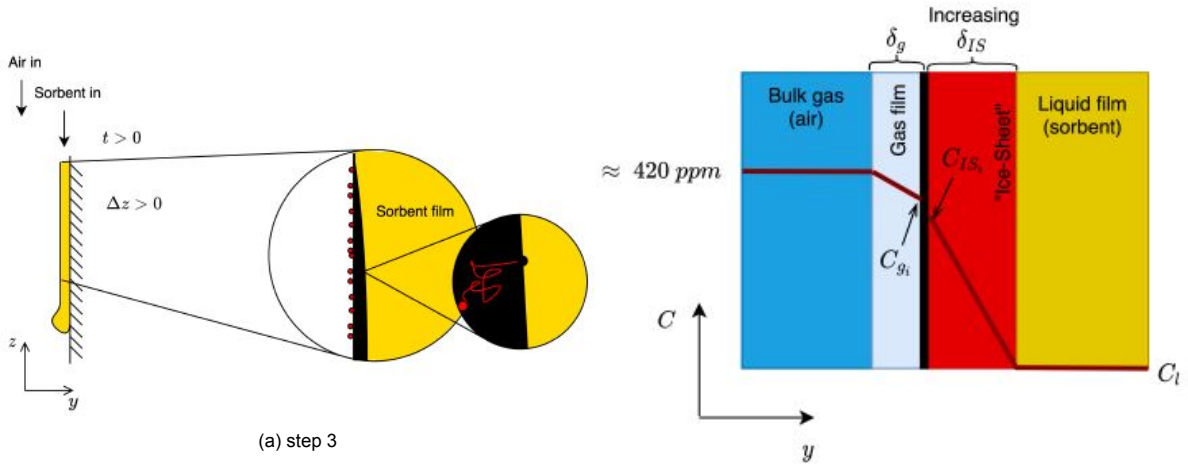

(a) step 3

(b) Concentration profile according to the ”Ice-Sheet” theory

Figure 2.13: Absorption of CO_2 into a polyamine sorbent [82]

At time t > 0, CO_2 gas molecules will keep diffusing towards the gas-liquid interface even when there is an ”Ice-Sheet” on the sorbent layer. Therefore, since there is an ”Ice-Sheet” at the interface, CO_2 molecules cannot react instantaneously with the sorbent, but have to diffuse through the ”Ice-Sheet” layer before they are able to react with the sorbent as is displayed in figure 2.13a. When the CO_2 molecules have diffused through the layer they immediately react with the sorbent. Consequently, the reacted CO_2 molecule will itself become a part of the ”Ice-Sheet” layer. Because of this, Figure 2.13a shows that the thickness of the fully saturated ”Ice-Sheet” layer varies along the plate, since the layer will grow over time and the sorbent which is lower on the plate will have absorbed CO_2 molecules for a longer duration. In other words, a slower flowing sorbent will generate a ticker ”Ice-Sheet”, thus slowing

down the absorption process even more. Figure 2.13b shows a possible concentration profile across the gas-liquid interface, where it must be noted that the concentration of CO_2 within the bulk (liquid film) stays zero before mixing. Matteis et al. tested a solution to this problem, which is to ”break the ice” by actively mixing the sorbent stream.

van de Poll et al. focused his research on validating the stage-by-stage stripper model which was the product of Dowling’s research. This model is the basis for the full DAC model which will be designed for this research project. His research led to the most up to date ZEF DAC design prior to this research project with its specifications specified at the end of section 2.4.2.

2.4.2. System Overview

This thesis covers the sorbent selection for the DAC unit at ZEF, but selecting the optimal sorbent does not depend on one single parameter being optimized, as the sorbent flows through the entire DAC unit. The DAC unit at ZEF can be divided into two main parts, the absorber, where the CO_2 and H_2O are absorbed into the sorbent, and the stripper, where the CO_2 and H_2O are stripped from the sorbent, as can be seen in figure 2.14. The other parts such as the heat exchanger (HEX) between the lean and the rich stream, the flash tank, the cooler and the reboiler are sub parts for a higher efficiency or better separation.

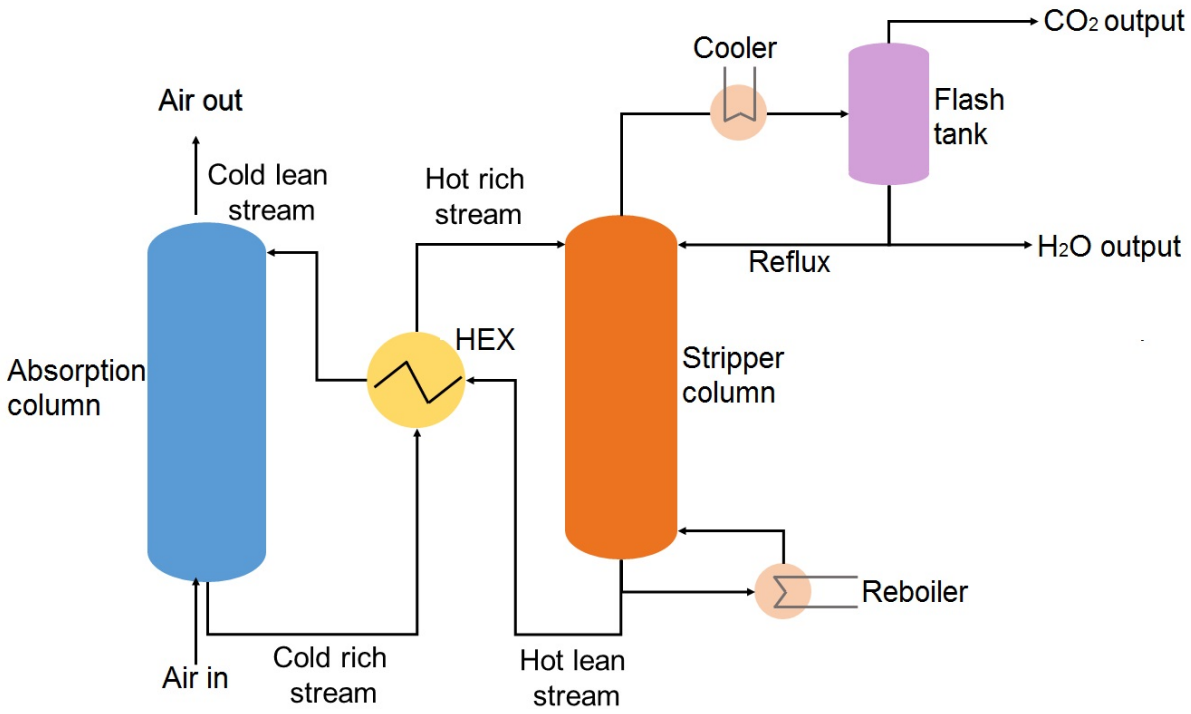

Figure 2.14: ZEF DAC system overview as made by Dowling et al. [36]

Absorber

The absorption column aims at maximizing the surface area between the sorbent and the ambient air as can be seen in figure 2.15. Where the sorbent and air flow in opposite direction to maximise the concentration difference throughout the absorber. For the absorber column there are several parameters to be set which influence the entire system. These parameters are graphically displayed in figure 2.16. When the sorbent comes in contact with ambient air the loading of CO_2 commences. It is assumed the absorption of CO_2 adheres the "Ice-Sheet" theory which was proposed by Matteis as was explained in section 2.4.1 [82]. The amount of CO_2 in the rich sorbent stream coming from the absorber is called the **rich loading**. The rich loading is generally given in $\frac{mol_{CO_2}}{kg_{sorbent}}$, is one of the design parameters that can be set to a specific value and has a big influence on the other main parameter for the absorber; the **Space-Time-Yield** (STY) which is generally given in $\frac{mol_{CO_2}}{m^2 s}$ and is calculated with equation 2.14. The Space-Time-Yield depends on the type of absorber, the specifications of the sorbent but most importantly the rich loading. The STY can be used to calculate the required absorber area, thus absorber size. For the sake of highlighting the effect of setting a certain rich loading two base cases have been set out in figure 2.16, case A and B. If, for example, the lower rich loading of A compared to B is chosen, it coincides with a higher STY as can be seen in figure 2.16. A higher STY, meaning a higher CO_2 absorption per unit area, means a smaller required absorber size and thus lower capital costs. On the other hand, the lower rich loading of A compared to B depicts a lower cyclic capacity, which in turn results in a higher sorbent mass flow since the output of CO_2 from the DAC system is a set value of 825 grams per eight hours. A higher sorbent mass flow results in a larger sensible heat ($E_{sensible}$) requirement, thus a higher energy demand for regeneration of the sorbent in the stripper according to equation 2.22. This thesis strives to find the optimum for these parameters.

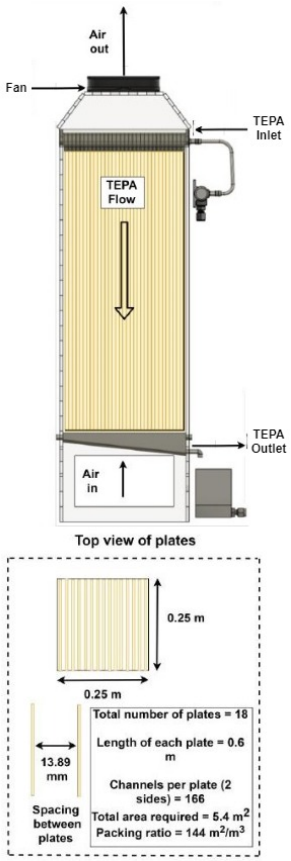

Figure 2.15: Absorber prototype 3 made by Sinha [112]

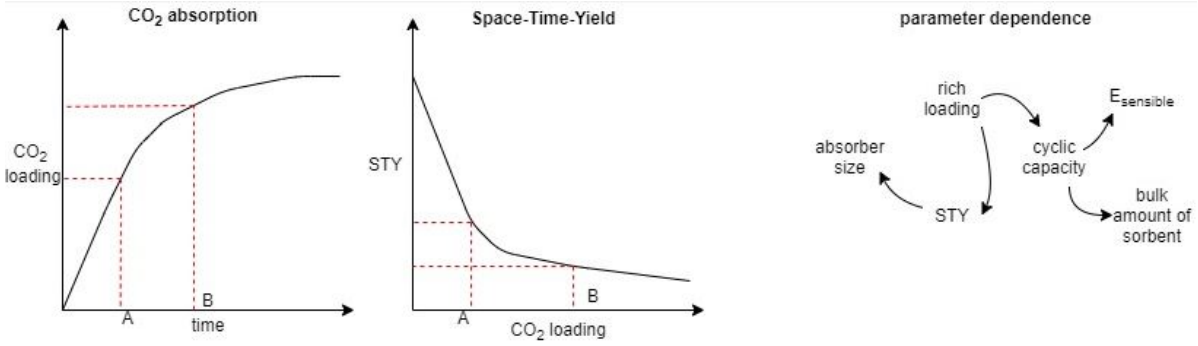

Figure 2.16: Graphical display of significant absorber parameters

Stripper

In the stripper the feed stream enters at the top of the stripping column as can be seen in the schematic of the stripper in figure 2.17. The heat required to desorb the CO_2 and H_2O from the sorbent is supplied by the reboiler, which is stationed at the bottom of the column. The desorbed gasses rise through the column and flow therefore counter current to the falling liquid feed mixture. As the bottom of the column is heated and the colder feed stream enters at the top of the column, a temperature gradient is present. The energy needed for stripping is called the **regeneration energy** as was stated in equation 2.22 and is strongly dependent on the **temperature of the stripper** and the operating **pressure of the stripper**. Who both are key parameters for its performance. It requires a certain amount of time for the desired amount of CO_2 and H_2O to desorb from the sorbent. Therefore, there is a minimum amount of time that the sorbent remains in the stripper. This time is called the **hold-up time**. The hold-up time is depicted by the time it takes the reverse the reaction between the CO_2 molecules and the sorbent molecules, i.e. the reaction time, and by the time it takes for the CO_2 molecules to diffuse from the liquid sorbent into the gas phase, i.e. the diffusion time. The absorbed CO_2 and H_2O is never fully stripped from the sorbent, hence the sorbent leaving the stripper will always contain an amount of absorbed product [42]. This is called the bottom product. The desorbed CO_2 and H_2O exit the top of the column in the gas phase as the top product. The reflux condenser and the reflux drum make up the top of the column. In this section the evaporated H_2O condenses and is partially fed back to the stripper column. The amount of condensed H_2O fed back over the amount of top product discarded from the column is called the **reflux ratio** as can be seen in equation 2.24. Part of the stream leaving the bottom of the stripper is evaporated in the reboiler and fed back into the column. The amount that is fed back to the column over the bottom product, which is discarded from the column is called the **boilup ratio** as can be seen in equation 2.25. The reboiler and reflux are used to further purify the product streams. The stripper column can be a single stage or multiple staged, where more stages are beneficial for the degree of desorption, but does require more energy. When an infinite number of theoretical stages is assumed a minimum reflux ratio (RR_{min}) exists and when an infinite reflux is assumed a minimum number of stages exist for a given feed composition, operating pressure and desired degree of desorption. For optimization, a design trade-off is made between the reflux ratio and the number of stages [42].

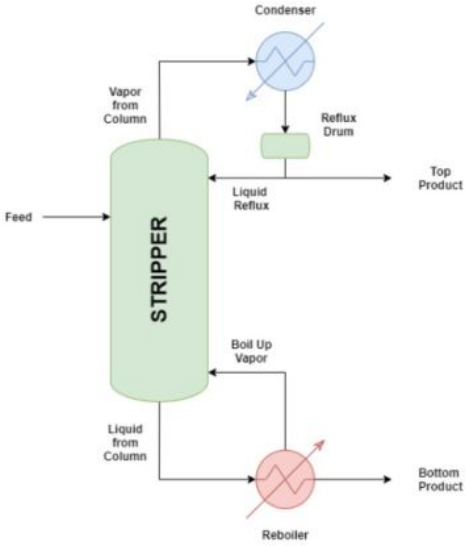

Figure 2.17: Schematic of general stripping column by van de Poll

$$RR = \frac{L_{cond}}{D_{top,product}} \tag{2.24}$$

$$V_B = \frac{V}{B} \tag{2.25}$$

where

L_{cond}	=	condensed vapor fed back to the column $[kg/s]$
$D_{top,product}$	=	top product discarded from system $[kg/s]$
V	=	liquid fed back to the column $[kg/s]$
B	=	bottom product discarded from system $[kg/s]$

According to van de Poll's research the stripper design which meets ZEF's requirements best at the start of this thesis project consists of a 5 stage stripping column with a reboiler temperature of 120°C, operates at 1 bar absolute pressure and has a reflux ratio of 0.55. The feed stream would be preheated up to 105°C in a counterflow heat exchanger. The sorbent, which his setup theoretically used, is aqueous TEPA loaded to 6.9 moles of CO_2 per kg of TEPA and contains 30wt% H_2O in the feed stream. Resulting in a cyclic capacity of 3.3 moles of CO_2 per kg of TEPA and a regeneration energy demand of 1762 kWh/ton$_{CO_2}$.

2.4.3. Current Sorbent Challenges at ZEF

Despite previous research at ZEF showing that TEPA holds great promise as a direct air capturing sorbent, there are still a lot of challenges to be faced. That is where the importance of this thesis comes to light. These challenges are set out in this section in order to get a clear view of where improvements can and have to be made.

Viscosity & Kinetics

The research of Barthe and Matteis revealed that the absorption of CO_2 was diffusion limited. In other words, when CO_2 is absorbed in the absorption column, the initial mass transfer of CO_2 from air to the amine is high as the concentration difference is high, until the point when the CO_2 concentration of the surface layer of the amine, the "Ice-Sheet", reaches equilibrium with the overflowing air. It then takes a long time for the CO_2 molecules to diffuse further into the bulk of the amine, hence the very low average diffusion coefficient of CO_2 in TEPA of only $D = 10^{-10}\, m^2/s$ as was found by Barthe et al. and an even lower diffusion coefficient through the "Ice-Sheet" layer of only $D = 10^{-15}\, m^2/s$ [82]. This could be due to the fact that when an amine is loaded with CO_2 the viscosity rises exponentially with increasing CO_2 concentration, as was concluded by Sinha et al. [112]. The uptake of CO_2 at the surface of the amine results in multiple layers in the bulk of the amine with a difference in viscosity. This increase in viscosity is due to the formation of a hydrogen bond network when CO_2 is absorbed [10]. There is a clear trade-off between the sorbent viscosity and its CO_2 physical solubility. According to R. Wanderley et al., the corresponding Henry coefficient H_A for a valid trade-off decreases exponentially with the viscosity μ. In other words, in order to enhance the kinetics, the viscosity of a possible diluent plays a much bigger role than its CO_2 solubility [100]. Figure 2.18 shows a rise in viscosity up until 10% of H_2O and from there a dip in viscosity when a CO_2 loaded sample is increased in water concentration. This could indicate that a higher amount of H_2O acts as a diluent. A sorbent with a high viscosity not only results in a higher pumping duty, it also results in very slow CO_2 capture kinetics. This is the reason why Dowling et al. concluded that the high viscosity of TEPA, even at optimal process conditions, will be its bottleneck for its use in a continuous absorption and stripping process.

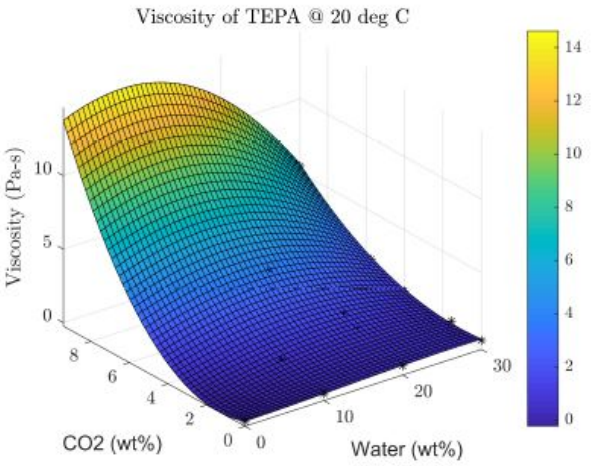

Figure 2.18: 3D plot for viscosity of TEPA with varying CO_2 and H_2O concentrations made by Sinha [112]

VLE

The VLE experiments of Dowling et al. provided a first approximation of the energy demand of a system utilizing TEPA as a CO_2 capturing sorbent. Her results showed that a TEPA driven system has a three times higher energy demand than existing systems utilizing monoethanolamine (MEA), which is the benchmark sorbent for post-combustion CO_2 capture [36]. The larger energy demand of TEPA can be attributed to the difficulty of reaching a high rich loading from the low concentration of CO_2 in ambient air. The difference between the rich CO_2 loading, obtained from ambient conditions, and the lean loading, obtained from the stripper conditions, is the cyclic capacity. In other words, how much CO_2 can be caught and released to the system by the DAC unit. A higher rich loading would result in a higher cyclic capacity, which in turn would reduce the energy demand of the system.

Ambient Sorbent Specifications

The absorption experiments of Matteis et al. showed a great influence by the ambient conditions in the absorption of H_2O, and with that the sorbent conditions changed. ZEF needs to know the exact concentrations of CO_2 and H_2O which are absorbed at specific ambient conditions in order to do precise VLE experiments and to make statements on what kind of sorbent would work in specific climates. Even a slight deviation in concentration of the sample loaded in the VLE experiment could result a

very different outcome of the expected energy demand of the system. Up until now, no research has been done within ZEF on the ambient loading at specific ambient conditions. Since the concentration of CO_2 in the sorbent will be the highest when the sorbent flows from the absorber, where absorption happens at ambient conditions, it is evident that viscosity tests will have to be conducted at the exact concentrations obtained at ambient conditions.

Evaporation
Gowda et al. found that evaporation losses are influenced by the following factors:

- Vapour pressure, which indicates the bias of molecules to escape from the surface of the liquid. When the vapor pressure is high, the evaporation of the liquid is high. This is a result of the inter-molecular forces, since stronger inter-molecular forces prevent the liquid from evaporating into the gas phase.
- Surface area, since evaporation takes place at the surface, a larger surface area results in more molecules escaping the liquid at the liquid-gas interface.
- Temperature, since the kinetic energy of the molecules increases as the temperature is increased, in turn speeding up the evaporation.
- Flow rate of the gas. The gases flowing above the liquid enlarge the mass transfer of vapor from the liquid to the gas phase. Therefore, a higher flow rate of the gases above the liquid interface coincide with a higher evaporation rate.

When evaporation of the sorbent at ambient conditions occurs it means that the amount of sorbent in the system is declining, which would mean that sorbent would have to be added on a regular basis for the DAC unit not to run out of sorbent. This ramps of operational costs and furthermore, could possibly harm the environment. Since evaporating a chemical into the atmosphere is not desirable when one of the goals of the ZEF system is to cleanse the atmosphere.

Degradation
Previous research at ZEF showed the degradation of the sorbent. Sorbent degradation reveals itself as amine site loss. Amine sites are the locations in the molecular structure where the CO_2 molecule can attach with the amine molecule. A loss in amine sites corresponds with a loss in CO_2 absorption capacity. Sorbent degradation possibly occurs as a cause of the following:

- Thermal degradation. By subjecting the sorbent to heat, amine site losses have been observed by Gowda et al.
- Oxidative degradation. O_2 induced degradation has been observed by Gowda et al. Quyen T. Vu and Yogo reported a change in the composition of the with TEPA impregnated silica sorbent due to oxidative degradation, resulting in a loss of the CO_2 absorption capacity. According to them this is mainly caused by changes in the functional groups of TEPA [98]. Furhtermore, Srikanth and Chuang also reported oxidative degradation of a silica-supported amine sorbent comprised of TEPA and virious species of PEG [114].
- CO_2 induced degradation been observed by Gowda et al. Furhtermore, Abdelhamid Sayari and Yang concluded a significant deactivation in the presence of dry CO_2 at ambient conditions after extensive adsorption-desorption cycling of various amine adsorbents. They attributed the decrease in CO_2 uptake to the formation of urea linkages at the expense of amine groups [3].
- Stainless steel induced degradation has been observed by Fong et al. Where stainless steel possibly acts as a catalyst for sorbent degradation.

2.4.4. Key Performance Indicators
Due to the endless list of possibilities regarding sorbent formulation, the problems of coming up with a new, optimized sorbent may be as cumbersome as frantically guessing which mixture of chemicals would benefit a DAC system. In order to address this complexity, this chapter presents the most important parameters for the sorbent that will have to be determined. Research within ZEF and literature have

provided the answer to the following research question: **What are the key performance indicators for the ZEF DAC unit?** The findings are explained in this section along with the **design specifications set by ZEF** per key performance indicator. Quantitative knowledge on these key performance indicators (KPI) is necessary in order to design an entire DAC unit. Some of the answers for these KPI's can be found through literature, some of them through experiments and others require a model. The full list of KPI's for the ZEF DAC unit are depicted in green in figure 2.19. A more elaborate explanation including their significance is given below.

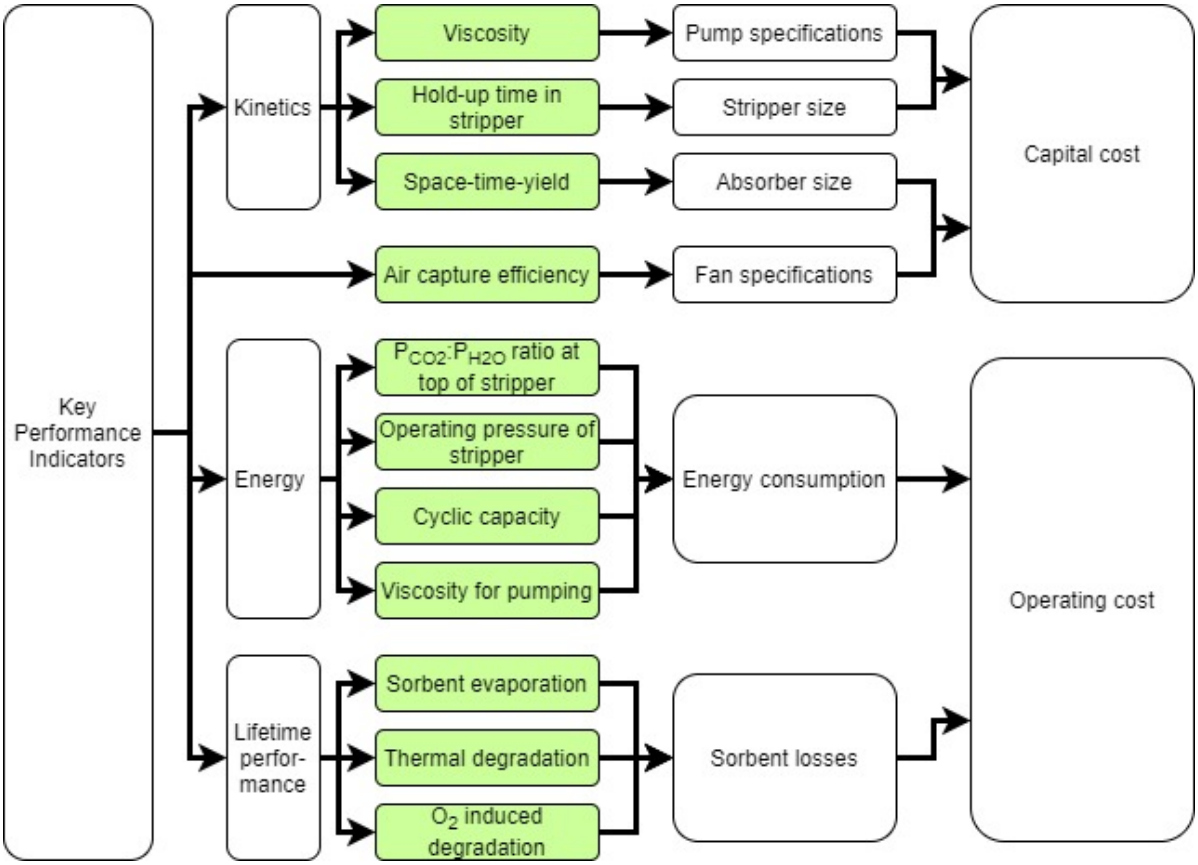

Figure 2.19: Overview of the key performance indicators (green) for the ZEF DAC unit and their determining factors.

Viscosity

The viscosity of the sorbent is one of the main points of improvement stated by previous research at ZEF. A higher viscosity for the sorbent results in a larger pumping duty in order to overcome the pressure drop. But more importantly, the viscosity is a proxy for the kinetics of the sorbent. According to the Stokes-Einstein relation (equation 2.10) diffusion scales inversely with viscosity. In other words, diffusion of CO_2 into the sorbent will be fastest if the viscosity is as low as possible. ZEF has set a limit for the viscosity of **2** $Pa \cdot s$ **maximum**.

Optimal Pressure Ratio

The methanol synthesis reactor converts CO_2 and H_2 at a molar ratio of 1:3 into a mixture of methanol and water. In other words, the DAC system would operate the most energy efficient if it would provide its products, CO_2 and H_2O, at a molar ratio of 1:3. For every mol of H_2O higher than that, there is an extra energy expense of 40.8 kJ/mol as it is fed back into the stripper column through the reflux, where it has to be vaporized again. As the molar ratio scales with the partial pressure ratio, it is beneficial for the product stream coming from the stripper to be $\mathbf{P_{CO2}:P_{H2O} = 1:3}$. Furthermore, it is highly beneficial for the stripper to operate at atmospheric pressure, since it reduces the need for pressure valves, which would cost energy to be operated and controlled. Hence, the optimal absolute pressure in the stripper would be $\mathbf{P_{abs} = 1\ atm}$.

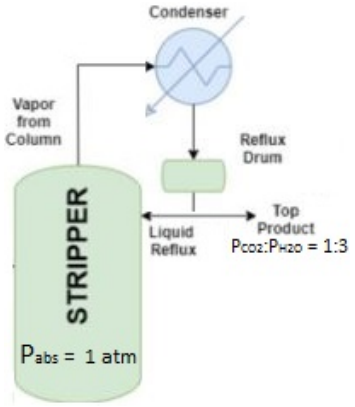

Figure 2.20: Optimal stripper operating conditions.

Cyclic Capacity

The amount of CO_2 which can be stripped per passing of the sorbent through stripper is called the cyclic capacity, therefore it is the difference in CO_2 loading of the rich sorbent stream entering the top of the stripper and the lean sorbent stream exiting the bottom of the stripper. In other words, **Cyclic capacity = Rich CO_2 loading - Lean CO_2 loading**. As from the start of this thesis there is no set optimal value for this parameter, since there is a trade-off to be made which is explained by the following. If, for example, the system could operate with a high cyclic capacity, that would mean that the rich loading of CO_2 would have to be high. The research of Sinha et al. has shown that a high concentration of CO_2 coincides with a high sorbent viscosity, which, as explained earlier, has a negative effect on the size of the absorber, pumping power and overall absorption kinetics. On the other hand, if the system would operate with a low cyclic capacity that would mean that the mass flow of sorbent going into the stripper will have to be much higher to produce the set amount of 825 grams of CO_2 per day. A higher mass flow results in a higher energy demand for the stripper, as the sensible heat required to heat up the feed stream to the desired temperature scales with the mass flow according to equation 2.23. This thesis strives to find the optimum for this trade-off.

Space-Time-Yield

As is stated in section 2.4.2, the space-time-yield is a key parameter in designing the DAC unit for ZEF. It depends strongly on the chosen rich loading and can be used to calculate the required area of the absorber. Furthermore it can be used to compare different sorbents on their performance as it is the parameter that represents the absorption kinetics. The higher the STY, the faster the CO_2 is absorbed in the sorbent, the smaller the required size of the absorption column.

Hold-up time stripper

The hold-up time of the stripper depicts the time it takes for the required amount of CO_2 and H_2O to be stripped from the sorbent mixture and is therefore the time that it takes for a single passing of the sorbent through the stripper. It depends on the reaction time of CO_2 molecules with the sorbent molecules and the diffusion time. It is assumed that the diffusion time is longer than the reaction time. Therefore, the hold-up time strongly depends on the kinetics of desorption. It is a key performance indicator as it determines the size of the stripper.

Sorbent evaporation

ZEF strives at keeping the operational cost of the ZEF system as low as possible. Extensive sorbent evaporation coincides with the need to frequently add diluent to the system. This would negatively affect the operational cost. More importantly, the ZEF system is designed to clean the atmosphere from pollutant gasses, thus extensive evaporation of the sorbent is not possible. The evaporation limit set by ZEF is set to a maximum of **100 grams per year** based on the assumption that the system operates with 1.5kg of sorbent. That equals to a maximum sorbent loss of only 6.67%.

Sorbent degradation
For the ZEF system to be able to operate for a long duration of time the sorbent can not degrade too much. The research of Gowda et al. showed that pure TEPA is susceptible to O_2 induced degradation. Furthermore, research has shown that pure TEPA is also effected by exposure to heat. Therefore, **oxidative degradation** and **thermal degradation** are two KPI's which have to be mapped.

Cost of sorbent
The cost of the sorbent is a key performance indicator as it is directly linked to the cost of the system. Mass production could eventually bring the cost of the sorbent down, therefore the cost of the sorbent has to be researched in $€/ton$ instead of $€/kg$. ZEF has set no upper limit for the cost but strives to find the least expensive sorbent that meets the requirements set by ZEF.

The other KPI's which are not listed above fall outside the scope of this thesis, where this thesis focuses on the effect of adding a diluent on the sorbent performance. It is only when all these KPI's are quantified an entire DAC unit can be designed.

2.4.5. Preceding Sorbent Selection
Literature shows that adding a diluent to TEPA could potentially benefit the system. However, the list of physical absorbents is long. Since there is not enough time for any student at ZEF to test all the chemicals on their performance regarding the DAC system a background check is defined to filter through the long list of chemicals and obtain the ones that could potentially increase the sorbent performance.

Background check
Before a chemical is chosen to enter the test phase, it is subjected to an initial background check which is given in the chart below.

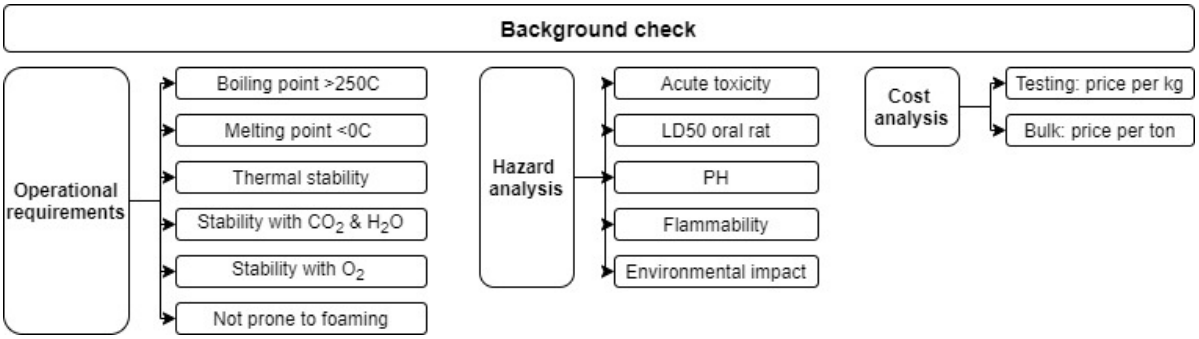

Figure 2.21: Initial background check

2.5. Diluents
Adding a diluent to TEPA could potentially increase the performance of the sorbent. An increase in CO_2 capacity is proposed by various researchers due to the coupling of physical and chemical absorption [103][74][102]. However, for low-to-moderate CO_2 partial pressures, it was observed not to be the case by R. Wanderley et al.. Perhaps an increase in CO_2 capacity could be attributed to the reduction of the viscosity of the sorbent when it is loaded with CO_2. In this section the research on possible diluents is set out.

2.5.1. Selection Criteria for Diluents
The selection criteria for diluents coincides with the performance characteristics for amines which are listed in section 2.3.1. yet for diluents the list of criteria is expanded, since the diluent has to be mixed with TEPA. The main selection criteria is a high physical solubility of CO_2, as it is understood that this enhances mass transfer rates [100]. Which is is the main function of the diluent. The solubility of the diluent in TEPA is one of equal importance, problems such as separation of the sorbent could occur if the diluent would not mix properly with TEPA. As one of the aims of this research project is to reduce

the viscosity of the sorbent, a low viscosity is one of the main criteria. Furthermore, ease of desorption is highly beneficial, as it reduces the regeneration temperature and pressure, which reduces the energy demand for regeneration. Evaporation of the sorbent is one of the problems faced by ZEF, thus a low vapour pressure, high thermal stability as well as long-term stability are desirable in order to prevent the loss of sorbent. Finally, the cost and environmental toxicity have to included in the selection criteria, especially when evaporation of sorbent is taken into account. The selection criteria can be summarized by the following:

- Solubility of CO_2 at ambient temperature
- Solubility of diluent in TEPA
- Low viscosity at ambient temperature
- Low energy demand for regeneration
- Low vapour pressure
- High thermal stability
- Cost
- Environmental toxicity

2.5.2. List of Candidates

The following diluents where stated in literature, all with their own characteristics which could potentially improve the sorbent performance.

Polyethylene glycol

Polyethylene glycol (PEG) is a synthetic polyether compound which is well established as a chemical all the way from the pharmaceutical industry to industrial manufacturing. PEG has multiple important advantages such as being amphiphilic, soluble in water, nontoxic, biodegradable, nonvolatile and cheap [10]. Its general molecular structure is displayed in figure 2.22. Its molar mass ranges from 62.07 g/mole all the way up to 100.000 g/mole depending on the amount of repeating groups. PEGs chemical formula is $C_{2n}H_{4n+2}O_{n+1}$ with n depicting the number of repeating groups. When n=2 it is called **diethylene glycol** or (DEG), and from n>4 it is called polyethylene glycol. In contrary to amines, PEGs physically absorb CO_2 rather than chemically, which is easier to reverse, hence regeneration would be less energy intensive. Originally, acid-base reactions of the acidic CO_2 with the electron-rich ether oxygen which are present in the PEG molecule was ought to be the mechanism behind the high solubility of CO_2 in liquid PEGs, However, solvents such as selexol show lower CO_2 solubility in spite of their ether groups, thus that can not be the only mechanism behind CO_2 absorption [8]. Despite the fact that CO_2 is a non polar gas, interaction with polar groups occurs through the polarity of the individual C-O bonds in the CO_2 molecule. It is very plausible that the terminal -OH groups have a higher affinity for CO_2 molecules and therefore increase the absorption of CO_2 compared to chemical containing only ether groups. The molecular structure of PEG contains a free -OH group for every repeating group. These -OH groups are the functional groups that can increase the absorption of CO_2 due to strong polar interactions between the -OH groups and the CO_2 molecules [8], as can be seen in figure 2.23.

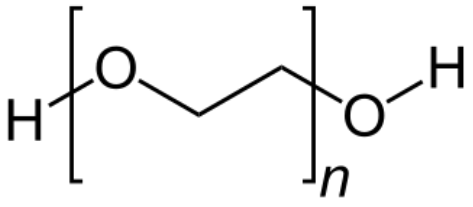

Figure 2.22: General molecular structure of PEG

Aschenbrenner and Styring researched PEGs with a molar weight of 200, 300 and 600 g/mol on their CO_2 solubility and thermal stability. They concluded that PEG is superior in CO_2 solubility compared to PEI, where PEG-200 and PEG-300 could absorb 5 times, and PEG-600 almost 3 times as much CO_2 compared to PEI [8]. They also concluded that PEG-600 scored similar results as PEI on thermal stability, where they are equal in vapor pressure. It must be noted that the vapor pressure usually

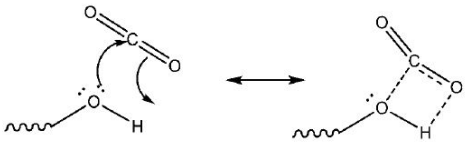

Figure 2.23: Polar interaction between -OH group and CO_2 molecule [8]

scales inversely with molar mass, in other words, the higher the molar mass, the lower the vapor pressure, the lower the change of evaporation of the diluent. On the other hand, viscosity scales with molar mass, the higher the molar mass, the higher the viscosity. As was concluded by Aschenbrenner and Styring, where they observed that the solubility of CO_2 in PEG-200 and PEG-300 was almost identical, as these solvents are quite similar in -OH and -O- groups. PEG-600 on the other hand has a much larger molecule, which severely reduces the amount of available -OH groups with a high affinity to CO_2. Additionally, the viscosity of PEG-600 is higher compared to PEG-200 and PEG-300 since there are more carbon atoms per molecule, and therefore making it harder for CO_2 molecules to diffuse through the solvent. Resulting in the lower solubility of PEG-600 compared to PEG-200 and PEG-300. Lower CO_2 solubility will therefore be expected for PEGs with higher molar mass.
B. Zhang and Yu tested the effect of adding PEG-200 to an ionic liquid of tetraethylenepentamine acetic acid ([TEPA]Ac) at high temperature. They observed that the viscosity increase after CO_2 absorption was severely decreased by adding PEG-200. Therefore, they concluded that adding PEG-200 could increase the efficiency of absorption and desorption significantly [10]. However, the solubility of CO_2 into the sorbent decreased with increasing PEG-200 content. This implies that the PEG-200 itself does not absorb CO_2 at the tested conditions, but only acts as a diluent for the [TEPA]Ac to increase the absorption efficiency. Srikanth and Chuang et al. performed a spectroscopic investigation into the oxidative degradation of silica-supported amine sorbents for CO_2 capture, consisting of TEPA combined with PEG-200 and PEG-600, and concluded that the addition of PEG-200 and PEG-600 to the supported amine sorbents both improved the CO_2 capture capacities and reduced the oxidative degradation of the sorbent [114]. Since diethylene glycol (DEG) is used for dehydration of CO_2 for the purpose of enhanced oil recovery, Jou et al. tested the solubility of CO_2 in DEG at different temperatures and pressures [61]. They concluded that a substantial amount of CO_2 can be absorbed in DEG even at ambient temperatures.

Table 2.3: General properties of polyethylene glycol

Diluent	M	**CO_2 solubility**	P_{vap}	T_{melt}	T_{boil}	μ **at 20°C**	C_p	**Cost**
Type	**[g/mol]**		**[Pa]**	**[°C]**	**[°C]**	**[mPa-s]**	**[kJ/kgK]**	**[€/ton]**
DEG	106.12 [4]	2.38 g/l at 25 °C and 1 bar [61]	2.8 at 25 °C [89]	-9 [22]	245.5 [22]	20 [89]	2.343 [22]	28,800.- [4]
PEG-200	190-210 [4]	15.1 g/l at 25 °C [8]	0.0112 at 25 °C [64]	-50 [4]	202 [8]	63.8	2.135 [4]	27700,- [4]
[TEPA]Ac/PEG-200		1.24 $Mol_{CO2}/Mol_{[TEPA]Ac}$ at 1.01 bar and 80°C [10]						
PEG-300	300 [8]	15.1 g/l at 25 °C [8]	1.5 at 95 °C [8]		272 [8]			
PEG-600	600 [8]	8.7 g/l at 25 °C [8]	0.2 at 95 °C [8]		404 [8]			

Selexol

Selexol is perhaps the best-known physical absorbent of CO_2 which is currently used in the industry [8]. Selexol is the trade name for the dimethyl ethers of polyethylene glycol (DEPG). It has basically the same structure as PEG but has methyl groups (CH_3) at the end of the molecule instead of hydroxyl groups (OH), as can be seen in its molecular structure 2.24. Its chemical formula is $C_{2n+2}H_{4n+6}O_{n+1}$, where n is between 2 and 11 [19]. Its molar mass ranges from 240 to 530 g/mol [85]. Selexol is inexpensively produced and has been used in the industry as a liquid physical solvent to remove acid gas and CO_2 from synthetic or natural gas streams since the early 1970s. Desorption of the rich selexol solvent can be done by flashing, so thermally, or by a stripping gas [106]. According to literature, the selexol solvent has a low vapor pressure which limits its evaporation losses,

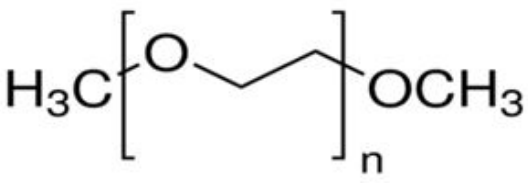

Figure 2.24: General molecular structure of selexol

a low viscosity which avoids large pressure drops, a high chemical and thermal stability, is nontoxic, non-corrosive, inherently non-foaming and moreover, has a low heat requirement for regeneration [16]. Bucklin and Schendel found that selexol holds great promise for applications involving CO_2 removal in hydrocarbon systems, as it proved less costly compared to a Rectisol process.

Table 2.4: General properties of selexol

Diluent	M	**CO_2 solubility**	P_{vap}	T_{melt}	T_{boil}	μ	C_p	**Cost**
Type	**[g/mol]**	**[g/l]**	**[Pa]**	**[°C]**	**[°C]**	**[mPa-s]**	**[kJ/kgK]**	**[€/ton]**
Selexol 250	250	7.17 at 25 °C [19]	0.0973 at 25 °C [19]	-28 [19]	275 [19]	5.8 at 25 °C [19]	0.49 at 25 °C [19]	170300.- [4]
Selexol 500	530.65		<1 [4]	13 [84]	>250 [4]			174800.- [84]

Glycerol

Glycerol is the trade name of 1,2,3-propanetriol, which is a basic polyol compound. It is widely used in the pharmaceutical industry and as a sweetener in the food industry. Glycerol is plentifully available as a byproduct of the biodiesel industry. Therefore, it is inexpensive and biodegradable. Furthermore, glycerol is non-toxic, stable, and liquid at slight vapor pressure points [87]. Glycerol has a high boiling point and is nonvolatile at atmospheric pressures. The viscosity on the other hand, is relatively high. Its molar mass equals 92.094 g/mol and the chemical formula is $C_3H_8O_3$. Aschenbrenner and Styring observed that glycerol, just like PEG-200 and PEG-300, has a high solubility of CO_2, this can be attributed to the high density of free -OH groups [8]. Shamiri et al. added glycerol to mixtures of MEA and methanol and observed improvements in CO_2 absorption capacity and a decrease in regeneration energy compared to an aqueous MEA solution [109]. They observed that the solubility of the MEA + glycerol solution actually increased by adding glycerol up to 10% at lower pressures, that is below 1000 kPa. With that, they confirmed that the solvent could be applied in low-pressure CO_2 absorption processes. However, Jie et al. found that the cyclic absorption capacity decreases when Glycerol is added to MEA. When Seo et al. added glycerol to a solution of ammonia improvements in CO_2 absorption and a reduced vaporization was observed [108]. Compared to PEG-300, PEG-600 and PEI, glycerol has the highest molar solubility of CO_2 [86].

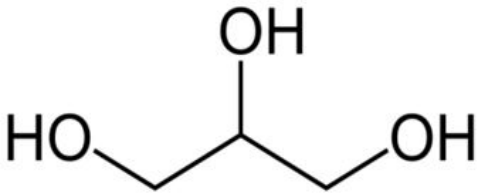

Figure 2.25: General molecular structure of glycerol [26]

Table 2.5: General properties of glycerol

Diluent	M	**CO_2 solubility**	P_{vap}	T_{melt}	T_{boil}	**μ at 20°C**	C_p	**Cost**
Type	**[g/mol]**	**[g/l]**	**[Pa]**	**[°C]**	**[°C]**	**[mPa-s]**	**[kJ/kgK]**	**[€/ton]**
Glycerol	92.09 [4]	59.01 at 30.81 °C [87]	0.0224 at 25 °C [32]	18.2 [75]	290 [84]	1069 [73]	2435 at 25 °C [73]	115,500.- [4]

1,4-Butanediol

1,4-Butanediol is an organic compound and a primary alcohol. It is used industrially as a solvent and for the manufacturing of certain plastics, elastic fibers and polyurethanes. With a world production of over one million metric tons per year it has a relatively inexpensive market price of €1,600 per ton [41]. Its molar mass equals 90.122 g/mol and the chemical formula is $C_4H_{10}O_2$. Although there is very little research done on the capability of butandiol as a CO_2 sorbent it is very much an interesting candidate. Since its molecular structure is quite similar to that of PEG and it is from the glycol family, where the synonym for 1,4-butanediol is Tetramethylene glycol.

Figure 2.26: General molecular structure of 1,4-butanediol [41]

Table 2.6: General properties of 1,4-Butanediol

Diluent	M	CO_2 solubility	P_{vap}	T_{melt}	T_{boil}	μ at 20°C	C_p	Cost
Type	[g/mol]	[g/l]	[Pa]	[°C]	[°C]	[mPa-s]	[kJ/kgK]	[€/ton]
1,4-butanediol	90.12 [4]	-	1.3998 at 25 °C [32]	20.1 [37]	235 [37]	84.9 [53]	1.9751 at 25 °C [21]	1,600.- [41]

Sulfolane

Sulfolane is an organosulfur compound with the formula $(CH_2)_4SO_2$, which is a cyclic sulfone as can be seen in figure 2.27. Sulfolane is soluble in water and because of its low corrosion and high stability, it is used extensively as an aprotic polar solvent in the physical absorption of acid gasses. Usually to be used in extractive distillation. Sulfolane can enhance the absorption rate and solubility of CO_2 during chemical absorption without participating in the chemical reaction [76]. Lidong Wang and Chen et al. researched the application of sulfolane as a phase splitter combined with traditional MEA absorption technology for CO_2 capture. Sulfolane facilitates the absorption of CO_2 by its strong affinity with acid gases, hence the system utilizing the mixture of MEA and sulfolane resulted in an absorption rate 2.7 times higher than a conventional MEA process [76]. Furthermore, they observed a substantial decrease of 31% in the required regeneration heat when they simulated the process. Moreover, the heat of vaporization and the sensible heat both decreased remarkably by 47.9% and 62.7%.

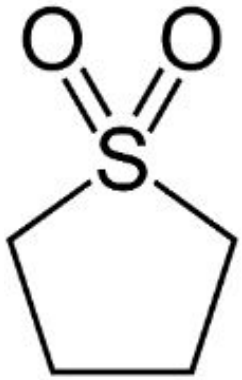

Figure 2.27: General molecular structure of sulfolane [46]

Table 2.7: General properties of Sulfolane

Diluent	M	CO_2 solubility	P_{vap}	T_{melt}	T_{boil}	μ at 25°C	C_p	Cost
Type	[g/mol]	[mol_{CO_2}/kg_{sulf}]	[Pa]	[°C]	[°C]	[mPa-s]	[kJ/kgK]	[€/ton]
Sulfolane	120.27 [4]	0.103 [5]	1.333 at 20°C [4]	20-26 [4]	285 [4]	10.3 [11]	1.513 at 30°C [11]	2,086.- [23]

2.6. Background Research Conclusion

Based on previous research at ZEF, the current challenges regarding the sorbent for the DAC unit at ZEF and literature, the following points can be concluded which specify the steps that have to be taken in order to characterize and optimize a sorbent/solvent system for the DAC unit at ZEF.

- Based on the research of previous teams it is evident that pure TEPA does not meet the design specifications set by ZEF. Recommendations and literature have shown that adding a diluent could potentially improve the sorbent performance. Therefore, a performance analysis will be conducted and evaluated on the addition of different diluents to TEPA.
- Research has shown that there are countless of parameters on which a sorbent for ZEF can be judged. In order to characterize the performance of a sorbent, a set of key performance indicators for the ZEF DAC system has been defined as specified in section 2.4.4.
- Based on the key performance indicators, a framework for sorbent selection has to be developed. Considering time is limited during this thesis, this framework will have to be developed accordingly.
- Knowledge on CO_2 and H_2O loading at specific ambient conditions is not readily available, but necessary for exact energy demand and sizing predictions. Therefore, a test setup has to be developed in order to precisely measure the loading of CO_2 and H_2O at specific ambient conditions.
- Previous research at ZEF indicates that the elevated viscosity after CO_2 absorption is one of the main drawbacks of TEPA as a sorbent. Therefore, a viscosity analysis of the rich sorbent stream, obtained from ambient conditions, will have to be conducted.
- Research at ZEF has shown that TEPA is prone to degradation induced by heat, oxygen, CO_2 and stainless steel. Therefore, the optimized sorbent has to be tested accordingly.

- The following diluents are be mixed with TEPA in various ratio’s and will be tested through the developed framework of sorbent selection.
  - Diethylene-glycol
  - PEG-200
  - PEG-400
  - PEG-600
  - Selexol-250
  - Selexol-500
  - Glycerol
  - 1,4- butanediol
  - Sulfolane

3

Experimental Investigation

Due to the multitude of sorbent possibilities, the issue of coming up with an optimized sorbent can be as cumbersome as swiftly mixing a few chemicals together. Therefore, this chapter will provide the framework of testing to which every sorbent is going to be tested at ZEF. From where a qualitative, and to a certain extend, quantitative evaluation of all the important parameters can be performed. The layout of this chapter is as presented in figure 3.1.

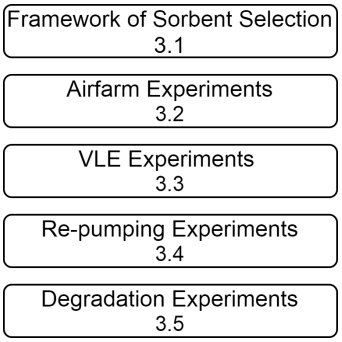

Figure 3.1: Experimental investigation setup

3.1. Framework for Sorbent Selection

If the optimum out of all testable sorbents has to be found, there are countless of samples to test. Due to time constraints this is not possible for the duration of this thesis. Therefore, a framework for sorbent selection is designed such that bad candidates can be crossed off the list with the least amount of time, effort and expense. The entire framework will be split into three different test phases as can be seen in figure 3.2.

Sample Identification

Since the amount of testable sorbents is so vast, a systematic manner of labeling different sorbent mixtures is desirable. This makes handling the amount of data easier while keeping a good overview of what has or has not been tested yet. Therefore, all the different sorbents tested at ZEF will get a unique sample identification (sample ID). In this sample ID the type of polyamine, the type of diluent and their mixing ratio is specified as can been seen in table 3.1.

Table 3.1: Example of sample ID1

ID:1	**Type**	**wt%**
Polyamine	TEPA	90
Diluent	PEG-200	10

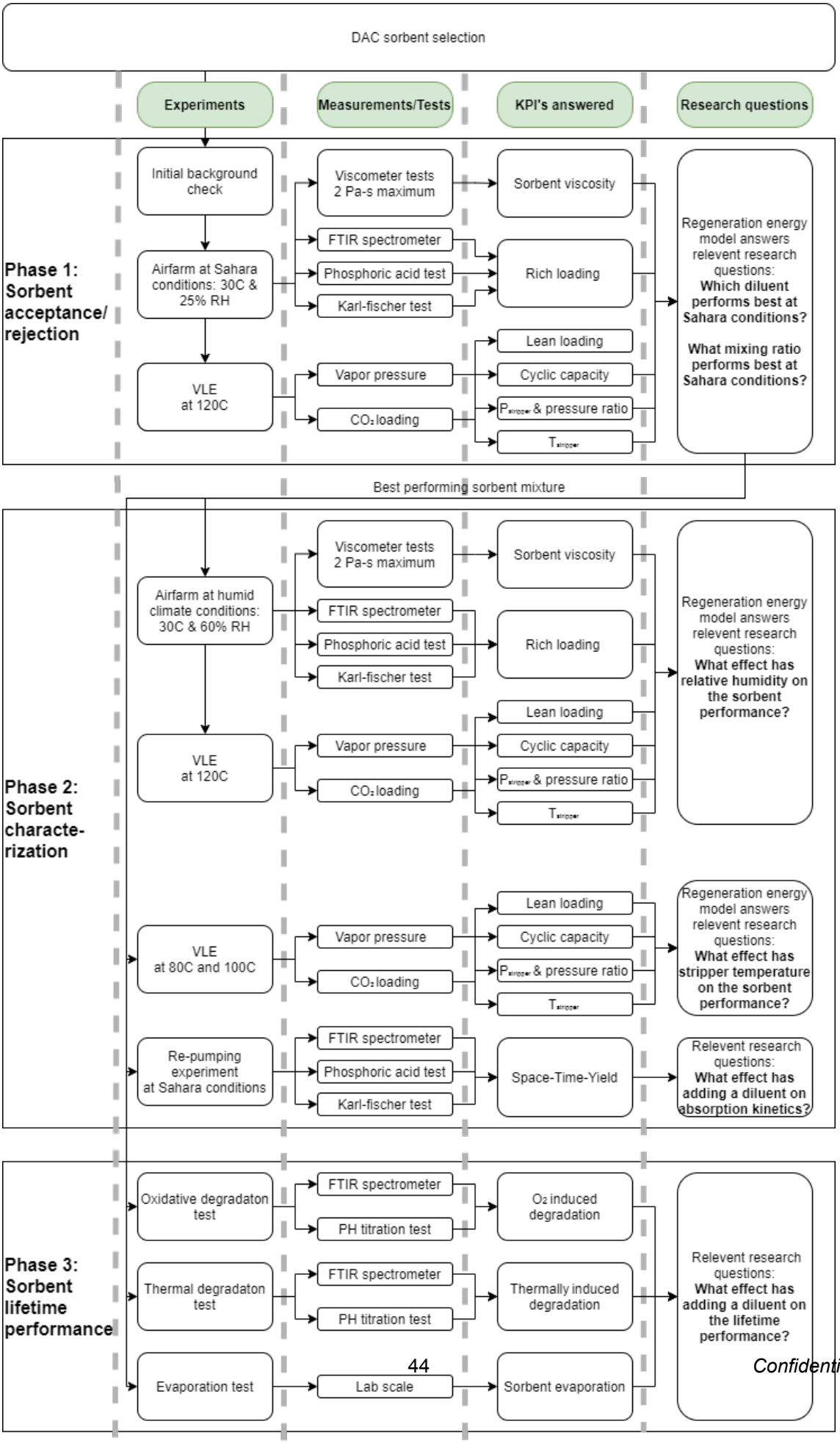

Figure 3.2: Framework of sorbent selection

3.1.1. Phase one: Sorbent Acceptance/Rejection

Phase one of testing has the primary goal to eliminate sorbent candidates as fast and as easy as possible. The following step are taken in phase one of testing:

1. The first thing that is done in phase one is a **full background check** on the polyamine and the diluent of which the sorbent is comprised of. If one of the substances fails the background check as it is specified in figure 2.21, it is of no use to further test that sorbent as it will not work in the ZEF DAC unit.

2. After the initial background check, the next step is to evaluate the performance of the sorbent at the Sahara's ambient conditions in the **Airfarm** experiment. The Airfarm experiment is the second step of phase one since it provides quantitative knowledge on two of the most important KPI's; the viscosity and the rich loading. If a sorbent scores pore on one of these KPI's, it can be eliminated from the possible sorbent list. This prevents wasting time on performing more experiments on that specific sorbent. In the Airfarm the 1:1 and 1:3 mixing ratios of TEPA:diluent will be tested of every diluent in order to compare them.

   One of the main goals of adding a diluent to the sorbent is to reduce the viscosity, and research has shown that the viscosity decreases when an increasing amount of H_2O is absorbed by the sorbent. Therefore, the choice was made to compare the effects of adding different diluents in a climate where it should have the biggest effect on the viscosity. In other words, in a dry climate, less H_2O will be absorbed, thus the increase in viscosity after CO_2 absorption will be most evident. Therefore, the initial Airfarm experiments will be performed at the **Sahara's ambient conditions**, these base case conditions correspond to 30°C and 25% relative humidity.

3. After the sorbent has successfully passed the Airfarm experiment the next step is to test the sorbent in the **VLE experiment** at stripper conditions. The H_2O concentration of the sample which is tested in the VLE follows from the ambient H_2O loading of the Airfarm experiment. It has to be noted that the H_2O concentration drawn from the Airfarm experiment holds for the sorbent which has also absorbed CO_2. As the starting sample of VLE experiment is without any CO_2, the H_2O concentration has to be adjusted accordingly. One of the most important outcomes of the VLE experiment is the lean loading of CO_2 and H_2O. As the cyclic capacity (CC) is calculated from the rich and the lean loading, at this point in the process the CC can be calculated. Furthermore, since the cyclic capacity is now known, as well as the operating pressure and pressure ratio of the stripper, the regeneration energy demand can be calculated with the regeneration energy model. Research at ZEF has shown that the regeneration energy is the biggest energy consumption of the ZEF DAC unit [36]. Therefore, this is the perfect KPI to compare the performance of the different diluents.

At the end of phase one of testing it will be clear which of the tested diluents performs best at Sahara conditions. Furthermore, it will provide valuable information on which mixing ratio's are beneficial to the ZEF DAC unit. The overall best performing sample will be further evaluated in phase two.

3.1.2. Phase two: Sorbent Characterization

The best performing sample at Sahara conditions picked from phase one of testing will be examined more thoroughly in phase two, where the following steps will lead to more insight in the performance of that specific sorbent.

1. The first step of phase two is to test the sorbent at a **different climate**. The same test sequence of phase one is performed again, yet this time with a climate of **30°C and 60% relative humidity**, as this climate corresponds to the average climate at the south side of the Mediterranean sea. By only altering the relative humidity while keeping the temperature constant, this will shine light on what effect the relative humidity will have on the sorbent performance. Altering the relative humidity will have an effect on the H_2O absorbance of the sorbent as the research of Barthe et al. showed in section 2.4. The first step of phase two of testing will provide quantitative data on the effect of the relative humidity on the sorbent viscosity, rich and lean loading of H_2O and CO_2, the cyclic capacity, the operating conditions and the energy demand of the stripper.

2. The second step of phase two is to perform the **VLE experiment at different operating temperatures**. This will provide insight in the effect of altering the stripper operating temperature on the lean loading, cyclic capacity, operating pressure and regeneration energy demand of the stripper.

3. The third step of phase two is to run the **re-pumping experiment at Sahara conditions**, as this will provide knowledge on the absorption kinetics of the chosen sorbent at the base case conditions. From this experiment the Space-Time-Yield can be calculated and with that, the required, sorbent specific, size of the absorbtion column can be calculated.

At the end of test phase two the complete ZEF DAC unit can be designed according to the specific sorbent specifications.

3.1.3. Phase three: Sorbent Lifetime Performance

For the ZEF DAC unit to be able to operate in real life, the sorbent will have to last for a longer duration of time. Therefore, in test phase three the lifetime performance of the sorbent is examined.

1. Research of Gowda showed that TEPA was sensitive to O_2 degradation. Therefore, the first step of test phase three is to perform an **oxidative degradation test** on the best performing sample of test phase one.

2. Since the sorbent will pass through the complete cycle of heating and cooling for numerous times during its lifetime the next step of phase three is to perform a **thermal degradation test** at a test temperature of the stripper, as this will provide quantitative data on the thermally induced degradation.

3. The last step of the test phase is to perform an **evaporation test**. This test will provide quantitative data on the amount of sorbent evaporation at ambient conditions.

At the end of the test phase, all the data needed to design an entire ZEF DAC unit and make accurate predictions on the capital and operating costs is within hand. At this point in the process, all the data will have to processed with the help of multiple mathematical models. These models are elaborated in the next chapter.

3.2. Airfarm Experiments

One of the main challenges regarding the sorbent selection at ZEF is the absence of knowledge on the loading of CO_2 and H_2O at specific ambient conditions as discussed in section 2.4.3. Therefore, a test setup has been designed to acquire the much needed data at ambient conditions of every sorbent mixture tested. This setup is called the **Airfarm** as it harvests results at specific ambient air conditions. This experiment will provide quantitative knowledge on the possible rich loading of CO_2 and H_2O and the viscosity of the sorbent at those specific conditions, as depicted in red in figure 3.3.

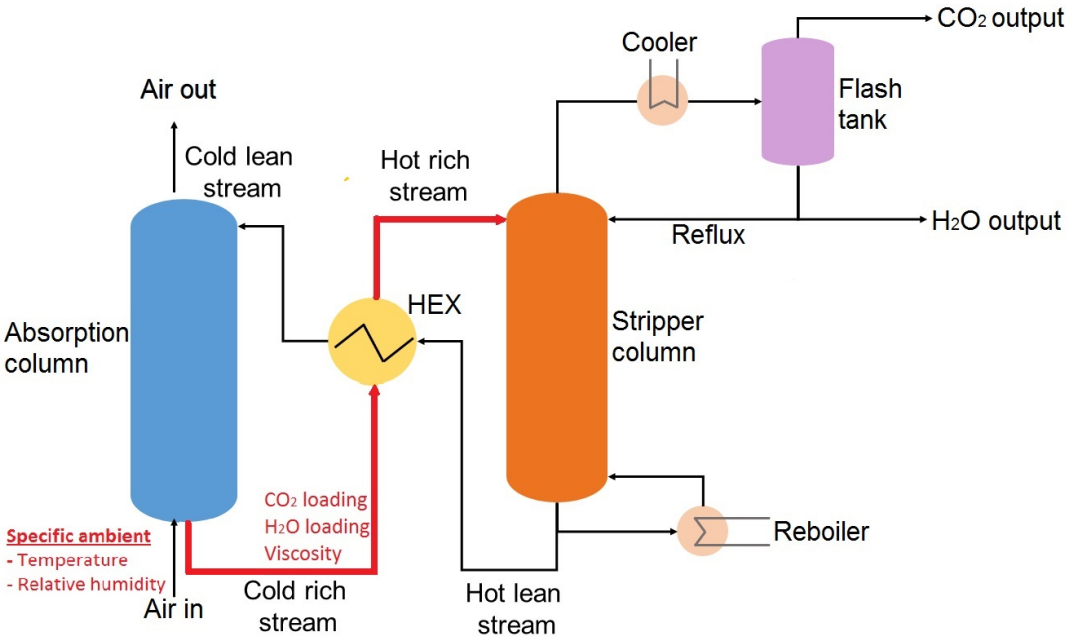

Figure 3.3: Overview of the parameters concerning the Airfarm experiment, depicted in red.

3.2.1. Requirements

Quantitative knowledge on certain parameters at ambient conditions which is needed in order to compare different sorbent mixtures on their CO_2 and H_2O capturing performance leads to certain design requirements of the Airfarm setup. The engineering and manufacturing of the setup is based on those requirements.

- On of the main difficulties of testing a sorbent on its performance is the difficulty of **obtaining repeatable results**. Sample collection will have to be done in a way which is easily repeatable for every sample, such that the results will not be influenced by human errors.
- Since the setup will have to shine light on the performance at specific ambient conditions the whole setup will have to fit and be able to operate inside a **climate chamber**. Where the experimental setup can be operated at a specific temperature and relative humidity.
- A method of facilitating a **large contacting area between the test sample and ambient air** within the climate chamber has to be designed, since the time it takes to absorb an amount of CO_2 or H_2O is directly proportional to the gas-liquid surface area. In other words, a larger contact area, enhanced absorption, thus faster test results.
- The concentration of CO_2 in ambient air is around 420 ppm [28], during the writing of this thesis, and is relatively constant all over the surface of the earth. A process will have to be designed which assures a **steady CO_2 concentration inside the climate chamber**, while the temperature and relative humidity remain constant.
- Regarding the vast amount of sorbents which can be tested on their performance, it is desirable to be able to test **as many samples as possible at the same time in the climate chamber**.

- Research has shown that ”breaking the ice” reduces the absorption time. Therefore, it is necessary to **constantly mix the test samples** while they are in contact with ambient air.
- According to previous research at ZEF absorption of CO_2 can be a slow process. Therefore, the Airfarm has to **be able to operate for multiple days straight**.

Figure 3.4: Climate chamber

Figure 3.5: Fusion 3D design of Airfarm test setup

3.2.2. Setup Description

The complete setup has to be able to operate within the climate chamber at the ZEF laboratory, which is a *Hielkema* climate chamber that can be set to a certain constant temperature and relative humidity as can be seen in figure 3.4. This was the starting point of the design phase, as that provided the dimensions of the Airfarm setup. In order to find the optimal sizing and setup, a design in the 3D CAD software *Fusion360* was made which can be seen in figure 3.5. The climate chamber can accommodate four 100ml gas washing bottles of the brand *Lenz*, through which ambient air from the chamber is pumped by four 12V dual head *Hargraves* gear pumps. As the test samples will absorb CO_2 from the air and the climate chamber can only regulate its climate regarding the temperature and the relative humidity, a solution was found to ensure a steady CO_2 concentration inside the climate chamber. Ambient air from outside the TU Delft laboratory was compressed and dried before it was supplied via a hose to the climate chamber. The climate chamber continuously controls its climate by measuring the conditions inside the chamber, therefore adding completely dry air with an unknown temperature does not effect the climate in the chamber, but it merely ensures a steady CO_2 concentration, equal to that of the ambient air in Delft, the Netherlands.

Figure 3.6: Aifarm setup

Figure 3.7: final assembly of Airfarm setup inside the climate chamber

The gas washing flask ensures that the ambient air is dispersed into tiny gas bubbles which travel

upward through the sample, thus creating a large gas-liquid surface area and therefore, allowing the sample to absorb the CO_2 and H_2O at the exact conditions specified in the climate chamber.

3.2.3. Methodology

For this thesis and the ease of understanding, the experimental procedure of the Airfarm experiment can be divided into three parts - Airfarm Sampling, Measurement of Viscosity and Measurement of Concentrations. All three steps require conscientious and strict experiment methodology, in order to avoid experimental errors.

Table 3.2: Airfarm parameters

Parameters	
Input	**Output**
Ambient temperature	CO_2, rich loading
Ambient relative humidity	H_2O, rich loading
	Viscosity at rich loading

Airfarm Sampling

The goal of the sampling method is to eliminate as much uncertainty factors as possible and provide a structured way of collecting samples which will increase the probability of gaining reliable and repeatable data. The experimental parameters for the Airfarm experiment are listed in table 3.2. After the specific ambient conditions are selected the experiment is started. The samples are collected daily and the time at which the samples are taken is carefully noted.

Figure 3.8: Airfarm experiment in operation inside the climate chamber.

Measurement of Viscosity

The setup shown in figure 3.7 is used to bubble the ambient air at specific conditions through a specific sorbent mixture. However, this is only the first part of the Airfarm experiment. The second part is to test every sample taken from the Airfarm on its dynamic viscosity in the *Contraves low shear 40 rheometer*, which is shown in figure 3.9. Around 2 ml per drawn sample was used for one viscosity experiment at a test temperature of 20°C. At the beginning of the test phase of this experiment the decision was made to continue the Airfarm test until equilibrium was reached between the concentration of CO_2 in the sorbent and ambient air. In other words, keep on testing until the viscosity of the same sample drawn from the Airfarm at a different day became constant, since the viscosity is highly dependent on the CO_2 concentration as described in section 2.4.3. It became evident after the first test phase that some of the test samples became extremely viscous, presumably, too viscous to work with in the final product. Therefore, the decision was made to set a limit for the maximum viscosity of 2 $Pa \cdot s$. It is assumed that a viscosity of 2 $Pa \cdot s$ is the maximum viscosity of the sorbent used in the ZEF DAC unit, and therefore, the rich loading is decided either by the loading when the sample reaches the viscosity of 2 $Pa \cdot s$ or when it reaches its equilibrium loading before reaching the viscosity of 2 $Pa \cdot s$, which meant a change in testing with the Airfarm was needed.

Measurement of Concentrations
After the samples are collected and tested on the viscosity, the third step is to measure the CO_2 and H_2O concentration. Therefore, the samples are taken to the *Cary 630 FTIR Spectrometer* to be analysed, which is shown in figure 3.10. The output of the spectrometer measurements is in the form of a graph of absorbance vs wave number. These graphs can be quantified through calibration via a software called *TQ Analyst*^{TM}. The steps for calibration and functioning of the spectrometer are extensively discussed in Appendix A.3 due to their complexity. Validation of results is done by testing the samples on CO_2 concentration in the phosphoric acid test setup, of which the details can be found in Appendix A.4, and by testing the samples on H_2O concentration in the Karl-Fischer titrator, of which the details can be found in Appendix A.2.

Figure 3.9: Contraves low shear 40 rheometer

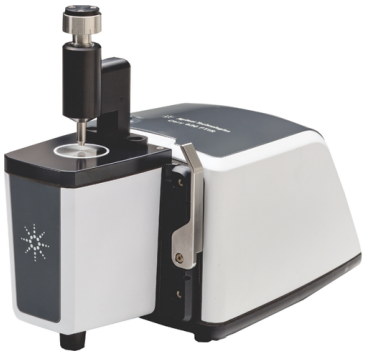

Figure 3.10: Cary 630 FTIR Spectrometer

The final result of the Airfarm experiment consists of three different plots. A viscosity vs time, CO_2 concentration vs time and an H_2O concentration vs time. The quantitative knowledge on these parameters is used to compare the different sorbents on their performance at specific ambient conditions.

3.2.4. Assumptions
Despite the fact that the amount of data collected from the Airfarm experiments is gigantic, the limitations of this data has to be pointed out as well as the validations of the assumptions made during the experiments. Three key assumptions are mentioned below along with their respective validation in order to prove the validity and quality of the data collected during the Airfarm experiments.

1. **Sample collection process is valid.** Considering taking samples during the Airfarm experiments involves subtracting a small portion of the test sample every day, the quality of the data relies on the method of collecting by the experimentalist. All the Airfarm experiments were performed inside the climate chamber. When samples had to be taken the climate chamber had to be opened, therefore, changing the climate inside the climate chamber. During the drawing of samples the air pumps are turned off, and are only turned back on again when the climate chamber reaches it desired climate again. The climate variation during this short period of times was assumed to have no affect on the absorption of CO_2 and H_2O. This thesis assumes that the sample collection procedure is consistent, and experiments are repeatable.

   Validation of assumption 1: Due to time constraints, not all Airfarm experiments could be duplicated. Therefore, during the initial phases of testing, multiple duplos were performed to asses the quality of data being produced.

2. **No depletion of CO_2 inside climate chamber.** During the entirety of the Airfarm experiments fresh, dried air from outside the lab is fed to the climate chamber in order to keep the concentration of CO_2 constant during the absorption of CO_2 inside the chamber. The assumption is made that the ambient CO_2 concentration of the air in Delft represents the average CO_2 concentration of CO_2 around the world, and is equal to roughly 420 ppm. The concentration of CO_2 remained constant inside the climate chamber throughout the duration of the Airfarm experiments.

Validation of assumption 2: During the Airfarm experiments, measurements where performed with a *Telaire T6713* CO_2 sensor in order to check if the concentrations remained constant inside the climate chamber. Figure 3.11 shows the CO_2 concentration in the climate chamber during a full day of Airfarm testing. It can be seen that the concentration of CO_2 remains fairly constant between 500 and 600ppm. The noise in this measurement could be due to the very low concentration of CO_2 of only 0.05%, at such low values, an error of 0.01% is probably due to the accuracy of the sensor itself.

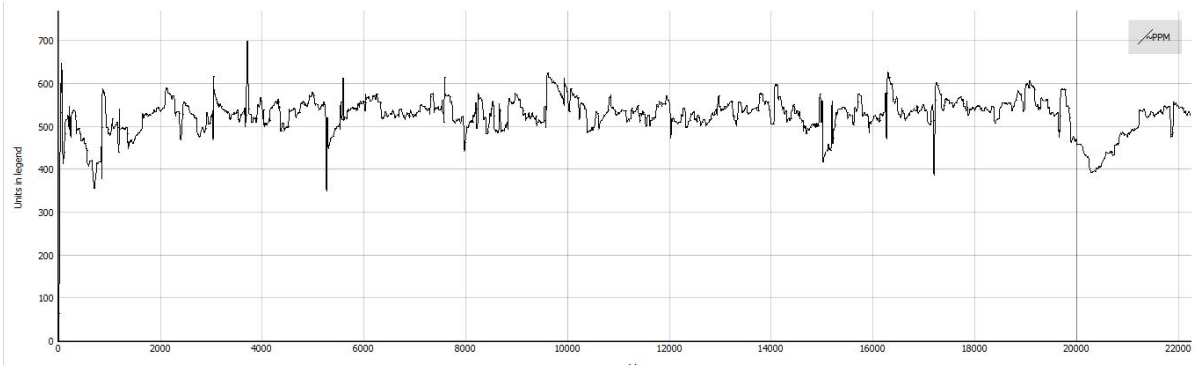

Figure 3.11: CO_2 concentration inside climate chamber during an Airfarm experiment.

3. **Average concentration is obtained from FTIR.** Furthermore, it is assumed that the concentration of CO_2 and H_2O is the average concentration of the test sample, due to the fact that the samples are continuously mixed.

   Validation of assumption 3: All samples in the Airfarm are continuously mixed, as well as being mixed by hand just before extracting the sample from the climate chamber. Multiple drops of the same sample should have the same CO_2 and H_2O concentration for the analysed data to represent the average concentration, and therefore, the plots generated by the FTIR software should overlap and provide the same concentrations. This is the case as can be seen in figure: 3.12

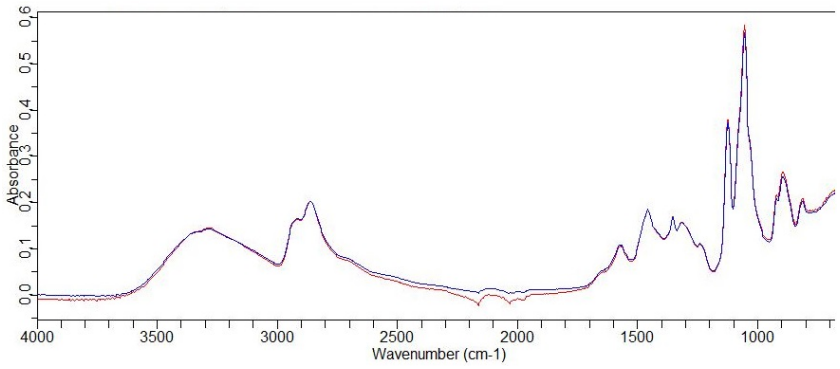

Figure 3.12: Overlapping FTIR graphs from a duplo of samples.

3.3. Vapor-Liquid-Equilibrium Experiments

This thesis covers the entire DAC unit. Where the Airfarm experiments shine light on the specifications of the sorbent streams leaving the absorber, the **Vapor-Liquid-Equilibrium** or **VLE** experiments shine light on the specifications of the streams leaving the stripper. It is for a big part the same test setup as was used by Dowling et al. and will give quantitative knowledge on the conditions of the stripper, as well as the outgoing streams of the stripper, as depicted in red in figure 3.13.

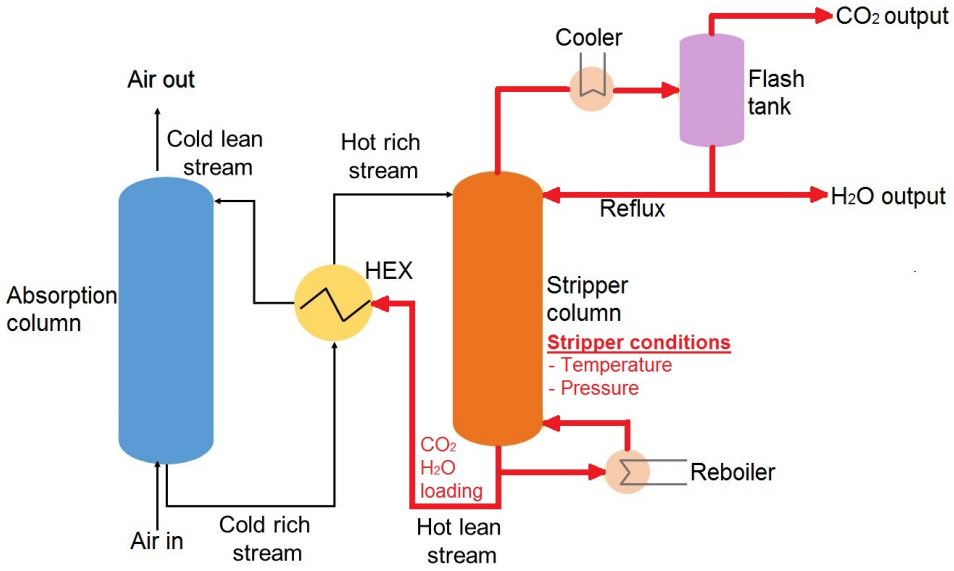

Figure 3.13: Overview of the parameters concerning the VLE experiment, depicted in red.

3.3.1. Requirements

Quantitative knowledge on certain parameters at specific stripper conditions is needed in order to compare different sorbent mixtures on their CO_2 and H_2O capturing performance leads to certain design requirements of the VLE setup. The engineering and manufacturing of the setup is based on those requirements.

- On of the main difficulties of testing a sorbent on its performance is the difficulty of **obtaining repeatable results**. Duplo's will have to be conducted to check if the results are repeatable.

- Since the setup will have to shine light on the performance of the sorbent at specific stripper conditions the whole setup will have to **operate at a specific temperature**. Therefore, accurate temperature control is one of the key requirements for this setup. Furthermore, a **uniform temperature distribution** is desired for accurate results. Hence, good insulation is necessary in order to maintain the pre-set temperature with minimum fluctuation.

- A method of creating a **uniform CO_2 concentration** inside the sample has to be obtained, since it will ensure faster absorbance of CO_2 compared to the situation when a heavily loaded "Ice-Sheet layer" is situated at the gas-liquid interface of the sample. Stirring the sample will ensure a uniform CO_2 concentration in the sample and therefore, decrease the experimental time. Hence, the sample will have to be continuously, mechanically stirred.

- The system will have to be operated at a wide range of pressures, from a vacuum to an over pressure. Therefore, it is necessary to have a well **enclosed system** without any leaks.

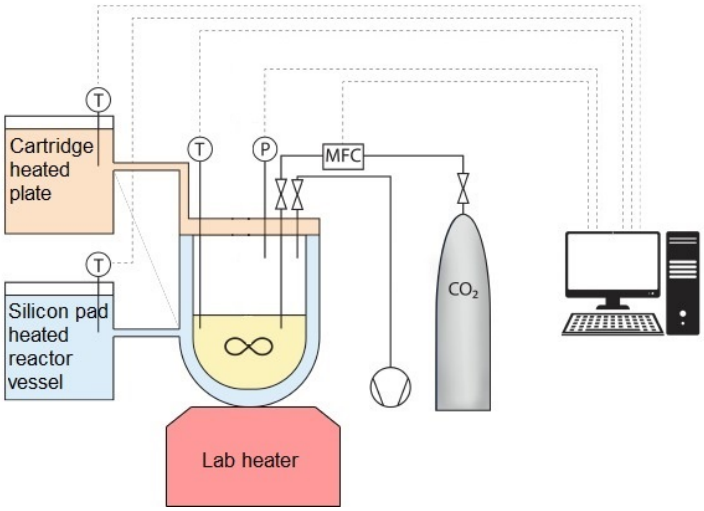

Figure 3.14: Schematic of the VLE test setup as designed by Dowling et al. [36]

3.3.2. Setup Description

A schematic of the setup is shown in figure 3.14. It consists of a reactor vessel, which is custom made out of *Tri-Clamp* tubing for ease of access. Its temperature is controlled by a *MENGSHAX 5V-380V* silicon heating pad surrounding the vessel, by two *Yancheng Yuheng Electric* cartridge heaters placed inside the top plate of the vessel and by a lab heater placed underneath the vessel. The lab heater is a *DLAB MS-H280-Pro* which can be heated up to 280°C and at the same time, continuously mechanically stir the sample at a speed up to 1500 rpm. The top plate of the vessel is custom made out of aluminium and has two functions. It not only holds the two cartridge heaters and a temperature sensor, it also acts as a insulating buffer between the top of the vessel and the outside air. All the tubing is *PFA* flexible tubing and all the fittings are from *Swagelok*, to ensure leak tight fitting, easy installation and resistance for corrosion. Since the setup will have to be able to control the amount of gas supplied to the system three solenoid valves are used. These 12V solenoid valves from *JP Fluid Control* are made of stainless steel and have a maximum operating pressure of 10 bar. In order to know exactly what the feed and operating pressure of the vessel is, two pressure sensors from *AE Sensors BV* are used in this setup. The operating pressure of the vessel ranges from vacuum to 3 bar, and the feed pressure ranges from 1 to 3 bar. Hence the sensors are specified accordingly. In total there are three *Tegg NTC* temperature sensors used per VLE setup with an operating temperature range of -40°C to 300°C. They are installed inside the top plate, between the silicon heating pad and the vessel and inside a thermowell in the vessel. The control of the system is done via a *Printed Circuit Board* or PCB.

3.3.3. Methodology

This setup is used to perform two types of experiments: vapor curve measurements and CO_2 loading measurements, these experimental procedures are both discussed in the following sections.

Table 3.3: VLE experiment parameters

Parameters	
Input	**Output**
Stripping temperature	CO_2, lean loading
Stripper operating pressure	H_2O, lean loading
Sorbent composition	Cyclic capacity (combined with Airfarm results)

Measurement of Vapor Pressure

The aim of this experiment is to measure the equilibrium pressure between the sorbent mixture and H_2O as a result of changing temperature without the addition of any CO_2, as it can shine light on the following KPI's: the pressure ratio of H_2O and CO_2 coming from the stripper as well as the operating pressure of the stripper itself. For this experiment the only parameters which can be varied are the composition of

the sorbent, and the temperature range. After the specific sorbent mixture is loaded in the test vessel the temperature is set to 298.15 K or 25°C. Then the system is evacuated such that a vacuum exists above the liquid inside the vessel. After that, the temperature of the vessel is gradually increased to 393.15 K or 120°C. All the while the vapour pressure above the liquid is measured and logged together with the operating pressure. Which can be compiled into a vapor pressure vs temperature curve, as can be seen in figure 3.15, which shows an example of the vapor curves of pure TEPA with various amounts of H_2O as was researched by Dowling et al. [36].

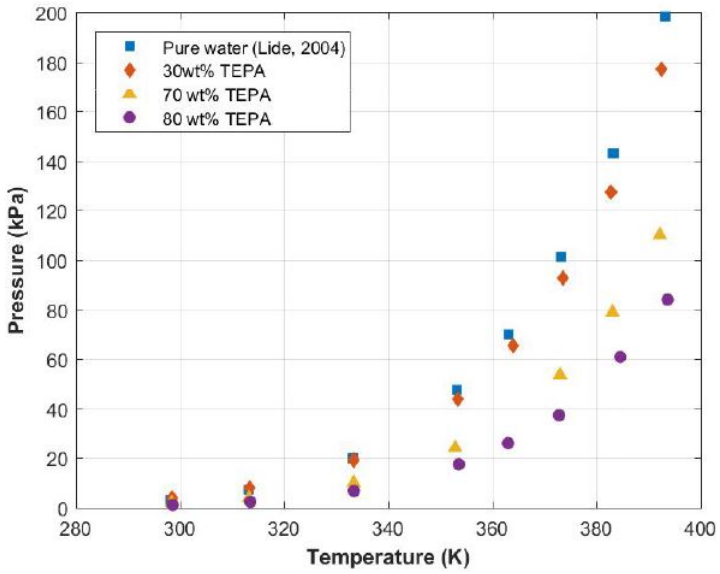

Figure 3.15: Example of vapor curve experiment outcome: the equilibrium vapor pressure vs temperature plot of pure TEPA with various amounts of H_2O [36].

Measurement of CO_2 Loading

The aim of this experiment is to measure the vapor liquid equilibrium between TEPA, diluent, H_2O and CO_2 at different temperatures and compositions. This will provide quantitative knowledge on the amount of CO_2 which is still absorbed at specific stripper conditions, in other words, it provides the CO_2 loading of the lean sorbent stream leaving the stripper. Together with the outcome of the Airfarm experiments this will provide the cyclic capacity of that specific sorbent. The loading of CO_2 in this setup is done by puffing pulses of CO_2 into the test vessel. During each puff, the pressure inside the vessel increases rapidly, followed by a decrease in pressure, as the CO_2 is absorbed by the sorbent mixture. The software recognizes that equilibrium is reached when the pressure inside the test vessel stabilizes and the next puff of CO_2 is added to the vessel. This continues until a pre-set maximum pressure is reached. For this experiment the only parameters which can be varied are the composition of the sorbent, and the temperature, which represents the stripper operating temperature. The experimental procedure consists of three important steps: sample preparation, the loading of CO_2 and cleaning the vessel. The software produces two data files. One raw data file and one VLE data file. In the VLE data file the exact size of the CO_2 puff is logged as well as the partial pressure of the gas in the vessel just before a CO_2 puff, which equals the equilibrium pressure. The equilibrium partial pressure of CO_2 is calculated by equation 3.1. The pressure measured before the first puff of CO_2 is equal to the vapor pressure of H_2O, $p_{H_2O,eq}$. The amount of CO_2 per puff added to the system is calculated from the mass flow controller data, which is provided in normal liters. A normal liter represents a liter of gas at standard pressure and temperature (STP), which is 100kPa and 273.15K. Combined with the ideal gas law, the amount of CO_2 entering the vessel can be converted to moles as in equation 3.2. And from there the total amount of CO_2 inside the vessel can be calculated by the sum of all gas puffs up to that point with equation 3.3.

$$p_{CO_2,eq} = P_{total,eq} - p_{H_2O,eq} \quad (3.1)$$

$$n_{puff} = \frac{P_{STP} * V_{puff}}{R * T_{STP}} \quad (3.2)$$

$$n_{CO_2,total} = \sum_i n_{puff}, i \quad (3.3)$$

where

$p_{CO_2,eq}$ = equilibrium partial pressure of CO_2 [Pa]
$P_{total,eq}$ = equilibrium total pressure of the test vessel [Pa]
$P_{H_2O,eq}$ = equilibrium partial pressure of H_2O [Pa]
n_{puff} = amount of CO_2 in one puff [mol]
P_{STP} = standard pressure, equals 100.000 [Pa]
V_{puff} = volume of one puff [l]
R = gas constant [$\frac{J}{K*mol}$]
T_{STP} = standard temperature, equals 273.15 [K]
$n_{CO_2,total}$ = total amount of CO_2 in test vessel [mol]

The amount of CO_2 inside the vessel which is the gas phase is calculated from the equilibrium pressure with the ideal gas law as can be seen in equation 3.4. From there, the amount of CO_2 which is absorbed can be calculated with equation 3.5. The loading is either defined as the amount of moles of CO_2 absorbed per kilogram of sorbent or per kilogram of TEPA and can be calculated with equations 3.6 and 3.7.

$$n_{CO_2,g} = \frac{p_{CO_2,eq} * (V_{vessel} - V_{sorbent})}{R * T} \quad (3.4)$$

$$n_{CO_2,abs} = n_{CO_2,total} - n_{CO_2,g} \quad (3.5)$$

$$\gamma_{CO_2,sorbent} = \frac{n_{CO_2,abs}}{m_{sorbent}} \quad (3.6)$$

$$\gamma_{CO_2,TEPA} = \frac{n_{CO_2,abs}}{\chi_{TEPA} * m_{sorbent}} \quad (3.7)$$

where

$n_{CO_2,g}$ = amount of CO_2 in the gas phase [mol]
V_{vessel} = total volume of the vessel [l]
$V_{sorbent}$ = volume of the sorbent inside the vessel [l]
T = temperature of the vessel [K]
$n_{CO_2,abs}$ = amount of CO_2 absorbed by the sorbent [mol]
$\gamma_{CO_2,sorbent}$ = the loading of CO_2 into the sorbent [$\frac{mol_{CO_2}}{kg_{sorbent}}$]
$\gamma_{CO_2,TEPA}$ = the loading of CO_2 into the sorbent [$\frac{mol_{CO_2}}{kg_{TEPA}}$]
χ_{TEPA} = mass fraction of TEPA in the sorbent [$wt\%$]
$m_{sorbent}$ = mass of sorbent in vessel [g]

The outcome of this experiment is an absorption isotherm, in the form of a CO_2 partial pressure vs. CO_2 loading plot as is displayed in figure 3.16. This plot provides quantitative knowledge on what the amount of CO_2 in the sorbent is at stripper conditions, which is crucial knowledge for calculation the regeneration energy demand. How this is calculated is elaborated in the section 4.1.

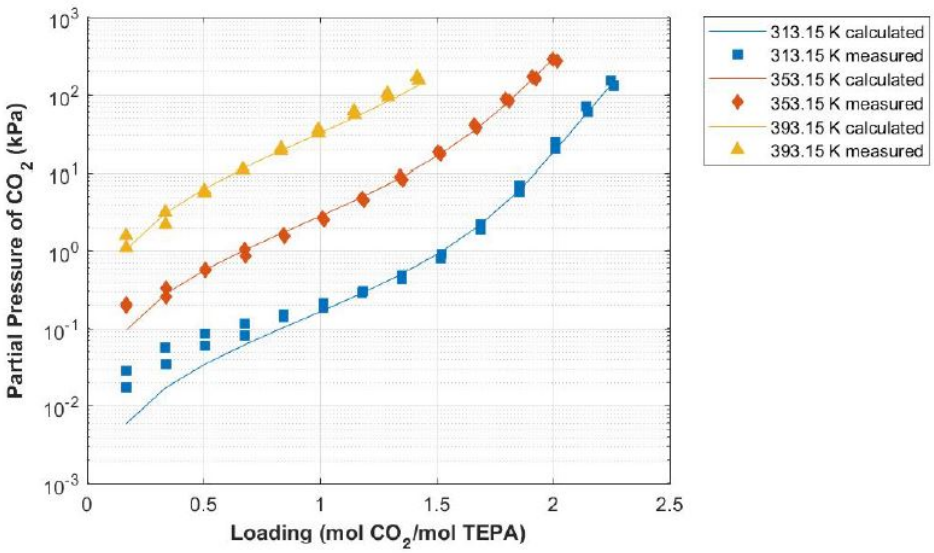

Figure 3.16: Experimental VLE data of equilibrium CO_2 absorption in an aqueous solution of 30 wt% TEPA at 313.15, 353.15 and 393.15 K with her model predictions Dowling et al. [36]

3.3.4. Assumptions

The VLE experiments give valid results only when certain assumptions are met. These assumptions are listed here under.

1. **Ideal gas law is valid for the calculating the amount of CO_2 in the gas phase.** The general gas equation can be used to give a good approximation of the amount of moles of CO_2 in the gas phase. When the operating pressure is low this is a reasonable assumption.

2. **Constant volume of the gas phase in reactor vessel**. During the entire experiment the volume above the liquid is assumed to be constant. In other words, the liquid volume is assumed to remain constant and therefore, the density of the liquid has to remain constant. Even tough it is known that varying the temperature and changing the amount of H_2O and CO_2 in the liquid phase, as it happens during the experiment, changes the liquid volume, following the equation given below:

$$\Delta V = V_0 \cdot \beta \cdot \Delta T \tag{3.8}$$

   where

   ΔV = Difference in liquid volume due to a temperature change $[m^3]$
   V_0 = Liquid volume of original sample $[m^3]$
   β = Thermal expansion coefficient $[1/K]$
   T = Temperature change of liquid $[K]$

   For a pure TEPA sample of 200 ml, going from 20°C to 120°C, combined with a thermal expansion coefficient found for TEPA of 0.000681 [54], this corresponds to a volume change of the liquid phase of 6.8%. Considering that the volume of the gas phase is at least 4 times bigger compared to the liquid phase in the reactor, it is assumed that this change in volume of the gas phase is negligible.

3. **$P_{H_2O,eq}$ is constant**. For the entire run of a CO_2 loading experiment it is assumed that the vapor pressure of H_2O is to remain constant. In other words, the formation of ions in the liquid phase as a consequence of the addition of CO_2 to the system, has a trivial effect on the partial pressure of H_2O in the gas phase. It is only with the help of this assumption the equilibrium partial pressure of CO_2 can be calculated using equation 3.1. It is known that this assumption is not completely true, but in order to be able to calculate the CO_2 loading this has to be assumed.

4. **Equilibrium in reactor vessel is reached.** It is assumed that equilibrium is reached within the reactor vessel when the pressure variation is to remain within 25 mbar.

5. **Uniform CO_2 loading in liquid phase.** It is assumed that continuously stirring the liquid in the test vessel results in a homogeneous CO_2 loading inside the sample.

   Validation of assumption 5: In order to validate assumption 5 multiple samples where drawn from the same test sample and evaluated in the FTIR to check if the CO_2 loading was homogeneous. Variation of the amount of CO_2 was within 0.9% and is therefore assumed to be negligible.

6. **Leak tight reactor vessel.** The reactor vessel is assumed to be leak tight and that no condensation of H_2O is taking place.

   Validation of assumption 6: After the reactor vessel was evacuated to 0.04 bar, it was observed that the pressure inside the vessel remained constant, hence the system had to be leak tight.

7. **No H_2O evaporation at lowest operation pressure.** It is assumed that negligible H_2O evaporation occurs when the vessel was evacuated. In other words, the ratio of sorbent to H_2O is assumed to be constant.

3.4. Re-pumping Experiments

Quantitative knowledge on the kinetics of absorption is needed in order to make statements on the size of the absorber. The main goal of this experiment is to get a better understanding of the absorption performance of the sorbent in a ZEF DAC absorption setup. Following the research of Matteis et al. where he found that actively mixing the sorbent in the absorption column proved beneficial regarding the performance of the absorption process, a similar setup is used to characterize the kinetics of absorption of the sorbent in the **re-pumping experiments**. The re-pumping experiment utilizes a similar setup to Matteis's active mixing setup and is therefore explained in this section.

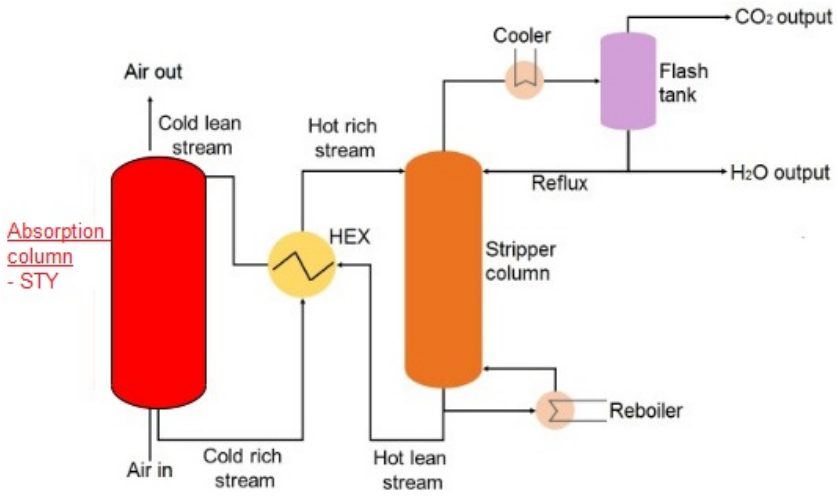

Figure 3.17: Overview of the sorbent parameters concerning the re-pumping experiment, depicted in red

3.4.1. Requirements

The requirements of the re-pumping experiments are stated below.

- The sorbent has to be **actively mixed** while the absorption process is taking place. This reassures a homogeneous CO_2 concentration and therefore, increases the absorption performance of the sorbent.
- **Sample collection** has to be possible **without stopping** the experiment.

- Since the absorption performance is dependent on the **flow rate of the sorbent and the flow rate of the overflowing air, both need to be adjustable**.

- Since the absorption of CO_2 occurs at the gas-liquid interface, **maximizing its surface area** is desirable.

- As the absorption performance depends strongly on ambient conditions it is necessary to be able to **fit the entire setup inside the climate chamber**.

3.4.2. Setup Description

A schematic of the setup is shown in figure 3.18. It was designed by previous students at ZEF [82] and is utilized for this research for sorbent performance analysis. With the exception of the absorber channels, where Matteis et al. utilized plates with flow channels, the setup used during this research utilizes a new absorber design with wire guides, as designed by Hanafi et al. The absorption section is custom made from polyactic acid (PLA) at ZEF and aims to maximize the surface area between the sorbent and the overflowing air. The setup consists out of a gear pump from *Surflo KGP-001 12V*, which pumps the sorbent from the reservoir to the top of the absorption plate. The operational voltage of the pump can be altered to adjust the flow rate of the sorbent. The air flow is provided by an *ADDA plastic fan*, which can provide a maximum airflow up to 5.247 m^3/min. The container is a laboratory graded glass beaker in which the sorbent is stirred by a *Dlab MS-H280-pro* magnetic stirrer. This way the sorbent completes the loop and is continuously stirred.

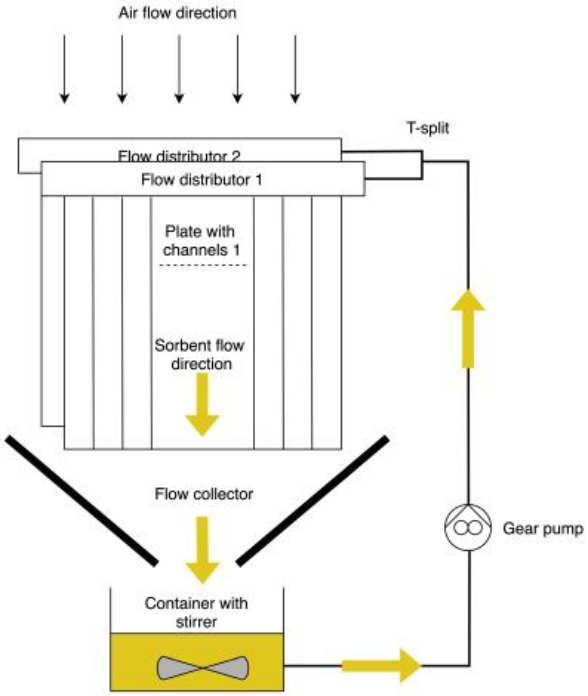

Figure 3.18: Schematic of the re-pumping experiment as designed by Matteis et al. [82]

3.4.3. Methodology

The methodology of the re-pumping experimental investigation include the parameters depicted in table 3.4. The experiment commences with a fresh sorbent, without CO_2 and H_2O, which is then pumped through the setup. Sample collection is done using a 1 ml transfer pipette, at the outlet of the flow collector at specific time intervals. All the samples are evaluated in the *Carry 360 FTIR spectrometer* for CO_2 and H_2O concentration until equilibrium is reached and the experiment is finished.

Table 3.4: Experimental parameters: re-pumping experiments

Parameters	
Input	**Output**
Initial sorbent conditions	CO_2, rich loading
Air flow rate (or fan power)	H_2O, rich loading
Sorbent flow rat (or pump power)	Space-Time-Yield
Absorber area	

The *TQ Analyist*^{TM} software presents the concentrations in wt% from where the rich loading of CO_2 and H_2O in moles per kilogram of sorbent can be calculated using the following equation:

$$\gamma_{CO_2,H_2O} = \frac{1000 * \chi_{CO_2,H_2O}}{\chi_{sorbent} * M_{CO_2,H_2O}} \tag{3.9}$$

where

χ_{CO_2,H_2O} = mass fraction of CO_2 or H_2O in the sample $[wt\%]$
$\chi_{sorbent}$ = mass fraction of the actual sorbent in the sample $[wt\%]$
M_{CO_2,H_2O} = molar weight of either CO_2 or H_2O $[\frac{g}{mol}]$

From where, two different types of space-time-yield can be calculated. The absolute STY represents the amount of CO_2 or H_2O over the area of absorption at a specific time interval and the cumulative STY is that absorbed amount over the area of absorption at a specific time from the start of the experiment. The can be calculated using the following equations:

$$STY_{absolute} = \frac{\Delta\chi_{CO_2,H_O} * m_{sorbent}}{1000 * A * \Delta t} \tag{3.10}$$

$$STY_{cumulative} = \frac{\chi_{CO_2,H_O} * m_{sorbent}}{1000 * A * t} \tag{3.11}$$

where

STY = Space-time-yield, flux of CO_2 or H_2O into sorbent per area $[\frac{mol}{m^2 s}]$
$m_{sorbent}$ = initial weight of the sorbent used in the experiment $[mol]$
A = total area of absorption in the test setup $[m^2]$
t = time of the absorption process $[s]$

The outcome of this experiment is a STY vs CO_2 loading curve, which, not only helps to asses the performance of the absorption process, but also provides an operating window regarding the STY for the sorbent in the absorber. An example of such a curve is presented in figure 3.19. Furthermore, from the obtained STY, the required area of the actual ZEF DAC unit can be approximated.

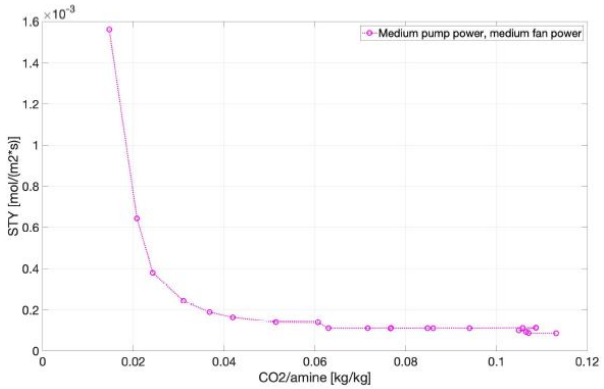

Figure 3.19: Cumulative STY vs CO_2 loading curve. Example of re-pumping experiment outcome by Matteis et al. [82].

3.4.4. Assumptions

The assumptions relevant to the re-pumping experiment are described below:

1. **All three assumptions for the Airfarm experiment hold for the re-pumping experiment.** As the sample collection and environment is quite similar to the Airfarm experiment, the same assumptions are relevant to this experiment. They can be seen in section 3.2.4.

2. **No reduction in overall amount of sorbent.** Collecting the samples will reduce the overall amount of sorbent. However, as every drawn sample is less than 1ml, this is a negligible amount compared to the overall amount. Therefore, during the experiment it is assumed that the initial amount of sorbent is conserved.

3.5. Degradation Experiments

Previous research at ZEF proved the degradation of the sorbent [48]. Sorbent degradation in the form of amine site losses can possibly be caused by subjection to oxygen, CO_2 and/or stainless steel. Therefore, a method of testing is set up which varies only one variable per test, to see which variable plays the biggest part in sorbent degradation and if the added diluent has an effect on it. The degradation process is known to be accelerated at higher temperatures [48]. The maximum temperature of the DAC system is set by ZEF to be 120°C for the stripper, thus the degradation tests will be performed at 120°C. These experiments are merely performed to give an indication of the degree of degradation, in order to make statements about the effect of adding a diluent on sorbent degradation and provide a heading for future research at ZEF through the recommendations.

3.5.1. Requirements

The requirements of the degradation experiments are stated below.

- **The temperature** of the sorbent has to be **uniform** and needs to be **adjustable**.
- **Sample collection** has to be possible **without stopping** the experiment.
- The sample will have to be **continuously mixed** to ensure a uniform mixture.
- Some of the experiments require the lack of oxygen, hence the **reactor vessel will have to be airtight**.

3.5.2. Setup Description

For the thermal degradation experiments two different setups will be used. In the first setup the sorbent can be open to the surrounding air, as this might affect the degradation due to the presence of oxygen. The second setup requires the sorbent to be closed of from the surrounding air, as this setup is used to map the degradation in the absence of oxygen.

Open Setup

The open setup, as schematically displayed in figure 3.20, consists of a laboratory graded glass reactor vessel, which is isolated with glass wool. The reactor vessel is heated and magnetically stirred with a *Stuart US-152* lab heater. The lab heater can be set to a certain temperature or let the temperature be controlled with the *SCT1* digital contact thermometer, which is submerged in the test sample for high accuracy. The temperature of the sample will be double checked by a *BENETECH GM300* infrared thermometer.

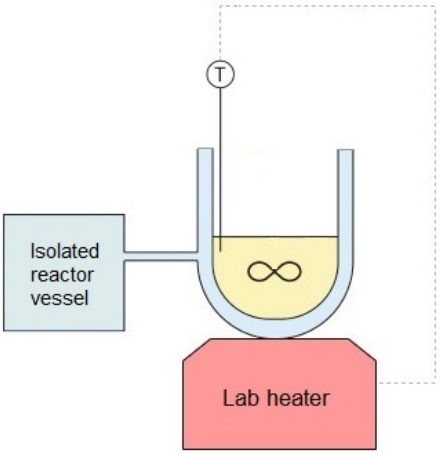

Figure 3.20: Schematic of the open to air setup for the thermal degradation experiments

Closed of Setup

The airtight laboratory graded glass reactor vessel, in which the sample is closed of from oxygen, is placed inside a *BINDER E028-230V-T* furnace as can be seen in figure 3.21.

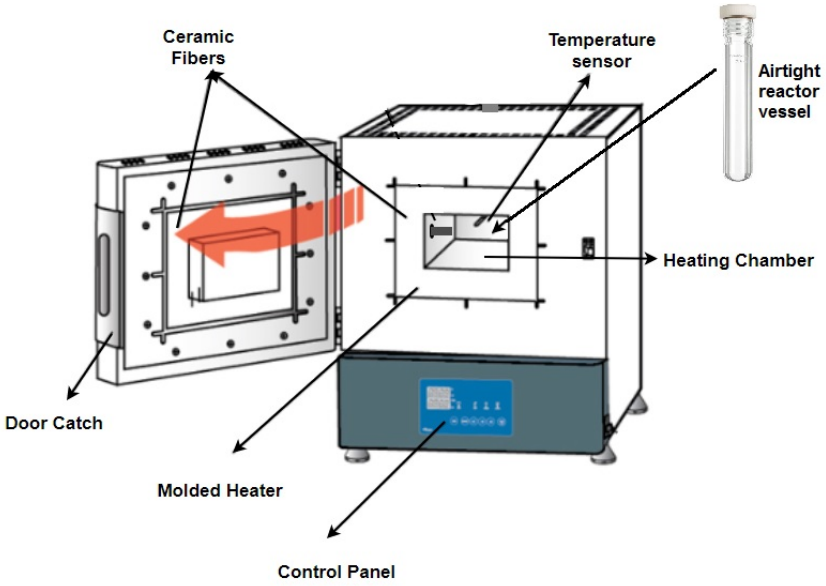

Figure 3.21: Schematic of the furnace containing the closed of reactor vessel

3.5.3. Methodology

The methodology of the degradation experimental investigation include the parameters depicted in table 3.5. All the experiments will be performed at 120°C to which the temperature of the sample is gradually increased. The following four experiments will be performed with the optimized sorbent obtained from test phase one:

- Fresh, unloaded sorbent, so without CO_2 and H_2O, The samples are flushed with nitrogen to evacuate the reactor tubes from air, thus this experiment is without O_2. The sorbent is not in contact with stainless steel and at a temperature of 120°C. To see if only applying heat will degrade the sorbent.
- This experiment is under the same conditions as the first one but with a loaded sorbent, so with CO_2 and H_2O according to the equilibrium loading obtained from the Airfarm experiments. Yet

without O_2 and without stainless steel at 120°C. To evaluate if CO_2 and H_2O play a role in the degradation of the sorbent.

- Fresh, unloaded sorbent at the start, so without CO_2 and H_2O. Although this time in contact with the surrounding air, thus in contact with O_2. The sorbent will therefore absorb CO_2 and H_2O as the experiment proceeds, so these concentrations will have to monitored. This experiment is without stainless steel at 120°C. To see if the presence of oxygen plays a big role in the degradation of the sorbent.
- Fresh, unloaded sorbent at the start, so without CO_2 and H_2O, in contact with the surrounding air, thus in contact with O_2. The sorbent will therefore absorb CO_2 and H_2O as the experiment proceeds, just like the previous experiment. However, this experiment is with the stainless steel temperature probe submerged in the sorbent, which is also at 120°C. To see if the presence of stainless steel accelerates the degradation of the sorbent.

For every experiment samples are drawn every 24 hours for the duration of 7 days. Every sample is evaluated in the *Carry 360 FTIR spectrometer* for analysis. Samples which show alterations in the FTIR results will be analysed through titration on amine site loss. An extensive manual on the titration is provided in Appendix A.5.

Table 3.5: Experimental parameters: thermal degradation experiments

Parameters	
Input	**Output**
Initial sorbent concentration	Amine site loss
Temperature	Formation of urea

4

Modelling Framework

This chapter describes the models which are developed and used during this thesis project. Firstly, the regeneration energy model is explained. Secondly, the full DAC model used for the design of the DAC unit is elaborated.

4.1. Regeneration energy model

The regeneration energy consumption accounts for the biggest part of the total energy consumption of the DAC unit. Therefore, one of the key parameters on which a sorbent is scored is its regeneration energy consumption. In order to be able to decide on which diluent will perform best at the end of phase one of testing, the regeneration energy model is used to evaluate the data obtained from the Airfarm and the VLE experiments.

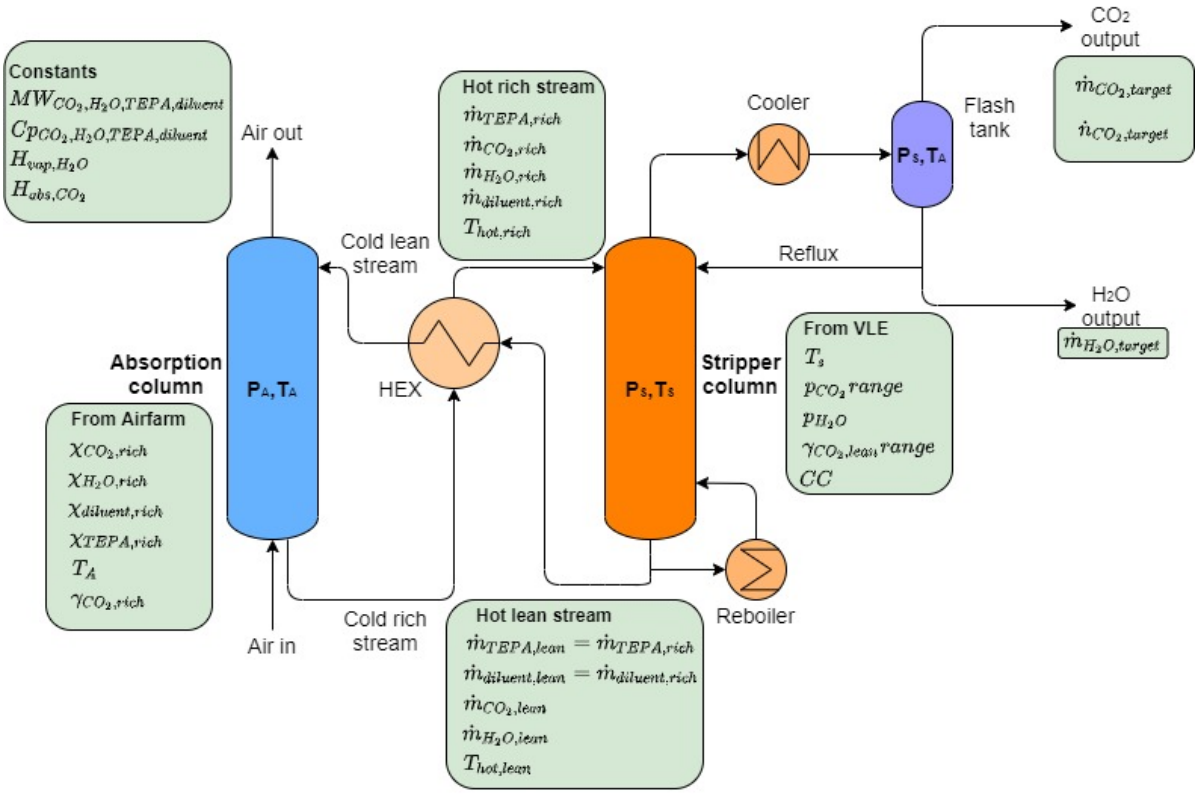

Figure 4.1: Schematic overview of the ZEF DAC unit including the process parameters needed for the regeneration energy model.

4.1.1. Model Assumptions

The regeneration energy model is used to compare the different diluents on their regeneration energy demand. Therefore, some assumptions are made which simplify the model, as this model is not used to make accurate predictions of the sorbent in the real ZEF DAC unit, but merely to compare the different diluents on their performance after phase one of testing. These assumptions are listed below:

- The stripping column is assumed to be a **single stage** flash separator.
- It is assumed that the column operates at **steady state**. In other words, no accumulation of mass or energy occurs inside the stripper column.
- The stripping column is assumed to **operate at equilibrium**. In other words, the VLE and vapor curve assume equilibrium inside the stripper column.
- **Heat losses** from the stripper column are assumed to be **negligible**.
- It is assumed that no loss of sorbent occurs inside the stripper column. In other words, **negligible evaporation of TEPA + diluent** occurs. Therefore, the p_{CO_2} and p_{H_2O} are assumed to be the only contributors to the absolute pressure inside the stripper column.
- The vapor curve obtained from the VLE experiments as described in section 3.3.3 is based on the vapor pressure of H_2O alone, hence without CO_2. It is assumed that the presence of **CO_2 in the vapor phase has a negligible effect on the vapor curve**. It is known that this is not true, but Dowling et al. proved that the effect of CO_2 on the vapor curve is relatively small [36].
- **The specific heat** of the different components is assumed to be **constant**. Therefore, **average values** are used for the calculations. The specific heat is based on the weight fraction of the individual components in that specific stream. This gives a fair indication of the specific heat of the present mixtures even though it deviates slightly from reality.
- **The heat of absorption** of the different components is also assumed to be **constant**, and based on **average values**. This holds true for temperatures above 80 °C. As the stripping column operates at 120°C, this is a valid assumption. The constants are listed in table 4.1.
- It is assumed that the **heat ex-changer (HEX) can heat the rich stream up to 70°C** making use of the hot lean stream leaving the stripper column.
- ZEF has specified a **daily CO_2 target of 18.75 moles**, assuming the solar-powered plant can operate for 8 hours a day, this results in $\dot{m}_{CO_2,target}$ equaling 2.344 mol/hr or 0.103 kg/hr.
- For the ZEF plant to work effective, H_2 and CO_2 have to react in a molar ratio of 3:1 to form methanol. Therefore, the **daily capture target for H_2O is 56.3 moles**, which results in $\dot{m}_{H_2O,target}$ equaling 7.031 mol/hr or 0.127 kg/hr. Every mole of H_2O which is separated above this is purged from the system for simplicity of the model. It must be noted that this is not desirable, as for every extra mole of H_2O that is vaporized an energy expense of roughly 40 kJ is wasted.

4.1.2. Model inputs

To start, the model requires certain constants as input, which are set out in table 4.1.

Table 4.1: Overview of constants for regeneration energy model.

Constant	Description	TEPA	H_2O	CO_2	Units	Source
M	Molar weight	189.314	18.015	44.010	$[g/mol]$	[115]
c_p	Specific heat	2.554	4.217	0.911	$[kJ/kgK]$	[115]
H_{abs}	Heat of absorption	0	0	85	$[kJ/mol]$	[36]
H_{vap}	Heat of vaporization	0	2202.1	0	$[kJ/kg]$	[115]
		DEG	PEG-200	Butanediol		
M	Molar weight	106.12	196	90.12	$[g/mol]$	[115]
c_p	Specific heat	2.303	2.157	2.21	$[kJ/kgK]$	[115]

A number of inputs obtained from the Airfarm and the VLE experiment is required to run the regeneration energy model. These are listed in table 4.2

Table 4.2: Overview of inputs for regeneration energy model.

Input	Description	Unit	Experiment
χ_{rich}	Mass fractions of rich sorbent stream	$[wt\%]$	Airfarm
$T_{hot,rich}$	Hot, rich feed stream temperature	$[^{\circ}C]$	
T_s	Stripper temperature	$[^{\circ}C]$	VLE
$\dot{n}_{CO_2,target}$	CO_2 capture target	$[mol/s]$	ZEF
p_{CO_2}	Partial pressure of CO_2 range	$[mbar]$	VLE
p_{H_2O}	Partial pressure of H_2O at 120°C	$[mbar]$	VLE
$\gamma_{CO_2,lean}$	Lean loading range	$[mol_{CO_2}/kg_{TEPA}]$	VLE

4.1.3. Model Description

The desired outcome of the model is a the regeneration energy demand of the stripper using a specific sorbent. However, this depends on a number of process parameters, such as the temperature of the stripper (T_s) and the operating pressure of the stripper (P_s). The operating temperature of the stripper is set to 120°C, which is the same temperature at which the VLE experiments are conducted. The operating pressure of the stripper depends on the partial pressure of H_2O (p_{H_2O}) which is obtained directly from the vapor pressure curve of the VLE experiment, and the partial pressure of CO_2 (p_{CO_2}). The model depicts the regeneration energy use at this pressure ratio of p_{H_2O}:p_{CO_2} of $3:1$ and shows the absolute operating pressure when this ratio is met, this parameter makes it easy to compare the different diluents. By calculating the energy use the following KPI's is obtained: the energy use per mole of CO_2 at the desired pressure ratio.

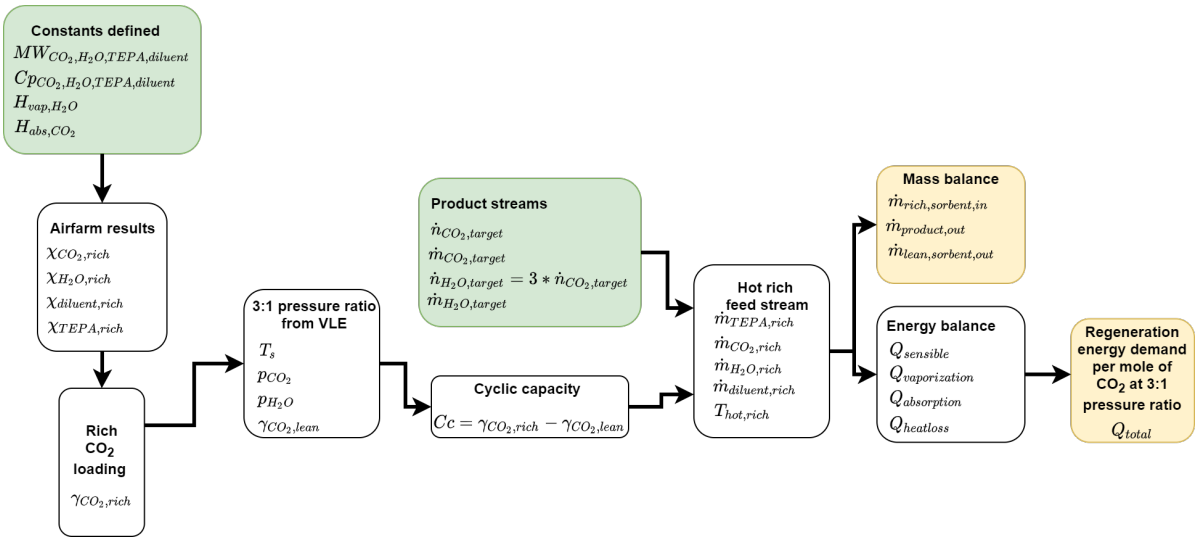

Figure 4.2: Visual interpretation of the regeneration model.

The model commences by calculating all the inputs which are necessary to setup the mass balance, which in turn is necessary to setup the energy balance. The first step is to calculate the rich loading of CO_2 from the concentrations obtained from the Airfarm experiment with the following equation:

$$\gamma_{CO_2,rich} = \frac{1000 * \chi_{CO_2,rich}}{\chi_{TEPA,rich} * M_{CO_2}} \qquad \left[\frac{mol_{CO_2}}{kg_{TEPA}}\right] \tag{4.1}$$

From there, the partial pressure of H_2O (p_{H_2O}) is obtained from the VLE experiments at a temperature of 120°C. Due to the required pressure ratio of p_{H_2O}:p_{CO_2} of $3:1$, the partial pressure of CO_2 (p_{CO_2}) is assumed to be one third of p_{H_2O}. The absolute pressure of the stripper is calculated by: $P_{abs} = p_{CO_2} + p_{H_2O}$. The lean CO_2 loading is obtained from the VLE data at the specific p_{CO_2} from where the

cyclic capacity can be calculated using the equation as can be seen in figure 4.2. The next step is to calculate the mass flow of TEPA, under the assumption that no TEPA evaporates. Consequently, the mass flows of the other three components is calculated through the mass balance. Now all the mass flows are known, the energy balance can be setup which is comprised of the following:

$$Q_{tot} = Q_{sens} + Q_{vap} + Q_{abs} \tag{4.2}$$

It must be noted that for this model, it is assumed that the stripper suffers from negligible heat loss. The model produces the total regeneration energy demand in the following units: W, kJ/mol_{CO_2}, MJ/kg_{CO_2} and kWh/ton_{CO_2}.

4.2. Full DAC Model

One of the main research goals of this thesis project is to design a ZEF DAC unit utilizing the optimized sorbent. In this section, the model which is used to design the DAC unit is described. The goals of the model is to have a tool for predicting the specifications of the DAC design utilizing the optimized sorbent. Close observation of the system overview in figure 2.14 shows that the system can be dissected into two main subsystems; the absorption column and the stripper column. The DAC model will be setup accordingly.

4.2.1. Absorber Model: Description

The absorber side of the model will be used to make predictions on the size and energy use of the absorption column. A model regarding the mass transfer of CO_2 into pure TEPA has been previously researched by Matteis et al. [82]. Originally, this model was ought to be updated for the optimized sorbent and used for this research project. Unfortunately, at this point of ZEF's research, there are too many unknowns for the new optimized sorbent for the mass transfer model to give accurate predictions. Which specific characteristics that have to be researched regarding the new sorbent in order for the mass transfer model to be accurate is stated in the recommendations section 7.2. It is for these reasons that the predictions on the performance and size of the absorber are based on the experimental values obtained from the re-pumping experiments. The re-pumping experiments provide an absolute STY vs CO_2 loading curve. This curve is used as the input for the absorber side model. A schematic overview regarding all the important process parameters is provided in figure 4.3.

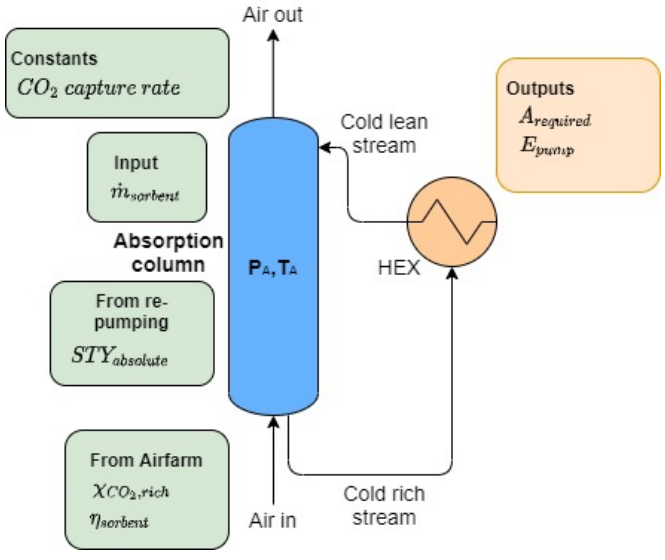

Figure 4.3: Schematic overview of the absorber side of the ZEF DAC unit including the process parameters needed for the absorber model.

The required absorber area will be calculated using the following equation:

$$A = \frac{CO_2 \ capture \ rate}{STY_{absolute}} \tag{4.3}$$

As seen before in figure 3.19 of section 3.4, the STY is a function of the CO_2 concentration of the sorbent. Consequently, the required area of the absorber is a function of the rich CO_2 loading, which will be obtained for the optimized sorbent from the Airfarm experiments. When a certain range of rich CO_2 loading is chosen for the absorption column, this will provide an operating range of the STY. This relation will be evaluated in section 6.1. The required energy demand for the gear pump in the absorber depends on the sorbent mass flow rate, the sorbent viscosity and the diameter of the pipes. The diameter of the pipes is set to 1cm according to recommendations from Matteis's research [82].

4.2.2. Absorber Model: Assumptions

The following assumptions hold for the absorber model:

- **During absorption it is assumed that the sorbent properties remain constant.** The change in CO_2 concentration over one pass through the absorption column is ought to be small enough for the viscosity of the sorbent to be assumed constant throughout the absorption column. In reality, it has been observed that the viscosity rises during absorption. Research of Matteis et al. proved this to be a valid assumption as the changes in residence time of the sorbent on the absorption column were very slim. Indicating that the viscosity does not effect the flow velocity by much.

- **It is assumed that the pressure drop regarding the air side is negligible compared to the pressure drop on the sorbent side.** Therefore, it is assumed a fan of with a power of 20 W operating at full power is sufficient for the airflow through the absorption column [82].

4.2.3. Stripper Model: Description

The stripper side of the model used for this research project will be an evaluation of the proven stripper model following van de Poll's research. The model is setup through different steps as can be observed on the next page in figure 4.4. The model solves its equations individually for each stage via a stage-by-stage approach which is displayed in figure 4.4 by the dashed area. Experimental data following the VLE experiments as well as certain inputs and initial guesses are required for the model to start. The experimental data is fitted to obtain an entire field of water curves and isotherms. From these isotherms a certain p_{CO_2} and p_{H_2O} is obtained for every stage. A mass balance, an energy balance and Rachford-Rice are solved to obtain the stage specific unknowns. Subsequently, these obtained unknowns are compared to the initial guesses. The final answers are presented when the error is small enough. When the error is still too large, the obtained answers are then used as inputs for the new loop making this an iterative process. Each step is elaborated in the following sections.

4.2.4. Stripper Model: Inputs

The following inputs are required to run the stripper model:

Table 4.3: Overview of inputs for stripper model.

Input	Description	Unit
N	Number of stages	[-]
RR	Reflux ratio	[-]
T_{reb}	Reboiler temperature	$[^{\circ}C]$
T_{feed}	Feed temperature	$[^{\circ}C]$
P	Operating pressure	$[mbar]$
γ_{feed}	CO_2 loading of feed	$[mol_{CO_2}/kg_{TEPA}]$
χ_{feed}	Mass fractions of feed	$[wt\%]$
F_{rich}	Mass flow of feed	$[mol/s]$

The reflux ratio (RR) is defined as the reflux stream divided by the product stream. Apart from the inputs listed above the model requires the specific heat of the liquid ($C_{p,liq}$) and vapor ($C_{p,vap}$) phase and the heat of absorption (H_{abs}) of all the substances which are present in the stripper. The exact constants used for the full DAC design using the optimized sorbent are listed in table 6.1 in section 6.2.

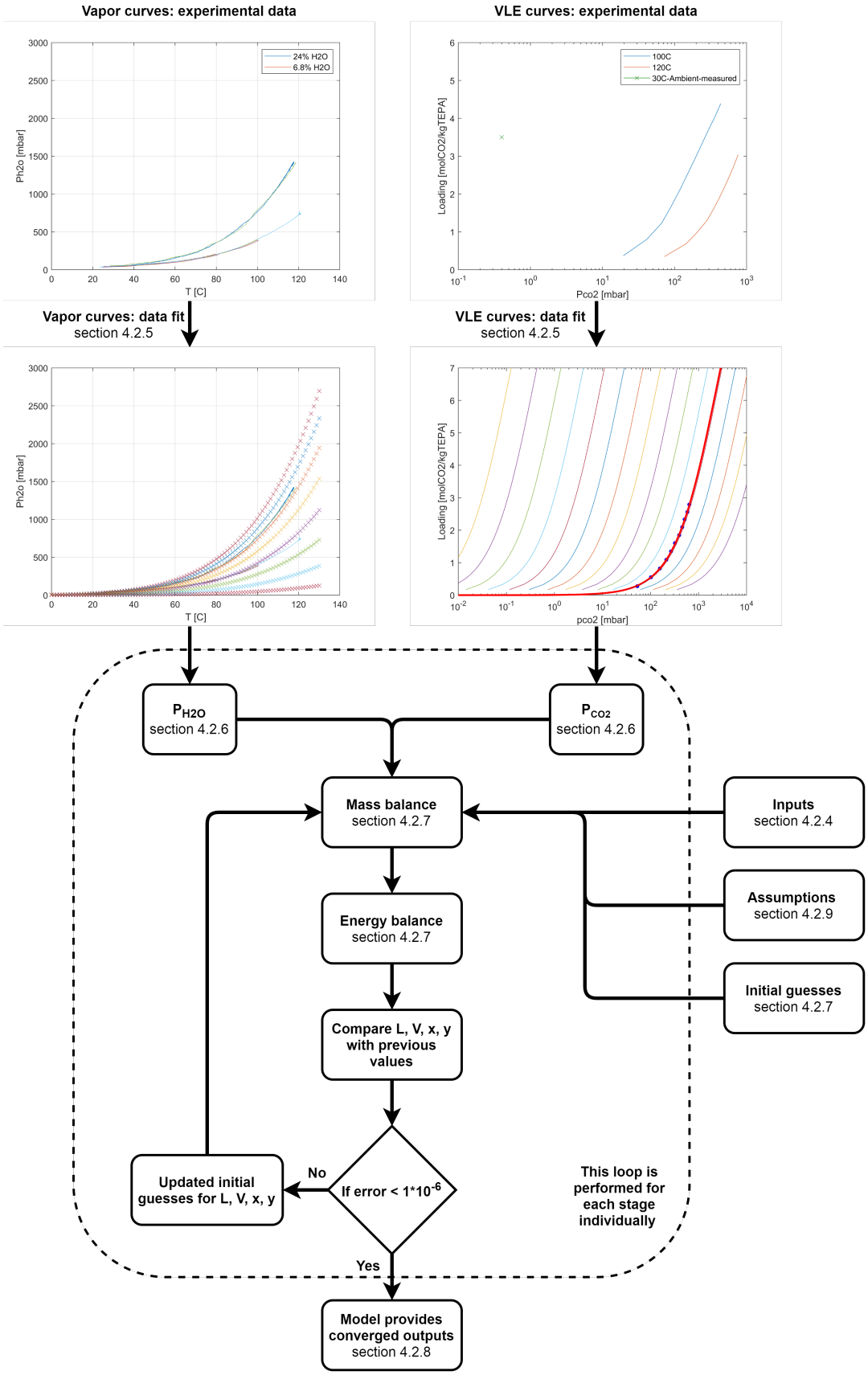

Figure 4.4: Schematic overview of the stripper side of the the model.

4.2.5. Stripper Model: Data Fitting

For the stripper model to run, an entire field of water curves and isotherms has to be present. It would take too much time to run the VLE experiment at every temperature from 0°C to 120°C, while varying the H_2O concentration. Therefore, the experimental data obtained from the VLE experiments will have to be accurately fitted. A comparison between the following five methods of data fitting will be made, where after the best fit will be utilized to produce the field of isotherms.

- Linear
- Langmuir
- Freundlich
- Sips
- Toth

The comparison and the specific fit used for the DAC design is provided in Appendix B.5. Regarding the VLE data curves, the Clausius-Clapeyron equation allows for the calculation of a second data point with a different partial pressure of CO_2 ($P_{CO_2,2}$) and different temperature (T_2) at a constant loading using equation 4.4 [36].

$$ln\left(\frac{P_{CO_2,2}}{P_{CO_2,1}}\right) = \frac{-H_{abs}}{R}\left(\frac{1}{T_2} - \frac{1}{T_1}\right) \tag{4.4}$$

This equation holds for low temperatures and pressures, such that the gas may be approximated by the ideal gas law. For this iteration of the Clausius-Clapeyron relation it is assumed that the specific volume of the gas phase greatly exceeds the specific volume of the liquid phase at these low temperatures [129]. Furthermore, the assumption that the heat of absorption (H_{abs}) remains constant over the temperature range between T_1 and T_2 is made, as is evaluated for the optimized sorbent in section 6.2.2. Lastly, R depicts the universal gas constant.

4.2.6. Stripper Model: Partial Pressure Functions

After the experimental data is fitted to form an entire data set of water curves and isotherms, the partial pressure of CO_2 and H_2O both have to be obtained from these data sets. Therefore, two functions have been created which are depicted below.

$$p_{CO_2} = f(T, \chi_{feed}, \gamma_{feed}, H_{abs}) \tag{4.5}$$

$$p_{H_2O} = f(T, x) \tag{4.6}$$

Where x depicts the composition vector of the liquid phase. The function for CO_2 utilizes the Clausius-Clapeyron relation (equation 4.4) and the fitted data set to obtain the partial pressure of CO_2 at any given temperature and loading.

The function for H_2O utilizes the modified Raoult's law, as presented in equation 4.7, which is an extension of the Raoult's law. As the modified law allows for correction of the liquid phase non-idealities [99]. Subsequently, Antoine's Equation (4.8) is used for the pure component vapor pressure of H_2O, followed by Wilson's theory for a binary system [36]. The equations used for this function are presented below in chronological order. The Wilson parameters (Λ_{12} & Λ_{21}) will be fitted such that the generated water curves coincide with the experimental water curves, a comparison for the fitted water curves is provided in Appendix B.2. The activity coefficient (γ_i) for a binary system is calculated using equation 4.9, obtained from Wilson's theory. Finally, the modified Raoult's law is rewritten to equation 4.10 to calculate the partial pressure of H_2O, while neglecting the vapor phase non-ideality [36].

$$y_i \phi_i P_{tot} = x_i \gamma_i P_i^{sat} \tag{4.7}$$

$$log_{10} P_{H_2O}^{sat}(T) = A - \frac{B}{C + T} \tag{4.8}$$

$$ln(\gamma_1) = -ln(x_1 + \Lambda_{12} x_2) + x_2 \left[\frac{\Lambda_{12}}{x_1 + \Lambda_{12} x_2} - \frac{\Lambda_{21}}{x_2 + \Lambda_{21} x_1}\right] \tag{4.9}$$

$$p_{H_2O} = \gamma_1 x_1 P_{H_2O}^{sat}(T) \tag{4.10}$$

Where y_i resembles the vapor mole fraction, ϕ_i resembles the fugacity coefficient, x_i resembles the liquid phase mole fraction, P_i^{sat} resembles the saturation vapor pressure of the pure component i and P_{tot} resembles the total pressure of the system. The Antoine coefficients were obtained from the Dortmund Databank [12] and are stated in appendix C.2. The partial pressures of CO_2 and H_2O are then obtained for the stage specific conditions.

4.2.7. Stripper Model: Single Stage

At the heart of the stripper model lies the set of equations it solves per stage [117]. The first simplification that has been made is that every stage is modelled as a flash tank as is schematically illustrated in figure 4.5. The flow into the stage is combined to the feed mass flow F_i as in equation 4.11, with its composition $z_{i,j}$ as in equation 4.12.

$$F_i = A_i + L_i + V_{i+1} \tag{4.11}$$

$$z_{i,j} = \frac{A_i z_{Ai,j} + L_i x_{i,j} + V_{i+1} y_{i+1,j}}{F_i} \tag{4.12}$$

Where F_i resembles the total feed mass flow flowing into single stage i, A_i resembles the additional mass flow into stage i, L_i resembles the liquid flow entering stage i from the stage above, V_{i+1} resembles the vapor flow entering stage i from the stage below. Furthermore, $z_{i,j}$ resembles the composition of the total feed mass flow and $z_{A_{i,j}}$ resembles the composition of the additional mass flow into stage i. In order to solve the stage specific unknowns, a mass and energy balance are solved for every stage.

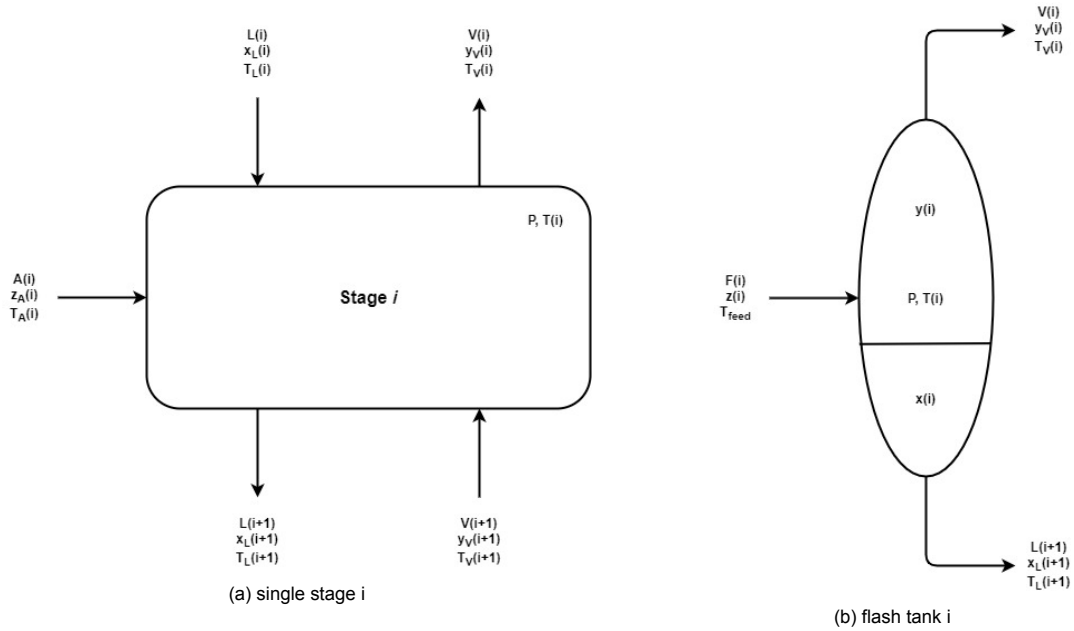

Figure 4.5: Schematic of single stage simplification to a flash tank at pressure P_i and temperature T_i including the relevant characteristic of the in- and outgoing flows. The schematics were made by van de Poll [117].

Mass Balance

For each stage the mass balance of the in- and outgoing total and component specific flows is solved through a trial-and-error iterative method as described in Appendix B.3 with the help the following equations [117]:

$$F_i - L_{i+1} - V_i = 0 \tag{4.13}$$

$$F_i z_{i.j} - L_{i+1} x_{i+1,j} - V_i y_{i,j} = 0 \tag{4.14}$$

The calculation for this iterative solution is obtained with the Rachford-Rice equation (equation B.3) and is extensively elaborated in Appendix B.3. From this all the stage specific flows are calculated.

Energy Balance
The energy balance of a single stage i is comprised of the heat of absorption, heat of desorption and the sensible heat of the mass flows flowing in and out of the stage. The energy balance solved is the following: [117]

$$Q_{tot,i} = Q_{L_i} + Q_{V_i} + Q_{A_i} + Q_{abs_i} \tag{4.15}$$

Where $Q_{tot,i}$ resembles the total amount of heat flowing into the stage i, Q_{L_i} resembles the sensible heat by the liquid inflow, Q_{V_i} resembles the sensible heat by the vapor inflow, Q_{A_i} resembles the sensible heat by the additional feed into the stage and Q_{abs_i} resembles the heat of absorption required to absorb the difference between the gas in- and out flow. All the sub factors of the energy balance are further elaborated in Appendix B.4. Note that the assumption is made that the heat loss of the stripper is negligible. Consequently, this factor is left out of equation 4.15.

The calculated total amount of energy flowing into the stage is also used to calculate the stage specific temperature. In order to do that, the average heat capacity of the vapor and liquid mixture in the stage is calculated and multiplied with the total mass flow flowing into the stage. Which in turn, should equal the multiplication of the corresponding heat capacity with the liquid and vapor mass flow out of stage i as is presented in equation 4.16. The temperature difference between the assumed and the calculated value is then calculated with equation 4.17 from where the temperature is updated with a decreased step size to prevent overshooting with equation 4.18.

$$F_i C_p = \sum_{j=1}^{C} L_{i+1} x_{i+1,j} C_{p,liq} + \sum_{j=1}^{C} V_i y_{i,j} C_{p,vap} \tag{4.16}$$

$$dT_i = \frac{Q_{tot,i}}{F_i C_p} \tag{4.17}$$

$$T_{new,i} = T_i + \frac{dT_i}{500} \tag{4.18}$$

Where C_p resembles the average specific heat of the mixture in stage i, dT_i resembles the temperature difference between the assumed stage temperature (T_i) and the newly calculated temperature of stage i ($T_{new,i}$). The visual interpretation of this section of the model is provided in figure B.4 in Appendix B.4. The single stage script produces the outputs presented in table 4.4

Table 4.4: Overview of outputs for stage specific script

Output	Description	Unit
T	Stage temperature	$[°C]$
A_{feed}	Feed stream	$[mol/s]$ (for each component)
L_{in}	Liquid flow in	$[mol/s]$ (for each component)
L_{out}	Liquid flow out	$[mol/s]$ (for each component)
V_{in}	Vapor flow in	$[mol/s]$ (for each component)
V_{out}	Vapor flow out	$[mol/s]$ (for each component)
p_{CO_2}	Partial pressure of CO_2	$[mbar]$
p_{H_2O}	Partial pressure of H_2O	$[mbar]$
χ_{TEPA}	Mass fraction of TEPA	$[wt\%]$
γ	Loading of mixture	$[mol_{CO_2}/kg_{TEPA}]$

Only when the mass and energy balance of the single stage i are established, multiple stage are connected together to form the multi-stage stripper column as is explained in the next section.

4.2.8. Stripper Model: Multi-Stage

The multi-stage stripper model solves the single stage script for the N number of single stages, which is an input of the model. Figure 4.6 shows how the numbering is setup, with the top stage being stage 1 and the bottom stage N the reboiler. The reflux stream is assumed to be only H_2O, enters in the top stage and is a function of the vapor stream leaving the stripper column as can be seen in equation 4.19.

$$L_1 = V_1 y_{1,2} \frac{RR}{1 + RR} \tag{4.19}$$

Where L_1 resembles the liquid reflux stream, V_1 resembles the vapor stream leaving the top stage, $y_{1,2}$ resembles the H_2O molar fraction of stream V_1 and RR resembles the reflux ratio. Furthermore, as no vapor enters the system in the bottom stage, it means that $V_{n+1} = 0$. The temperature of stage N (T_n) remains constant as this is an input of the model. At the same time, heat is required for the sensible heat and the heat of desorption in the bottom stage, which is supplied by the reboiler and equals $Q_{reb} = -Q_{tot}$.

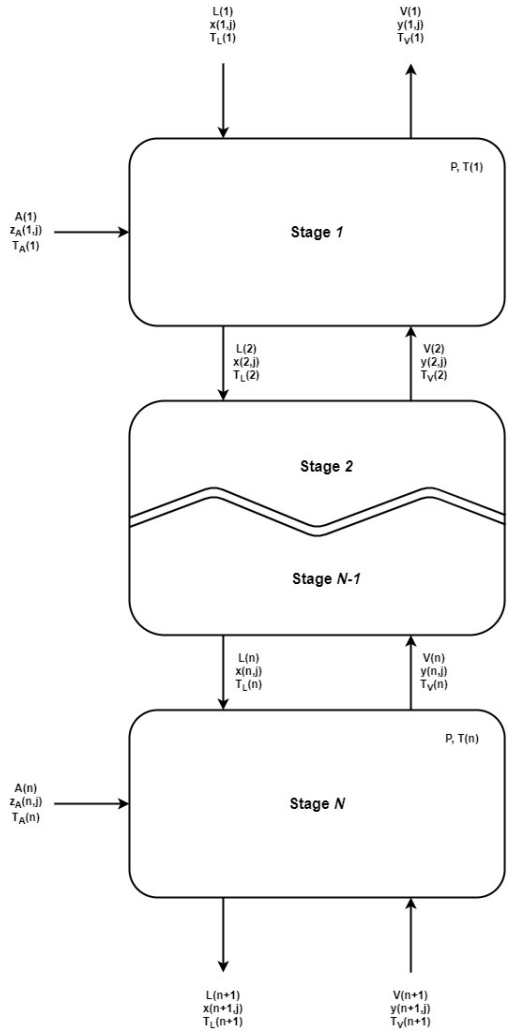

Figure 4.6: Schematic overview of the stripper model with N stages. Schematic made by van de Poll [117]

It is only when the temperature and mass flows of all the stages are stable and within the error as depicted in figure 4.4, the model produces its final outputs which are listed in table 4.5. Close observation of table 4.5 reveals two different outputs for the energy demand of the stripper. E resembles the energy use per mole of CO_2 without taking into account the extra energy expenses if the 3:1 top ratio is not satisfied. $E_{3:1}$ resembles the energy demand per mole of CO_2 taking the 3:1 top ratio into account, and assumes that the excess CO_2 or H_2 can be purged from the system, or possibly be stored for later use.

Table 4.5: Overview of outputs produced by the stripper model.

Output	Description	Unit
Q_{reb}	Reboiler duty	$[W]$
E	Energy demand without taking R_{top} into account	$[kJ/mol_{CO_2}]$
$E_{3:1}$	Energy demand when 3:1 product ratio is satisfied	$[kJ/mol_{CO_2}]$
R_{top}	Product vapor ratio	[-] $(H_2O : CO_2)$
CC	Cyclic capacity	$[mol_{CO_2}/kg_{TEPA}]$

4.2.9. Stripper Model Assumptions

The stripper model produces its outputs under the condition of several assumptions. These assumptions are listed below:

- **Heat losses are assumed to be negligible for the stripper model.** Therefore, the model will be utilized to predict a best case scenario.
- It is assumed that the column operates at **steady state**. In other words, no accumulation of mass or energy occurs inside the stripper column.
- **The stripping column is assumed to operate at equilibrium**. In other words, the VLE and vapor curve assume equilibrium inside the stripper column.
- It is assumed that no loss of sorbent occurs inside the stripper column. In other words, **negligible evaporation of TEPA + diluent** occurs. Therefore, the p_{CO_2} and p_{H_2O} are assumed to be the only contributors to the absolute pressure inside the stripper column.
- The vapor curve obtained from the VLE experiments as described in section 3.3.3 is based on the vapor pressure of H_2O alone, hence without CO_2. It is assumed that the presence of **CO_2 in the vapor phase has a negligible effect on the vapor curve**. It is known that this is not true, but Dowling et al. proved that the effect of CO_2 on the vapor curve is relatively small [36].
- **The specific heat** of the different components is assumed to be **constant**. Therefore, **average values** are used for the calculations. The specific heat is based on the weight fraction of the individual components in that specific stream. This gives a fair indication of the specific heat of the present mixtures even though it deviates slightly from reality.
- **The heat of absorption** of the different components is also assumed to be **constant**, and based on **average values**. This holds true for temperatures above 80 °C. As the stripping column operates at 120°C, this is a valid assumption. The sorbent specific constants are listed in table 6.1 in section 6.2.2.
- It is assumed that the **heat ex-changer (HEX) can heat the rich stream to a temperature of 10°C below the reboiler temperature** making use of the hot lean stream leaving the stripper column.

5

Results & Discussion

The main goals of this research project include providing an overview of all key performance indicators and the design specifications regarding the ZEF DAC system. Moreover, research goals and objectives include the characterization of the system regarding the sorbent performance. Finally, all the different answers obtained during the investigation will provide an optimization of the sorbent mixture for different climates.

In this chapter, all the relevant obtained results are presented for each research goal. That includes **results from the literature study, experimental investigation as well as results from the regeneration energy model.** The design of the ZEF DAC unit utilizing the optimized sorbent is provided in chapter 6.

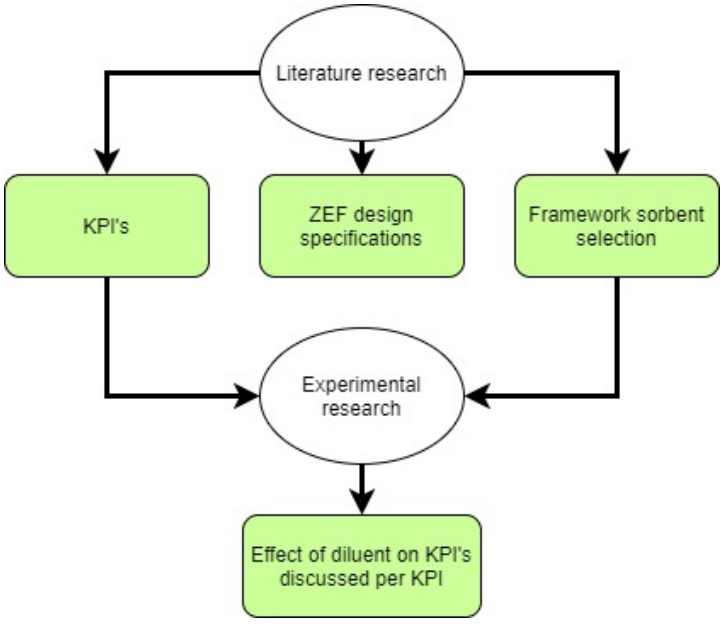

Figure 5.1: Schematic overview regarding this chapter.

5.1. Key Performance Indicators & ZEF Design Specifications

The first question of this project is: **"What are the key performance indicators that influence the DAC process at ZEF?"**. This subject has been thoroughly discussed in section 2.4.4, but is listed below in table 5.1 for completion of this chapter.

Table 5.1: The key performance indicators along with the design specifications of the ZEF DAC unit.

KPI	ZEF Design specification
Viscosity of the rich sorbent at 20°C	maximum of 2 $Pa \cdot s$
Optimal pressure ratio of stripper products	p_{H_2O}:p_{CO_2} = 3:1
Operating pressure of the stripper	as close to 1 atm as possible, can not be lower than 1 atm
Operating temperature of the stripper	no set optimal value, depends on sorbent characteristics
Cyclic capacity of sorbent	no set optimal value, depends on specific system energy demand
Rich CO_2 loading	as high as possible
Lean CO_2 loading	as low as possible
Regeneration energy demand	as low as possible
Space-Time-Yield	as high as possible
Sorbent evaporation	100 gr per year maximum
Sorbent degradation	as low as possible
Hold-up time stripper	as low as possible
Cost of sorbent	as low as possible

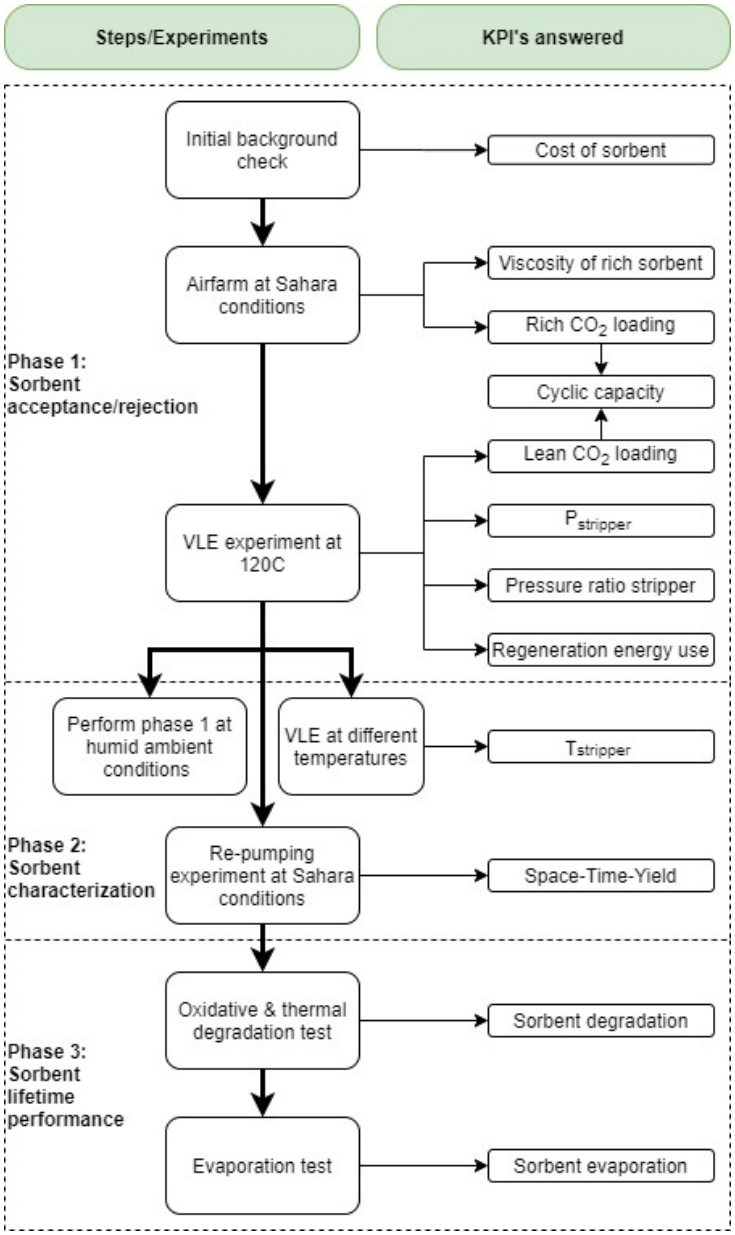

Figure 5.2: Schematic summary of the framework of sorbent selection

5.2. Framework of Sorbent Selection

All sorbents tested during this project are characterized and assessed by these KPI's. Therefore, one of the research goals of this project was: **"Develop a framework of sorbent selection"**. This has been extensively explained in section 3.1, but for completion a schematic overview is provided on the previous page in figure 5.2.

5.3. Experimental Phase one: Results

The key performance indicators provide the framework on which every sorbent at ZEF is assessed. This section comprehends the results from the experimental investigation and strives to answer the following research question: **"What is the effect of adding a certain diluent on the key performance indicators?"**. Therefore, the significant results of all the experiments are presented for each phase of testing.

5.3.1. Phase one: Airfarm Experiments

Phase one of testing is part of the characterization of the sorbent for **Sahara conditions**. The Sahara climate was chosen as the base case ambient condition as this climate is extremely dry, it provides the biggest challenge regarding the sorbent viscosity and it is a likely location where the ZEF plant could be utilized. The results of the phase one Airfarm experiments have been set out below in table 5.2.

Table 5.2: Results of phase one Airfarm experiment

ID	Diluent	Ratio $TEP:Dil$	Viscosity $[Pa \cdot s]$	CO_2 $[wt\%]$	H_2O $[wt\%]$	Rich CO_2 loading $[mol_{CO_2}/kg_{TEPA}]$	Rich CO_2 loading $[mol_{CO_2}/kg_{sorbent}]$	Comment
1	Pure TEPA	-	2.492*	5.01	11.73	1.37	1.14	
2	DEG	1:1	2.586*	5.2	5	2.61	1.17	
3	DEG	1:3	0.448	3.6	6.1	3.63	0.82	
4	PEG-200	1:1	1.443*	3.0	6.4	1.48	0.67	
5	PEG-200	1:3	0.931	3.2	7.7	3.28	0.73	
6	Selexol-250	1:1	N/A	N/A	N/A	N/A	N/A	Layer separation
7	Selexol-250	1:3	N/A	N/A	N/A	N/A	N/A	Layer separation
8	Glycerol	1:1	N/A	N/A	N/A	N/A	N/A	Very viscous
9	Glycerol	1:3	N/A	N/A	N/A	N/A	N/A	Very viscous
10	1,4-butanediol	1:1	1.755*	4.1	6.0	2.08	0.94	
11	1,4-butanediol	1:3	0.457	2.8	9.9	2.94	0.64	
12	Sulfolane	1:1	N/A	N/A	N/A	N/A	N/A	Layer separation
13	Sulfolane	1:3	N/A	N/A	N/A	N/A	N/A	Layer separation

* The asterisk symbol in the viscosity column indicates that specific sample crossed the 2 $Pa \cdot s$ maximum during the Airfarm experiment

A total of six different diluents where tested in the Airfarm setup in two different mixing ratios with TEPA. The TEPA:diluent mixing ratios correspond to a 1:1 and a 1:3 ratio, as preliminary viscosity experiments (Appendix B.1) showed the viscosity still rising way above the limit of 2 $Pa \cdot s$ for less diluted samples. Pure TEPA was tested as a base case for the sake of comparison, but close observation of table 5.2 shows that the viscosity advanced well above the 2 $Pa \cdot s$ limit before it reached equilibrium. The table also shows three of the six diluents tested listed as not applicable (N/A). In the case of selexol-250 and sulfolane the samples separated in multiple layers after the sample was loaded with CO_2. R. Wanderley et al. also reported phase separation in amino-mixtures upon CO_2 absorption. Phase separation eliminates these sorbents from possible diluents as this would result in huge uncertainties in a real life continuous DAC setup. The glycerol samples got extremely viscous after only 24 hours in the Airfarm, with sample ID 9 reaching 5.896 $Pa \cdot s$ and ID 8 even reaching 11.8 $Pa \cdot s$. Moreover, these values where still rising as the samples had not yet reached their equilibrium CO_2 loading. Therefore, eliminating glycerol as a possible diluent.

Rich CO_2 Loading

The CO_2 loading obtained from the Airfarm experiment corresponds to the rich loading of the sorbent flowing from the absorption column to the stripper column in the full DAC setup. Furthermore, the cyclic capacity depends strongly on the rich loading. Therefore, the rich CO_2 loading of the remaining tested sorbents is presented in figure 5.3. It must be noted that the black dots depict the CO_2 loading of the data points presented in table 5.2, which are the closest to the viscosity limit of 2 $Pa \cdot s$. The rich CO_2 loading is provided in $mol_{CO_2}/kg_{sorbent}$ and is calculated using equation 5.1.

$$\text{Rich } CO_2 \text{ loading} = \frac{\frac{wt\%_{CO_2}}{wt\%_{TEPA}+wt\%_{Diluent}+wt\%_{CO_2}+wt\%_{H_2O}}}{44.01} * 1000 \quad [mol_{CO_2}/kg_{sorbent}] \qquad (5.1)$$

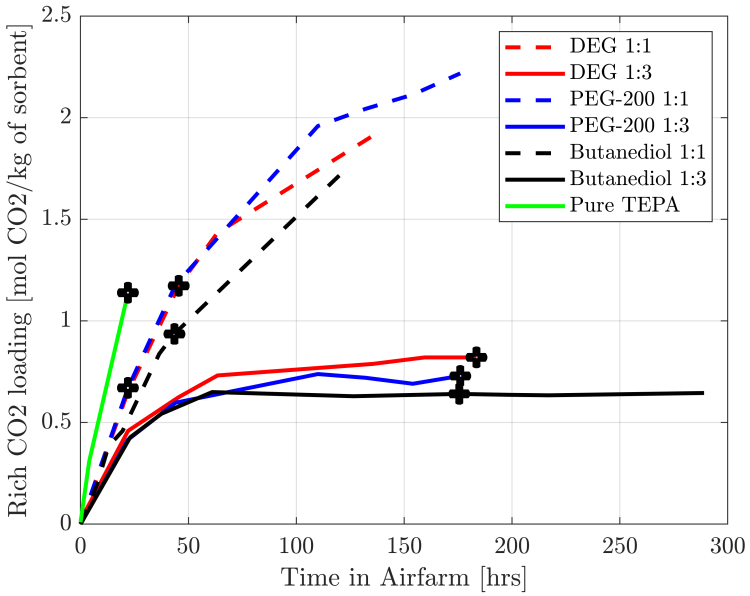

Figure 5.3: CO_2 loading vs time in the Airfarm at Sahara conditions

*The black dots are the data points closest to a viscosity of 2 $Pa \cdot s$.

The most important conclusions drawn from figure 5.3 are that the 1:1 samples and the pure TEPA sample are all still absorbing CO_2 when they cross the 2 $Pa \cdot s$ viscosity limit, indicating that the samples had not yet reached their equilibrium CO_2 loading. On the other hand, all three 1:3 samples are very close to their equilibrium loading as their gain in CO_2 loading remained within 5% for more than 100 hours. The rich CO_2 loading does not provide a conclusive answer on the best performing diluent, as the sorbent has to meet the design specifications set by ZEF. Therefore, the next step is to evaluate the viscosity of the samples.

Viscosity

When the viscosity at 20°C of all tested samples is obtained in the *Contraves Low Shear Rheometer* (Appendix A.1) and the results are plotted in a chart, figure 5.4 is obtained. The red arrows indicate that the viscosity is still rising at the moment the final sample was taken. The limit for the viscosity at 20°C is set by ZEF at 2 $Pa \cdot s$. Meaning that sorbents that cross this limit before reaching their equilibrium rich CO_2 loading are discarded for being too viscous. As a high viscosity of the rich sorbent would result in problems in the absorption column, such as the poor pumping ability of a highly viscous fluid. Furthermore, it would require more energy from the PV panels to power the pump which is undesirable for the ZEF system. The higher viscosity levels of the 1:1 samples as observed in figure 5.4 can be attributed to their higher CO_2 loading compared to the 1:3 samples, as was also observed by Sinha [112].

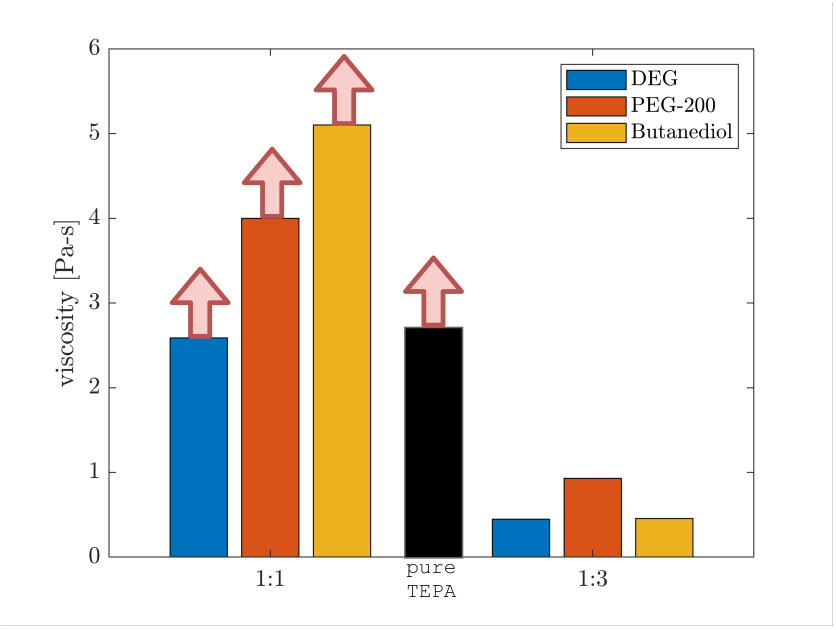

Figure 5.4: Viscosity at 20°C of the Airfarm samples. [$Pa \cdot s$]

*The red arrow indicates it was still rising when the final sample was drawn.

Conclusion phase one: Airfarm Experiments
Based on the performance parameters regarding the Airfarm experiment, the following conclusions can be drawn:

1. For pure TEPA the viscosity advanced well above the 2 $Pa \cdot s$ limit before it reached equilibrium.
2. Sorbents comprised of TEPA mixed with selexol-250 or sulfolane both split into multiple layers after CO_2 is absorbed, eliminating them from possible diluents as this would result in huge uncertainties in a real life continuous DAC setup.
3. Sorbents comprised of TEPA mixed with glycerol get extremely viscous upon CO_2 loading. Therefore, eliminating glycerol as a possible diluent.
4. The viscosity of the more diluted 1:3 samples remained much lower than the 1:1 samples at the Sahara's ambient conditions as was expected beforehand.
5. What is remarkable though, is that the rich, near to equilibrium, CO_2 loading of the more diluted 1:3 samples is in the same range as the less diluted 1:1 samples when the latter crossed the 2 $Pa \cdot s$ viscosity limit, while the 1:3 samples remained significantly lower in viscosity at roughly the same CO_2 loading. This supports the assumption that adding a diluent reduces the sorbent viscosity.
6. From the 1:3 diluted samples, the DEG sample seems to remain lowest in viscosity while having the highest CO_2 loading compared to the PEG-200 and 1,4-butanediol samples, although the difference is only marginal.

In other words, at this point of the process, the three remaining diluents; DEG, PEG-200 and 1,4-butanediol, especially the 1:3 samples, all hold great promise as a low viscosity sorbent for the ZEF DAC unit. The next step in the process is to test their performance at higher temperatures in the VLE setup.

5.3.2. Phase one: VLE Experiments

The sorbents containing the three remaining diluents; DEG, PEG-200 and 1,4-butanediol are tested in the VLE setup in order to provide quantitative knowledge on the KPI's listed below.

- Lean CO_2 loading
- Cyclic capacity
- Pressure ratio of stripper top products
- Operational pressure of the stripper
- Operational temperature of the stripper
- Regeneration energy demand

The VLE test setup is thoroughly described in section 3.3. It must be noted that the VLE experiments have been performed together with R. Phougat [95]. After the sorbent with the equivalent H_2O concentration, obtained from the Airfarm experiments, is loaded in the VLE setup two graphs are produced; a vapor curve of H_2O (figure 5.5) and a CO_2 loading curve (figure 5.6). From these graphs the KPI's can be evaluated, as is described in following section.

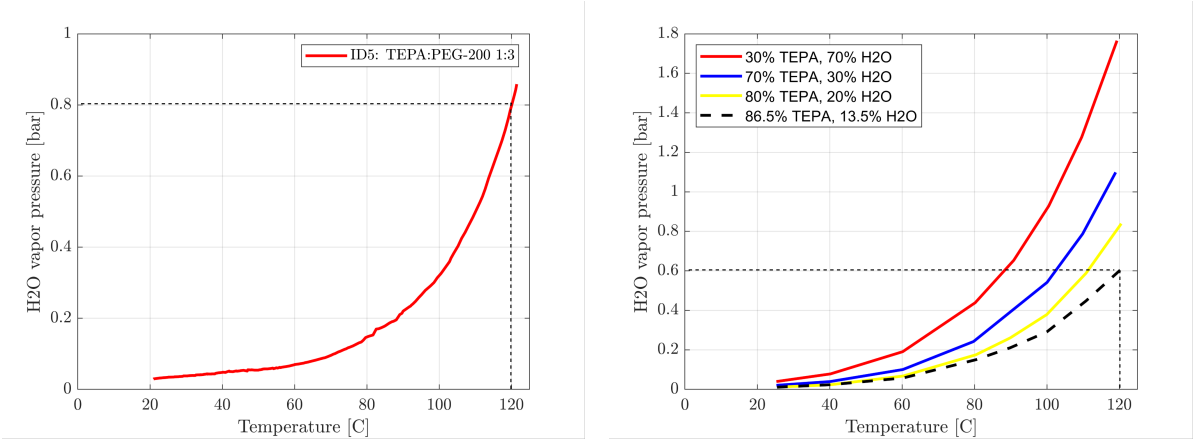

(a) ID5, TEPA:PEG-200 of 1:3

(b) Aqueous mixtures of TEPA, obtained by Dowling et al.[36]

Figure 5.5: H_2O vapor curves with Sahara equivalent H_2O loading

*The black broken curve in figure b is extrapolated from the other three vapor curves.

The procedure of obtaining the regeneration energy demand is explained for sorbent ID 5 and pure TEPA. Figure 5.5 shows the vapor curves obtained for sorbent ID 5 and various aqueous solution of TEPA. These specific graphs are displayed in order to clarify how the data is evaluated. From figure 5.5a it can be seen that sorbent ID 5, at the Sahara equivalent H_2O loading, corresponds to a water vapor pressure of 0.8 bar, assuming the stripper temperature is set to 120°C, as is denoted by the dotted lines. Figure 5.5b is obtained from the experimental data of Dowling et al. where she tested mixtures of aqueous TEPA in three different ratio's. The vapor curve for TEPA, at the Sahara equivalent H_2O loading, is extrapolated from these three curves and results in an equivalent water vapor pressure of approximately 0.6 bar. Again, assuming the stripper operates at 120°C.

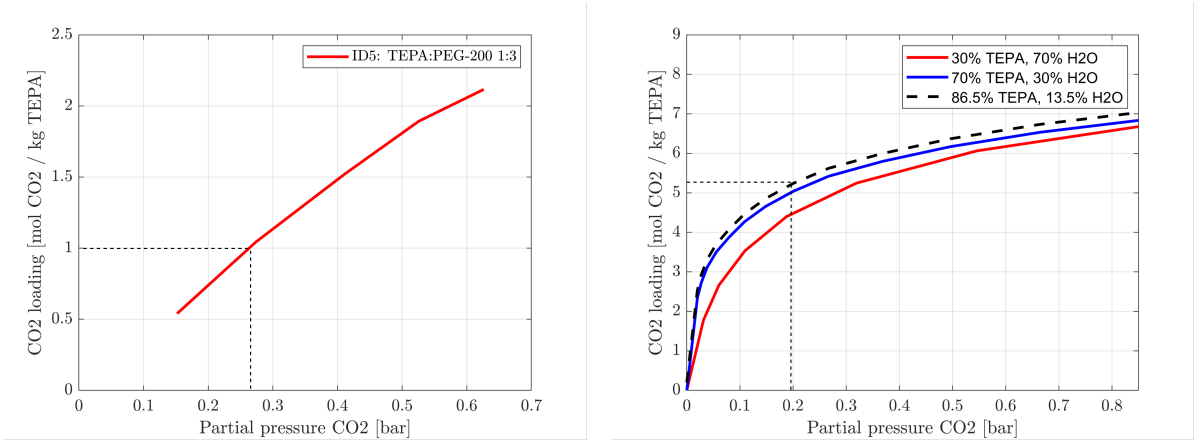

(a) ID5, TEPA:PEG-200 of 1:3

(b) Aqueous mixtures of TEPA, obtained by Dowling et al.[36]

Figure 5.6: VLE CO_2 loading curves with Sahara equivalent H_2O loading

*The black broken curve in figure b is extrapolated from the other three vapor curves.

In order to obtain the equivalent CO_2 loading at stripper temperatures the assumption is made that the stripper operates p_{H_2O}:p_{CO_2} of 3:1. In other words, the partial pressure of CO_2 is one third of the vapor pressure of H_2O. As the partial pressure of CO_2 is now known, the equivalent CO_2 loading at the 120°C stripper temperature can be evaluated from figure 5.6. For ID 5 at Sahara conditions the water vapor pressure equals 0.8 bar, resulting in an equivalent partial pressure of CO_2 of $\frac{0.8}{3} = 0.267$ bar, which in turn results in an equivalent lean CO_2 loading of *1.01 mol_{CO_2}/kg_{TEPA}*, which equals *0.25 $mol_{CO_2}/kg_{sorbent}$*. This, together with the rich CO_2 loading of *0.73 $mol_{CO_2}/kg_{sorbent}$* obtained from the Airfarm experiment, corresponds with a cyclic capacity of $0.73 - 0.25 = 0.48$ *$mol_{CO_2}/kg_{sorbent}$*. Assuming the stripper operates at 120°C the absolute operating pressure of the stripper equals *$p_{CO_2} + p_{H_2O} = 0.267 + 0.8 = 1.067$ bar*. When these inputs are implemented in the regeneration energy script as described in 4.1 the regeneration energy demand is obtained. For ID 5 the regeneration energy demand equals *2706 kWh/ton_{CO_2}*. Close observation of figures 5.5b and 5.6b reveals a problem when the same procedure is done for pure TEPA. As the lean CO_2 loading obtained for pure TEPA at Sahara's equivalent H_2O concentration equals *5.3 $mol_{CO_2}/kg_{sorbent}$*. While the rich CO_2 loading for pure TEPA obtained from the Airfarm experiments equals *1.14 $mol_{CO_2}/kg_{sorbent}$*. Consequently, this would result in a negative cyclic capacity, which theoretically, would reverse the system and absorption would happen in the stripper column. It must be noted that the lean loading for TEPA is equal for both units, *mol_{CO_2}/kg_{TEPA}* and *$mol_{CO_2}/kg_{sorbent}$*, as the sorbent has no diluent in it. Furthermore, it would require the absolute pressure of the stripper column to be 0.8 bar. This highlights why **pure TEPA would definitely not work for the ZEF DAC system operating at the Sahara conditions**, under the condition that the viscosity of the rich sorbent may not surpass 2 $Pa \cdot s$, the stripper temperature may not exceed 120°C and the absolute pressure of the stripper can not be lower than atmospheric pressure according to ZEF's design specifications. The procedure to obtain the regeneration energy demand is done for every sorbent and results in the following table 5.3. Close observation shows the strong decrease in lean CO_2 loading when a diluent is added to the amine. This decrease in lean CO_2 loading was also observed by R. Wanderley et al.. Where they described a shift of the VLE curve toward less CO_2 absorption for fixed CO_2 partial pressure. Hypothetically, as a result of the increased destabilization of the carbamate for water-lean sorbents [100].

Table 5.3: VLE experiment results of phase one of testing

ID	Diluent $TEP:Dil$	Rich CO_2 loading $[mol_{CO_2}/kg_{sorbent}]$	Lean CO_2 loading $[mol_{CO_2}/kg_{TEPA}]$	Lean CO_2 loading $[mol_{CO_2}/kg_{sorbent}]$	Cyclic capacity $[mol_{CO_2}/kg_{sorbent}]$	Absolute stripper pressure $[bar]$	Regeneration $[kWh/ton_{CO_2}]$	energy $[MJ/kg_{CO_2}]$
1	Pure TEPA	1.14	5.3	5.3	-4.16	0.8	N/A	N/A
3	DEG 1:3	0.82	0.78	0.20	0.63	0.766	2410	8.68
4	PEG-200 1:1	0.67	1.61	0.80	-0.13	0.853	N/A	N/A
5	PEG-200 1:3	0.73	1.01	0.25	0.48	1.067	2706	9.74
10	1,4-butanediol 1:1	0.94	1.5	0.75	0.19	0.840	4150	14.94
11	1,4-butanediol 1:3	0.64	1.05	0.26	0.38	0.916	3100	11.16

Conclusion phase one: VLE Experiments
The regeneration energy demand of the tested sorbents is displayed in figure 5.7 for the sake of comparison. From the phase one VLE experiments the following conclusions can be drawn:

1. Pure TEPA would clearly not work as a sorbent in the ZEF DAC unit operating at Sahara conditions under the design specifications set by ZEF.
2. The 1:1 ratio sorbents drop either due to the 2 $Pa \cdot s$ viscosity limit, or due to the negative cyclic capacity.
3. All the 1:3 ratio samples score within the same range regarding the regeneration energy demand.

Therefore, in order to conclude which of the three remaining diluents performs best for the ZEF DAC application the sorbent evaporation limit was set by ZEF as is discussed in the next section.

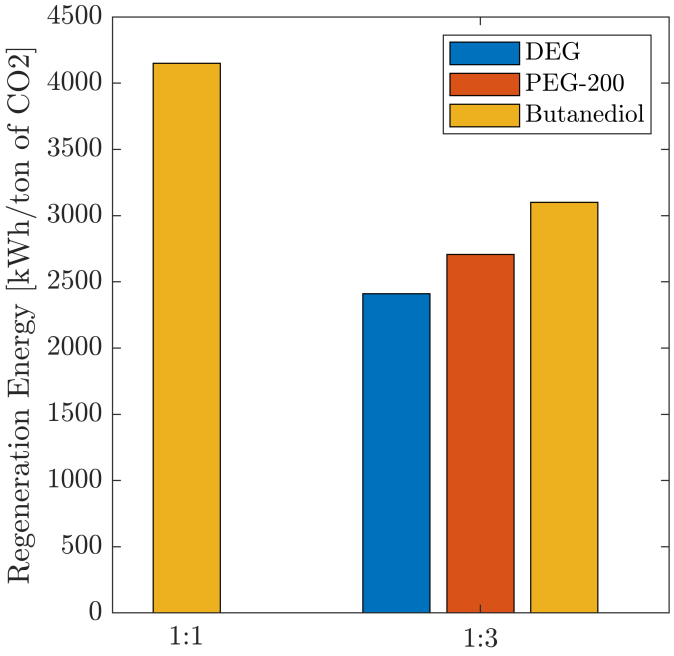

Figure 5.7: Regeneration energy demand [MJ/kg_{CO_2}]

5.3.3. Phase one: Evaporation Limit

The three diluents which are left at this point of the process score reasonably even in energy consumption. Therefore, the next step to evaluate which diluent would work best is to calculate the theoretical evaporation rate. It was at this point in the process the evaporation limit of 100 gr/yr was set by ZEF. The allowable vapor pressure of the sorbent is calculated by the following. When a total amount of 1500 grams of sorbent in the ZEF DAC unit is assumed, the evaporation limit is set to 100 grams per year and the molar mass of the sorbent is assumed to be between 100 and 200 g/mol. The highest acceptable molar flow of the evaporating sorbent is equal to:

$$\dot{n}_{sorbent,evap} = \frac{sorbent\ loss}{M_{sorbent}} = \frac{100 g/yr}{100 \leftrightarrow 200 g/mol} = 0.5 \leftrightarrow 1\ mol/yr \tag{5.2}$$

The ZEF unit powered by three solar panels has an airflow through the absorption column of 619 kg/hr according to Matteis et al. This airflow equals roughly $21.3 * 10^3$ mol/hr assuming the molar mass of dry air to be 28.97 g/mol [115]. The molar fraction of the evaporating sorbent is calculated by the following equation:

$$\chi_{sorbent} = \frac{\dot{n}_{sorbent,evap}}{\dot{n}_{air}} = \frac{0.5 \leftrightarrow 1}{21.3 * 10^3 * 365 * 8} = 8.01 * 10^{-9} \leftrightarrow 1.60 * 10^{-8} \tag{5.3}$$

This holds under the assumption that the sun provides enough energy to power the plant for 8 hours per day and the plant operates 365 days per year. Assuming the partial pressure of the sorbent ($p_{sorbent}$) to be much smaller than the partial pressure of the overflowing air (p_{air}) and the partial pressure of the sorbent resembles the vapor pressure of the sorbent, the molar fraction of the sorbent adheres the following equation:

$$\chi_{sorbent} = \frac{p_{sorbent}}{p_{total}} = \frac{p_{vap}}{p_{air}} \quad \text{thus} \quad p_{vap} = \chi_{sorbent} * p_{air} = 8 * 10^{-4} \leftrightarrow 1.6 * 10^{-3} Pa \tag{5.4}$$

In other words, if the evaporation limit set by ZEF has to be met, the maximum allowable vapor pressure of the sorbent is in the order of magnitude of 1 mPa at ambient temperatures. Literature provides various numbers for the vapor pressures of the pure substances, as they are presented in table 5.4. Close observation of table 5.4 reveals that only a few of the values found for pure TEPA come close to 1 mPa, with PEG-200 being the closest of the three diluents. The vapor pressure of DEG and 1,4-butanediol is roughly three orders of magnitude higher than the allowable 1 mPa. While for pure PEG-200, the vapor pressure is only one order of magnitude higher. **Consequently, based on these findings, PEG-200 is chosen for further testing, as it performs best out of the tested diluents.**

Table 5.4: Vapor pressure of pure substances from different sources

Chemical	**M** [g/mol]	**P_{vap}** [Pa]
TEPA	189.31 [91] [54]	<0.3 at 20°C [24] 0.0019 at 20°C [90] <1 at 20°C [34] 1.06*10^{-4} <->1,3 at 20°C [48] 0.1213 at 20°C from TGA experiments [48]
DEG	106.12 [4]	2.8 at 25°C [89] 1.33 at 20°C [4] 2.7 at 20°C [57] 0.8 at 25°C [83] 0.25 at 20°C [101] 0.81 at 30°C [101]
PEG-200	190-210 [4]	0.0112 at 25°C [63] 0.0113 at 25°C [63] 0.0158 at 25°C [92] 0.0169 at 25°C [29] 0.0203 at 30°C [63]
1,4-butanediol	90.12 [4]	1.3998 at 25°C [32] <133 at 38°C [56]

The fact that that the vapor pressure is known to go down when CO_2 is absorbed or when two substances are mixed introduces an uncertainty. Therefore, for an exact analysis the evaporation has to be tested on the chosen sorbent. Unfortunately, due to time constraints, this is not within the scope of this thesis.

5.3.4. Phase one: Ratio Optimization

The final stage of phase one of testing comprises of the same test phase as performed before, yet this time various sorbents comprised of TEPA and PEG-200 at different mixing ratio's are tested in order to find the optimal mixing ratio. The viscosity of sample ID 5 rose up to 0.93 $Pa \cdot s$ after it reached its equilibrium CO_2 loading in the Airfarm. This left room for improvement, as the maximum allowable viscosity is 2 $Pa \cdot s$. Having relatively more TEPA in the sorbent would result in a higher CO_2 absorption capacity, under the assumption that TEPA is the absorbing substance and PEG-200 merely acts as a diluent. This is a fair assumption as PEG-200 only physically absorbs CO_2 at high partial pressures. Research of Sinha has shown that a higher concentration of CO_2 in the sorbent corresponds to a higher sorbent viscosity. Therefore, the same test phase has been performed with various sorbent mixing ratio's between 1:1 and 2:7, of which the results are presented in table 5.5.

Table 5.5: VLE results of PEG-200 ratio optimization

ID	Ratio $TEP:Dil$	Viscosity $[Pa \cdot s]$	Rich CO_2 loading $[mol_{CO_2}/kg_{sorbent}]$	Lean CO_2 loading $[mol_{CO_2}/kg_{sorbent}]$	Cyclic capacity $[mol_{CO_2}/kg_{sorbent}]$	Absolute stripper pressure $[bar]$	Regeneration energy $[kWh/ton_{CO_2}]$	$[MJ/kg_{CO_2}]$
14	9:1	1.79*	1.08	N/T	N/T	N/T	N/T	N/T
15	3:1	1.68*	0.99	N/T	N/T	N/T	N/T	N/T
4	1:1	1.44*	0.67	0.80	-0.13	N/A	N/A	N/A
16	2:3	1.69*	1.00	N/T	N/T	N/T	N/T	N/T
17	1:2	2.28*	1.13	N/T	N/T	N/T	N/T	N/T
18	2:5	1.50	0.90	0.35	0.55	0.977	2498	8.99
5	1:3	0.93	0.73	0.25	0.48	1.067	2706	9.74
19	2:7	0.66	0.55	0.19	0.36	1.187	3161	11.38

* The asterisk symbol in the viscosity column indicates that specific sample crossed the 2 $Pa \cdot s$ maximum during the Airfarm experiment

Close observation of table 5.5 shows sample ID 18, TEPA:PEG-200 2:5, is the sample richest in TEPA which is not capped by the viscosity limit. Therefore, the samples richer in TEPA were not tested further in the VLE setup. Furthermore, sample ID 18 would require *2498 kWh/ton$_{CO_2}$* for regeneration of the sorbent, which is, apart from ID 3 with DEG, the lowest theoretical energy expense of all tested sorbents so far. When this energy demand for the reboiler is compared to the theoretical *1762 kWh/ton$_{CO_2}$* obtained from the research for pure TEPA as a sorbent of van de Poll et al.it can be concluded that the energy demand for sorbent ID 18 is 41% higher. However, the value obtained for pure TEPA was obtained under the assumption that TEPA could be loaded in the absorber to a rich loading of *6.9 mol$_{CO_2}$/kg$_{TEPA}$* while reaching a viscosity of 6.26 $Pa \cdot s$ [117]. The viscosity limit set by ZEF prevents this from being a realistic operating condition. Therefore, energy demand obtained for ID 18 is assumed to be the more realistic value.

5.3.5. Phase one: Conclusion

Sample ID 18, TEPA:PEG-200 2:5, is chosen as the optimized sorbent based on the following:

- The sorbents comprised of TEPA and PEG-200 show excellent mixing properties and remain fluid at the tested conditions even after the sorbent was loaded with CO_2.
- The sorbents diluted with PEG-200 show the lowest tendency to evaporate, as the vapor pressure of PEG-200 is two orders of magnitude lower compared to DEG and 1,4-butanedol.
- The highest measured viscosity of ID 18 was 1.5 $Pa \cdot s$, this is well within the 2 $Pa \cdot s$ limit.
- From the VLE experiments it was concluded that sorbent ID 18 also reached the highest cyclic capacity of all sorbents tested comprised of TEPA and PEG-200.
- Results from the regeneration energy model showed sorbent ID 18 required the least amount of energy for regenerating the sorbent.

Therefore, sample ID 18, TEPA:PEG-200 2:5, is the sorbent which performs best, out of all the tested sorbents, at the Sahara's ambient conditions for the given ZEF DAC design specifications.

5.4. Experimental Phase two: Results

The purpose of phase two is the characterization of sorbent ID 18. This has been done in three steps. The first step consists of the performing test phase one again but at a more humid ambient climate, to map the effects of relative humidity on the sorbent performance. The second step comprises of VLE testing at different stripper temperatures, to map the effect of the stripper temperature on the sorbent performance. The third step consist of performing the re-pumping experiment on ID18, to make qualitative statements on the effect of the diluent on the absorption kinetics of the sorbent.

5.4.1. Phase two: Airfarm Experiments

Phase two of Airfarm testing is done at a more humid climate in order to see the effect of the relative humidity on the optimized sorbent. The **climate of the Mediterranean sea** has been chosen for phase two of optimization. The Mediterranean climate would benefit a DAC system as it is close to the equator

compared to ZEF's current location. This means that the energy of the sun is plentiful but the relative humidity is around 60% compared to the 25% of the Sahara. The Airfarm results are presented below in table 5.6.

Table 5.6: Phase two: Airfarm results at Mediterranean climate.

ID	Ratio TEPA:PEG-200	Viscosity $[Pa \cdot s]$	CO_2 $[wt\%]$	H_2O $[wt\%]$	Rich CO_2 loading $[mol_{CO_2}/kg_{sorbent}]$
15	3:1	1.522*	8.6	26.2	1.95
4	1:1	1.110	7.61	23.0	1.73
18	2:5	0.229	3.52	24.62	0.80
5	1:3	0.188	2.87	24.06	0.65

* The asterisk symbol in the viscosity column indicates that specific sample crossed the 2 $Pa \cdot s$ maximum during the Airfarm experiment

Rich H_2O Loading

When the loading of H_2O inside the Airfarm is plotted figure 5.6 is obtained. What is striking is how fast the H_2O equilibrium loading is reached, usually within 24 hours of testing, which is much faster than the time it takes for CO_2 to reach its equilibrium loading. This indicates that the absorption process for H_2O differs from the one for CO_2. Where CO_2 is chemically absorbed, H_2O is physically absorbed [122], as was confirmed by previous research at ZEF [82]. Furthermore, an increase of relative humidity from 25% to 60% results in an increase of H_2O loading from 5-10% to 23-26%. Close observation of figure 5.8 also shows a trend of the less diluted 3:1 samples having a higher equilibrium H_2O loading, albeit only marginally.

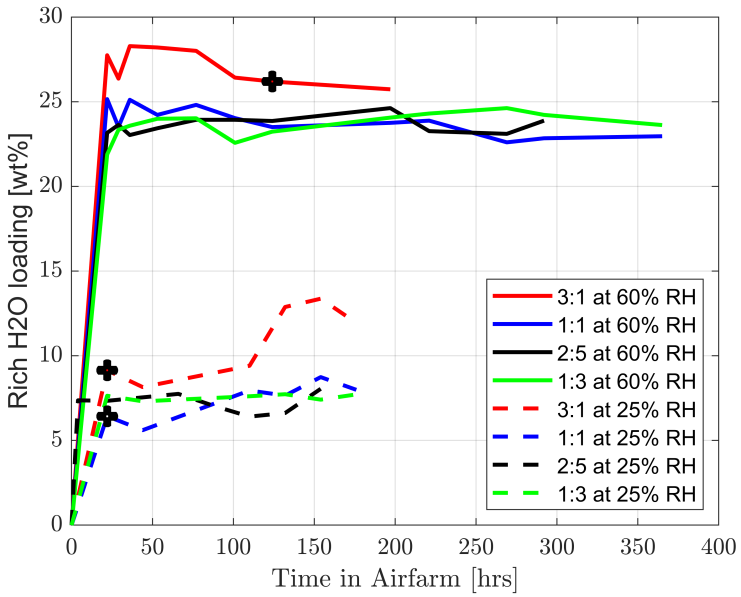

Figure 5.8: Rich H_2O loading at Mediterranean climate (60%RH) compared to Sahara climate (25%RH)

Viscosity

Research of Sinha et al. showed that a higher H_2O concentration corresponds to a lower sorbent viscosity for aqueous TEPA. This is also observed during this research. As can be seen in figure 5.9, where the more diluted sample ID's 18 and 5 reduced in viscosity by 85% and 80% at their equilibrium loading. Furthermore, where sample ID 4 was capped by the viscosity limit of 2 $Pa \cdot s$ at the Sahara's conditions, at the Mediterranean conditions it was not, reaching 1.11 $Pa \cdot s$ at its equilibrium CO_2 loading.

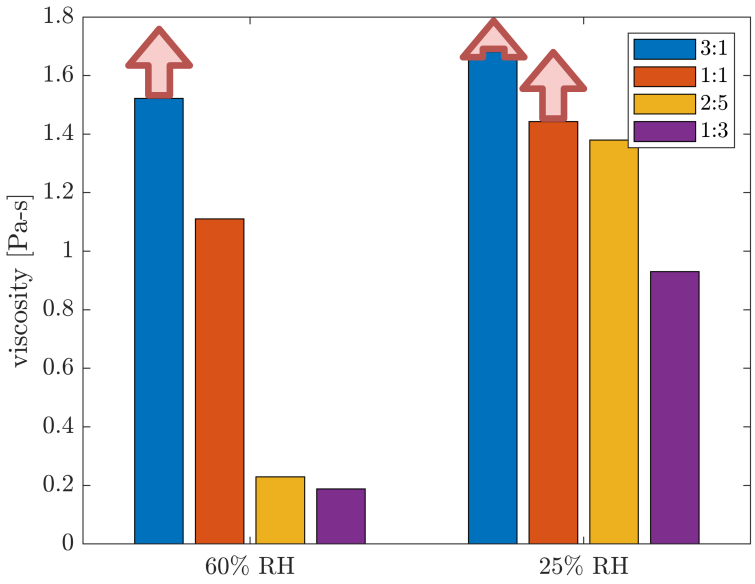

Figure 5.9: Viscosity of TEPA:PEG-200 samples at various mixing ratio's comparing two different H_2O loading corresponding to the Mediterranean climate (60%RH) and the Sahara climate (25%RH)

The red arrow indicates it was still rising when the final sample was drawn.

Rich CO_2 Loading

The reduction in viscosity at more humid conditions means that a less diluted sorbent can be used. Less diluent means more amine and more amine means more amine sites for the CO_2 to bond with. Which in turn certainly has an effect on the CO_2 absorption capacity within the 2 $Pa \cdot s$ viscosity limit. The rich CO_2 loading graph obtained from the Airfarm experiments for both climates is presented here under in figure 5.10.

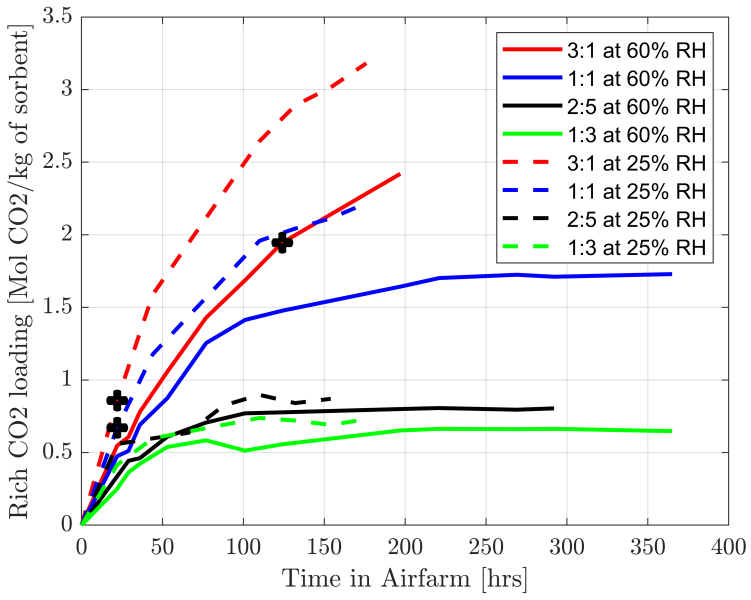

Figure 5.10: Rich CO_2 loading of TEPA:PEG-200 samples at various mixing ratio's comparing two different ambient climates corresponding to the Mediterranean climate (60%RH) and the Sahara climate (25%RH)

The black dots are the data points closest to a viscosity of 2 $Pa \cdot s$.

If for example, sample ID 4, which is TEPA:PEG-200 1:1, is observed. The sample was capped by the

viscosity limit at the Sahara conditions, reaching a CO_2 concentration of 3 wt% and an H_2O concentration of 6.4 wt% at a viscosity of 1.443 $Pa \cdot s$. This was the sample closest to the 2 $Pa \cdot s$ viscosity limit. While, at the more humid Mediterranean conditions, the CO_2 concentration more than doubled at 7.61 wt%. Yet the viscosity only rose to 1.11 $Pa \cdot s$ as the H_2O concentration almost tripled at 23 wt%. This indicates that **a more humid climate requires less diluent for the sorbent to stay within the 2 $Pa \cdot s$ limit**, as was expected beforehand.

5.4.2. Phase two: VLE experiments

The VLE tests of phase two have been performed for insights in two different cases. Firstly, to map the effects of the more humid Mediterranean climate in conjunction with sorbent ID 18 on the regeneration energy demand and secondly, to map the effects of varying the stripper temperature on the regeneration energy demand. Figure 5.11a shows a comparison of the H_2O vapor curves corresponding to the H_2O loading of the different climates. As expected, the H_2O vapor pressure corresponding to the more humid Mediterranean climate is much higher than the one corresponding to the less humid Sahara climate.

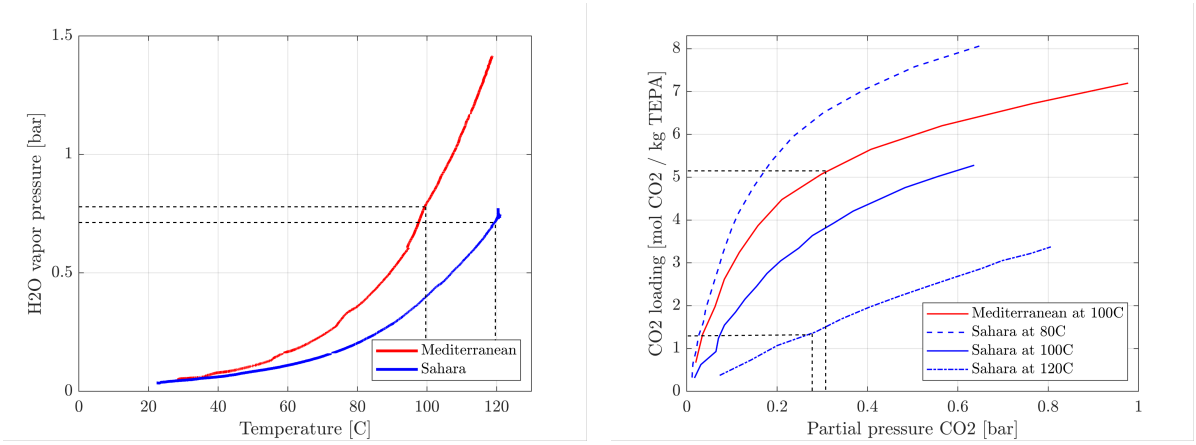

(a) H_2O vapor curves of ID 18.

(b) CO_2 loading curves of ID 18 at varying stripper temperatures.

Figure 5.11: Phase two VLE graphs corresponding to the loading of the Mediterranean climate (60%RH) and the Sahara climate (25%RH)

The performance of sorbent ID 18 is discussed for varying stripper temperatures.

- **120°C;** it is interesting to note that the absolute pressure of the stripper would be well above one bar when sorbent ID 18 would be used at the Mediterranean climate, if the stripper would be operated at 120°C. Therefore, it would be a logical step to lower the stripper temperature. Since the vapor pressure of H_2O might already be sufficient at a stripper temperature of a 100°C. For operation at the Sahara climate, sorbent ID 18 proved to be the optimal sorbent following section 5.3.

- **100°C;** when the equilibrium CO_2 loading at a stripper temperature of a 100°C for the Mediterranean equivalent sorbent is evaluated it reveals a problem. As the lean CO_2 loading would be higher than the rich loading. Resulting in a hypothetical negative cyclic capacity. For the Sahara climate, lowering the stripper temperature to 100°C would result in an absolute operating pressure of the stripper below one bar which is highly undesirable as this would require vacuum pumps accompanied with additional energy expense..

- **80°C;** lowering the stripper temperature below 100°C would for both climates result in an absolute pressure of the stripper well below one bar.

The VLE results of phase two are presented on the next page in table 5.7.

Table 5.7: VLE Results of sorbent ID 18, climate comparison

ID	Climate	Rich CO_2 loading $[wt\%]$	Rich H_2O loading $[wt\%]$	Viscosity at 20°C $[Pa \cdot s]$	Rich CO_2 loading $[mol_{CO_2}/kg_{sorbent}]$
18	Sahara (S)	3.95	6.4	1.50	0.90
18	Mediterranean (M)	3.5	24.6	0.23	0.80
ID	Stripper temperature [°C]	Lean CO_2 loading $[mol_{CO_2}/kg_{sorbent}]$	Cyclic capacity $[mol_{CO_2}/kg_{sorbent}]$	Absolute stripper pressure $[bar]$	Regeneration energy demand $[kWh/ton_{CO_2}]$
18 (S)	120	0.35	0.55	0.98	2498
18 (M)	120	0.89	<0	1.87	N/A
18 (M)	100	1.39	<0	1.06	N/A
18 (M)	80	>0.91	<0	0.48	N/A

Consequently, **sorbent ID 18 can not be used in the ZEF DAC system which operates at the Mediterranean climate in conjunction with ZEF's design specifications**, if the data is evaluated as described in section 5.3.2. It would be very interesting to test how sorbent ID 4, TEPA:PEG-200 would perform at Mediterranean conditions as the rich CO_2 loading at these conditions is much higher than sorbent ID 18. Unfortunately, due to time constraints, this was not tested during this research project, but it is highly recommended for future research at ZEF.

5.4.3. Phase two: Re-pumping Experiments

Sorbent ID 18 is tested in the re-pumping setup to evaluate its performance at the absorption side of the DAC unit. The results are presented in this section. Due to time constraints, the re-pumping experiments have been performed by Hanafi et al., who was an intern at ZEF during this period.

Rich CO_2/H_2O Loading

Figure 5.12 shows the loading of CO_2 and H_2O vs. time obtained with the FTIR during the re-pumping experiments. It can be seen that for both climates the increase in loading of H_2O is much greater than the one for CO_2, just like the Airfarm experiments showed. What is remarkable though, is that the CO_2 loading at the Sahara climate rose to *1.02* $mol_{CO_2}/kg_{sorbent}$, which is higher than the presumed equilibrium loading found in the Airfarm experiments, where a maximum loading of *0.90* $mol_{CO_2}/kg_{sorbent}$ was obtained. Indicating that the sample had not yet reached its equilibrium loading in the Airfarm setup. This could be attributed to the difference in contacting area between the sorbent and the ambient air, being significantly larger in the re-pumping setup and therefore, reaching equilibrium much faster or perhaps due to the fact that in the Airfarm setup, there is a portion of the sorbent below the gas dispersion disc of the gas washing flask which is not in contact with the gas and is therefore, not uniformly mixed.

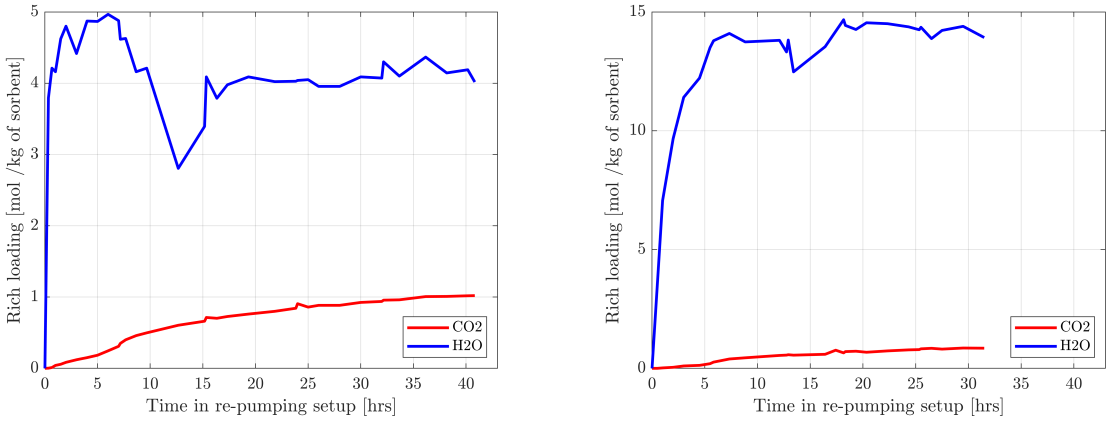

(a) Sahara conditions, 30°C & 25% relative humidity

(b) Mediterranean conditions, 30°C & 60% relative humidity

Figure 5.12: CO_2 and H_2O loading vs time in the re-pumping setup obtained by Hanafi [52].

Space-Time-Yield

When the absolute STY for CO_2 is calculated using equation 3.10 with the loading data from the FTIR and plotted against the rich CO_2 loading the following two plots of figure 5.13 are obtained. What can

be seen from the experimental data is that there is a lot of noise in the data. This is confirmed by the low R^2 values for the linear regression, indicating that the linear regression line is not representative for the changes in STY along different loading values. Theoretically, the absolute STY should be high at first and go down as the CO_2 concentration increases. The concentration difference is the driving force for the mass transfer of CO_2 from the ambient air to the sorbent. Meaning that when the sorbent is fresh the rate of CO_2 uptake is high, gradually going down and finally going to zero as the CO_2 concentration reaches the equilibrium loading, as was proved by previous research at ZEF by Matteis et al. The linear regression does confirm the trend of the STY going down, but it does not reach zero in the end. This could mean the sample has not yet reached equilibrium at the end of the experiment or perhaps that the uncertainty of the measurements of the FTIR plays a role. When the values for the STY are compared to the values found for pure TEPA by Matteis et al. the values are in the same range. Unfortunately, as the STY is dependent on the specific area of the absorption column used for testing, the STY values for pure TEPA of Matteis are not comparable to the STY values of this re-pumping experiment. A new absorber design was used during this research. The noise in the data is most likely caused by the way the samples were drawn from the sump of the setup, even though the sump is continuously stirred, it could well be that the sorbent in the sump is not uniformly mixed, which would result in fluctuations in CO_2 loading. **For future research of the absorption characteristics, it is highly recommended that the samples collection needs to be at a stationary point in the setup, for example after the pump to ensure good mixing of the sorbent mixture. By that, eliminating human error in that process**.

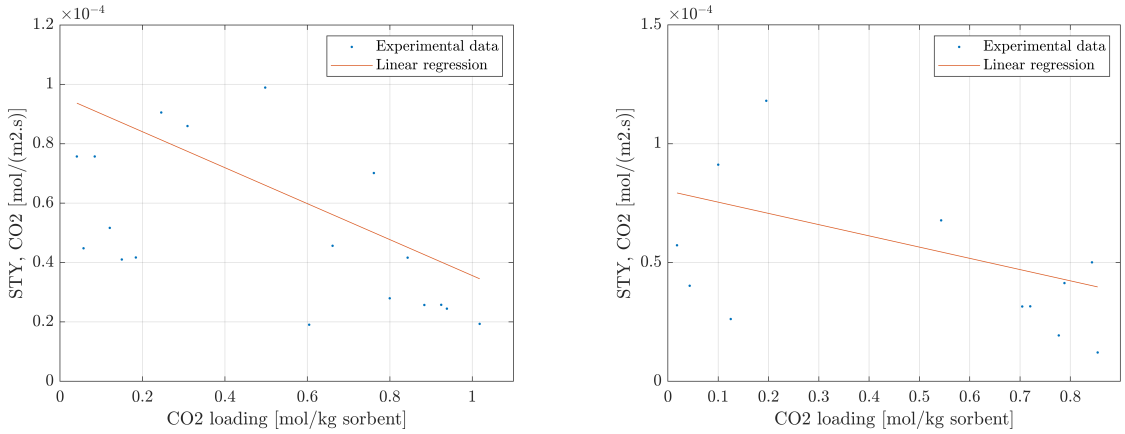

(a) Sahara conditions

(b) Mediterranean conditions

Figure 5.13: Absolute STY of CO_2 vs CO_2 loading for the re-pumping setup obtained by Hanafi [52].

Despite the fact that the data is noisy, the values for the absolute STY will be used for the design of the absorption column in the next chapter. This will provide the most accurate prediction on the absorber characteristics as the acquired STY data is obtained for the new updated absorber design using the optimised sorbent found during this research project.

5.5. Experimental Phase three: Results

Phase three of testing is performed to make qualitative statements on the lifetime performance of the sorbent. As previous research by Gowda et al. at ZEF indicated that the sorbent was prone to degradation due to exposure to oxygen and heat. Furthermore, sorbent evaporation has to be evaluated.

5.5.1. Phase three: Sorbent Degradation

Thermal sorbent degradation tests have been performed as they were described in section 3.5. The FTIR spectra of every drawn sample from these experiments is presented in figure 5.14 and is evaluated per experiment below.

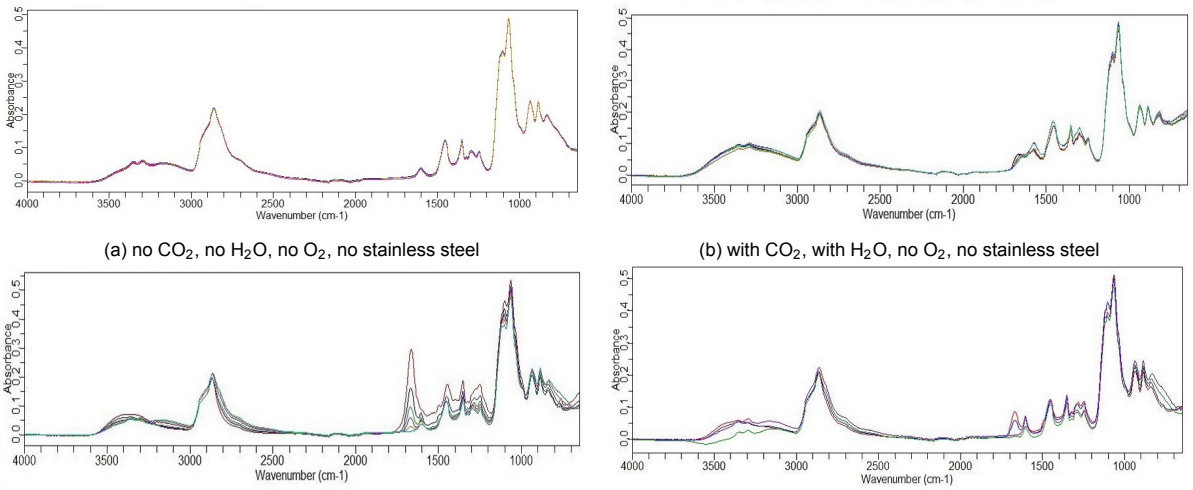

(a) no CO_2, no H_2O, no O_2, no stainless steel

(b) with CO_2, with H_2O, no O_2, no stainless steel

(c) no CO_2 and no H_2O at start, with O_2, no stainless steel

(d) no CO_2 and no H_2O at start, with O_2, with stainless steel

Figure 5.14: FTIR spectrum of the thermal degradation experiments at 120°C of ID 18

- **Experiment A**, of which the FTIR spectra is provided in figure 5.14a, shows no significant changes after a full week at 120°C and being closed of from oxygen. Meaning that a fresh, unloaded sorbent most likely does not degrade significantly in the absence of oxygen during the tested time span. Titration of the first and last sample confirms this, as there is no loss in amine sites measured.

- **Experiment B**, of which the FTIR spectra is provided in figure 5.14b, does show a slight change in the spectrum at the 1200-1700 cm^{-1} range of the wavelength after a full week at 120°C and being closed of from oxygen. According to K.Li et al. peaks at 1258, 1276, 1496, 1562 and/or 1685 cm^{-1} can be attributed to the formation of urea linkages in amines [68]. Where the most significant difference for this experiment is noted for a wavelength of 1560 cm^{-1} this could be the result of COO^- stretching of the carbamate species according to the spectral characterization chart of W. C. Wilfong et al. which is presented in Appendix C.1. This observation is in line with the expectations as the addition of CO_2 would result in the formation of carbamates according to equation 2.16. Titration of the final sample resulted in a measured amine site loss of 16.7% compared to the loaded sample at the start of the experiment.

- **Experiment C**, of which the FTIR spectra is provided in figure 5.14c, shows a big change in the spectrum at the 1200-1700 cm^{-1} range of the wavelength after a full week at 120°C and being open to the surrounding air. With the largest peak formation at a wavelength of around 1680 cm^{-1}, which can be attributed to C=O stretching. The C=O stretching indicates that CO_2 is present in the amine sample as is confirmed by the FTIR, since the sample absorbed CO_2 from the surrounding air, going from 0 wt% CO_2 to 1.2 wt% after one full week of testing. The alteration in the FTIR spectra hints towards the formation of urea linkages as a result of CO_2 reacting with the amine at temperatures above 100°C [68]. Titration of the first and final sample confirms this suspicion as an amine site loss of 87.4% between the first and final sample was measured. From this result it can be concluded that the presence of oxygen accelerates the degradation of the sorbent at 120 °C significantly.

- **Experiment D**, of which the FTIR spectra is provided in figure 5.14d, shows a change in the spectrum at the 1200-1700 cm^{-1} range of the wavelength after a full week at 120°C, being open to the surrounding air and in contact with the stainless steel temperature probe. However, the growth of the peak at 1680 cm^{-1} is not as significant as the one from experiment C, which is against the expectation of stainless steel accelerating the degradation process. This could possibly be explained by the lesser amount of CO_2 in the final sample. This is backed up by the titration of the first and final sample, showing an amine site loss of 47.3%.

Table 5.8: Thermal degradation test titration results after 168 hours of subjection to the elements.

Test	CO_2 $[wt\%]$	H_2O $[wt\%]$	Amine site loss
A: ID 18, fresh, no O_2	0%	0%	0%
B: ID 18, loaded, no O_2	2%	7.5%	16.7%
C: ID 18 with O_2	0% at start, 1.2% final sample	0% at start, 13.4% final sample	87.4%
D: ID 18 with O_2 & SS	0% at start, 0.33% final sample	0% at start, 5.71% final sample	47.3%

A discussion following the degradation experiments is given below:

- From this sequence of degradation tests it can be concluded that the presence of CO_2 causes the sorbent to degrade at elevated temperatures as was concluded by Gowda et al. and that this process is highly accelerated by the presence of oxygen. On the other hand, the presence of stainless steel does not seem to accelerate the degradation process, counter intuitively so. This has to be researched further to make proven statements about this subject.

- Duplo's in the titration of the samples revealed inconsistencies in the amount of amine site loss. This could be due to the need to manually titrate the sample in the setup used. During this procedure it is necessary to add 0.1 ml of HCl to the sample for more than 100 times per titration experiment resulting in this process being highly susceptible to human error. **Therefore, it is highly recommended to use an automatic titrator for future testing at ZEF**, as this eliminates the human factor in this matter.

- The difference in CO_2 concentration between experiment C and experiment D indicate an inconsistency in the experimental approach. As both samples where open to the surrounding air for the same duration, but during experiment C significantly more CO_2 and H_2O was absorbed by the sample. Perhaps this can be attributed to the test temperature not being consistent between the two tests or not being uniform throughout the sample. Or else because part of the sorbent has evaporated. **It would be advised for future thermal degradation tests at ZEF to design a test setup from which the sorbent can not evaporate and a method of keeping a uniform temperature in the sample, such as in a thermal bath**.

5.5.2. Phase three: Evaporation Experiment

Unfortunately, due to time constraints regarding this thesis project the evaporation of the optimized sorbent has not been tested. The largest part of the evaporation of the sorbent will most likely be occurring inside the stripper column, as the stripper temperature is much higher than the absorber temperature. However, implementing a gas washer stage after the stripper could prevent the sorbent from escaping the system. Therefore, the conditions at which the evaporation would have to be tested are the absorber conditions, which are the ambient conditions. Unfortunately, due to the relatively low temperatures, evaporation would be very slow, hence experimenting this would take very long. It is for these reasons **it is recommended for future research at ZEF to design a sorbent evaporation setup** which can precisely measure the sorbent evaporation without taking a whole year or more to be tested.

5.6. Sorbent Comparison

Previous research at ZEF by van de Poll focused the design of the DAC column based on aqueous TEPA as a sorbent. van de Poll's research proved that a 5 stage column, operated at 1 bar absolute pressure with a reboiler temperature of 120°C, a feed temperature of 105 °C and a reflux ratio of 0.55 required the least amount of energy per mole of CO_2 for CO_2 capture. When the stripper column is simulated using sorbent ID 18 in the advanced stripper model as described in section 4.2.3 to the exact same specifications as in van de Poll's research, the results shown in table 5.9 are obtained.

Table 5.9: Comparison of sorbents in equal stripper set-up. The values for Aqueous TEPA were obtained by van de Poll [117].

Output results	Aqueous TEPA	ID 18 TEPA:PEG-200 2:5 Sahara climate	ID 18 TEPA:PEG-200 2:5 Mediterranean climate	Unit
γ_{rich,CO_2}	6.9	3.5	3.895	$[mol_{CO_2}/kg_{TEPA}]$
R_{rich,H_2O}	0.3	0.25	1.20	$[kg_{H_2O}/kg_{TEPA}]$
$\mu_{rich,sorbent}$	6.26	1.50	0.23	$[Pa * s]$
γ_{lean,CO_2}	3.6	1.41	0.0005	$[mol_{CO_2}/kg_{TEPA}]$
CC	3.3	2.09	3.8945	$[mol_{CO_2}/kg_{TEPA}]$
R_{top}	3	1.43	17.52	[-] (H_2O:CO_2)
$\dot{m}_{feed}$	0.31	1.22	0.81	$[g/s]$
E	279	209	833	$[kJ/mol_{CO_2}]$

Close observation of table 5.9 reveals that sorbent ID 18 at Sahara's climate would require less energy to regenerate than the 'old' aqueous TEPA sorbent. However, the problem is depicted in red. Where the design specification regarding the top ratio of H_2O:CO_2 of 3:1 is not met, as the ratio is 1.43:1. In other words, the DAC system of these specific specifications using sorbent ID 18 at the Sahara conditions does not produce enough water compared to CO_2 for the ZEF plant to operate efficiently. When sorbent ID 18 with the Mediterranean climate equivalent H_2O loading is evaluated in the stripper model the energy use is much higher compared to the 'old' sorbent. One of the main reasons for this is that the top ratio of H_2O:CO_2 is 17.52:1, meaning that way too much water is produced if sorbent ID 18 would be used at the Mediterranean climate. It must be noted that the stripper specifications of van de Poll's research were optimized for aqueous TEPA with a rich loading of $6.9\,mol_{CO_2}/kg_{TEPA}$, in a real life situation at the Sahara conditions the sorbent viscosity would have reached well above 2 $Pa \cdot s$, and is therefore too viscous for the system to be effective. The system specifications will have to be updated for sorbent ID 18 to find the optimal design in terms of energy use while all ZEF's design specifications are met. This optimized design is elaborated in section 6.2.

6

DAC System Engineering

This section will provide the design of the entire DAC unit with the help of a sensitivity analysis for both the absorption column and stripper column for the new optimized sorbent. The first section will elaborate the absorption column design followed by the stripper column design. Lastly, a cost analysis of the entire DAC unit is provided.

6.1. Absorption Column Design

The absorption column of the DAC unit is designed in this section to make solid statements on its energy use and size. The basis for the design of the contacting device between the sorbent and the air is obtained from Hanafi et al. [52]. As stated before, the daily CO_2 capture target of the ZEF DAC unit is 18.75 moles per day. Assuming the sun provides enough energy to power the plant for 8 hours per day and that all CO_2 will be captured by the absorption column, **the required CO_2 capture rate of the absorber equals** $6.5 * 10^{-4}\ mol/s$**.** This value will be used in equation 4.3 together with an operating range for the STY to obtain the required contacting area of the absorber. Consequently, the required absorber size can be determined.

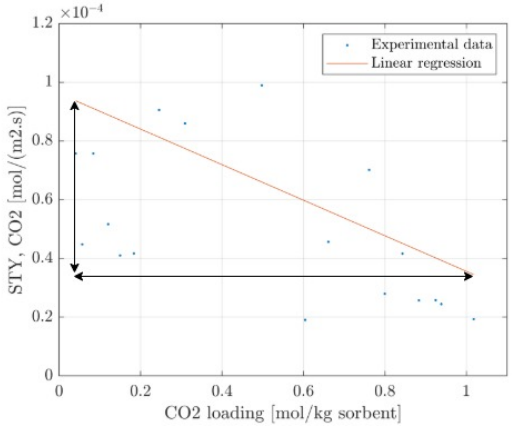

(a) A schematic of the operating range of the absolute STY of sorbent ID 18 at Sahara conditions, data obtained by Hanafi [52]

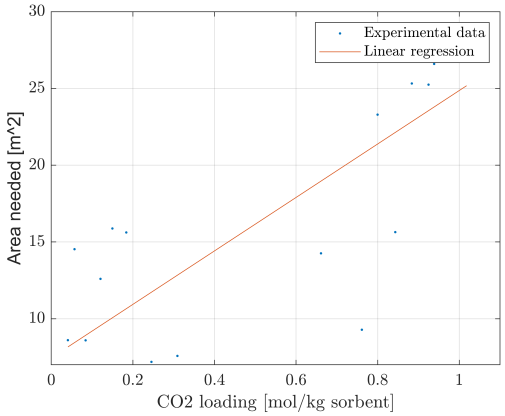

(b) The minimal required contacting area of the absorption column using sorbent ID 18 at Sahara conditions vs the operating rich loading.

Figure 6.1: Absorber area data evaluation

6.1.1. Sensitivity Analysis

The area of the absorber is a function of the STY and the STY is a function of the loading of CO_2 in the sorbent. The re-pumping experiments performed by Hanafi et al. provided the absolute STY vs CO_2 loading curve as presented below in figure 6.1a for sorbent ID 18 operated at the Sahara's conditions . Close observation shows the absolute STY of the sorbent being in the range of $0.35{*}10^{-4} \leftrightarrow 0.94 * 10^{-4}\ mol/m^2 s$, but a certain minimum loading of CO_2 is required for the system to be effective.

Assuming that minimum CO_2 loading equals $0.6\,mol_{CO_2}/kg_{sorbent}$ results in a STY operating range of $0.35*10^{-4} \leftrightarrow 0.6*10^{-4}\,mol/m^2s$. This is a valid assumption since the lean loading for sorbent ID 18 at the Sahara conditions equals $0.35\,mol_{CO_2}/kg_{sorbent}$. For the Mediterranean climate the absolute STY varies between $0.4 * 10^{-4} \leftrightarrow 0.5 * 10^{-4}\,mol/m^2s$ as can be observed in figure 5.13b in section 5.4.3, which is in the same range as for the Sahara climate. Assuming it is possible to choose an operating CO_2 loading of the sorbent in the absorption column, the required area can be calculated and plotted as in figure 6.1b. The linear regression assists to evaluate the fluctuating STY data, this way the required absorption area can still be approximated.

6.1.2. Optimized Absorber Design

In order to size the final the absorption design, the assumption is made that a contacting area of 100 m^2 per cubic meter of absorption column can be realized. This assumption is valid according to ZEF's latest absorption column design [52]. As the range of required contacting area is between $16 \leftrightarrow 25\,m^2$, the required absorber volume is $0.16 \leftrightarrow 0.25\,m^3$. **Therefore, the minimal required absorber volume for an absorber using sorbent ID 18 at the Sahara's conditions is** $0.25\,m^3$**.** That would mean that an absorber of $0.4\,m * 0.4\,m * 1\,m$ would be of sufficient size to acquire the 825 grams of CO_2 per day when sorbent ID 18 is used in the Sahara desert. Different dimensions of the absorption column are a possibility as long as the required volume of $0.25\,m^3$ is achieved. The contacting area of 25 m^2 is slightly more than the 17.82 m^2 area of the absorber, which was designed for pure TEPA as a sorbent by Matteis [82]. This could be attributed to the slightly higher area density of 107 m^2/m^3 that was used for that setup, or because of the absolute STY of pure TEPA being slightly higher than that of sorbent ID 18. As the design of the new column is slightly taller, the actual base area is kept smaller. The mass flow of the sorbent through the absorption column for both climates is calculated under the assumptions that the mass flow through the absorption column needs to be 100 times the mass flow through the desorption column, followed by Matteis's research [82]. Lastly, it must be noted that the area is calculated using the minimum STY obtained from the re-pumping experiments and that minimum STY is lower for the Sahara climate compared to the Mediterranean climate. Meaning that the absorber designed for the Sahara climate is of sufficient size to be operated at the Mediterranean climate using sorbent ID 18, TEPA:PEG-200 in the 2:5 ratio.

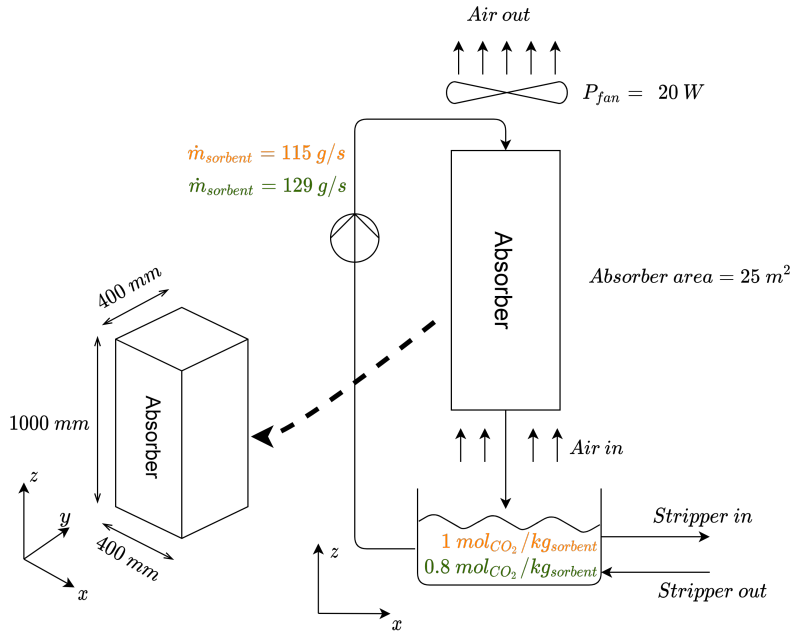

Figure 6.2: Optimized absorber design utilizing sorbent ID 18 at Sahara and Mediterranean conditions.

6.2. Stripper Column Design

The design of the stripper column will be based on the stripper model as described in detail in section 4.2.3, utilizing sorbent ID 18, the stripper design will be optimized for the Sahara climate and the Mediterranean climate. In this section, first the operating requirements of the stripper are set out. Secondly, the assumptions and data fitting regarding the specific data for sorbent ID 18 is elaborated from where a sensitivity analysis will be performed and finalized with an optimized stripper design is proposed.

6.2.1. Operating Requirements

In order to reach the methanol production target of 600 grams per day as set by ZEF the only operating requirements regarding the stripper column that has to be met is that **the stripper column will have to produce 18.75 moles of CO_2 per 8 hours of operation.** All the other requirements set by ZEF have room to play with and are therefore listed in the next section under the assumptions.

6.2.2. Assumptions

A number of assumptions will have to be made in order to set the boundary conditions for the stripper column to operate in. These assumptions are listed below:

- **A 3:1 molar ratio of H_2O to CO_2 is required in the product stream of the stripper column to produce methanol as efficiently as possible in the synthesis reactor.** The model will provide the top stage ratio of the partial pressures, which is equal to the molar ratio of the product stream. Any deviations from this will cause extra energy expense in the form of extra heat of vaporization, which will have to be accounted for, as is depicted by the $E_{3:1}$.
- **The stripper column has to operate at 1 bar absolute pressure.** This is due to the simplicity of the system, as a different operating pressure would result in extra pumps and/or valves. Any deviations from 1 bar will have to be accounted for in the energy expense.
- The heat of absorption of CO_2 into the sorbent is obtained from the experimental VLE data. When the heat of absorption is calculated, using the isotherms of 100°C and 120°C of ID 18, with the help of the Clausius-Clapeyron equation (equation 4.4), figure 6.3 is obtained. It can be seen that from a loading of $0.3\ mol_{CO_2}/kg_{TEPA}$ on wards the average heat of absorption during the absorption of CO_2 is $85\ kJ/mol_{CO_2}$, this is the heat of absorption due to the formation of carbamates, the main reaction when CO_2 is absorbed [65]. Therefore, **the heat of absorption is assumed to be $85\ kJ/mol_{CO_2}$ and remains constant throughout the stripper column.** This is backed up by the research of R. Wanderley et al., where they concluded the heat of absorption of CO_2 for water lean sorbents could be assumed to be $H_{abs} = 85\ kJ/mol_{CO_2}$ following the average of that obtained experimentally [100]. The other constants used for the stripper model are presented in table 6.1 on the next page.

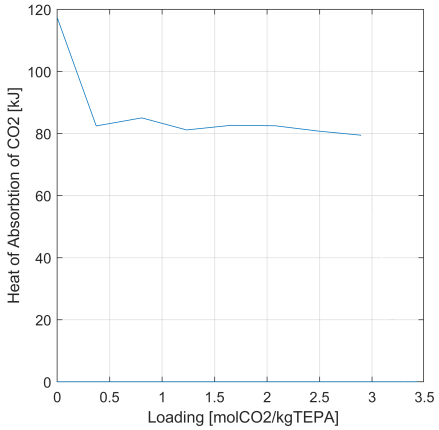

Figure 6.3: Heat of absorption of CO_2 vs Rich CO_2 loading of ID 18 at Sahara conditions.

- **The maximum reboiler temperature is set to 120°C**, as previous research at ZEF indicated that TEPA heavily degrades at temperatures above that [48].
- **The rich loading of the sorbent, obtained from the Airfarm experiments, is assumed to be the maximum loading the sorbent can acquire.** The loading could theoretically be lower than the value obtained form the Airfarm experiment, which makes this a parameters to play with.

Table 6.1: The constants used for the stripper model

Constant	Description	TEPA	PEG-200	H_2O	CO_2	Units
$C_{p,liq}$	Specific heat liquid phase	460	427	75	160	$[J/molK]$
$C_{p,vap}$	Specific heat vapor phase	0	0	33.5	37	$[J/molK]$
H_{abs}	Heat of absorption	0	0	40	85	$[kJ/mol]$

6.2.3. Optimized Stripper Design

As explained in section 4.2.5, the stripper model requires an entire field of water curves and isotherms to be able to calculate the stage specific conditions. For sorbent ID 18 the method of fitting the experimental data is presented in Appendix B.5. From there, a sensitivity analysis has been performed as is presented in Appendix B.6. Based on the sensitivity analyses an optimized design is proposed in this section. The regeneration energy demand while the 3:1 top ratio is met is the parameter that weighs heaviest in the decision making, as this value resembles the real life regeneration energy demand of the stripper closest as ZEF needs its products in that ratio. In the case of too much CO_2 or too much H_2O, it is assumed that the surplus is purged from the system or possibly stored for later use. The optimized design is made for both the Sahara and the Mediterranean climate utilizing sorbent ID 18, TEPA:PEG-200 of 2:5, of which the results are displayed below in table 6.2.3.

Table 6.2: Optimized design parameters utilizing sorbent ID 18, TEPA:PEG-200 2:5, for both the Sahara and Mediterranean climate.

Parameter	Sahara	Mediterranean	Unit
γ_{rich,CO_2}	3.5	3.9	$[mol_{CO_2}/kg_{TEPA}]$
R_{rich,H_2O}	0.25	1.20	$[kg_{H_2O}/kg_{TEPA}]$
$\mu_{rich,sorbent}$	1.50	0.23	$[Pa*s]$
N	1	5	[-]
RR	4.7	0.5	[-]
P	1000	1000	$[mbar]$
T_{reb}	120	104	$[°C]$
T_{feed}	110	94	$[°C]$
γ_{lean,CO_2}	1.28	1.43	$[mol_{CO_2}/kg_{TEPA}]$
CC	2.22	2.47	$[mol_{CO_2}/kg_{TEPA}]$
R_{top}	2.67	3.00	[-] $(p_{H_2O} : p_{CO_2})$
$\dot{m}_{feed}$	1.15	1.29	$[g/s]$
E	236	259	$[kJ/mol_{CO_2}]$
$E_{3:1}$	246	259	$[kJ/mol_{CO_2}]$

Close observation of table 6.2 shows the process parameters of the two different optimized stripper column designs for two different climates. Where the DAC unit in the Sahara climate would benefit from a single stage column, the DAC unit in the Mediterranean climate would operate best with a 5 stage column. This has all to do with the different amounts H_2O in the feed stream for the two different climates. For the Mediterranean climate, the reboiler temperature and the feed temperature have been lowered in order to get closer to the 3:1 top ratio. Furthermore, it has been chosen for both units to operate at 1000 mbar absolute pressure for the sake of simplicity of the system. The temperature of the feed is for both systems 10 °C lower compared to the reboiler temperature. This ΔT is within the limits of a counter flow heat exchanger which is used to heat up the feed stream with the outgoing lean sorbent stream. The temperature of the reboiler has been set to 120 °C for the Sahara climate, as this is the maximum temperature before the sorbent is known to degrade according to previous research at

ZEF [48]. For the Mediterranean climate the reboiler temperature is set to 104 °C, as this results in a lower p_{H_2O} compared to p_{CO_2} in the top stage. Consequently, the top ratio of 3.00 $p_{H_2O} : p_{CO_2}$ is obtained for the Mediterranean setup, which benefits the required regeneration energy. **Both systems, while utilizing sorbent ID 18, TEPA:PEG-200 2:5 as a sorbent, require less energy for regeneration compared to using aqueous TEPA.** For the Sahara climate a reboiler duty of 246 kJ/mol_{CO_2} or 1554 kWh/ton_{CO_2} and for the Mediterranean climate a reboiler duty of 259 kJ/mol_{CO_2} or 1636 kWh/ton_{CO_2} is required, opposed to 279 kJ/mol_{CO_2} or 1762 kWh/ton_{CO_2} for a system using aqueous TEPA as a sorbent, according to van de Poll's research [117]. It must be noted that the calculated regeneration energy demand resembles the best case scenario, as the heat losses are assumed to be negligible.

6.3. DAC System Design

This section combines the absorption column as designed in section 6.1 with the stripping column as designed in section 6.2 to provide an estimate on the total energy demand of the ZEF DAC unit operating in the Sahara climate and the Mediterranean climate. For this research, the design of the absorption column has been limited to the sorbent side. The following operating conditions are assumed:

- **The viscosity of the sorbent depends on the CO_2 loading and H_2O loading.** However, for the ease of calculating the pump power, the sorbent is assumed to have a constant viscosity which equals the maximum viscosity obtained from the Airfarm experiments. The viscosity of sorbent ID 18 equals 1.50 $Pa \cdot s$ for the Sahara climate, and 0.23 $Pa \cdot s$ for the Mediterranean climate.

- **The mass flow rate of the sorbent through the absorption column is assumed to be a 100 times larger than the mass flow rate of the stripper column. [82]**. For the Sahara climate, the $\dot{m}_{abs}$ equals 115 g/s and for the Mediterranean climate the $\dot{m}_{abs}$ equals 129 g/s, produced by a gear pump.

- The energy demand of the gear pump on the absorber side of the plant is defined by the viscosity and the mass flow rate of the sorbent. **Based on a pipe diameter of 1 cm, an energy demand of 1016 kWh/ton_{CO_2} was calculated for the Sahara climate, and 211 kWh/ton_{CO_2} for the Mediterranean climate.** The big difference in required pumping energy is a result of the big difference in sorbent viscosity for both climates. The exact calculations can be found in Appendix B.7.

- **The pressure and temperature of the flash tank are chosen to be 1000 mbar and 40 °C.**

- **The absorption column operates at ambient temperature, which is 30 °C for both climates.** Therefore, the streams between the absorption column and the heat exchanger are assumed to be 30 °C.

- **The condenser on top of the stripper column is assumed to be naturally cooled, which means that the top condenser does not add up to the total energy demand of the system.** In other words, the duty of the top condenser does not add up to the energy balance of the DAC system. Nonetheless, the duty for the top condenser was found to be 78.1 W for the system in the Sahara climate and 85.1 W for the system in the Mediterranean climate [121].

- **A counter flow heat exchanger is utilized in order to reduce the sensible heat requirement of the stripping column.** A HEX duty of 263.7 W was found for the system in the Sahara climate and 269.1 W for the system in the Mediterranean climate [117].

- **The air mass flow rate of the absorber is left outside of the scope of this thesis.** The fan used to suck enough air through the absorption column is assumed to have a power of 20 W for both climates and is continuously operating at full power [82]. This energy consumption equals 194 kWh/ton_{CO_2}.

An overview of the two entire DAC units optimized for both climates including all the important parameters is presented in figure 6.4. The parameters for the Sahara setup are depicted in yellow and for the Mediterranean climate in green.

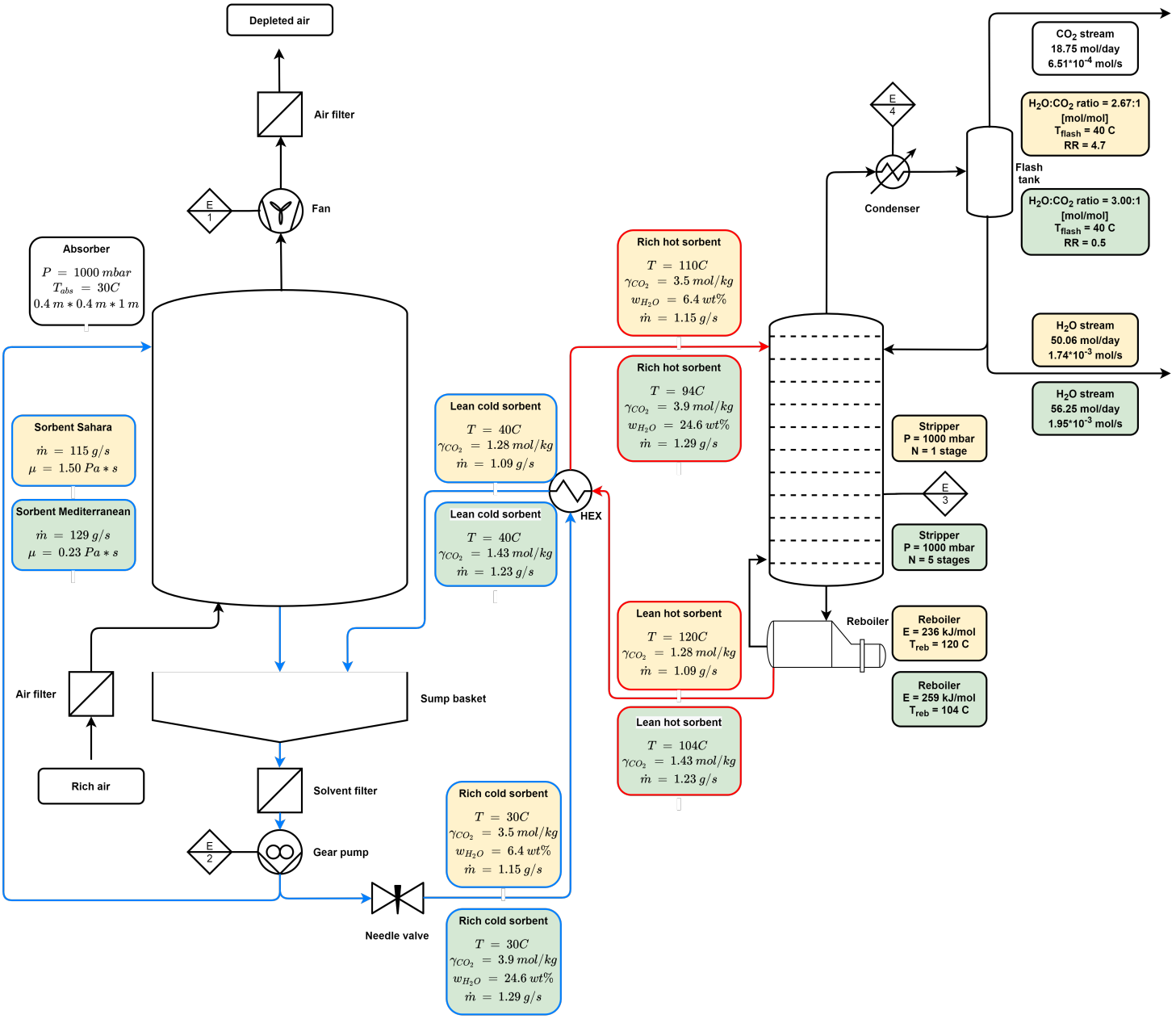

Figure 6.4: Process flow diagram of the ZEF DAC unit utilizing sorbent ID 18 at Sahara and Mediterranean conditions.

Close observation of figure 6.4 shows how the sorbent flows through the system. It flows down the absorption column into the sump, from where a gear pump provides the pumping power to pump the sorbent through the system. Most of the sorbent is pumped back up the absorption column, but a fraction of that flows to the stripper column. The magnitude of that flow is regulated by a needle valve. Before the rich sorbent enters the top stage of the stripper it flows through a counter flow heat exchanger which heats up the rich sorbent with heat supplied by the hot lean sorbent stream leaving the stripper column. The rich sorbent stream is heated up to 10 °C below the reboiler temperature before entering the stripper column. Looking at the system operating conditions in figure 6.4 and at the total amount of captured CO_2, it can be concluded that **the proposed conceptual DAC system design satisfies the system requirements as proposed in chapter 1**.

6.3.1. Cost Analysis

The previous section about the design will be used to estimate the capital costs (CAPEX). In order to make statements on the operational costs (OPEX) the energy demand of the entire DAC unit is

calculated through an energy balance based on the energy demand of the reboiler in the stripper, the gear pump and the fan on top of the absorption column, as can be seen in equation 6.1.

$$E_{tot} = E_{reb} + E_{pump} + E_{fan} \tag{6.1}$$

An overview for the energy demand of the DAC unit for both climates is provided below in table 6.3.

Table 6.3: Overview of energy demand of the ZEF DAC unit utilizing sorbent ID 18, TEPA:PEG-200 2:5

Name	Sahara	Mediterranean	Unit
E_{reb}	1554	1636	$[kWh/ton_{CO_2}]$
E_{pump}	1016	211	$[kWh/ton_{CO_2}]$
E_{fan}	194	194	$[kWh/ton_{CO_2}]$
$E_{condenser}$	757	825	$[kWh/ton_{CO_2}]$
E_{tot}	2764	2041	$[kWh/ton_{CO_2}]$

The condenser is naturally cooled so it does not add up to the total energy demand.

It must be noted that the energy use for the Sahara system is that much higher compared to the Mediterranean system because of the higher sorbent viscosity, resulting in a much higher pumping duty. Furthermore, the duty of the top condenser for both climates is relatively high, which means the top condenser to be naturally cooled could be an optimistic assumption. Therefore, more research concerning the top condenser is required. When the required energy demands of the ZEF systems are compared to the other DAC companies which were presented in chapter 2, table 6.4 is obtained.

Table 6.4: Comparison of the energy demand between ZEF and several of the leading DAC companies.

Company	Electrical energy	Heat	Unit
ZEF (Sahara)	2764	-	$[kWh/ton_{CO_2}]$
ZEF (Mediterranean)	2045	-	$[kWh/ton_{CO_2}]$
Carbon engineering	366	1460	$[kWh/ton_{CO_2}]$
Climeworks	200-300	1500-2000	$[kWh/ton_{CO_2}]$
Global Thermostat	150-160	1190-1400	$[kWh/ton_{CO_2}]$

From table 6.4 it can be concluded that ZEF's DAC unit scores in the same range as the other leading DAC companies.

In order to make statements on the CAPEX and OPEX various assumptions on inputs will have to be made, which are listed below in table 6.5.

Table 6.5: Inputs for the cost analysis

Parameter	Value	Unit
Absorber area cost	10	$[€/m^2]$
Cost per stripper stage	80	$[€/stage]$
Amount of sorbent per stage	0.2	[kg]
Amount of sorbent absorber	3	[kg]
Cost of sorbent	40	$[€/kg]$
Cost of heat exchanger	200	[€]
Maintenance cost	100	$[€/year]$
Energy cost	0.02	$[€/kWh]$

When all the assumption are taken into account and the CAPEX and OPEX are calculated for both systems it results in the following table 6.6.

Table 6.6: Overview of costs for one year to produce one tonne of CO_2 production

Climate	CAPEX	OPEX
Sahara	€2632	€155 per ton_{CO_2}
Mediterranean	€4040	€141 per ton_{CO_2}

The CAPEX is calculated for the production of one tonne of CO_2, which results in the need for four DAC units, assuming to produce 825 grams of CO_2 each and every day. The CAPEX is single investment which has to be earned back. The OPEX is calculated through the energy costs per tonne and the assumed €100 per year maintenance cost. It must be noted that this cost analysis is a qualitative analysis, as these numbers are rough estimates, since most of the cost analysis inputs are estimates.

7

Conclusion & Recommendations

The main conclusions of this research project are collected in this final chapter. The conclusions are organized with respect to the relevant research goals and questions and are taken directly from chapter 2, 5 and 6. Subsequently the recommendations for future research at ZEF are provided.

7.1. Conclusions

Select a sorbent-diluent cocktail based on the key performance indicators to optimize ZEF's DAC process.
It was found through the literature research and proved by an extensive experimental research that adding a diluent to TEPA has a profound positive effect on the overall performance of the DAC unit. A total of nine diluents in combination with TEPA have been tested, out of which **PEG-200 proved the most promising**. How this positive effect manifests itself and why PEG-200 was chosen as the best diluent is explained by the hand of the key performance indicators.

What are the key performance indicators that influence the direct air capture process at ZEF?
The complete list of KPI's including their significance regarding the ZEF DAC system is provided in section 2.4.4. Nevertheless, an overview is provided below:

- Viscosity of the rich sorbent.
- Rich CO_2 loading.
- Lean CO_2 loading.
- Cyclic capacity of the sorbent.
- Optimal top ratio of the stripper products of p_{H_2O}:p_{CO_2}= 3:1.
- Operating pressure of the stripper.
- Operating temperature of the stripper.
- Regeneration energy demand.
- Space-Time-Yield.
- Sorbent evaporation.
- Sorbent degradation.
- Hold-up time stripper.
- Cost of sorbent.

How are these KPI's influenced by adding a diluent to the polyamine?
The following conclusions can be drawn regarding the KPI's affected by the optimized sorbent after phase one of testing at the Sahara climate; 30°C and 25% relative humidity.

- Following the results of the Airfarm experiment it was concluded that sorbents diluted with selexol-250, selexol-500 and sulfolane all suffer from **layer separation** after the absorption of CO_2. Eliminating them from possible diluents.
- The **viscosity** of the sorbents diluted with DEG, PEG-200 and 1,4-butanediol remained much lower after the absorption of CO_2 compared to pure TEPA as a sorbent. Furthermore, the highly diluted TEPA:diluent of 1:3 samples remained much lower in viscosity than the 1:1 samples and were the first sorbents ever at ZEF to remain below the 2 $Pa \cdot s$ viscosity limit after reaching its presumed equilibrium CO_2 loading, even at the dry Sahara conditions. Both the pure TEPA sorbent and the sorbent diluted with glycerol were observed to cross the viscosity limit well before they reached equilibrium and were therefore eliminated as a sorbent for the ZEF DAC unit operated at Sahara conditions.
- Following the results of the VLE experiments it was concluded that the highly diluted 1:3 samples required less **energy for regeneration** compared to the 1:1 samples, as a consequence of their higher **cyclic capacity**. Which in turn was a consequence of the 1:3 samples reaching a lower **lean loading** after the stripping column. The three 1:3 sorbents comprised of TEPA plus DEG, PEG-200 and 1,4-butanediol scored within the same range for the regeneration energy demand following the VLE experiments of phase one.
- A dive deeper into the **evaporation of the diluted sorbents** distinguished the three diluents. Where neither of the three remaining diluents would satisfy the evaporation limit set by ZEF as a pure substance. However, according to literature, pure PEG-200 has a magnitude of two orders lower in vapor pressure compared to the other diluents and is therefore the least likely to evaporate at ambient conditions. Therefore, **PEG-200 was chosen as the best tested diluent.** It must be noted that no data is available on the evaporation of the sorbent mixture at ambient conditions, hence this is a recommended area of research for the future of ZEF.
- It was concluded to be very challenging for the optimized sorbent to satisfy the **optimal top ratio of the stripper products of p_{H_2O}:p_{CO_2} = 3:1** for the very dry Sahara climate. Since adding a diluent to TEPA reduces the H_2O absorption capacity. However, a stripper column configuration was configured which comes very close to the optimal top ratio as was explained in section 6.2.

Following phase one of testing as presented in 5.3 it was concluded that **sorbent ID 18, TEPA:PEG-200 2:5 would perform best at the Sahara conditions for the ZEF design specifications**.

What is the effect of climate change on the characteristics of the optimized sorbent?
For phase two of testing, the more humid Mediterranean climate (30°C and 60% relative humidity) was investigated. Where the main conclusions drawn are listed below:

- The more humid conditions resulted in an **increase of the H_2O loading** in the tested sorbents. For sorbent ID 18 an increase 18.2% was observed.
- This increase in H_2O loading resulted in a **decrease of the sorbent viscosity** of all the four sorbents comprised of TEPA and PEG-200 that were tested at the more humid conditions. For sorbent ID 18, this meant a viscosity reduction of 85% compared to the Sahara conditions.
- **It was concluded, for a more humid climate, it requires less diluent for the sorbent to stay within the 2 $Pa \cdot s$ limit.**

Design a sorbent system/process taking into account the optimum KPI's
Through a sensitivity analysis of the full DAC model as described in chapter 6 and Appendix B.6 it was concluded that the optimal ZEF DAC unit design to fulfill ZEF's operating conditions while utilizing sorbent ID 18, TEPA:PEG-200 2:5, is equal for the absorption column design yet different in stripper column design for both researched climates.

The absorption column designed for both climates operates at ambient conditions of 1000 $mbar$ absolute pressure, 30°C and requires a contacting area of 25 m^2 between the sorbent and the overflowing air. This results in an absorption column size of $0.4\ m * 0.4\ m * 1\ m$. The airflow is provided by a 20 W fan. Lastly, the mass flows of the sorbent for the two systems differ, where the unit in the Sahara climate would require a sorbent mass flow of 115 g/s, the unit in the Mediterranean climate requires a sorbent mass flow of 129 g/s.

For the Sahara climate, a single stage stripping column was designed that operates with a reboiler temperature of 120°C, 1000 mbar absolute pressure and a reflux ratio of 4.7. The feed is preheated by a heat exchanger to 110°C, has a CO_2 loading of 3.5 mol_{CO_2}/kg_{TEPA}, contains 6.4 $wt\%$ H_2O and has a mass flow of 1.15 g/s. A vapor top ratio of 2.67 and a cyclic capacity of 2.22 mol_{CO_2}/kg_{TEPA} was achieved, resulting in an energy use for the stripper of 246 kJ/mol_{CO_2}, which equals 1554 kWh/ton_{CO_2}.

For the Mediterranean climate, a five stage stripping column was designed that operates with a reboiler temperature of 104°C, 1000 mbar absolute pressure and and a reflux ratio of 0.5. The feed is preheated by a heat exchanger to 94°C, has a CO_2 loading of 3.9 mol_{CO_2}/kg_{TEPA}, contains 24.6 $wt\%$ H_2O and has a mass flow of 1.29 g/s. A vapor top ratio of 3.00 and a cyclic capacity of 2.47 mol_{CO_2}/kg_{TEPA} was achieved, resulting in an energy use for the stripper of 259 kJ/mol_{CO_2}, which equals 1636 kWh/ton_{CO_2}.

A cost analysis for both DAC units has been performed and resulted in a CAPEX of €2632 for the Sahara climate and €4040 for the Mediterranean climate, this difference is attributed to the size difference of the stripping column. Furthermore, an OPEX of €155 per tonne of CO_2 for the Sahara climate and €141 per tonne of CO_2 for the Mediterranean climate was obtained, where the main difference in energy use is due to the required pumping duty of the Sahara unit being higher due to a higher sorbent viscosity.

The main goal of this thesis was to develop a sorbent selection method in order to characterize and optimize the sorbent/solvent system for the DAC unit at ZEF.
The method was developed as described in section 3.1 and ran through its phases to come up with an optimized sorbent. **Sorbent ID 18, TEPA:PEG-200 2:5 was concluded to be the optimal sorbent** at this stage of ZEF's research, as it requires less energy for regeneration for both climates compared to pure TEPA as a sorbent followed by van de Poll's research[117].

7.2. Recommendations

In this section all the recommendations for further research at ZEF regarding the sorbent selection method found during this research project are presented below:

- **More research is required to understand how the ratio of TEPA:PEG-200 would have to be altered for it to be effective in different climates.** During this research only the dry Sahara climate and the more humid Mediterranean climate were researched, varying only the relative humidity while keeping the temperature constant at 30 °C. More research in this area could lead to a map of different sorbents which would be optimal for different climates.
- **Sorbent ID 4, TEPA:PEG-200 1:1 showed promising results for the Mediterranean climate according to the VLE experiments of phase two of testing.** More VLE data of sorbent ID 4 at the Mediterranean conditions would enable the full DAC model to be ran with ID 4. Perhaps a lot of energy gains can be made as the CO_2 loading of sorbent ID 4 at the Mediterranean climate is much higher compared to sorbent ID 18.
- **Expand the full DAC model with the mass transfer model as used in Matteis's research for the absorption column [82]**. For this to be possible more research is needed regarding the 'ice-sheet' layer of sorbent ID 18, where the concentrations of the components need to be know as well as the diffusion coefficient of CO_2 through the layer. Adding the mass transfer model would provide a more realistic absorption column design and a more complete DAC model.
- **Further elaborate the thermal degradation tests.** As described in section 5.5.1 sorbent ID 18 is prone to degrade under the influence of heat, oxygen, CO_2 or stainless steel, yet due to time

constraints, this was more qualitative research than quantitative. More research is required to get a better understanding of what has the biggest influence. Furthermore, for the degradation experiments it is key to eliminate the manual titration as this is prone to human error and very time consuming. Lastly, during the degradation experiments open to air inconsistencies regarding the CO_2 uptake occurred, possibly evaporation of the components in the sample and/or keeping a uniform temperature in the sample could prove advantageous. A method of eliminating these uncertainties is needed for accurate statements in this area.

- **Design a sorbent evaporation test setup, to test sorbent evaporation at ambient conditions.** Research has shown that the pure component vapor pressure of all the components in the sorbent is too high to comply to evaporation limit as set by ZEF as concluded in section 5.3.3. However, the vapor pressure of a mixture is known to go down upon mixing and no data is available for the mixture of the components. Therefore, it would be very interesting to test the evaporation of sorbent ID 18 at ambient conditions.
- **Regarding the re-pumping experiments, design a sample collection method not prone to human error**. The noise in the data for the re-pumping experiments is most likely caused by the way the samples were drawn from the sump of the setup, even though the sump is continuously stirred. It could well be that the sorbent in the sump is not uniformly mixed, which would result in fluctuations in CO_2 loading. It is highly recommended that the samples collection needs to be at a stationary point in the setup, for example after the pump to ensure good mixing of the sorbent mixture. By that, eliminating human error in that process.
- **Decrease sample size for VLE experiments to make them faster executable and less expensive.** During this research, most of the VLE experiments were performed by Phougat [95], it was a very time consuming process and moreover, due to large amounts of chemicals needed a very costly process. A VLE setup with a smaller sample size could possibly reduce the experimental time and costs.
- **Expand stripper model dynamically**, to give more accurate predictions on startup time, extra energy expense during startup and varying weather conditions. Furthermore, the effects of the changing seasons could be accounted for in the model, which would provide a more realistic energy demand of the stripper, as well as showing possible alterations for the sorbent for different ambient conditions.
- **Research the possibility to store excess CO_2 or H_2O** if one of these substances is produced in excess in the DAC unit. This could lead to a reduction in the energy demand of the system, when a surplus could be stored and used at a different moment of the day.
- **Look into the possibility to use the H_2O distilled from the methanol and water product stream to be used again for the synthesis**. This way the DAC unit does not need to produce its products in the molar ratio of 3:1 of H_2O and CO_2. This could lead to more sorbents being adequate for the ZEF DAC unit and more importantly, could possibly reduce the energy demand of the DAC unit.
- **A complete analysis on the cooling duty of the top condenser of the stripper column is required**. It was found during this research that the duty of the top condenser for both climates is relatively high, perhaps too high to cool naturally. Therefore, more research concerning the top condenser is required.

A

Detailed measurement equipment and experimental methodology

The details of all measurement equipment used and techniques performed for this thesis are set out in this chapter of the appendix.

A.1. Viscometer

This section discusses the basic working of the **Contraves Low Shear 40 Rheometer**, which is the machine used for the viscosity tests, along with its user manual and all obtained data regarding the bob and cup comparison.

Figure A.1: Contraves Low Shear 40 Rheometer

A.1.1. Basic Working Principles

'The Low Shear 40 is a rotational rheometer which measures the dynamic viscosity based on the Couette principle [97]. It measures the moment of a static bob inside a rotating cup. The highly sensitive

torque measuring system ensures rapid response to changes in the torque value. It is, therefore, possible to observe the elastic behavior of such substances by the determination of relaxation curves. The temperature-regulated, interchangeable measuring cup is driven by a speedcontrolled motor incorporated in the measuring head. The speed is controlled by software and continuously variable programmed in the range 10^2 to 10^{-2} rpm. The measuring cup of the coaxial measuring system, rotating at accurately defined speeds, exerts a torque on the measuring bob through the test substance. The interchangeable measuring bob is attached to a tilting system on which is fixed a multi-pole magnet arrangement and mirror. The complete tilting system is suspended on a torsion wire. An arrangement of electromagnetic coils, concentric to the pivoted magnet system, is rigidly mounted within the measuring head. Using a photo-electric system, the angular position of the bob is monitored by the mirror. When the pivoting system undergoes a deflection caused by a torque exerted on the bob, a regulating current is produced by the photo-electric system in conjunction with the compensation amplifier. This regulating current passes through the electromagnetic coils, and produces an electromagnetic torque on the multipole magnet which is in equilibrium with the mechanical moment. This regulating current is proportional to the torque prevailing on the bob and thus also to the torque prevailing at the bob and thus also to the shear stress.' as stated by the online manual [97].

A.1.2. User manual for Viscometer

This is a manual on how to use the Contraves low shear 40 rheometer to perform viscosity tests.

1. Turn on the heater and the box on top of the heater by switching the green and black/green switches.

2. The screen on the box on top of the heater tank shows C error, press enter, and press the turquoise on/off button to turn it back on again.

3. Set the temperature for T1, which is the fluid that heats up the sample that needs to be tested, and press enter. It will take some time for the machine to heat up and keep a constant temperature. The machine can go to 0 °C but it is not accurate at that temperature, the operating range is from 10-80 °C.

4. Switch on the controller on the left side of the controller, a green switch.

5. Check if the type of bob matches the code which the screen shows. The codes per type of bob are listed in the manual. You can change the bob and cup after you lift the stirrer by flipping up the switch. Make sure you pull the bob straight down when you want to change it, to minimize the strain on the sensors. When you have the right bob and cup you can proceed to the next step.

6. Take the cup from the machine and load the sample into it. Make sure there are no air bubbles inside the sample, which would affect your measurement greatly. Put the loaded cup back into the machine.

7. Lower the bob into the cup until the light next to the switch turns green

8. Press the yellow button and then the 7, which is the offset button. The machine will calibrate the bob.

9. Set the range at 5.

10. Press a value for the rotation in rad/s. The operating range is around 0.1 to 2 rad/s. You can also reverse the rotation by pressing a negative value.

11. Press ‘D’ button

12. Press ‘run’, the machine starts running.

13. Push the ‘M’ button, check whether the value is more or less than 15%. When it is less, set the range to 4. Check the value again, more or less than 15%. When it is less, set the range to 3. Check the value again, more or less than 15%, and so on until the value is above 15%, this will give you the most accurate reading. **NEVER** let it get above 100%, this can potentially damage the machine.

14. Check the temperature of the cup by pushing the ‘T’ button; this is the closest you’ll get to the actual temperature of the sample. This value has an error of 0.9°C, therefore you should add 0.9 to the given temperature to obtain the actual temperature.

15. You can check the viscosity by pressing the ‘η’. The unit is [Pa*s], if there is a -2 before this it means xxx*10^{-2} pa*s

16. If the viscosity is still changing that means that your sample is not at uniform temperature yet and you have to wait until the viscosity becomes

17. Do various tests at different speeds, the viscosity should not change.

18. Register the temperature and viscosity.

19. The test is complete.

20. Raise the bob from the cup again.

21. Clean the bob and the cup.

22. It is logical to test different samples with the same temperature on the same day, because it takes time for the temperature to become constant.

23. Switch off the three devices.

A.1.3. Data Obtained from Viscometer

Comparison of bobs and cups

Since measurements of the viscosity of every Airfarm sample until 2 Pa-s will have to be taken, a smaller in volume size bob will have to be used in order to test the small daily Airfarm samples. A comparison between bobs has been made, the 41S/1S is the one that come closest to the MS-DIN 412/8S, and has the smallest of test volumes. A comparison between pure TEPA, PEI-600 and sample ID14 from the same bottle has been performed, as well as a sample close to 2 Pa-s to check the error.

MS-DIN 412/8S				pure TEPA					
Temp(degC)				20					
Deformation rate(rad/sec)	0,1	0,2	0.4	0.6	0.8	1	1.5	2	
Range	2	2	3	3	3	3	4	4	avg
Viscosity(pa-s) run 1	0,08512	0,08337	0,08055	0,08121	0,08115	0,081	0,08241	0,08197	0,082098
Viscosity(pa-s) run 2	0,08268	0,0839	0,08758	0,08687	0,08652	0,08636	0,0856	0,08592	0,085679
Viscosity(pa-s) run 3	0,09266	0,09064	0,08785	0,08829	0,08831	0,08827	0,09001	0,08993	0,089495

41S 1S				pure TEPA					
Temp(degC)				20					
Deformation rate(rad/sec)	0,1	0,2	0.4	0.6	0.8	1	1.5	2	
Range	2	2	3	3	3	3	4	4	avg
Viscosity(pa-s) run 1	0,2106	0,1045	0,14	0,1263	0,1206	0,1158	0,1174	0,1146	0,131225
Viscosity(pa-s) run 2	0,3132	0,1577	0,1394	0,1334	0,129	0,1277	0,1226	0,1216	0,155575
Viscosity(pa-s) run 3	0,2581	0,1316	0,1487	0,1523	0,1526	0,1513	0,1468	0,1433	0,160588

MS-DIN 412				pure TEPA					
Temp(degC)				20					
Deformation rate(rad/sec)	0,1	0,2	0.4	0.6	0.8	1	1.5	2	
Range	2	3	3	3	3	3	4	4	avg
Viscosity(pa-s) run 1	0,07302	0,07608	0,0764	0,07608	0,07576	0,07557	0,07604	0,07604	0,075624
Viscosity(pa-s) run 2	0,07767	0,07735	0,07841	0,07918	0,07888	0,07921	0,07928	0,07858	0,07857
Viscosity(pa-s) run 3	0,09872	0,09869	0,09764	0,09665	0,09626	0,09654	0,09661	0,09675	0,097233

MS-DIN 412/8S			pure PEI 600						
Temp(degC)				20					
Deformation rate(rad/sec)	0,1	0,2	0.4	0.6	0.8	1	1.5	2	
Range	4	5	5	5	5				avg
Viscosity(pa-s) run 1	2,753	2,759	2,752	2,746	2,739				2,7498
Viscosity(pa-s) run 2	2,772	2,766	2,759	2,75	2,736				2,7566
Viscosity(pa-s) run 3	2,78	2,772	2,752	2,743	2,732				2,7558

MS-DIN 412			pure PEI 600						
Temp(degC)				20					
Deformation rate(rad/sec)	0,1	0,2	0.4	0.6	0.8	1	1.5	2	
Range	4	5	5	5					avg
Viscosity(pa-s) run 1	2,706	2,725	2,677	2,658					2,6915
Viscosity(pa-s) run 2	2,799	2,799	2,778	2,757					2,78325
Viscosity(pa-s) run 3	2,738	2,736	2,714	2,702					2,7225

The MS-DIN 412 comes closest, at low viscosity and around 2 Pa*s. The deviation could be the cause of the bob having a larger surface area, so the sorbent absorbs more CO2 from the surroundings in between the runs. The deviation is within the acceptable range. The sample size for MS-DIN 412 is 1,75ml compared to 2,7ml for the MS-DIN 412/8S, this means that 2ml samples can be drawn from the Airfarm and tested daily on viscosity.

41S 1S			AF 4 cocktail ID 18						
Temp(degC)				20					
Deformation rate(rad/sec)	0,1	0,2	0.4	0.6	0.8	1	1.5	2	
Range	4	4	5	5	5	5			avg
Viscosity(pa-s) run 1	3,765	3,737	3,73	3,699	3,698	3,677			3,717667
Viscosity(pa-s) run 2	3,804	3,751	3,73	3,704	3,656	3,63			3,7125
Viscosity(pa-s) run 3	3,472	3,554	3,659	3,662	3,621	3,602			3,595

MS-DIN 412/8S			AF 4 cocktail ID 18						
Temp(degC)				20					
Deformation rate(rad/sec)	0,1	0,2	0.4	0.6	0.8	1	1.5	2	
Range	4	5	5	5					avg
Viscosity(pa-s) run 1	3,666	3,648	3,622	3,588					3,631
Viscosity(pa-s) run 2	3,565	3,608	3,584	3,573					3,5825
Viscosity(pa-s) run 3	3,573	3,588	3,552	3,539					3,563

A.2. Karl-Fischer Titrator

This section discusses the basic working of the *Mettler & Toledo V10S Volumetric KF Titrator*, which is the machine used to test the H_2O concentration in the samples, along with its user manual.

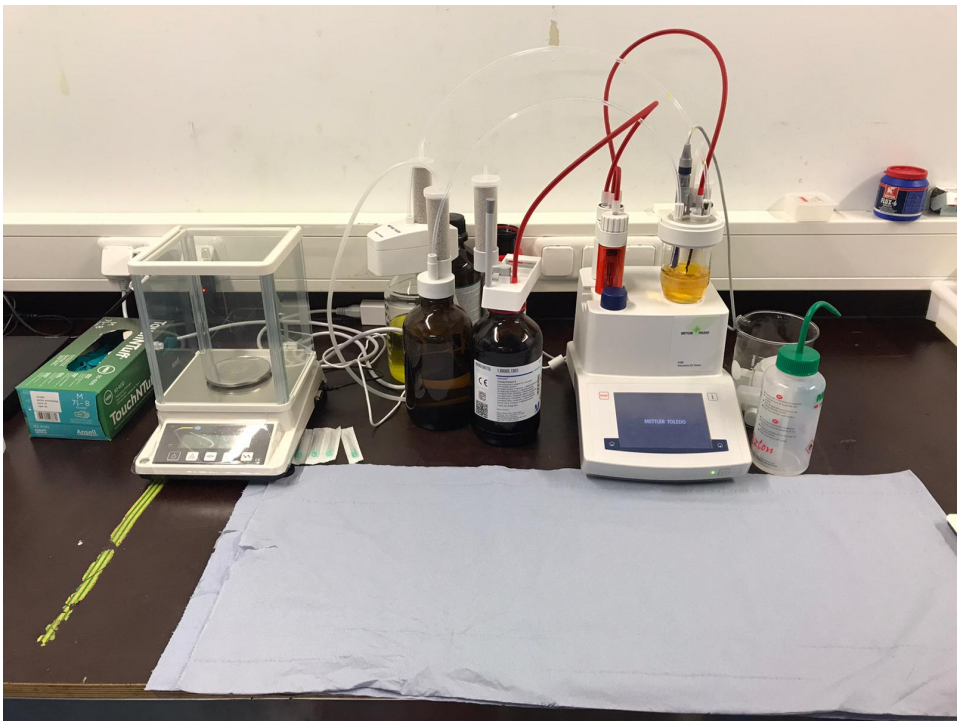

Figure A.2: Mettler & Toledo V10S Volumetric KF Titrator

A.2.1. Basic Working Principles

The Karl-Fischer test provides the amount of H_2O in the sample that is tested. Therefore, it provides the H_2O concentration of the sample. In the yellow container on the machine there is a sorbent, which is CH_2OH, Methanol. There is a titrant flowing to that container which delivers iodine to the container, after the sample has been added. The machine measures the resistance of the fluid in it through an electrode. When the sample is added, the machine slowly adds the iodine to the sample, which reacts with the water in the sample. The machine knows how much iodine has been added to the sample and therefore, it knows how much water is in the sample at the moment when the resistance of the sample is back to what it was before loading it. Since it knows how much iodine reacts with a certain amount of water; 1 mole of iodine reacts with 1 mole of H_2O. 1ml of iodine corresponds to 5mg of H2O, but the machine will do all the calculations. This does mean that the amount of H_2O that is loaded into the machine should be very small, otherwise the iodine will run out quickly. The test will take about 60 seconds when the amount of H_2O is not too big.

A.2.2. User manual for the KF titrator

This is a manual on how to use the *Mettler & Toledo V10S Volumetric KF Titrator* to analyse samples on the H_2O concentration.

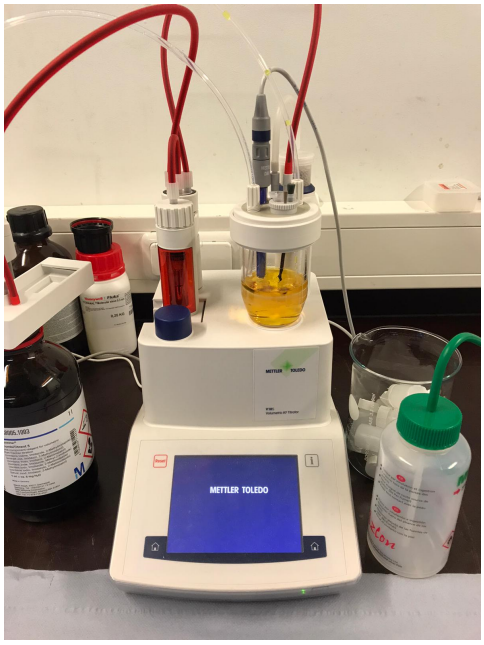

1. Take your amine sample, about 0.2g of it. Note the exact value and call it **A**.
2. Mix your sample with a lot of CH3OH, about 2g. Note the exact value and call it **B**.
3. Mix it very well.
4. Press play on the display.
5. Press *'run ZEF'*.
6. Make sure the 'drift' is less than 15. Drift is the error in the machine, so how much H_2O it senses without you having added anything. If it is not less than 15, you will not be able to start the test and you will have to take the H_2O out first.
7. Press *'start sample'*.
8. Take a small sample from the mixture, about 0,3ml.
9. Wipe the syringe clean.
10. Way the syringe and set the scale to zero.
11. Add the sample into the container trough the small nipple on top, after removing the small rubber cork. Make sure that no fluid of the injected sample hits the inner wall of the container such that everything directly hits the sorbent on the bottom.
12. Put the syringe on the scale and the negative number now represents the weight of the mixture that you have added. Note this exact value and call it **C**.
13. Enter the weight of the added sample into the machine.
14. Wait until the machine gives the amount of H2O that you've put into the machine in % of the sample that has gone into it. Note this exact value and call it **D**.
15. Now the mass concentration of H_2O can be calculated using the following equations:

$$X_{H_2O} = \left(\frac{D}{100} * C\right) * \left(\frac{A+B}{A*C}\right) * 100\% \quad \text{(A.1)}$$

A.3. Fourier-Transform Infrared Spectroscopy

'The vibrational spectrum of any molecule can be considered as a unique physical property which would be characteristic of the molecule. The atoms of every molecule are always vibrating. Infrared spectroscopy is the study of interaction of light with matter. When a molecule absorbs infrared radiation, its chemical bonds vibrate. The bonds can stretch, contract, wag and bend. This is why infrared spectroscopy is a type of vibrational spectroscopy. The measurements obtained in infrared spectroscopy gives an infrared spectrum, which is a plot of measured infrared intensity versus wavelength (or wavenumber) of light. Solids, Liquids, gases, semi-solids, powders and even polymers can be analysed by identifying the positions of their peaks, intensities, width and shapes of the plot obtained by infrared spectroscopy. Fourier-transform infrared spectroscopy (FTIR) is an analytical technique used to identify organic (and in some cases inorganic) materials.' as explained by Sinha, 2019, 120 [112]

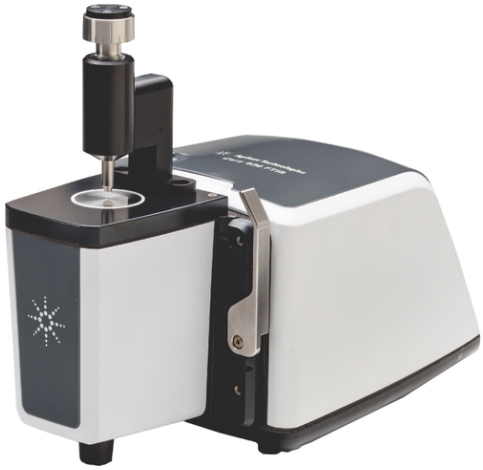

Figure A.3: FTIR setup of *Agilent Cary 630*.

A.3.1. Basic Working Principles

Figure A.4 depicts the working principle of FTIR. The general components of a Fourier Transform Infrared Spectrometer include a source, an interferometer, a sample compartment, a detector and a computer. The source would emit infrared energy. This beam would pass through an aperture which would control the amount of energy being provided to the sample, and ultimately to the detector. The beam enters the interferometer in which the interference of two beams of light would be employed to make precise measurements. The resulting interferogram signal would exit the interferometer and enter the sample compartment. This is where specific frequencies of energy which are uniquely characteristic of the sample are absorbed. The beam passes into the detector for final measurement and the measured signal is digitized and sent to the computer where the Fourier transform takes place. The final infrared spectrum is showed on the computer for further analysis [44]. as explained by Sinha, 2019, 122 [112]

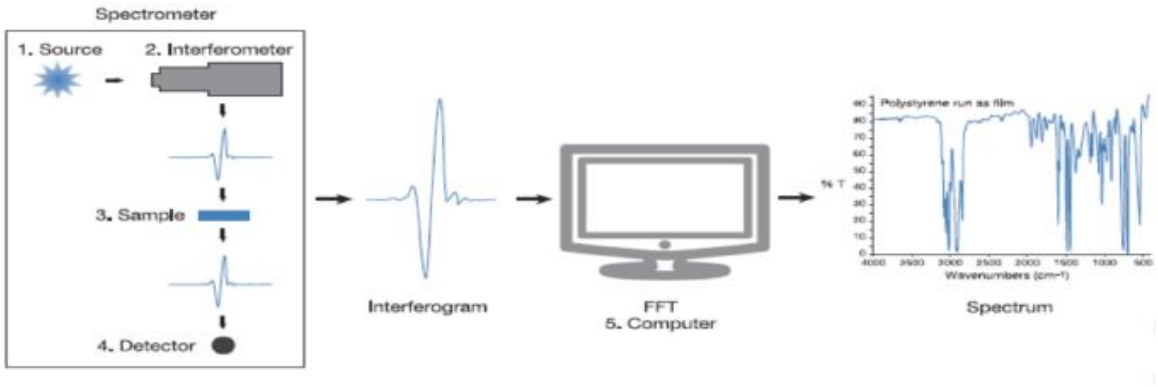

Figure A.4: Schematic of the working principle of the FTIR. [44]

A.3.2. User manual for the FTIR

1. Plug the machine in.
2. Turn it on, the light will start to flicker .
3. Open *Microlab PC* on the pc, when the light becomes stable and green.
4. Press start.
5. Clean the crystal which will shine the light on the sample, clean it with methanol.
6. If you want to test a solid you need to clamp it down.
7. Click that you've cleaned the crystal, it will now make a background spectrum.
8. Put a drop of fluid from the sample on top of the crystal.
9. Make sure it is in the center and that the entire crystal is covered, there should be no air gaps.
10. Press next.
11. It already gives the spectrum it detects.
12. Save it with a clear sample ID.
13. Click next.
14. No it gives the spectrum.
15. The files are stored in A2R file in the C-disk, users, public, public documents, agri, results.
16. Open *TQ Analyst*, where you can quantify the concentrations, if the FTIR is calibrated.
17. For the calibration of the FTIR there is referred to Sinha's thesis report [112], page 127.

A.4. Phosphoric acid test

This section discusses the basic working of the phosphoric acid test setup, which is the machine used to test the CO_2 concentration in the samples, along with its user manual.

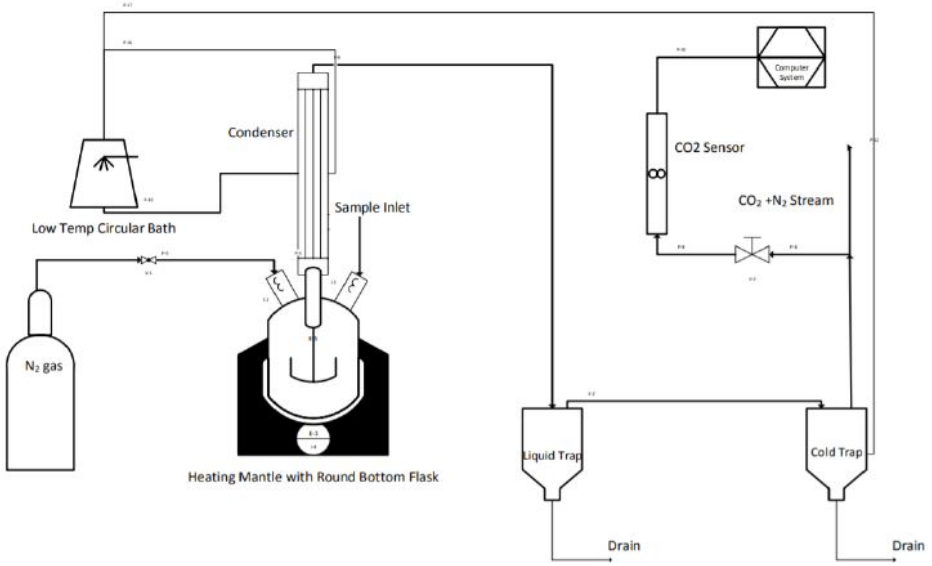

Figure A.5: A schematic of the phosphoric acid setup [1]

A.4.1. Basic Working Principles

'The round bottom flask contains about 350 ml of 85% phosphoric acid. With a constant temperature of the heating mantle at about 240±C, the phosphoric acid in the round bottom flask can be maintained at around 150±C which provides sufficient heat to desorb the amines containing CO_2. Small sample of loaded amine can be inserted in the round bottom flask leading to desorption of CO_2 due to esterification between the amine and hot phosphoric acid. The resultant gases desorbed flow through a condenser which is kept at around 8±C to condense water vapours before the gas stream enters the CO_2 analyzer. A nitrogen tank is used to dilute these gases and constantly flows through the round bottom flask to the CO_2 analyzer. The CO_2 gas carried by nitrogen enters the CO_2 analyzer which records voltage changes and calibrates it to CO_2 partial pressure. Through the partial pressure of CO_2, the mass flow rate of CO_2 is calculated and a total amount of CO_2 is displayed on the user interface on the computer' as explained by Sinha, 2019, 119 [112] [1].

A.5. Manual Acid-Base Titration

Manual Acid-Base titration was used during this research to determine the loss of amine sites in the sorbent after it was exposed to heat, oxygen, CO_2 and stainless steel.

A.5.1. Basic Working Principles

'An acid-base titration is an experimental procedure used to determined the unknown concentration of an acid or base by precisely neutralizing it with an acid or base of known concentration. This lets us quantitatively analyze the concentration of the unknown solution. Acid-base titrations can also be used to quantify the purity of chemicals. The solution in the flask contains an unknown number of equivalents of base (or acid). The burette is calibrated to show volume to the nearest 0.001 cm3. It is filled with a solution of strong acid (or base) of known concentration. Small increments are added from the burette until, at the end point, one drop changes the indicator PH permanently. At the equivalence point, the total amount of acid (or base) is recorded from the burette readings. The number of equivalents of acid and base must be equal at the equivalence point.' as stated by Chemistry [25].

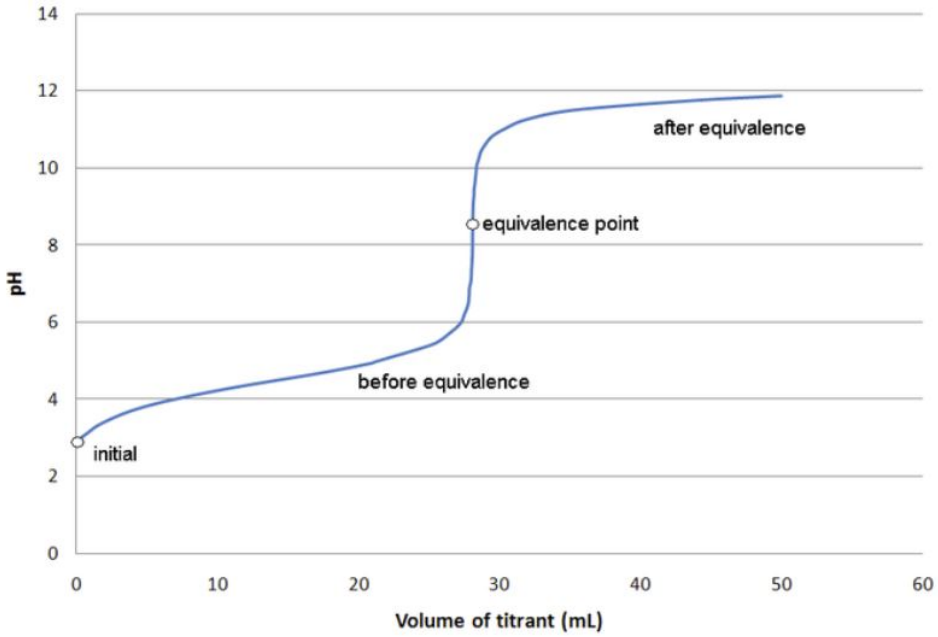

Figure A.6: Equivalence point of the titration curve. [25]

When the amount of acid, in our case HCl, which is added to the sample is known for the equivalence point, the concentration of amine sites can be calculated, as it is known that one mol of HCl neutralizes an equal amount of N molecules. One mole of TEPA contains 5 mole of N, by this, the amount of TEPA in the sample can be calculated. If this deviates from what has to be in there, that means amine site loss has occurred.

B

Experimental Data and Calculations

B.1. Preliminary viscosity test

%	PEG-200	PEG-400	PEG-600	Selexol-250	Selexol-500
79-10-1-10	0.430 0.193 0.105	0.388 0.177 0.090	0.414 0.194 0.100	0.236 0.118 0.064	0.285 0.146 0.075
39-10-1-50	0.395 0.190 0.101	0.440 0.209 0.113	0.500 0.245 0.127	0.115 0.059 0.046	0.305 0.149 0.072
76-10-4-10	1.373 0.592 0.286	1.460 0.604 0.287	1.360 0.576 0.275	0.800 0.360 0.183	1.836 0.730 0.325
36-10-4-50	0.994 0.455 0.224	0.820 0.422 0.224	1.365 0.575 0.275	Xxx Xxx Xxx	0.850 0.560 0.345
59-30-1-10	0.355 0.160 0.080	0.410 0.180 0.086	0.431 0.189 0.092	0.356 0.150 0.073	0.519 0.210 0.100
19-30-1-50	0.067 0.040 0.024	0.114 0.063 0.037	0.138 0.077 0.044	0.069 0.042 0.010	0.144 0.046 0.031
51-30-9-10	1.560 0.635 0.289	1.710 0.720 0.320	2.465 0.951 0.430	1.980 0.821 0.379	3.880 1.330 0.492
17-30-3-50	0.080 0.048 0.029	0.148 0.085 0.052	0.225 0.129 0.083	0.101 0.027 0.019	0.145 0.054 0.030
Pure TEPA	0.076 0.052 0.028	Pure PEG-200	0.067 0.040 0.027	Pure PEG-400	0.095 0.073 0.049
Pure PEG-600	0.173 0.109 0.073	Pure SEL-250	0.00669 0.00456 0.00450	Pure SEL-500	XXX 0.0280 0.0214

Figure B.1: Table of results of preliminary viscosity tests at 20, 30 and 40 °C in $[Pa \cdot s]$. % are in TEPA-H_2O-CO_2-Diluent. Green means easily mixed, orange means layers do separate but can be mixed manually, red means impossible to mix.

From this preliminary viscosity test sequence the following conclusion were drawn:

1. The lighter in mass diluents seem to have the biggest influence in reducing the viscosity of the sorbent.
2. The diluents comprised of selexol and TEPA were observed to separate from each other after the sample is loaded with CO_2, hence layer separation is an important characteristic to keep in mind.

B.2. Wilson Parameters

The Wilson parameters where fitted such that the water curves coincided with the experimental water curves obtained for sorbent ID18. The obtained Wilson parameters are listed below and they provide a water curve fit as presented in figure B.2.

$$\Lambda_{12} = 0.755054965 \tag{B.1}$$

$$\Lambda_{21} = 2.37976461968 \tag{B.2}$$

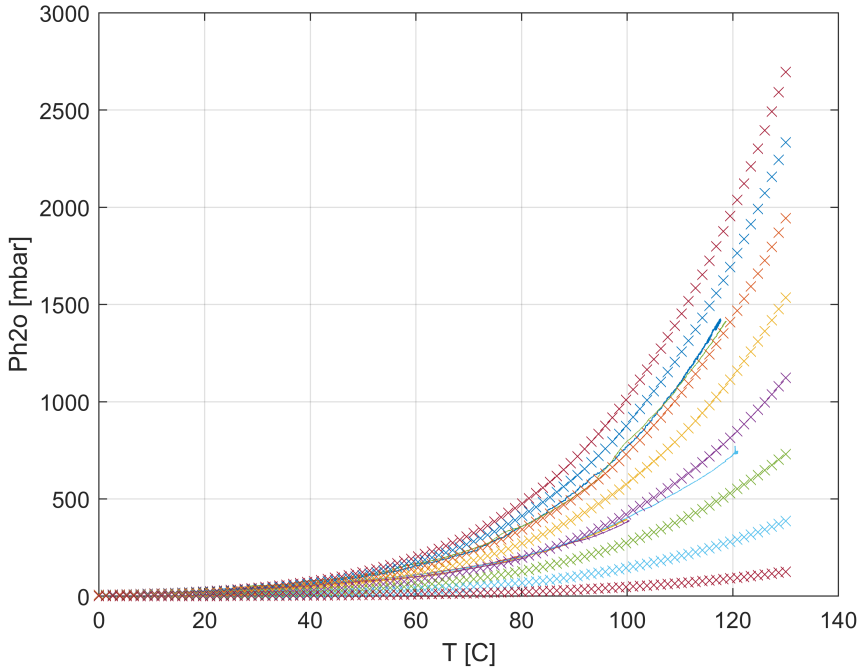

Figure B.2: Vapor curve fit for sorbent ID 18

B.3. Stripper Model: Mass Balance

A trial-and-error iterative solution is used to solve the mass balances for flash tank i. The Rachford-Rice equation (equation B.3) is used iteratively to calculated the composition vector of the liquid mixture [117].

$$x_{i,j} = \frac{z_{i,j}}{1 + \beta(K_j - 1)} \tag{B.3}$$

$$K_j = \frac{y_j}{x_j} \tag{B.4}$$

$$y_i = \left[0 \quad \frac{p_{H_2O}}{p_{H_2O} + p_{CO_2}} \quad \frac{p_{CO_2}}{p_{H_2O} + p_{CO_2}}\right] \tag{B.5}$$

Where β resembles the vaporized fraction of the feed, which is between 0 and 1 and K_j resembles the equilibrium constant for component j and is calculated with equation B.4. The partial pressures of H_2O and CO_2 determine the composition vector of the vapor mixture y_i as is defined in equation B.5. The Rachford-Rice equation is solved for β and K_j through a double looped bisection solver as is displayed below in figure B.3.

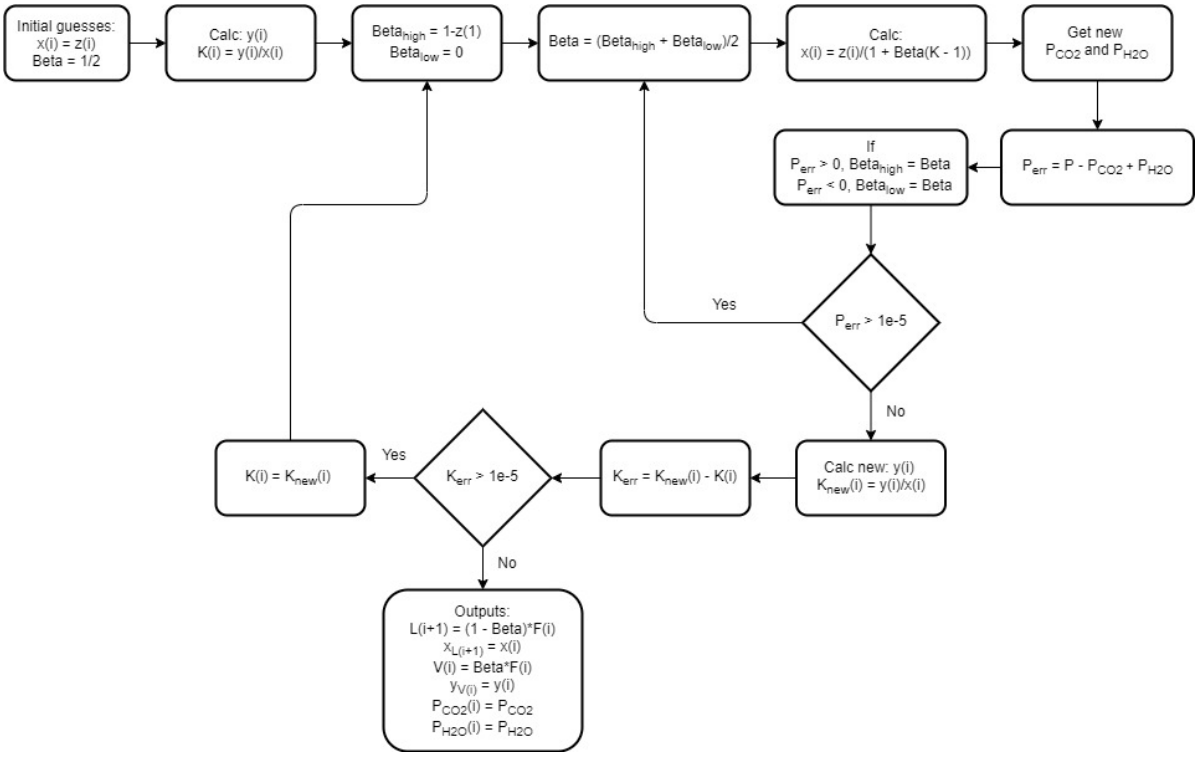

Figure B.3: Rachford-Rice solving methodology, using a double bisection numerical root-finder for a flash stage i. The flow chart was made by van de Poll [117].

B.4. Stripper Model: Energy Balance

The energy balance of a single stage i is comprised of the energy flows depending on the heat of absorption, desorption and the sensible heat of the mass flows flowing in and out of the stage. The energy balance solved is the following [117]:

$$Q_{tot,i} = Q_{L_i} + Q_{V_i} + Q_{A_i} + Q_{abs_i} \tag{B.6}$$

$$Q_{L_i} = \sum_{j=1}^{C} L_i x_{i,j} C_{p,liq}(T_{L_i} - T_i) \tag{B.7}$$

$$Q_{V_i} = \sum_{j=1}^{C} V_{i+1} y_{i+1,j} C_{p,vap}(T_{i+1} - T_i) \tag{B.8}$$

$$Q_{A_i} = \sum_{j=1}^{C} A_i z_{A_{i,j}} C_{p,liq}(T_{A_i} - T_i) \tag{B.9}$$

$$Q_{abs_i} = \sum_{j=1}^{C} (V_{i+1} y_{i+1,j} - V_i y_{i.j}) H_{abs} \tag{B.10}$$

Where $Q_{tot,i}$ resembles the total amount of heat flowing into the stage i, Q_{L_i} resembles the sensible heat by the liquid inflow, Q_{V_i} resembles the sensible heat by the vapor inflow, Q_{A_i} resembles the sensible heat by the additional feed into the stage and Q_{abs_i} resembles the heat of absorption required to absorb the difference between the gas in- and out flow. Furthermore, $C_{p,liq}$ resembles the heat capacity of the liquid components, $C_{p,vap}$ the heat capacity of the components in the vapor phase and H_{abs} resembles the heat of absorption of the components. The assumption is made that the heat loss of the stripper is negligible, therefor this factor is left out of equation B.6.

The temperature is updated as explained in section 4.2.7. The visual interpretation of the energy balance part of the model with the updated temperature is provided below. [117]

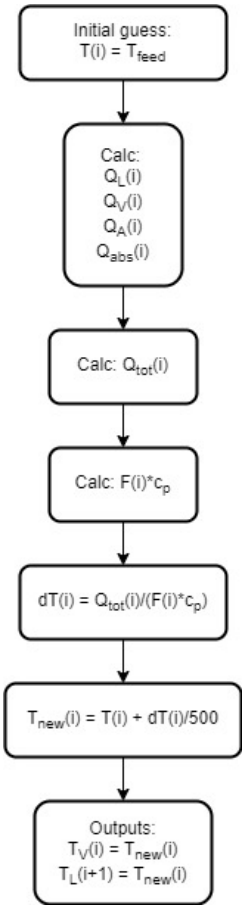

Figure B.4: Visual interpretation of the energy balance part of the stripper model. The flow chart was made by van de Poll [117].

B.5. Stripper Model: Experimental Data Fitting Sorbent ID 18

As explained in section 4.2.5, the stripper model requires an entire field of water curves and isotherms to be able to calculate the stage specific conditions. For sorbent ID 18 at the Sahara conditions, two isotherms and one ambient loading point where experimentally obtained as is displayed in figure B.5.

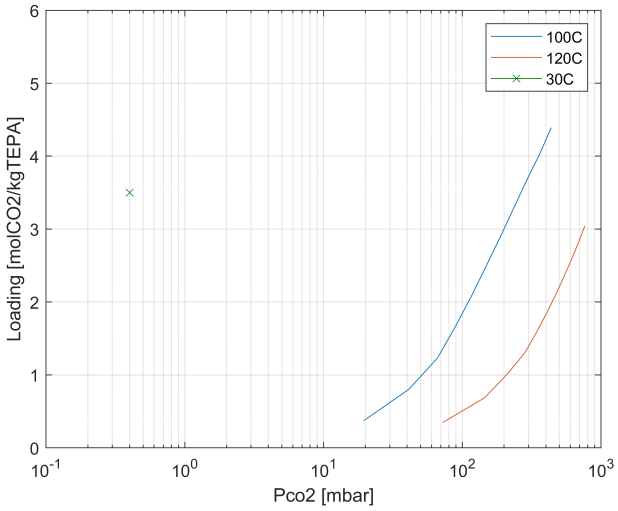

Figure B.5: Experimental VLE data of CO_2 for ID 18 at Sahara conditions.

When the two isotherms are fitted using five different methods of isotherm fitting the comparison between fits is obtained as is displayed in figure B.6. Close observation reveals that the best fit on the experimental data is obtained using the Toth method. As the linear fit is far off, both the Langmuir and the Sips fit seem to cross at higher loading, which is physically impossible and the Freundlich fit is off at lower loading. Consequently, the Toth fit is chosen to fit the experimental data of sorbent ID 18.

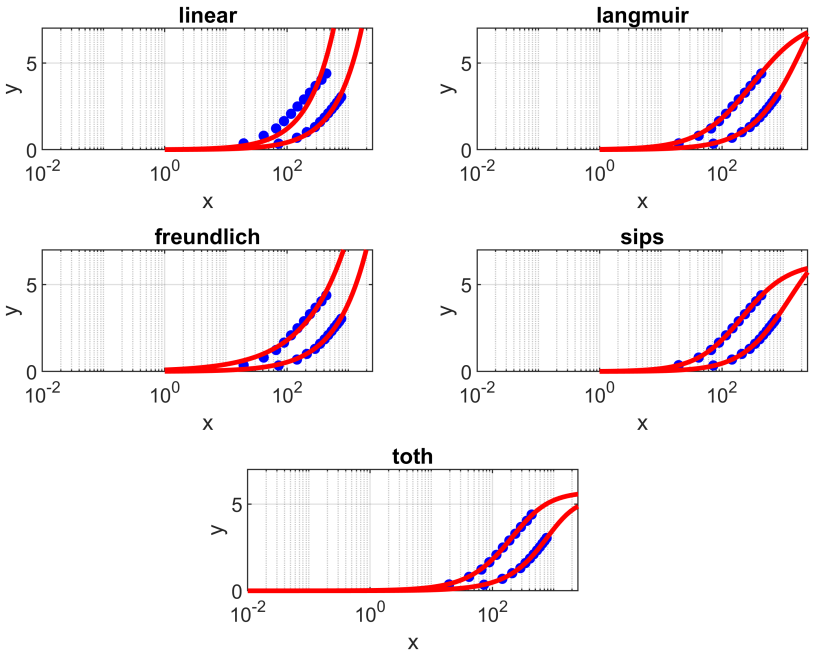

Figure B.6: Isotherm fit comparison

The next step in the process is to extrapolate the the Toth fitted data, to form the entire field of isotherms with the help of the Clausius-Clapeyron equation (4.4) as described in section 4.2.5. The field of

isotherms is displayed below in figure B.7. Close observation shows the partial pressure of CO_2, at the ambient loading data point of $3.5\ mol_{CO_2}/kg_{TEPA}$ obtained from the Airfarm experiments, being 0.430 mbar, which is equivalent to a CO_2 concentration of 425 ppm. This number is very close the actual average global CO_2 concentration in ambient air of 420 ppm [28]. Consequently, it is assumed that the fit is sufficient and that the assumption of the constant heat of absorption of CO_2 of 85 kJ/mol_{CO_2}, which is needed for the Clausius-Clapeyron equation, is valid.

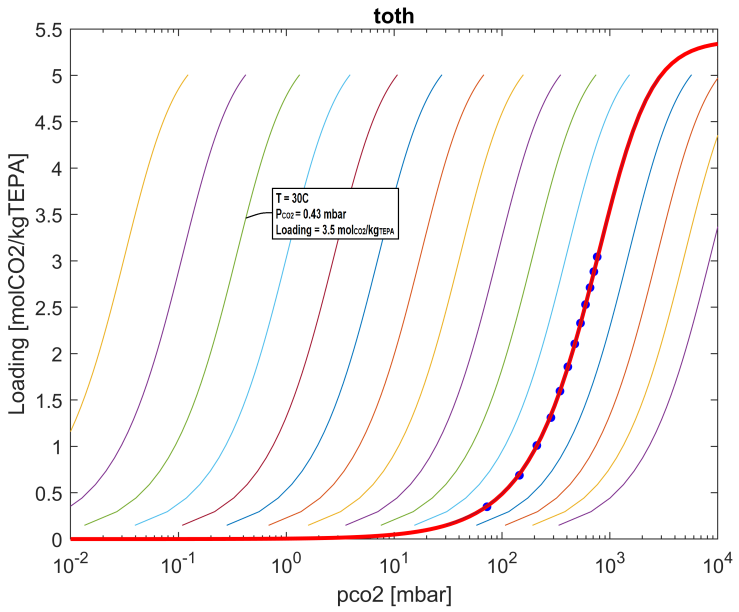

Figure B.7: Toth fitted field of isotherms for sorbent ID 18 at the Sahara conditions.

As the data for ID 18 at the Sahara conditions is now fitted, the next step in the process is to perform a sensitivity analysis with the help of the stripper model. Which will provide insights in how an optimized stripper design unitizing sorbent ID 18 is going to look like and from there, the DAC system can be designed.

B.6. Stripper Model: Sensitivity Analysis for Sorbent ID 18

In this section, a sensitivity analysis is performed to evaluate the effect of all the parameters on the performance of the stripper column. In order to compare the different configurations of the stripper column a base case has to be set out. The values of the base case are presented below in table B.1. For the base case, sorbent ID 18 with the CO_2 and H_2O concentrations as obtained from the Airfarm experiments is used along with the stripper column design as proposed by van de Poll [117]. For each parameter that is varied, all the parameters that are affected by this will be evaluated. As the regeneration energy is evaluated per mole of CO_2, it is assumed that the feed mass flow rate has no affect on the regeneration energy. Resulting from the sensitivity analysis, an optimization for the stripper column design will be proposed and presented in section 6.2.3.

Table B.1: Base case parameters utilizing sorbent ID 18, TEPA:PEG-200 2:5, Sahara climate

Parameter	Value	Unit
γ_{rich,CO_2}	3.5	$[mol_{CO_2}/kg_{TEPA}]$
R_{rich,H_2O}	0.25	$[kg_{H_2O}/kg_{TEPA}]$
γ_{lean,CO_2}	1.41	$[mol_{CO_2}/kg_{TEPA}]$
CC	2.09	$[mol_{CO_2}/kg_{TEPA}]$
R_{top}	1.43	[-] $(p_{H_2O} : p_{CO_2})$
T_{reb}	120	$[°C]$
T_{feed}	105	$[°C]$
N	5	[-]
RR	0.55	[-]
P	1000	$[mbar]$
E	209	$[kJ/mol_{CO_2}]$
$E_{3:1}$	302	$[kJ/mol_{CO_2}]$

Absolute Pressure

If the absolute pressure of the stripper is input parameter varied deviating from the base case scenario, the parameters which are affected by this are presented in table B.2. Close observation reveals that increasing the P_{abs} while keeping the T_{reb} constant increases the lean loading and therefore, decreases the cyclic capacity. Furthermore, as the P_{CO_2} rises significantly faster than the P_2O in the top stage, it decreases the amount of H_2O in the top ratio, as van de Poll also observer [117]. Consequently, the required energy demand to produce the 3:1 molar ratio of H_2O to CO_2 goes up. **So, increasing the absolute pressure results in lower lean loading, lower cyclic capacity and lower vapor top ratio.**

Table B.2: Effect of absolute pressure P_{abs} on performance parameters of stripper column.

P_{abs} $[mbar]$	γ_{lean,CO_2} $[mol_{CO_2}/kg_{TEPA}]$	CC $[mol_{CO_2}/kg_{TEPA}]$	R_{top} $[p_{H_2O} : p_{CO_2}]$	E $[kJ/mol_{CO_2}]$	$E_{3:1}$ $[kJ/mol_{CO_2}]$
500	0.35	3.15	3.16	252	259
750	0.75	2.75	1.98	214	258
1000	1.41	2.09	1.43	209	302
1250	2.11	1.39	1.13	232	373
1500	2.79	0.71	0.94	321	508

Reboiler Temperature

As the temperature of the feed is controlled by the temperature of the sorbent flowing from the stripper column, which is assumed to be equal to the reboiler temperature, the temperature of the feed is assumed to be 15 °C lower than the reboiler temperature. Furthermore, due to the fact that H_2O needs to boil from the mixture, P_{abs} is adjusted for the lower temperature range. P_{abs} is obtained from the vapor curve of ID 18 at the Sahara climate. The results are set out in table B.3. It can be seen that an increase in T_{reb} corresponds to a lower lean loading and therefore, a higher cyclic capacity. Furthermore, it increases the P_{H_2O} in the top stage. Resulting in less required energy to produce the 3:1 molar ratio of H_2O to CO_2. For this analysis, a minimum was obtained for $T_{reb} = 150°C$ and $T_{feed} = 135°C$ as this obtained the closest to 3:1 top ratio. **Increasing the reboiler temperature and feed temperature decreases the lean loading, thus increases the cyclic capacity. Furthermore, it increases the top ratio, but only when the absolute pressure is held constant.**

Table B.3: Effect of reboiler temperature T_{reb} on performance parameters of stripper column.

T_{reb} [°C]	T_{feed} [°C]	P_{abs} [mbar]	γ_{lean,CO_2} [mol_{CO_2}/kg_{TEPA}]	CC [mol_{CO_2}/kg_{TEPA}]	R_{top} [$p_{H_2O} : p_{CO_2}$]	E [kJ/mol_{CO_2}]	$E_{3:1}$ [kJ/mol_{CO_2}]
80	65	200	2.63	0.87	5.62	472	577
90	75	280	2.05	1.45	4.24	351	401
100	85	400	1.56	1.94	3.14	282	288
110	95	540	1.06	2.44	2.52	242	259
120	105	750	0.75	2.75	1.98	214	258
130	115	900	0.35	3.15	1.85	201	254
140	125	1000	0.08	3.42	2.00	202	245
150	135	1000	0.01	3.49	2.82	232	237
160	145	1000	0.00	3.50	3.54	257	279

Number of Stages

When the model is ran from the base case while only varying the number of stages of the column the results of B.4 is obtained. It can be seen that the regeneration energy demand per mole of CO_2 without taking H_2O in consideration (E) reaches a minimum from 4 stages onward because the top stage temperature T_{top} reaches a minimum. However, due to the fact that the top ratio goes down, as T_{top} goes down, the required energy demand to produce the 3:1 molar ratio of H_2O to CO_2 goes up when the number of stages is increased from 1. To conclude, **an increase in stages results in a lower lean loading and therefore, a higher cyclic capacity. However, it decreases the top ratio.**

Table B.4: Effect of the number of stages N on performance parameters of stripper column

N [-]	T_{top} [°C]	γ_{lean,CO_2} [mol_{CO_2}/kg_{TEPA}]	CC [mol_{CO_2}/kg_{TEPA}]	R_{top} [$p_{H_2O} : p_{CO_2}$]	E [kJ/mol_{CO_2}]	$E_{3:1}$ [kJ/mol_{CO_2}]
1	120.0	1.51	2.04	2.05	238	278
2	107.9	1.43	2.07	1.59	216	292
3	107.3	1.41	2.09	1.47	211	299
4	107.2	1.41	2.09	1.44	209	301
5	107.1	1.41	2.09	1.43	209	302
6	107.1	1.41	2.09	1.43	209	303
10	107.1	1.41	2.09	1.43	209	303

Reflux Ratio

The range between 0 and 10 is investigated for the reflux ratio of which the results are elaborated in table B.5. Just as van de Poll observed during his research, it can be observed that **an increase in reflux ratio results in a decrease in lean loading and therefore, increase in cyclic capacity.** Furthermore, **as the reflux ratio is increased the P_{H_2O} in the top stage increases.** Consequently, the required energy demand to produce the 3:1 molar ratio of H_2O to CO_2 goes down.

Table B.5: Effect of reflux ratio RR on performance parameters of stripper column

RR [−]	T_{top} [°C]	γ_{lean,CO_2} $[mol_{CO_2}/kg_{TEPA}]$	CC $[mol_{CO_2}/kg_{TEPA}]$	R_{top} $[p_{H_2O} : p_{CO_2}]$	E $[kJ/mol_{CO_2}]$	$E_{3:1}$ $[kJ/mol_{CO_2}]$
0	107.5	1.51	1.99	1.34	209	313
0.25	107.3	1.46	2.04	1.39	209	307
0.5	107.2	1.41	2.09	1.42	209	303
0.75	107.1	1.38	2.12	1.45	209	300
1	107.0	1.36	2.14	1.47	209	298
1.25	106.9	1.33	2.17	1.49	209	296
1.5	106.9	1.32	2.18	1.50	209	294
1.75	106.8	1.30	2.20	1.51	209	293
2	106.8	1.29	2.21	1.52	210	292
2.5	106.7	1.27	2.23	1.54	210	291
3	106.7	1.25	2.25	1.55	210	289
4	106.6	1.23	2.27	1.57	210	288
5	106.6	1.22	2.28	1.58	210	286
10	106.4	1.18	2.32	1.61	210	284

Feed Temperature

When the temperature of the feed increased, the required sensible heat to heat the feed up to the reboiler temperature decreases as a result of the decreasing difference between T_{feed} and T_{reb}. Therefore, it can be concluded that **the energy demand scales inversely with the temperature of the feed.** Furthermore, it can be seen that **an increasing feed temperature results in an increasing top stage temperature, and therefore, and increasing top ratio.** It must be noted that when the temperature of the feed is higher that the top stage temperature, absorption would take place in the top stage. Resulting, in that stage being unnecessary. An optimization regarding the amount of stages and feed temperature will be provided in section 6.2.3.

Table B.6: Effect of the feed temperature T_{feed} on performance parameters of stripper column

T_{feed} [°C]	T_{top} [°C]	γ_{lean,CO_2} $[mol_{CO_2}/kg_{TEPA}]$	CC $[mol_{CO_2}/kg_{TEPA}]$	R_{top} $[p_{H_2O} : p_{CO_2}]$	E $[kJ/mol_{CO_2}]$	$E_{3:1}$ $[kJ/mol_{CO_2}]$
30	90.4	1.26	2.24	0.65	497	807
40	93.0	1.28	2.22	0.74	460	719
50	95.3	1.30	2.20	0.84	423	642
60	97.6	1.32	2.18	0.94	385	572
70	99.7	1.34	2.15	1.04	349	509
80	101.8	1.36	2.14	1.15	308	444
90	103.9	1.38	2.12	1.26	269	386
100	106.0	1.40	2.10	1.37	229	330
110	108.3	1.42	2.08	1.49	189	275
115	109.4	1.43	2.07	1.54	168	248

Mass fraction of H_2O of the rich sorbent

Close observation of table B.1 reveals the top ratio is too low for sorbent ID 18 at the Sahara conditions to satisfy the design specification set by ZEF of 3:1. Assuming the mass fraction of H_2O can be varied, the following results are obtained as presented in table B.7. It must be noted that the amount of CO_2 is remained constant for this analysis. Close observation reveals **the lean loading going down as the mass fraction of H_2O is increased, resulting in the cyclic capacity going up** as the rich loading of the feed remains constant. A minimum in regeneration energy demand can be observed for $0.4\ kg_{H_2O}/kg_{TEPA}$, as a consequence of the top ratio getting closer to the required 3:1. The top ratio rises far beyond the 3:1 ratio as **the top ratio goes up with increasing H_2O mass fraction**, resulting in an increase in the required energy.

Table B.7: Effect of the mass fraction of H_2O of the feed on performance parameters of stripper column

R_{rich,H_2O} $[kg_{H_2O}/kg_{TEPA}]$	T_{top} $[^{\circ}C]$	γ_{lean,CO_2} $[mol_{CO_2}/kg_{TEPA}]$	CC $[mol_{CO_2}/kg_{TEPA}]$	R_{top} $[p_{H_2O} : p_{CO_2}]$	E $[kJ/mol_{CO_2}]$	$E_{3:1}$ $[kJ/mol_{CO_2}]$
0.1	110.7	2.45	1.05	0.68	237	527
0.2	108.2	1.73	1.77	1.18	210	341
0.25028 (S)	107.1	1.41	2.09	1.43	209	302
0.3	106.2	1.11	2.39	1.67	211	279
0.4	104.9	0.57	2.93	2.19	223	254
0.5	104.5	0.17	3.33	3.05	253	255
0.6	104.9	0.03	3.47	4.93	267	405
0.8	104.4	0.00	3.50	9.7	409	789
1	103.67	0.00	3.50	14.6	541	1183
1.1982 (M)	103.1	0.00	3.50	19.47	661	1575

Rich CO_2 loading of the sorbent

The effect of an increasing rich loading on the performance of the stripper is set up in table B.8. It can be seen that **an increase in the rich loading, results in an increase in lean loading**. However, as this increase is not as steep as the increase in rich loading, **the cyclic capacity is also increasing.** It must be noted that **the top ratio is going down**, so even when the E is going down with an increasing rich loading, the minimum energy expense when the 3:1 ration is met $E_{3:1}$ reaches a minimum for the Mediterranean equivalent CO_2 loading.

Table B.8: Effect of rich CO_2 loading of the feed γ_{rich,CO_2} on performance parameters of stripper column

γ_{rich,CO_2} $[mol_{CO_2}/kg_{TEPA}]$	T_{top} $[^{\circ}C]$	γ_{lean,CO_2} $[mol_{CO_2}/kg_{TEPA}]$	CC $[mol_{CO_2}/kg_{TEPA}]$	R_{top} $[p_{H_2O} : p_{CO_2}]$	E $[kJ/mol_{CO_2}]$	$E_{3:1}$ $[kJ/mol_{CO_2}]$
0.5	105.0	0.50	0.00	12.83	$>10^6$	$>10^6$
1	105.0	1.00	0.00	6.28	$>10^6$	$>10^6$
2	112.1	1.26	0.74	1.98	351	395
3	108.7	1.37	1.63	1.57	233	310
3.5 (S)	107.1	1.41	2.09	1.43	209	302
3.9 (M)	106.0	1.43	2.47	1.33	195	301
4	105.7	1.44	2.56	1.31	192	302
5	103.0	1.50	3.50	1.13	170	311
6	100.4	1.54	4.46	0.99	156	330

B.7. Absorption Column, Gear Pump Calculations

The duty for the gear pump on the absorber side has been calculated using equation B.11 for the pressure drop in the pipes. Following the pressure drop, the hydraulic pumping power is calculated with equation B.12, from where the energy demand for the pump can be calculated using equation B.13.

$$P = \rho_{avg} * g * h + \frac{128L}{\pi} * \mu * \frac{\dot{Q}}{D^4} \quad [pa] \tag{B.11}$$

$$P_h = \dot{Q} * P \quad [W] \tag{B.12}$$

$$E_{pump} = \frac{P_h * \Delta t_{ton,CO_2}}{1000} \quad [kWh/ton_{CO_2}] \tag{B.13}$$

The following assumptions are made for the calculations:

- g, the acceleration of gravity equals 9.81 m/s^2.
- ρ_{avg}, is the average density of the sorbent is calculated by multiplying the component concentrations with the individual components densities. The actual values used for the calculation are listed in table B.9.

Table B.9: Densities of the sorbent components

Chemical	Density [kg/m^3]
TEPA	993
PEG-200	1124
CO_2 (liquid)	1101
H_2O	997

- h depicts the height of the absorber, it was calculated to be 1 m in section 6.1.
- L resembles the length of the pipes of the absorber, this value is estimated to be 1.5 m.
- μ is the sorbent viscosity as obtained from the Airfarm experiments.
- $\dot{Q}$ resembles the sorbent volumetric flow rate through the absorber and is calculated by $\dot{Q} = \frac{100 * \dot{m_{stripper}}}{\rho_{avg}}$
- D resembles the diameter of the pipes, which is chosen to be 1 cm according to Matteis recommendations [82].
- $\Delta t_{ton,CO_2}$ depicts the time it takes for the DAC unit to produce a ton of CO_2, calculated from requirement of 18.75 $mol_{CO_2}/8hrs$
- The electrical efficiency of the pump has been left outside of the scope of this thesis and is therefore assumed to be 100%.

C

Relevant Theory

C.1. FTIR Spectral Chart

Figure C.1: IR band assignments for absorbed CO_2 Species obtained from [122].

wavenumber (cm^{-1})	assignment	species
3075–2975	NH_3^+ stretching	primary ammonium ions
2750–1750	N–H combination	primary/secondary ammonium ions
1696	C=O	dimer carbamic acid
1670–1630	NH_3^+ deformation	primary ammonium ions
1575–1525	COO^- stretching	carbamate
1486–1477	COO^- stretching	carbamate
1405	C–N stretching/$NCOO^-$ skeletal vibration	carbamate
1324–1305	$NCOO^-$ skeletal vibration	carbamate

C.2. Antoine's Equation

The function for H_2O in the stripper model utilizes the Antoine's Equation for the pure component vapor pressure of H_2O, followed by Wilson's theory for a binary system [36].

$$log_{10} P_{H_2O}^{sat}(T) = A - \frac{B}{C + T} \tag{C.1}$$

The Antoine coefficients were obtained from the Dortmund Databank [12].

Table C.1: Antoine coefficients for the temperature dependence of the pure water vapor pressure. [12]

	mmHg		mbar	
	T <100°C	T >100°C	T <100°C	T >100°C
A	8.07131	8.14019	8.196213	8.265093
B	1730.63	1810.94	1730.755	1811.065
C	233.426	224.485	233.5509	244.6099

Bibliography

[1] E. L. Goetheer A. Adeosun, N. El Hadri and M. R. AbuZahra. Absorption of co_2 by amine blends solution: An experimental evaluation. *International Journal Of Engineering And Science*, 3:12–23, 2013. http://www.researchinventy.com/papers/v3i9/B039012023.pdf.

[2] N. G. Chisholm-Q. T. Black D. D.Mumford-M. A. Nicholson A. D. Ebner, M. L. Gray and J. A. Ritter. Suitability of a solid amine sorbent for co2 capture by pressure swing adsorption. *Industrial Engineering Chemistry Research*, 50:5634, 2011.

[3] Aliakbar Heydari-Gorji Abdelhamid Sayari and Yong Yang. Co_2-induced degradation of amine-containing adsorbents: Reaction products and pathways. *J. Am. Chem. Soc.*, 134:13834–13842, 2012. doi: https://doi.org/10.1021/ja304888a.

[4] Sigma Aldrich. Chemical properties. *www.sigmaaldrich.com*, 2020. doi: sigmaaldrich.com.

[5] Farid Samani Masih Hosseini-Jena Amir Hossein Jalili, Mohammad Shokouhi. Measuring the solubility of co2and h2s in sulfolane and the density and viscosity of saturated liquid binary mixtures of (sulfolane + co2) and(sulfolane + h2s). *J. Chem. Thermodynamics*, 85:13–25, 2015. doi: https://doi.org/10.1016/j.jct.2015.01.001.

[6] Antecy. About us. *http://www.antecy.com/about-us/*, Accessed 15-10-2020.

[7] S. Gondal E. T. Hessen-T. Haug-Warberg A. Hartono-K. A. Hoff-H. F. Svendsen Aronu, U. E. Aronu and al. Solubility of co2 in 15, 30, 45 and 60 mass% mea from 40 to 120 c and model representation using the extended uniquac framework. *Chemical Engineering Science*, 66:6393–6406, 2011.

[8] O. Aschenbrenner and P. Styring. Comparative study of solvent properties for carbon dioxide absorption. *Energy & Environmental Science*, 3:1106–1113, 2010. doi: 10.1039/c002915g.

[9] O. Azzalini. Designing a carbon dioxide adsorption unit for producing sustainable synthetic fuels. *Ph.D. thesis, Delft University of Technology*, 2018.

[10] J. Wei T Zhang J Hu F. Li B. Zhang, A. Bogush and Q. Yu. Reversible carbon dioxide capture at high temperatures by tetraethylenepentamine acetic acid and polyethylene glycol mixtures with high capacity and low viscosity. *Energy and Fuels*, 31:4237–4244, 2017. doi: 10.1021/acs.energyfuels.6b03458.

[11] Dortmund Data Bank. Dortmund data bank data sheet. *ddbst.com*. doi: ddbst.com.

[12] Dortmund Data Bank. Saturated vapor pressure of water. Accessed on 13-04-2021.

[13] N. Serrano Barthe. Absorption of co2 from the air using polyamines: Experiments, modelling and design. *Master Thesis, Delft University of Technology*, 2019. doi: http://resolver.tudelft.nl/uuid:895913fc-987b-4f20-837e-28b369fe2fb3.

[14] Marland g. Boden, T.A. and R.J. Adres. Global, regional, and national fossil-fuel co2emissions. *Carbon Dioxide Information Analysis Center, Oak Ridge National Laboratory, U.S.*, 2017.

[15] F. Bougie and M. C. Iliuta. Sterically hindered amine-based absorbents for the removal of co2 from gas streams,. *Journal of Chemical Engineering Data*, 57:635–669, 2012.

[16] Steve Benson Brian Tande, Wayne Seames. Efficient regeneration of physical and chemical solvents for co2 capture. *University of North Dakota*, 2013. doi: DE-FE0002196.

[17] Weiland R.H. Browning, G.J. Physical solubility of carbon-dioxide in aqueous alkanolamines via nitrous-oxide analogy. *Journal of Chemical Engineering Data 39*, pages 817–822, 1994.

[18] R. W. Bucklin and R. L. Schendel. Comparison of physical solvents used for gas processing. *Energy Progress*, 1984.

[19] Barry Burr and Lili Lyddon. A comparison of physical solvents for acid gas removal. *GPA annual convention proceeding*, 1, 01 2008.

[20] J. Cakstins. Thermal properties of polyethyleneimine (pei) impregnatedmesoporous silica. *Journal of the Department of Chemical and Environmental Engineering: University of Nottingham*, 2015.

[21] Chemeo. Chemical properties of 1,4-butanediol (cas 110-63-4). *www.chemeo.com*, viewed 2020.

[22] TEXOL chemical. Technical data sheet texol. *http://www.dayioglupetrol.com.tr/PageContentImages/images/Te*

[23] Alibaba Chemicals. Chemicals.

[24] Dow chemicals. Datasheet tetraethylenepentamine. *www.dow.com*. doi: https://www.dow.com/content/dam/dcc/documents/en-us/productdatasheet/108/108-01354-01-tetraethylenepentamine-tepa-tds.pdf?iframe=true.

[25] Boundless Chemistry. Acid base titration. *Boundless Learning*, accessed on 3 May 2021. https://www.boundless.com/chemistry/textbooks/boundless-chemistry-textbook/.

[26] Bernd; Steinberner Udo; Dilla Wolfgang; Karinen Reetta Christoph, Ralf; Schmidt. Glycerol. *Ullmann's Encyclopedia of Industrial Chemistry*. doi: 10.1002/14356007.a12_477.pub2.

[27] Climeworks. Capturing co2 from air. *http://www.climeworks.com/co2-removal/*, accessed 14 October 2020.

[28] CO2.earth. Co2 statistics. 2020.

[29] EDB Union College.

[30] Rochelle G.T. Cullinane, J.T. Kinetics of carbon dioxide absorption into aqueous potassium carbonate and piperazine. *Industrial Engineering Chemistry Research 45*, pages 2531–2545, 2006.

[31] Giampaolo Manzolini Eric van Dijk Michiel Carbo Daniel Jansen, Matteo Gazzani. Precombustion co2 capture. *International Journal of Greenhouse Gas Control*, Februari 2015. doi: 10.1016/j.ijggc.2015.05.028.

[32] R.P. Danner. Daubert, T.E. Physical and thermodynamic properties of pure chemicals data compilation. *Taylor and Francis*, 1989.

[33] David St. Angelo David W. Keith, Geoffrey Holmes and Kenton Heidel. A process for capturing co2 from the atmosphere. *Elsevier, Joule*, pages 1573–1594, 2018. doi: https://doi.org/10.1016/j.joule.2018.05.006.

[34] Delamine. Product sheet tepa. doi: https://www.delamine.com/documenten/productsheets/s-sal313-06-spec-tepa.pdf.

[35] Veselovskaya J. Kardash T. Trubitsyn D. Okunev A. Derevschikov, V. Direct co2 capture from ambient air using k2co3/y2o3 composite sorbent. *Fuel*, 127:212–218, 2014. doi: https://doi.org/10.1016/j.fuel.2013.09.060.

[36] R. Dowling. An experimental and computational study of co_2 absorption in aqueous solutions of tetraethylenepentamine. *Thesis, Delft University of Technology*, 2020.

[37] Drugbank. 1,4-butanediol. *Drugbank*. doi: http://www.drugbank.ca/drugs/DB01955.

[38] Schwartz D.E. Amic S. Larner D.L. Zesch J. Torres F. Littau K. Eisaman, M.D. Energy-efficient electrochemical co2 capture from the atmosphere. *Technical Proceedings of the 2009 Clean Technology Conference and Trade Show*, 2009.

[39] Stephanie A. Didas Eloy S. Sanz-Pérez, Christopher R. Murdock and Christopher W. Jones. Direct capture of co_2 from ambient air. *Chemical Reviews*, 2016. doi: 10.1021/acs.chemrev.6b00173.

[40] Carbon Engineering. Carbon engineering, direct air capture. *http://carbonengineering.com/about-dac/*, Accessed 19 October 2020.

[41] Chemical Engineering. Commercial-scale production of bio-based bdo announced. *Chem. Eng.*, 2013.

[42] J. D. & Henley E.Seader. Seperation process principles. 36, 1999.

[43] NOAA National Centers for Environmental Information. State of the climate: Global climate report for annual 2019. 2020.

[44] G. Forensics. How does fourier transform infrared (ftir) spectroscopy work? last accessed on 3 May 2021. https://www.gossmanforensics.com/pdf-library/pdf-analytical-methods/fourier-transform-infrared.pdf.

[45] M. Maeder G. Puxty. The fundamentals of postcombustion capture. *Elsevier, CSIRO energy, Newcastle, NSW, Australia, Discipline of Chemistry, school of environmental and life sciences*, 2016. doi: http://dx.doi.org/10.1016/B978-0-08-100514-9.00002-0.

[46] Zhijie; Zhang Minghui; Li Wei; Tao Keyi. Ge, Shaohui; Wu. Industrial engineering chemistry research. *Industrial Engineering Chemistry Research*, 45:2229–2234, 2006.

[47] Lackner K. Han P. Slagle A. Wang T. Goldberg, D. Co-location of air capture, subseafloor co2 sequestration, and energy production on the kerguelen plateau. *Environ. Sci. Technol.*, 47:7521–7529, 2013.

[48] A. K. Gowda. Study of amine degradation in direct air capture. *Thesis, Delft University of Technology*, 2020.

[49] et al. Graves, Christopher. Sustainable hydrocarbon fuels by recycling co2 and h2o with renewable or nuclear energy. *Renewable and Sustainable Energy Reviews*, 15:1–23, 2011.

[50] Coyle I. Thambimuthu K. Gupta, M. Co2 capture technologies and opportunities in canada. *In 1st Canadian CCS Technology Roadmap Workshop*, 18:19, 2003.

[51] V. Becatinni Y.-C. Ng A. Steinfeld T. Zimmermann-P. Tingaut H. Sehaqui, M. E. G□lvez. Fast and reversible direct co2 capture from air onto all-polymer nanofibrillated cellulose—polyethylenimine foams. *Environ. Sci. Technol.*, 49:3167–3174, 2015. doi: https://doi.org/10.1021/es504396v.

[52] O. Hanafi. Development and design of the experimental setup of the absorber for direct air capture. *Zero Emission Fuels*, 1:1–26, 2021.

[53] Taylor P; Kirk-Othmer Hort EV. Acetylene-derived chemicals. *Encyclopedia of Chemical Technology.*, 2001.

[54] Huntsman. Technical data sheet tetraehtylenepentamine (tepa). 2008.

[55] IEAGHG. A brief history of ccs and current status. *IEA, green house gas*, 2020.

[56] Ilo. Datasheet 1,4-butanediol. doi: https://www.ilo.org/dyn/icsc/showcard.display?p_version=2&p_card_id=1104.

[57] Inchem. Datasheet diethylene glycol. doi: http://www.inchem.org/documents/icsc/icsc/eics0619.htm.

[58] R. J.Wrobel S.Mozia E. Piróg E. Kusiak-Nejman J. Serafin-A.W.Morawski J. Kapica-Kozar, B.Michalkiewicz and U. Narkiewicz. Adsorption of carbon dioxide on tepa-modified tio 2 /titanate composite nanorods. *New Journal of Chemistry*, 41:7870, 2017.

[59] universite Paris-SUD Jean Philibert, former professor of materials science. One and a half century of diffusion: Fick, einstein, before and beyond. *The Open-Access Journal for the Basic Principles of Diffusion Theory, Experiment and Application*, 2005.

[60] Y.; Feifei Z.; Xin C.; Ming-T.; Wanzhong-K.; Yanbo Z.; Jun L. Jie, G.; Jun. Study on absorption and regeneration performance of novel hybrid solutions for co2 capture. *Gas*, 15:15, 2016.

[61] F.-Y Jou, F.D Otto, and A.E Mather. Solubility of h2s and co2 in diethylene glycol at elevated pressures. *Fluid Phase Equilibria*, 175(1):53 – 61, 2000. ISSN 0378-3812. doi: https://doi.org/10.1016/S0378-3812(00)00440-4. URL http://www.sciencedirect.com/science/article/pii/S0378381200004404.

[62] Freitas Jr. The nanofactory solution to global climate change: Atmospheric carbon capture. *Institute for Molecular Manufacturing, Palo Alto, USA.*, 45, 2015, accessed 19 October 2020. doi: Availableat:http://www.imm.org/Reports/rep045.pdf.

[63] KEMS. Kems peg data collection. doi: https://www.research-collection.ethz.ch/bitstream/handle/20.500.11850/168628/PEGdataCollection.pdf?sequence=4&isAllowed=y.

[64] KEMS. Kems data. *Research Collection*, 2020. doi: https://www.research-collection.ethz.ch/bitstream/handle/20.500.11850/168628/PEGdataCollection.pdf?sequence=4&isAllowed=y.

[65] Inna Kim, Karl Anders Hoff, and Thor Mejdell. Heat of absorption of co2 with aqueous solutions of mea: New experimental data. *Energy Procedia*, 63:1446–1455, 2014. doi: 10.1016/j.egypro.2014.11.154.

[66] Jisook Lee Yunje Lee-Huiyong Kim-Eunseok Kim Kwang Soon Lee Kim et al., Junghwan Kim. Evaluation of aqueous polyamines as co2 capture solvents. *Elsevier, Energy*, 187, 2019. doi: https://doi.org/10.1016/j.energy.2019.115908.

[67] Jürg M. Matter A.-H. Alissa Park Allen Wright Klaus S. Lackner, Sarah Brennan and Bob van der Zwaan. The urgency of the development of co2 capture from ambient air. *Proceedings of the National Academy of Sciences*, 2012. doi: 10.1073/pnas.1108765109.

[68] X.Chen Y.Gao F.Yan S.Tian. K.Li, J.Jiang. Research on urea linkages formation of amine functional adsorbents during co2 capture process: Two key factors analysis, temperature and moisture. *The Journal of Physical chemistry*, 120:25892–25902, 2016. doi: https://doi.org/10.1021/acs.jpcc.6b08788.

[69] Ewa Knapik, Piotr Kosowski, and Jerzy Stopa. Cryogenic liquefaction and separation of co2 using nitrogen removal unit cold energy. *Chemical Engineering Research and Design*, 131:66–79, 2018. doi: https://doi.org/10.1016/j.cherd.2017.12.027.

[70] J. Kranendonk. Zero emission fuels. 2020.

[71] Sholl D. Kulkarni, A. Analysis of equilibrium-based tsa processes for direct capture of co2 from air. *Ind. Eng. Chem. Res.*, 51:8631–8645, 2012. doi: https://doi.org/10.1021/ie300691c.

[72] K. Lackner. Capture of carbon dioxide from ambient air. *Eur. Phys. J. Spec. Top.*, 176:93–106, 2009.

[73] Lange. Lange's handbook of chemistry. 10th ed.:1669–1674.

[74] I. L. L. Leites. Thermodynamics of co2 solubility in mixtures monoethanolamine with organic solvents and water and commercial experience of energy saving gas purification technology. *Energy Convers. Manage*, 39:1665–1674, 1998.

[75] D.R Lide. Crc handbook of chemistry and physics. *88th edition*, pages 3–268, 2007-2008.

[76] Rujie Wang Qiangwei Li Shihan Zhang Meng Li Jie Liu Lidong Wang, Yifeng Zhang and Bo Chen. Advanced monoethanolamine absorption using sulfolane as a phase splitter for co2 capture. *Environ. Sci. Technol.*, 52,24:14556–14563, 2018. doi: https://doi.org/10.1021/acs.est.8b05654.

[77] Rebecca Lindsey. Climate change: Atmospheric carbon dioxide. *Climate.gov*, February, 2020.

[78] G. Ruider R. Rossbacher M. Frauenkron, J.-P. Melder and H. Höke. Ethanolamines and propanolamines. *Ullmann's Encyclopedia of Industrial Chemistry (Wiley-VCH Verlag GmbH Co*, 2001. doi: DOI:10.1002/14356007.a10_001.

[79] S. Ochrimenko D. Fischer M. Jäger, S. Schubert and U. S. Schubert. Branched and linear poly(ethylene imine)-based conjugates: synthetic modification, characterization, and application. *Chemical Society Reviews*, 41:4755, 2012.

[80] P. Stephenson J. Sidders C. Ramshaw M. Wang, A. Lawal. Post-combustion co2 capture with chemical absorption: A state-of-the-art review. *Chemical Engineering Research and Design*, 89: 1609–1624, 2011. doi: https://doi.org/10.1016/j.cherd.2010.11.005.

[81] Christian Breyer Mahdi Fasihi, Olga Efimova. Techno-economic assessment of co2 direct air capture plants. *Elsevier, Journal of cleaner production*, pages 957–980, 2019. doi: https://doi.org/10.1016/j.jclepro.2019.03.086.

[82] A. De Matteis. Continuous direct air capture; understanding mass transfer in reactive absorption of carbon dioxide. *Thesis, Delft University of Technology*, 2020.

[83] Meglobal. Deg technical product brochure. doi: https://www.meglobal.biz/wp-content/uploads/2019/01/Diethylene-Glycol-DEG-Technical-Product-Brochure.pdf.

[84] Merck Millipore. Datasheet. *https://www.merckmillipore.com/*, attended 2020. doi: https://www.merckmillipore.com/.

[85] Merck Millipore. Polyethylene glycol dimethyl ether 500. *www.merckmillipore.com*, attended 2020.

[86] A.; Aroua M. K. Mirzaei, S.; Shamiri. A review of different solvents, mass transfer, and hydrodynamics for postcombustion co2 capture. *Rev. Chem. Eng.*, 31:521–561, 2015.

[87] Somayeh Mirzaei, Ahmad Shamiri, and Mohamed Kheireddine Aroua. Co2 absorption/desorption in aqueous single and novel hybrid solvents of glycerol and monoethanolamine in a pilot-scale packed bed column. *Energy & Fuels*, 34(7):8503–8515, 2020. doi: 10.1021/acs.energyfuels.8b04389. URL https://doi.org/10.1021/acs.energyfuels.8b04389.

[88] E. L. Goetheer N. El Hadri, D. V. Quang and M. R. A. Zahra. Aqueous amine solution characterization for post-combustion co2 capture process. *Applied energy*, 185:1433–1449, 2017.

[89] Nouryon. Technical data sheet nouryon. *https://ethyleneamines.nouryon.com/siteassets/tds-deg-mix-2019-11$_e$n.pdf,*.

[90] Nouryon. Tetraethylenepentamine. . doi: https://ethyleneamines.nouryon.com/globalassets/inriver/resources/pds-tetraethylenepentamine-tepa-en.pdf.

[91] Nouryon. Technical data sheet tetraehtylenepentamine (tepa). 2019.

[92] EDB University of Bristol.

[93] B. Ovaa. Direct air capture: an experimental approach on the desorption of co_2 and h_2o from pei and tepa. *Thesis, Delft University of Technology*, 2019.

[94] C. Saiwan R. Idem P. Muchan, J. Narku-Tetteh and T. Supap. Effect of number of amine groups in aqueous polyamine solution on carbon dioxide (co2) capture activities. *Separation and Purification Technology*, 184:128–134, 2017.

[95] R. Phougat. Vapor liquid equilibrium test sequence for the zef dac team. *Zero Emission Fuels*, 2021.

[96] Sakwa-Novak-M. Eisenberger P. Ping, E. Global thermostat low cost direct air capture technology. *International Conference on Negative CO2 Emissions*, 2018.

[97] ProRheo. Low shear viscometer user manual. *ProRheo*, 2020. doi: https://www.prorheo.de/images/Dokumente/Downloads/Englisch/User\%20manual\%20LS\%20300\%20RT-2016.pdf.

[98] Hidetaka Yamada Quyen T. Vu and Katsunori Yogo. Oxidative degradation of tetraethylenepentamine-impregnated silica sorbents for co2 capture. *Energy Fuels*, 33: 3370–3379, 2019. doi: 10.1021/acs.energyfuels.8b04307.

[99] J. M. Prausnitz R. C. Reid and B. E. Poling. The properties of gases and liquids. 1988.

[100] Hanna K. Knuutila R. Wanderley et al. Mapping diluents for water-lean solvents: A parametric study. *Industrial & Engineering Chemistry Research*, 59:11656–11680, 2020. doi: https://dx.doi.org/10.1021/acs.iecr.0c00940.

[101] Researchgate. Particle size magnifier for nano cn detection. doi: https://www.researchgate.net/publication/233253535_Particle_Size_Magnifier_for_Nano-CN_Detection/figures?lo=1.

[102] J. M. Rivas, O. R.; Prausnitz. Sweetening of sour natural gases by mixed-solvent absorption: Solubilities of ethane, carbon dioxide, and hydrogen sulfide in mixtures of physical and chemical solvents. *AIChE J*, 25:975−984., 1979.

[103] A. E. Roberts, B. E.; Mather. Solubility of co2 and h2s in a mixed solvent. *Chem. Eng. Commun.*, 72:201–211, 1988.

[104] Freeman S Van Wagener D Xu Q Voice A. Rochelle G, Chen E. Aqueous piperazine as the new standard for co2 capture technology. *Elsevier, Chemical engineering journal*, 171:725–733, 2011. doi: https://doi.org/10.1016/j.cej.2011.02.011.

[105] H. Shi S. Kim and J. Y. Lee. Co2 absorption mechanism in amine solvents and enhancement of co2 capture capability in blended amine solvent. *International Journal of Greenhouse Gas Control*, 45:181–188, 2016.

[106] William A. Poe Saeid Mokhatab. Handbook of natural gas transmission and processing. 2012.

[107] J. Seader and J. E. Henley. Separation process principles. *2nd ed.*, page 791.

[108] S.-B.; Kim J.-Y.; Lee G.-W.; Jung J.-H.; Oh K.-J. Seo, J.-B.; Jeon. Vaporization reduction characteristics of aqueous ammonia solutions by the addition of ethylene glycol, glycerol and glycine to the co2 absorption process. *J. Environ. Sci.*, 24:494–498, 2012.

[109] M. S.; Tee H. C.; Leo C. Y.; Aroua M. K.; Aghamohammadi N Shamiri, A.; Shafeeyan. Absorption of co2 into aqueous mixtures of glycerol and monoethanolamine. *J. Nat. Gas Sci. Eng.*, 35:605–613, 2016.

[110] Imada H. Maeda H. Hirata Y Shimonosono, T. Separation of hydrogen from carbon dioxide through porous ceramics. *Materials (Basel, Switzerland)*, 2016. doi: 10.3390/ma9110930.

[111] Darunte L. Jones C. Realff M. Kawajiri Y. Sinha, A. economic analysis of direct air capture of co2 through temperature vacuum swing adsorption using mil-101(cr)-pei-800 and mmen-mg2(dobpdc) mof adsorbents. *Ind. Eng. Chem. Res.*, 56 (3):750–764. doi: https://doi.org/10.1021/acs.iecr.6b03887.

[112] M. Sinha. Characterizing and design of a novel absorption process, dac. *ZEF reports*, 2019.

[113] Vaclav Smil and BP statistical review of world energy. Our world in data. 2020.

[114] Chakravartula S. Srikanth and Steven S. C. Chuang. Spectroscopic investigation into oxidative degradation of silica-supported amine sorbents for co2 capture. *ChemSusChem*, 5:1435–1442, 2012. doi: 10.1002/cssc.201100662.

[115] The Engineering Toolbox. *www.engineeringtoolbox.com*, attended 2020.

[116] P. D. Vaidya and E. Y. Kenig. Co2-alkanolamine reaction kinetics: a review of recent studies. *Chemical Engineering Technology: Industrial Chemistry-Plant Equipment-Process Engineering-Biotechnology*, 30:1467–1474, 2007. doi: https://doi.org/10.1002/ceat.200700268.

[117] N. van de Poll. Characterization and design of a stripper for a continuous direct air capture system. *Zero Emission Fuels*, 2021.

[118] R.W. van den Berg. Designing a direct air capture unit for methanol synthesis. *Thesis, Delft University of Technology*, 2018.

[119] D. van Laake. Characterization of a sorbent for a small scale direct air capture system. *Thesis, Delft University of Technology*, 2018.

[120] Van Dijck L.A.J. Van Swaaij W.P.M. Versteeg, G.F. On the kinetics between co2 and alkanolamines both in aqueous and non-aqueous solutions. an overview. *Chemical Engineering*, 144:113–158, 1996.

[121] Paul Vroegindeweij. Design and implementation of the zef 6 continuous direct air capture system. *ZEF reports*, 2020.

[122] S. S. C. Chuang W. C. Wilfong, C. S. Srikanth. In situ atr and drifts studies of the nature of adsorbed co2 on tetraethylenepentamine films. *Applied Materials and Interfaces*, 6:13617–13626, 2014. doi: https://doi.org/10.1021/am5031006.

[123] C. Sun T. C. Drage W. Zhang, H. Liu and C. E. Snape. Performance of polyethyleneimine–silica adsorbent for post-combustion co2 capture in a bubbling fluidized bed. *Chemical Engineering Journal*, 251:293, 2014.

[124] Brian Wang. World will blow through two degree co2 and have to look at geoengineering even if all electricity went solar and all cars are electric. *Next Big Future*, 2017. doi: https://www.nextbigfuture.com/2017/03/world-will-blow-through-two-degree-co2.html.

[125] Wikipedia. Timeline of human evolution. 2020.

[126] Chang P. Wilke, C.R. Correlation of diffusion coefficients in dilute solutions. *AIChe, Journal 1*, pages 264–270, 1955.

[127] Christopher W.Jones. Co_2 capture from dilute gasses as a component of modern global carbon management. *Annual reviews*, 2011. doi: 10.1146/annurev-chembioeng-061010-114252.

[128] Alexander Otto Martin Robinius Detlef Stolten Yuan Wang, Li Zhao. A review of post-combustion co2 capture technologies from coal-fired power plants. *Institute of Energy and Climate Research – Electrochemical Process Engineering (IEK-3), Forschungszentrum Jülich, D-52425 Jülich, Germany*, 2016.

[129] Michael A. Çengel, Yunus A.; Boles. Thermodynamics – an engineering approach. *McGraw-Hill Series in Mechanical Engineering*, 3, 1998. doi: ISBN978-0-07-011927-7.


TUDelft


ZEF